SEISMIC SITE-RESPONSE EXPERIMENTS FOLLOWING THE MARCH 3, 1985 CENTRAL CHILE EARTHQUAKE

(TOPOGRAPHICAL AND GEOLOGICAL EFFECTS)

Edited
by

M. Celebi

U.S. Geological Survey
Menlo Park, California

Open-File Report 86-90

TABLE OF CONTENTS

ACKNOWLEDGMENTS

A project of this type cannot be accomplished firstly without financial support and secondly without cooperation of institutions, officals and research personnel. The editor of this report gratefully acknowledges the partial financial support of the Office of Foreign Disaster Assistance (OFDA) of the Agency for International Development (AID). This support was administered through a grant to Dr. S.T. Algermissen of the U.S. Geological Survey (USGS). In addition to this partial support, Dr. Algermissen provided advice and consultation throughout the project. The mayor of the municipality of Viña del Mar, Madame Eugenia Garrido gave full moral support and inspiration to the project. Her staff, Luis Felipe Baeza, Hector Balbontin, Mario Mayo, and many others very significantly contributed to the success of this project, and their contributions are gratefully acknowledged.

Professors Rodolfo Saragoni and Edgar Kausel of the Civil Engineering Department and Institute of Geophysics, respectively, of the University of Chile, Santiago, and Professor Patricio Bonelli of the University of Santa Maria in Valparaiso contributed to the execution of and discussions related to the project.

Finally, Drs. Roger Borcherdt, William Joyner, and David Boore provided many helpful suggestions and discussions before and after the mission. Charles Mueller provided invaluable assistance in supervision of the data processing. Drs. Gerald Brady and Paul Spudich carefully and extensively reviewed the manuscript and offered valuable comments. Ray Eis and Lorraine M. Hollis contributed with their artistic draft work. Barbara Gessner, as always, patiently went through several drafts of typing effort. Gene Sembera and Chris Dietel worked late hours and weekends during the field work and Felipe Baeza was always there when we needed assistance. Without such advice and support, a successful mission cannot be undertaken.

M. Celebi
Editor

INTRODUCTION

M. Celebi

The 3 March 1985 Central Chile Earthquake (M_S=7.8) occurred with significant foreshocks and was followed by significant aftershocks (March 15, M=6.3; March 17, M=6.6; March 20, M=6.0, and April 8, M=7.2). The main population centers affected by the main shock and the aftershocks are shown in Figures 1 and 2.

The main event and the aftershocks caused a variety of natural hazards ranging from liquefaction and slope failure to failure of some unique engineered structures. These phenomena have been observed and preliminarily evaluated. Initial efforts in assessment of these effects of the earthquake are being compiled in comprehensive reports by the Earthquake Engineering Research Institute (Wyllie, and others, 1985), the United States Geological Survey (Algermissen, editor, 1985) as well as the Chilean scientists (Saragoni and others, 1985). The latter report contains extensive information on the accelerogram records obtained during the main event .

In this report, some unique experiments performed almost five months after the main event on the Central Chilean coast will be described. These experiments entail the study of specific site-response effects in the coastal town of Viña del Mar, and Canal in Beagle, a subdivision of the same town. In this report, the term site-response refers to variations in ground motions caused by variations in geological structure and topography. The overall geological formations of Viña del Mar, Canal Beagle, and Renecá, as well as general topography and coordinates of the region are depicted in Figure 3. The primary reasons for concentrating the efforts in this particular area were:

- the extent of damage in some and yet lack of damage in other taller structures (up to 24 stories) in Viña del Mar,
- the observations made during the previous trip (Celebi, 1985) immediately after the main event that: a) at Canal Beagle there is a possibility of geological and topographical (ridge) effects, and b) in Viña del Mar, there is a possibility of amplification of ground motions at alluvial and sand sites compared with firmer rock sites.
- the strong desire to correlate the damage distribution information compiled by the Municipality of Viña del Mar with site-related amplification studies.

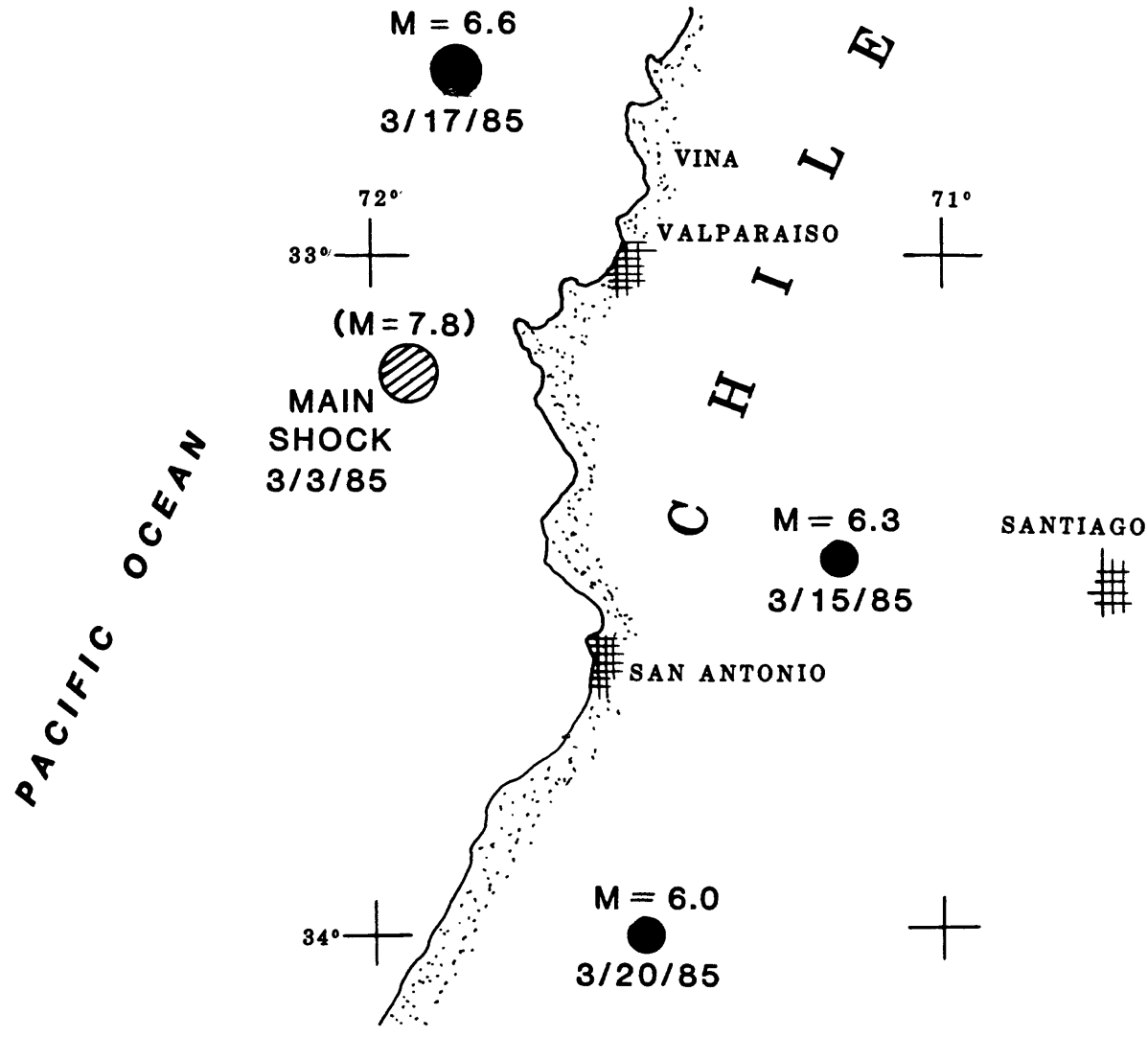

Figure 1. General epicentral locations of the 3 March 1985 (M = 7.8) central Chile Earthquake and its aftershocks and main affected centers.

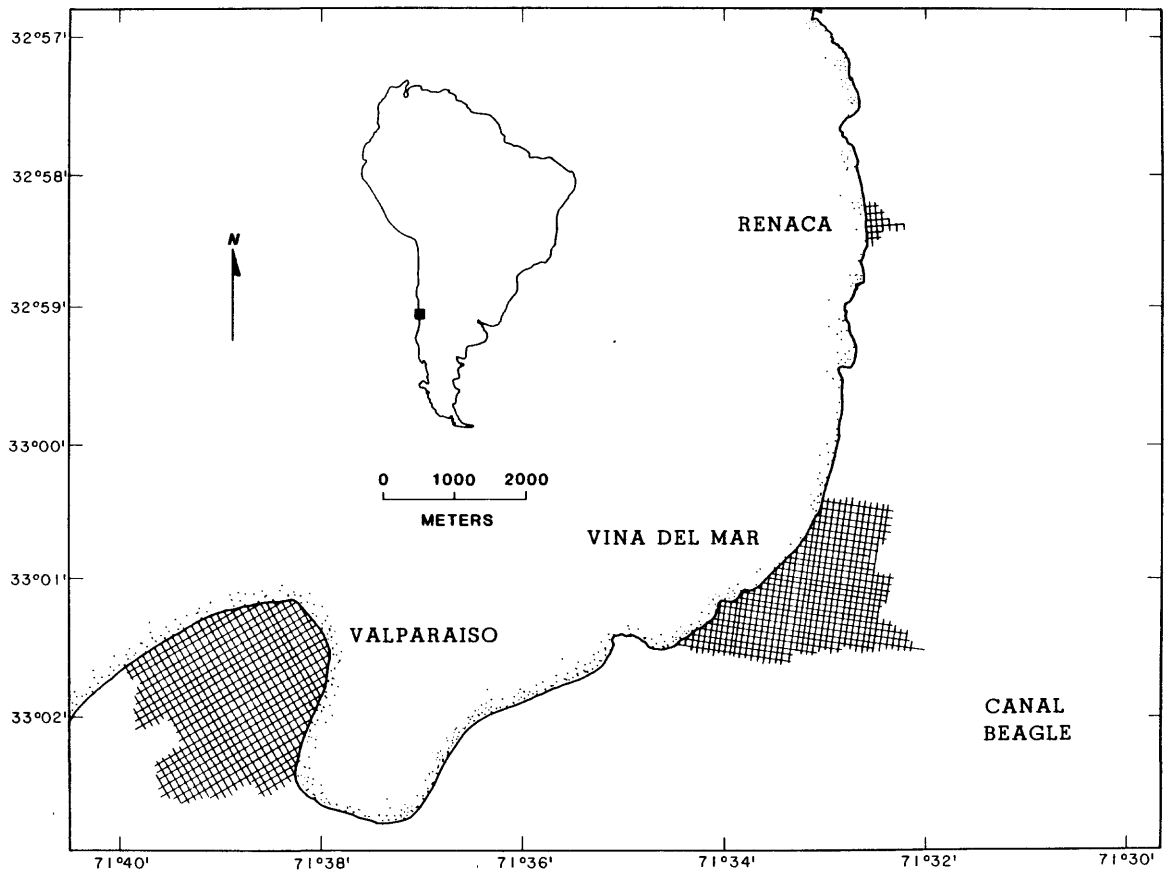

Figure 2. General locations of central Chile coast where the experiments were performed.

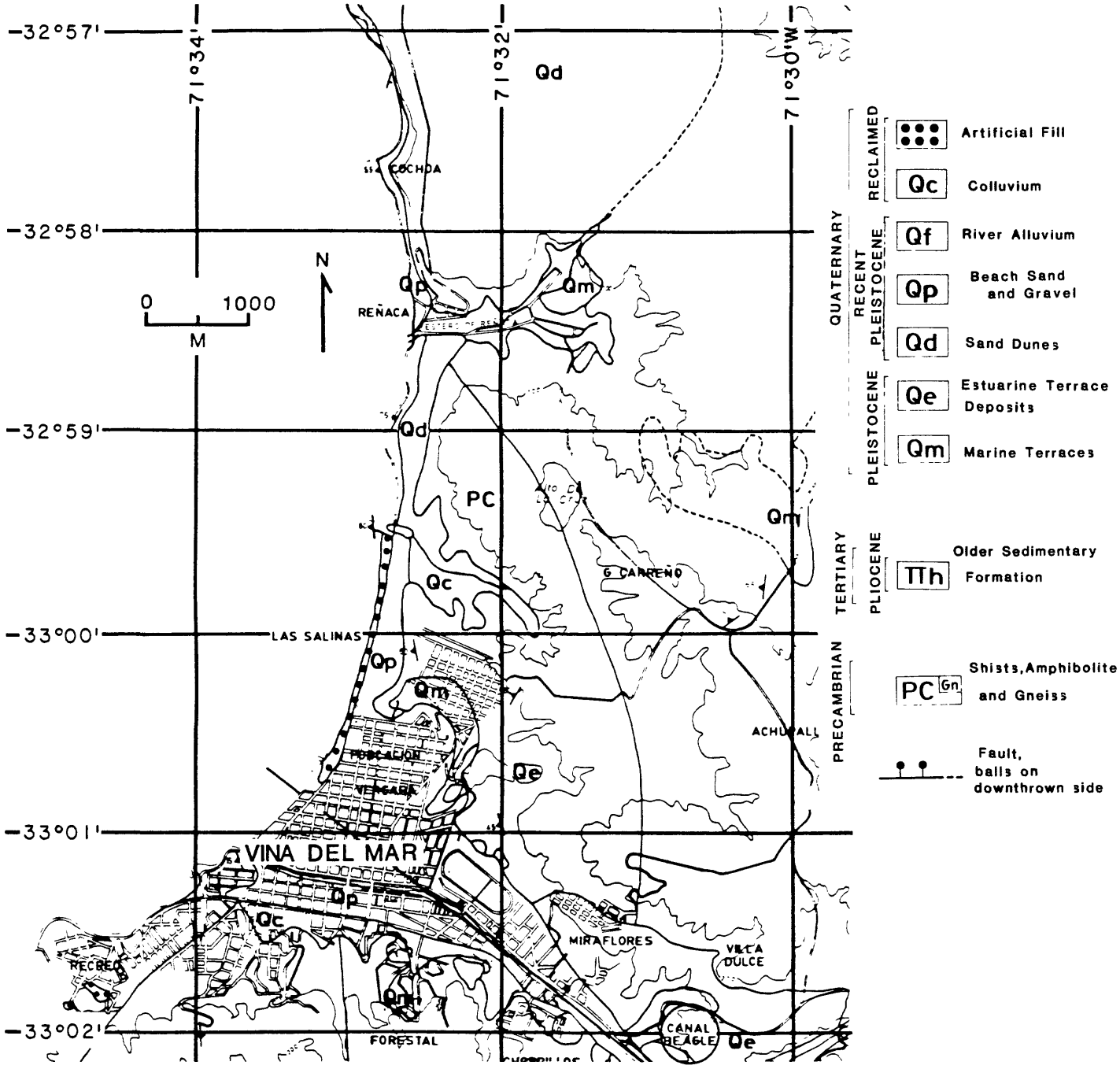

Figure 3. General geology, topography, and coordinates of Viña del Mar, Canal Beagle, and Reneca on the central coast of Chile.

The possibility that topography could cause the frequency-dependent amplification of seismic waves has been investigated empirically and theoretically by Boore (1972 and 1973), Bard and Tucker (1985) and Davis and West (1973). The current study presents a significant set of data reconfirming the frequency dependent amplification of seismic motions at ridges. One additional credit to be given to the current study is the fact that the seismograph array was located in a heavily populated region and a distinct damage pattern related to the ridge effect was observed. The other studies (Bard and Tucker, 1985; Davis and West, 1983) were performed in unpopulated or rural areas.

Studies of the type presented herein are necessary and useful for microzonation of local areas in seismic zones of the world. By quantifying amplification due to local topography (hills and ridges), we can contribute to both the local and overall understanding of this type of amplification. It may be possible that similar topographical and geological conditions may exist in close proximity to one another in other locales; therefore, results derived from one location can be generalized to be applied at others subsequent to additional studies. In Chile, for example, near Viña del Mar and beside Canal Beagle there are several other subdivisions founded on ridges. One such subdivision visited by the author was Gomez Carreño off Avenue Ste. Ines. The four-story structures in this subdivision were of concrete-block or brick masonry construction. A considerable number of these structures suffered extensive damage during the 3 March 1985 event.

Extensive review and experimentation of amplification of ground response at alluvial and other soft soil sites has been made in the San Francisco Bay Area (Gibbs and Borcherdt, 1974) and in the Los Angeles area (Rogers, and others, 1984) using pre-scheduled events of nuclear test explosions at Nevada. Certainly, the 19 September 1985 earthquake records in Mexico City (M_S=8.1) show that during that strong motion event the peak accelerations recorded in Mexico at a rock site and an alluvial site were 0.034 g and 0.17 g, respectively (Prince and others, 1985). Both of these records were obtained approximately 400 km from the epicenter.

The field work described herein was carried out between July 26 and August 10, 1985. This report describes the specific steps implemented during the field work and the extensive data set that has been obtained. Preliminary results and conclusions derived from the processing of the data set are pre-

sented. Participants in this field work were M. Celebi, E. Sembera, and C. Dietel as well as Mr. Luis Felipe Baeza of the Municipality of Viña del Mar. Planning of the experiments and day-to-day decisions were made by the author. The significant quantity of data obtained was played back and processed under the supervision of C. Mueller.

EXPERIMENTS CONDUCTED AND SCOPE OF THIS REPORT

The original objective of the field experiments as described above were:

1. To study topographical/geological amplification of ground motions at the Canal Beagle subdivision of Viña del Mar;
2. To study geological amplification effects in Viña del Mar.

The scope of this report covers these two experiments only. However, in addition to the above experiments, two additional experiments because of convenience and scheduling practicality were conducted, although the objective of the mission did not require them. These additional experiments were:

3. Ambient and free-vibration tests of selected structures at Canal Beagle and Viña del Mar;
4. Earthquake response of a 22-story structure in Viña del Mar.

These additional experiments are not within the scope of this report and will be documented separately.

Furthermore, all data and results presented in this report are derived from velocity recordings of motions. Studies of the data from acceleration recordings of motions are currently being carried out.

REFERENCES

Algermissen, S.T. (editor), 1985, Preliminary Report of Investigations of the Central Chile Earthquake of March 3, 1985: *U.S. Geological Survey Open-File Report 85-542.*

Bard, P.Y., and Tucker, B.E., 1985, Underground and ridge site effects: A comparison of observation and theory (paper submitted for publication - advance copy courtesy of B. Tucker).

Boore, D.M., 1972, A note on the effect of simple topography on seismic SH waves: *Bulletin, Seismological Society of America*, **62**, No. 1, pp. 275-284.

Boore, D.M., 1983, The effect of simple topography on seismic waves: Implications for the accelerations recorded at Pacoima Dam, San Fernando Valley, California, *Bulletin, Seismological Society of America*, **63**, No. 5, pp. 1603-1609.

Borcherdt, R.D., Fletcher, J.B., Jensen, E.G., Maxwell, G.L., Cranswick, E., VanSchaak, J.R., Warrick, R.E., 1984. A General Earthquake Observation System (GEOS), submitted to *Bulletin, Seismological Society of America*.

Celebi, M., 1985, Preliminary Field Trip Report on Chile Earthquake of March 3, 1985: *Report to Earthquake Engineering Research Institute* (April 1985).

Davis, L.L., and West, L.R., 1983, Observed effects of topography on ground motion: *Bulletin, Seismological Society of America*, **63**, No. 1, pp. 283-298.

Gibbs, J.F., and Borcherdt, R.D., 1974, Effects of local geology on ground motion in the San Francisco Bay region, California--A continued study: *U.S. Geological Survey Open-File Report 74-222*.

IAEE, 1972, Regulations for earthquake resistant design of buildings in Chile from Earthquake Resistant Design Regulations - A World List): publication of *IAEE (International Association of Earthquake Engineering)*, Japan.

Prince, J., and others, 1985, Sismo del 19 de Septiembre *Informe IPS-10A, B, C*, Instituto de Ingenieria, UNAM (University of Mexico).

Rogers, A.M., Borcherdt, R.D., Covington, P.A., and Perkins, D.M., 1984, A comparative ground response study near Los Angeles using recordings of Nevada nuclear tests and the 1971 San Fernando earthquake: *Bulletin, Seismological Society of America*, **74**, No. 5, pp. 1925-1949.

Saragoni, R., Fresard, M., and Gonzalez, P., 1985, Analisis de los acelerogramas del terremoto del 3 de Marzo de 1985, Universidad de Chile, Publicacion ses 14/1985 (199), Dec. 1985.

Wyllie, L., and others, 1985, Chile Report (to be published by *Earthquake Engineering Research Institute)*.

DATA ACQUISITION SYSTEMS

J. Gibbs, G. Jensen, G. Maxwell, E. Sembera, J. Sena,
J. VanSchaack, R.F. Warrick, R.D. Borcherdt, C. Dietel, and J. Fletcher

The experiment conducted following the earthquake of March 3, 1985 on the west coast of Chile utilized a set of eight portable General Earthquake Observations Systems (GEOS). This chapter provides a general description of the instrumentation followed by a summary of the particular configuration used for experiments described herein. A detailed description is provided by Borcherdt and others (1985).

GENERAL DESCRIPTION OF RECORDING SYSTEM

The portable digital data acquisition system used for the experiments was developed by the U.S. Geological Survey for use in a wide variety of both active and passive experiments. The microcomputer based system was developed in order that the system could be easily configured in the field to record signals for a variety of different experiments, including studies of strong motion, structural response, source mechanisms, wave propagation studies of aftershock sequences, crustal structure, teleseismic earth structure, near-surface seismic structure, earth tidal strains, free oscillations and a variety of wave propagation studies such as those described in this report. Versatility in system application is achieved by isolation of the appropriate data acquisition functions on hardware modules controlled by a central microcomputer through a general computer bus. CMOS hardware components are utilized to reduce quiescent power consumption to less than 2 watts for use of the system as either a portable recorder in remote locations or in an observatory setting with inexpensive backup power sources. The GEOS, together with two sets of three-component sensors (force-balance accelerometers and velocity transducers) and a ferrite WWVB antenna is shown in Figure 1. The hardware modules comprising the system are shown in Figure 2.

The signal conditioning module for the GEOS is configured with six input channels, selectable under software control, to permit acquisition of seismic signals ranging in amplitude from a few nanometers of seismic background noise to 2g in acceleration for ground motions near large events. The analog-to-digital conversion module is equipped with a 16 bit CMOS analog-to-digital

converter which affords 96 dB of linear dynamic range or signal resolution; this, together with two sets of sensors, implies an effective system dynamic range of about 180 dB. A data buffer with direct memory access capabilities allows for maximum throughput rates of 1200 sps or 200 samples/second/channel. With sampling rates selectable under software control as any integral quotient of 1200, a broad and variable system bandwidth ranging from 10^{-5} Hz to $5x10^{2}$Hz is available for recording signals from a wide variety of sensor types.

Modern high density (1600-6400 bpi) compact tape cartridges offer large data storage capacities (1.25 - 33 Mbyte) in ANSI standard format, to facilitate data accessibility via minicomputer systems. Read capabilities of cartridge tape recorders can be utilized to allow recording parameters and system operational software to be changed automatically. Read capability can be utilized to allow systems equipped with modems to transmit data via telecommunications to a central data processing laboratory. Microcomputer control of time standard provides capability to synchronize internal clock to internal receivers (such as WWVB and satellite), external master clock, or conventional digital clocks. Convenient system set-up and flexibility to modify system in the field for a wide variety of applications is achieved using a 32 character alphanumeric display under control of the microcomputer. English language messages to operator executed in an interactive mode, reduce operator field set-up errors. A complete record of recording system parameters is recorded on each tape together with calibration signals for both the sensors and the recorders. These records assure rapid and accurate interpretation of signals, both in the field and in the laboratory.

Flexibility to modify the system to incorporate future improvements in technology is achieved using a ringed software architecture and modular hardware components. Incorporation of new hardware modules is accomplished in a straightforward manner by replacing appropriate module and corresponding segments of controlling software. The flexibility afforded by microcomputer technology to modify the system for specialized applications and to incorporate changes in technology allows seismic signals as detectable by a wide variety of sensors to be recorded over a broad band of frequencies with high resolution.

The system response designed for strong-motion and aftershock applications of the GEOS was intended to allow large amplitude near source signals of

1-10 Hz as detected by a forced-balanced accelerometer (FBA) to be recorded on scale, while at the same time permitting much smaller amplitude high frequency signals (50-100 Hz) as might be detected on FBA's or velocity transducers to be recorded with high signal resolution. The design system response together with that for two types of sensors frequently used for aftershock studies in the near source region of large earthquakes is shown in Figure 3. With digitization rates and anti-aliasing filters, selectable under software control, the design system response allows signals ranging from essentially DC to 500 Hz to be recorded at high resolution without aliasing. Gain settings, selectable under software control, allow two sets of three-component data, ranging in amplitude over 180 dB, to be recorded simultaneously. Specifications for the recording system are summarized in Table 1.

GENERAL DESCRIPTION OF DATA PLAYBACK SYSTEM

The read and write capabilities of the mass-storage module together with the D/A conversion module permits the GEOS to be used as an analog as well as digital (via RS-232) play back system in the field. Visual inspection of digitally recorded data is useful for determining instrument performance, evaluation of recording parameters, evaluation of environmental factors (*e.g.*, local noise sources, *etc.*). RS-232 capabilities of data playback unit and ANSI-standard tape cartridges permit playback of digital time series on minicomputer system in the field or laboratory. Digital playback of data is generally performed using an ANSI-standard serpentine tape reader as a peripheral to minicomputer system in the laboratory. Deployment of minicomputer digital playback systems in the field is generally most feasible for large scale high data volume experiments.

RECORDING SYSTEM CONFIGURATION USED FOR CHILE EXPERIMENTS

For these experiments the recording system was configured as a six channel system. Channels 1-3 were set up to record the vertical, north-south, and east-west components of motion as detected by 3 component force-balanced accelerometers (Kinemetric FBA-13). Channels 4-6 were set up to record the vertical, north-south, and east-west components of motion as detected by 3 components velocity transducers (Mark Product, L-22). Specifications for the sensors are summarized in Table 2. Calibration procedures for sensors are described by Eaton (1975).

Each recording system was operated in trigger mode to permit on-site detection of seismic events. Sampling rate for each channel was chosen at 200 sps, implying a Nyquist frequency of 100 Hz. High cut analog filters (seven pole Butterworth, 42 dB/octave) with corner at 50 Hz were chosen to prevent aliasing. Gain settings of 6 and 12 dB were chosen for the signals detected by the acceleration sensors to permit any large amplitude near source signals to be recorded on scale. Gain settings of 30 and 36 dB were used to record smaller amplitude signals from more frequent small magnitude aftershocks to be recorded on-scale with high resolution.

Accurate timing (± 5 msecs) for each of the recorders was obtained using a portable master clock (model Mark I) synchronized with satellite time obtained from the Geophysical Institute of University of Chile in Santiago. Sensor calibration (applied DC voltage, velocity transducer; applied ± 12 volts FBA) and recording system calibration (voltage impulse, 5 sec Dirac comb) were recorded on each cartridge tape to permit evaluation of system performance and accurate relative calibration of recorders and sensors with changing environmental conditions.

Data playback in the field was accomplished using a GEOS system configured with a digital-to-analog conversion module and appropriate playback software. Analog playbacks of data using a Soltec strip chart with light sensitive film were used to visually inspect data in the field. Playback of digital data to minicomputer was not undertaken in the field. A description of the digital data played back from these experiments is described by Watson and Mueller (this report).

REFERENCES

Aki, K., and Richards, P.G., 1980, *Quantitative Seismology Theory and Methods*, vol. 1, W.H. Freeman and Co., San Francisco, California, 557 p.

Borcherdt, R.D., Fletcher, J.B., Jensen, E.G., Maxwell, G.L., VanSchaack, J.R., Warrick, R.E., Cranswick, E., Johnston, M.J.S., and McClearn, R., 1985, A general earthquake observation system: *Bulletin, Seismological Society of America*, **75**, no. 6.

Eaton, J.P., 1975, Harmonic magnification of the complete telemetered seismic system, from seismometer to film viewer screen: *U.S. Geological Survey Open-File Report 75-99*.

TABLE 1 - GEOS+ Specifications

Microcomputer and Communications

Internal CPU: CMOS, 12 Bit.
External CPU: optional.
Data transfer:
  Internal: Direct Memory Access
  I/O Port: RS-232 compatible baud rate programmable to standard rates.
  Telecommunications: UART, Modems optional.
  Analog playback via A/D.

Program Memory

Executable Memory: 8K 12 Bit word CMOS RAM.
Program Storage: 16K 12 Bit word CMOS PROM.
Alternate Program Storage: Programs may be stored on magnetic tape for loading directly into program RAM.

Sensor Inputs and Signal Conditioning

Input Channels: 6 balanced differential inputs, program selectable.
Preamplifier Dynamic Range: greater than 100 dB at 0 dB gain, programmable in 6 dB steps 60 to 0 dB.
Filters: low pass Butterworth, 42 dB per octave; program selectable, 17 Hz, 33 Hz, 50 Hz, and 100 Hz; high pass .1 Hz 6 dB per octave.
Calibration: Internal, automatic with or without sensors.
Transient Protection: ± 15 V

Analog to Digital Conversion

Resolution: 16 bits (1 part in 65,536).
Stability and Linearity: ± 1 count-no missing codes over full temperature range of -20°C to + 60°C.
Conversion Rate (Total samples per second for all active channels): 1200 samples per second maximum, .29 samples per second minimum; programmable as 1,200/N where N is 1 through 4,096.

Pre-Event Data Memory

Size: 4,096 words, 16 bits per word.
Pre-trigger memory: Five, 512 word blocks minimum at 1,200 samples per second (2.14 seconds), six 512 work blocks at 300 samples per second (10.24 seconds), program selectable.

Mass Data Storage/Retrieval

Cartridge: Read/Write 3M type, 1600 bpi.
Tape capacity: 3,680 512 word blocks (1.88 million samples) typical for 450 ft. tape, 26 minutes continuous record time at the maximum sample rate.
Tape Speed: 30 ips write or read.
Slave Recorders: 2 optional, separate housing.

Time Control

External:
  WWVB Receiver: Automatic synchronization of internal clock to WWVB under program command.
  Master Clock: Synchronization of internal clock with external pulse and corresponding time corrections derivable at selectable times under program command.
  Manual: Time entered through keyboard and synchronized manually.
Internal:
  Frequency: 3 MHz.
  Temperature Stability: ± 1 x 10^{-6}; - 20°C to + 70° C.
  Aging Rate: less than 5 x 10^{-7} per year.

Operator Interface

Operation Environment: English language commands under software control.
Display: 32 character, alphanumeric display, 18 segment, character height .15 in. LED with optical filters.
Keyboard: Mechanical switch with dust cover and water seal, 20 button keyboard with numeric and function entry.
Status Checks: Time, battery voltage, no. of events, % of tape used, elapsed time since power on.
Debug: single and subroutine stepping.

Operating Modes

Self triggering:
  Near field: Selectable short term average (STA), long term average (LTA), ratio.
  Teleseismic: Comparative ratios for two selectable frequency bands.
Pre-set time: record at selectable times and intervals.
Both: operate in both pre-set time and self triggering modes.
Manual: record under keyboard control for start-stop functions.

Power Requirements

Voltage, current: + 24 VDC nominal ± 15%, 40 mA nominal in operating mode with display off, 300 mA nominal with display on, 600 mA with display on and recording.
Internal batteries: ± 24 V, 5 AH Gates type, will operate about 3 days on internal batteries, connector provided for internal battery charging or external battery operation.

Physical and Environmental Requirements

Case Type: Waterproof aluminum case, 20 1/2" long, 9 7/8' wide 13 3/4" high.
Weight: 47 lbs. with internal batteries.
Operating Temperature Range: - 20°C to + 60°C, 15% to 95% rel. humidity.

+ Patent pending.

TABLE 2 - Sensor Specifications

Velocity transducers:

L22-3D (Mark Products)
Natural freq.: 2 Hz
Coil Resistance: 5.5 K Ω
Output: 0.5 v/cm/s
Damping: 0.8 critical
3 component pkg.: da., 18 cm; ht. 12 cm.

Forced Balanced Accelerometers:

FBA-13 (Kinemetrics)
Range: ± 2 g full scale
Output: ± 10 v full scale
Natural Freq: 50 Hz
3 component pkg.; 14 x 14 x 8.5 cm

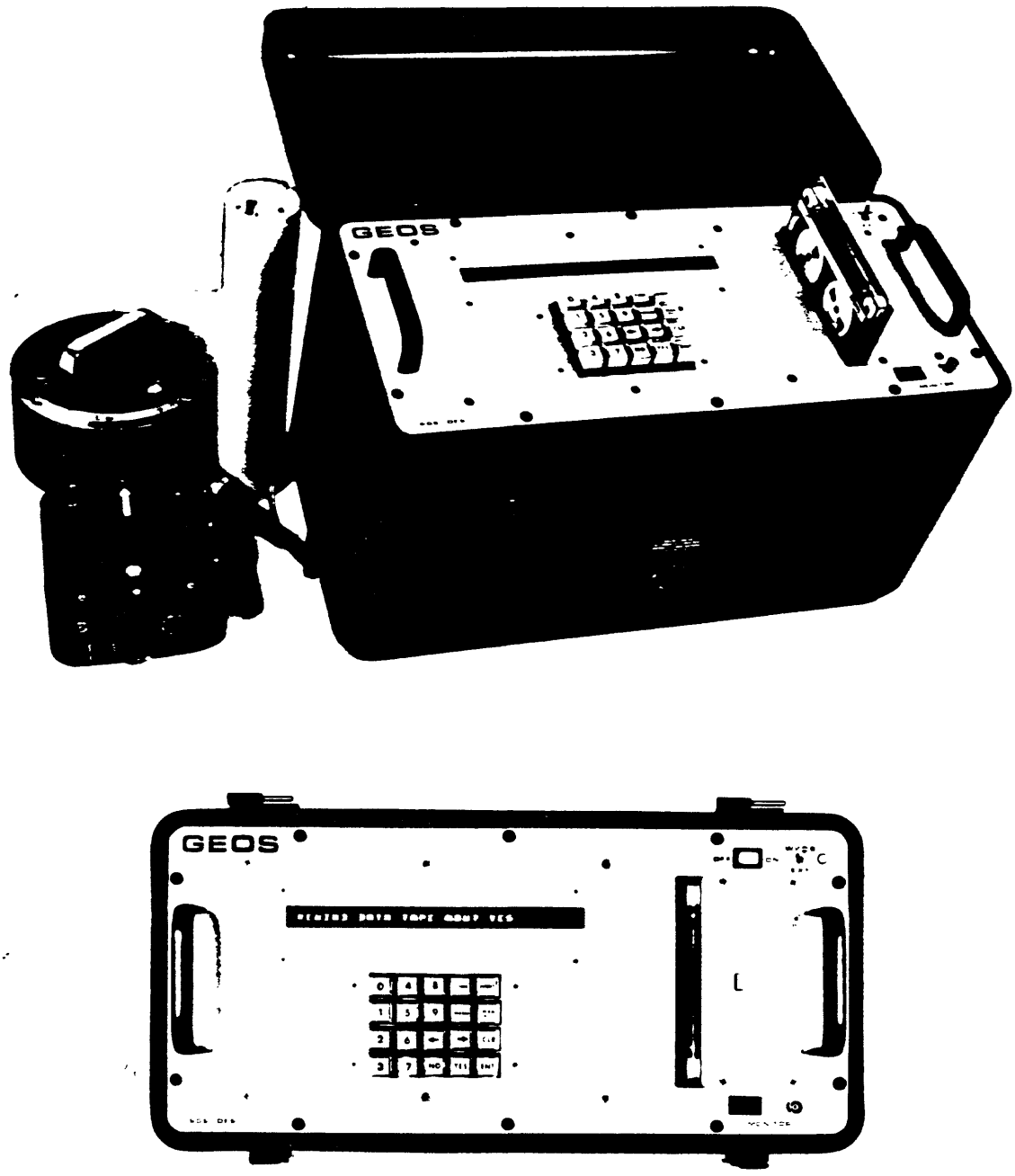

Figure 1. Side and front-panel view of the General Earthquake Observation System (GEOS), together with a WWVB ratio antenna and two sets of three-component sensors commonly used to provide more than 180 dB of linear dynamic range. System operation for routine applications requires only initiation of power. Full capability to reconfigure system in the field is facilitated by simple operator response to English-language prompts via keyboard.

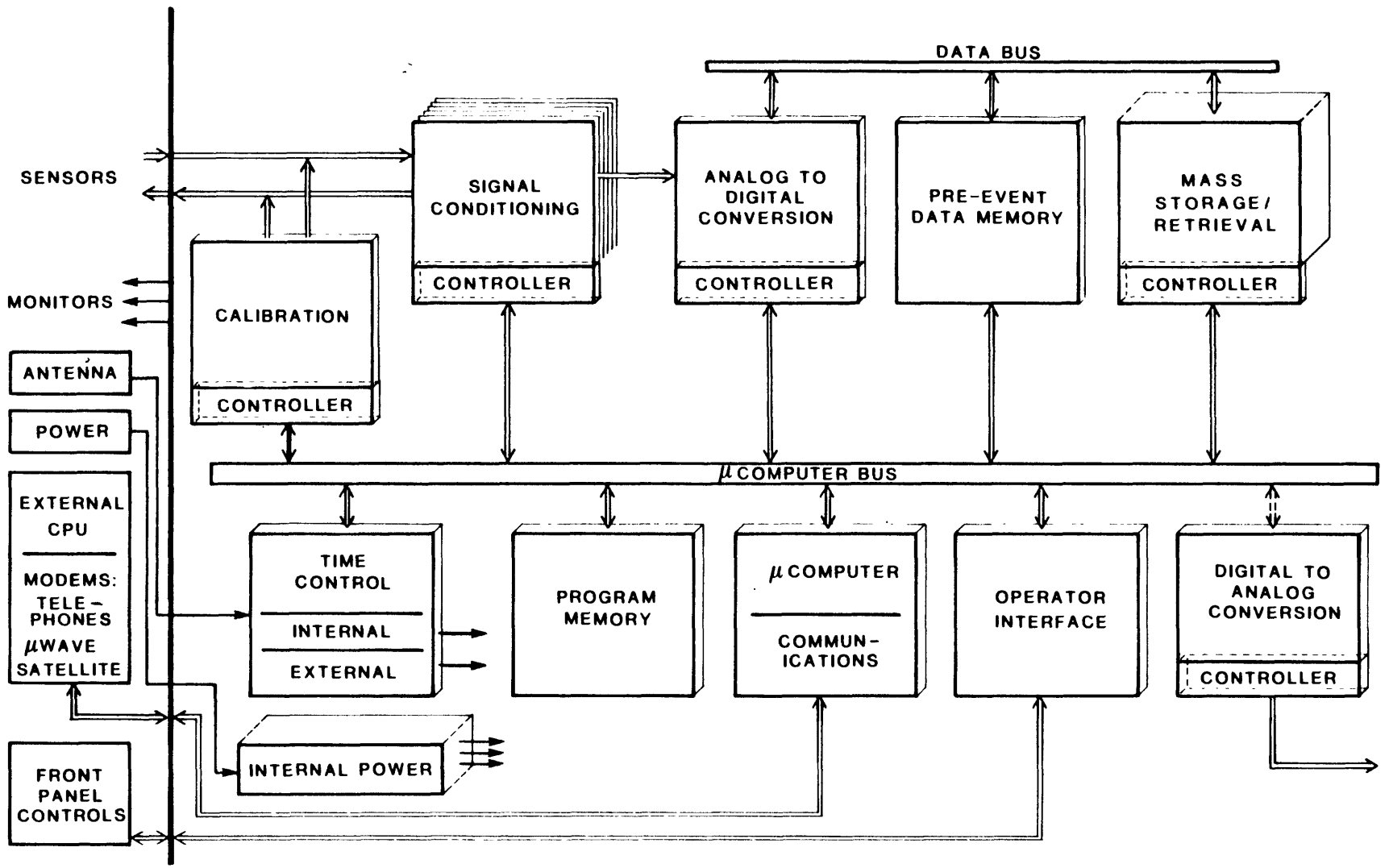

Figure 2. General system configuration for the GEOS, showing required system functions isolated on separate hardware modules. Central CPU control of each module via general computer bus permits full capability to configure system for most field applications and facilitates incorporation of improvements in technology.

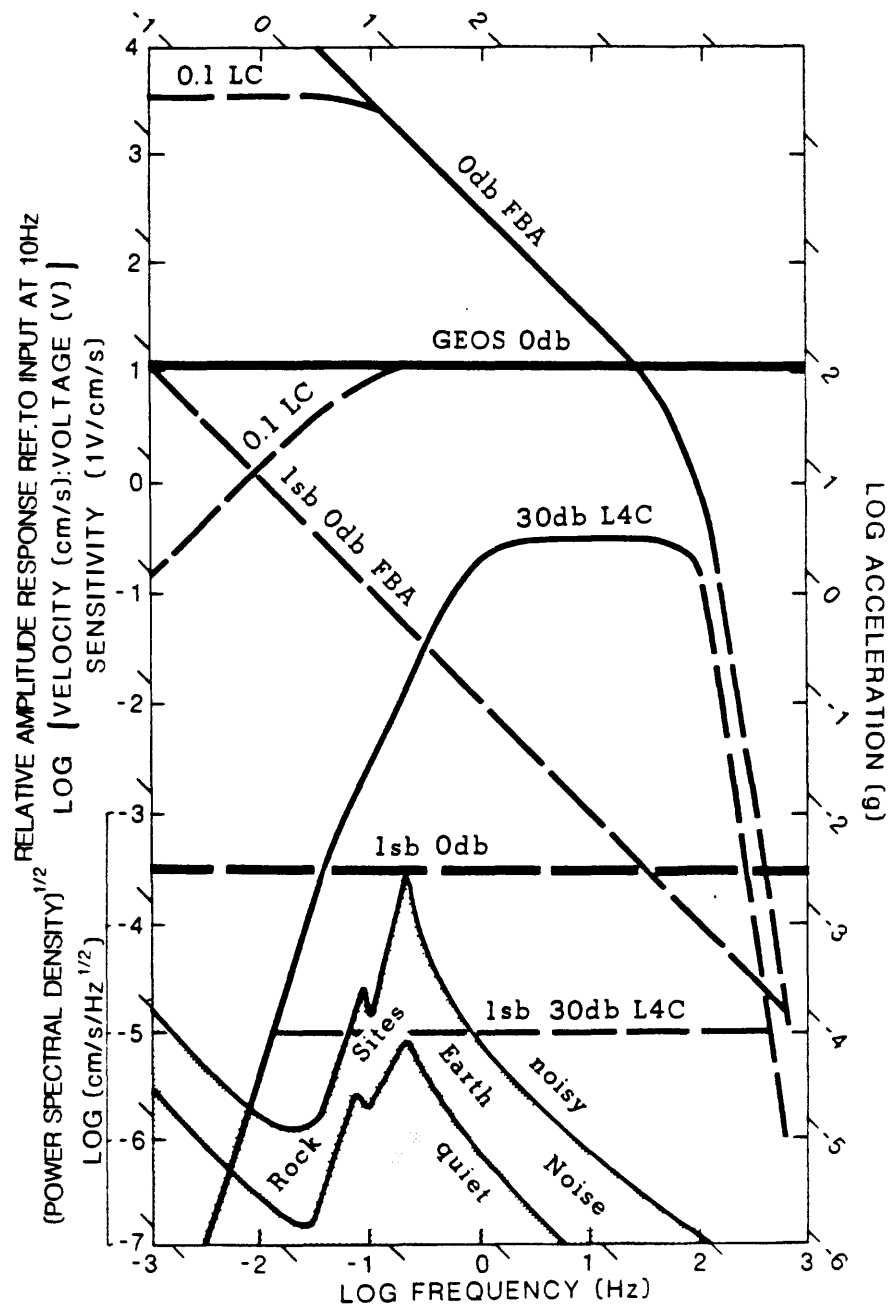

Figure 3. Unit-impulse response designed for the GEOS recorder, spectra for Earth noise [Aki, K., and Richards, 1980], and complete system response with two types of sensors (force balanced accelerometer at 0-dB gain and L4-C velocity transducer at 30-dB gain). Two sets of sensors and linear dynamic range of 96 dB (16 bit) offer capability to record without gain change 10-Hz signals on scale, with amplitudes ranging from 2 nm in displacement to 2 g in acceleration.

FIELD EXPERIMENT LAYOUT, SITE SELECTION, AND FIELD PLAYBACK

M. Celebi, E. Sembera, C. Dietel, L.F. Baeza

Deployment of the previously-described instruments at particular stations required consideration of:

- o Fulfillment of the objectives of the particular experiment;
- o Accessibility to the particular site;
- o Safety of the instruments;
- o Optimizing the set of data which could be obtained with the limited number of recording units available.

The two experiments constituting the subject matter of this report will be described as the Canal Beagle and Viña experiments, and will be presented in that order.

DEPLOYMENT OF INSTRUMENTS FOR CANAL BEAGLE EXPERIMENT

The main objective of the Canal Beagle experiment was to investigate possible a) geological, and b) topographical amplification. To achieve this, a network of stations was established at this particular subdivision of Viña del Mar. General location of these stations and topography can be seen in Figures 1 and 2. Specific descriptions of these stations are provided in Table 1. Descriptive photos related to the Canal Beagle are referenced in Table 1.

REFERENCE STATIONS

These experiments were performed by establishing stations in accordance with the described objectives. Throughout the whole duration of field work, a reference station (VAL) was maintained at the University of Santa Maria in Valparaiso. The location of this reference station is the same as one of the strong motion stations of the Chilean strong-motion network. The reason why this station was chosen as the reference station is two-fold:

- o Its geological feature (amphibolite and granite gneisses) which makes it the only rock site in close proximity to Viña del Mar.
- o To provide data to correlate with the strong motion records of the main event.

However, another reference station was established in downtown Viña del Mar at the basement of the Municipality Building (an alluvial site). The main reason for this choice was that it was impossible to occupy the same location as that

of the strong motion instrument site in Viña del Mar (also in the basement of a building) because of a continuously running motor pump which could have contaminated the low level motions at this site. However, the new station (MUN) was only one block from the actual strong motion station.

TABLE 1
Canal Beagle Experiment Stations
(General Layout Seen In Figures 1 and 2)

Station	Description	Reference Figure
Site Stations:		
CBA	At ground floor (no basement) of Type B* structure founded on a clear cut at canyon between two ridges. The structure and its twin next to it were not damaged. Geologic formation: sedimentary. (Building #1)	1, 2, 3-5
CBB	At ground floor of a Type B* structure on top of ridge where there is extensive damage. Geologic formation: Sedimentary and decomposed granite. (Building #7)	1, 2, 5, 11
CBC	(Same as above, CBB.) (Building #12)	1, 2, 6-8
CBD	At ground floor of a Type A* (single story) structure. This part of Canal Beagle is on the main body of the hill crowned by the ridges. (699 Ventisquero Street - at corner of Canal Kivke Street)	1, 2, 9
CBE	At ground floor (no basement) of Type C* (all 5 stories) structure located on top of emerging portion of the ridge. (Building #4 - Edificio Thomson)	1, 2, 13
CBF	At ground floor (no basement) of Type C* (all 5 stories) structure located at the top of the ridge. (Building #15 - Edificio Hyatt)	1, 2, 10, 12, 13
CBG	On a concrete floor of a single story structure located in the canyon between the two ridges. The structure is not part of Canal Beagle subdivision.	1, 2, 14
Reference Stations:		
VAL	On a concrete pedestal at the University of Santa Maria. Same location as the SMA station of the Chilean strong motion network. The site is amphibolite and granite gneiss formation.	15, 16
MUN	At basement of 2 story reinforced concrete structure on 615 Arlegui Street in Viña del Mar. The building is on alluvial ground and one block from the SMA station of the Chilean strong motion network.	17

* There are three types of structures in Canal Beagle. Type A structures are single and two-story buildings on top of the hill, whereas Type B structures are four-story buildings on one ridge and Type C structures are five-story buildings on another ridge. Two of the Type B structures are in a canyon at the entrance to the subdivision.

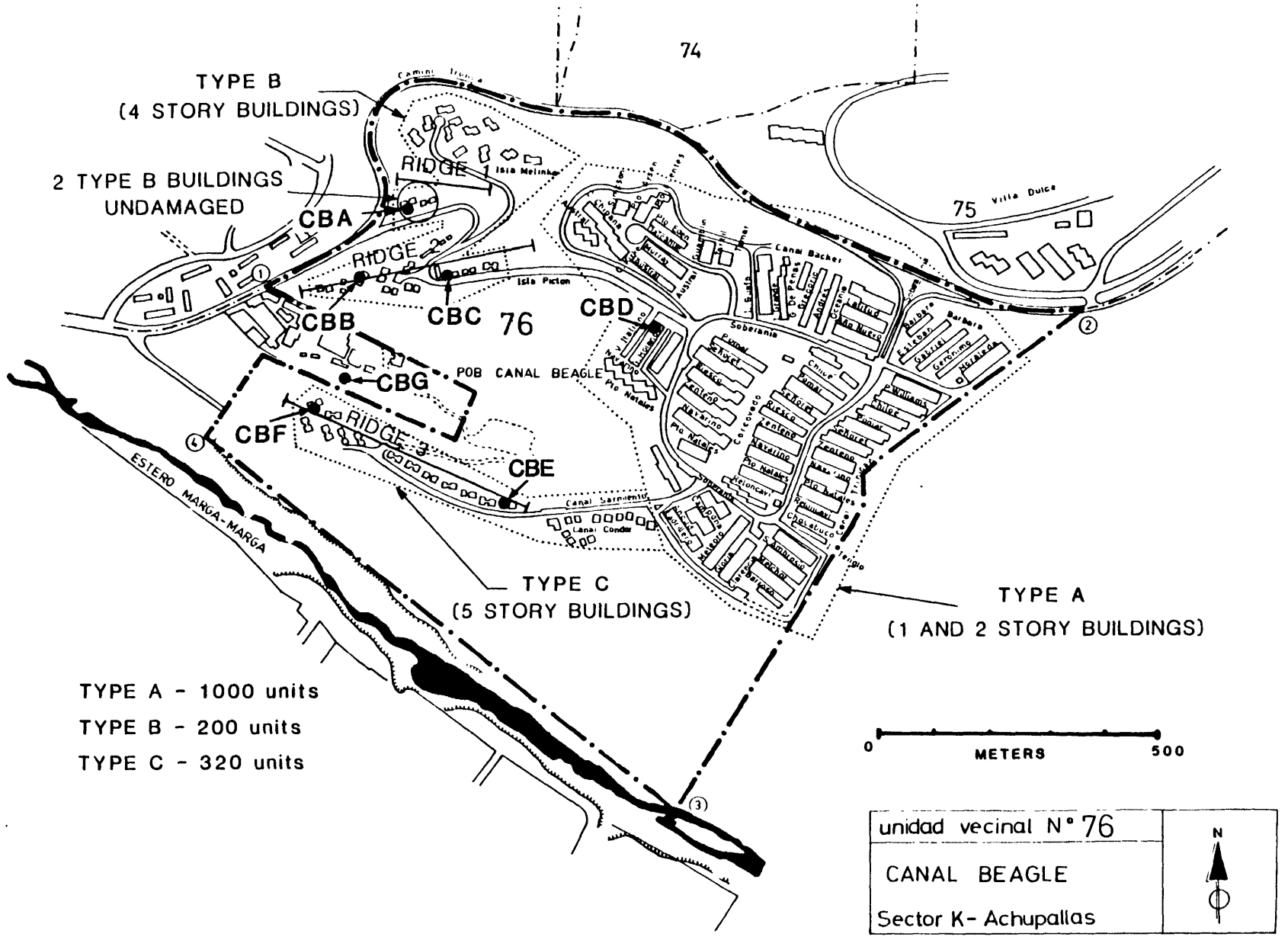

Figure 1. General layout of Canal Beagle subdivision. The three ridges crowning the main hilltop (where Type A buildings are located) are indicated. Damaged four story (Type B) and five story (Type C) buildings are located on ridges 2 and 3, respectively.

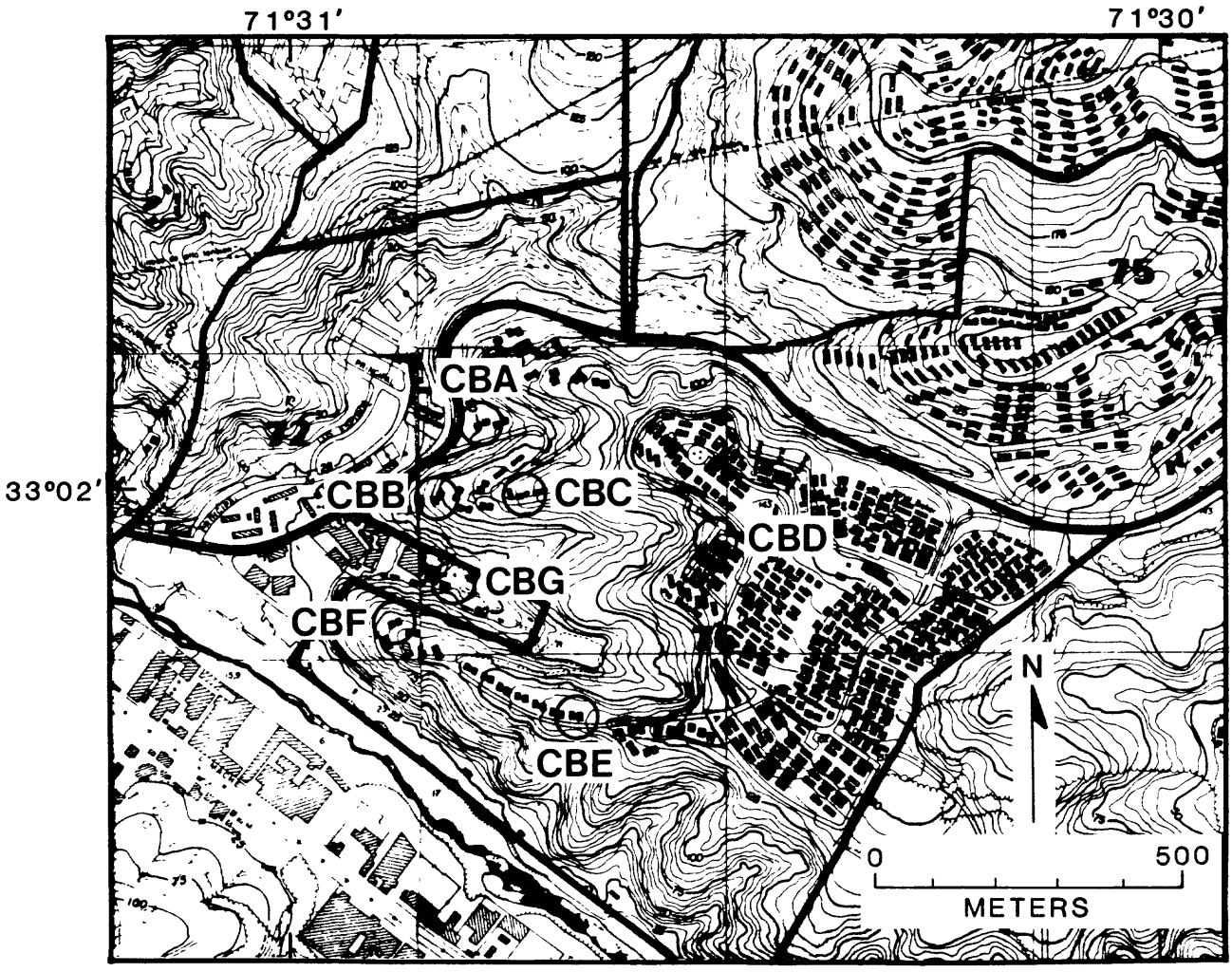

Figure 2. Detailed topography of Canal Beagle. The stations of the Canal Beagle site are indicated. Also a general scale and the latitudes and longitudes are shown.

Figure 3. Type B structure (no damage) at Canal Beagle where station CBA was sited. The structure is at the entrance to the Canal Beagle subdivision and is located in a canyon between two ridges.

Figure 4. Cut behind the two undamaged Type B buildings in the canyon at the entrance to Canal Beagle.

Figure 5. Type B structure (heavily damaged) on top of one of the ridges where station CBB was sited. A recent cut on the hillside displays the general status of the geological formation--alluvial conglomerates.

Figure 6. Type B buildings on the slopes of one of the ridges at Canal Beagle. The first building is the site of station CBC.

Figure 7. Site of station CBC. Note the extensive damage to the concrete walls and infill brick walls.

Figure 8. Close-up of damage to the Type B buildings (site of station CBC).

Figure 9. Site of station CBD - Type A building on top of the hill crowned by the ridges. There were no damages to this building or other Type A buildings.

Figure 10. Typical Type C buildings (5 stories) all extensively damaged.

Figure 11. Type B buildings on top of the ridge. General view of the ridges is seen here.

Figure 12. Type C buildng on top of the ridge. Station CBF was sited on the ground floor of the building. A general view of the ridge is also seen in the figure.

Figure 13. Panoramic view of Type C buildings (all five stories) on top of one of the ridges at Canal Beagle. All buildings are severely damaged. Note the steep slopes.

Figure 14. Locations of station CBG - in a canyon between two ridges. On top of the ridge, Type C buildings are seen.

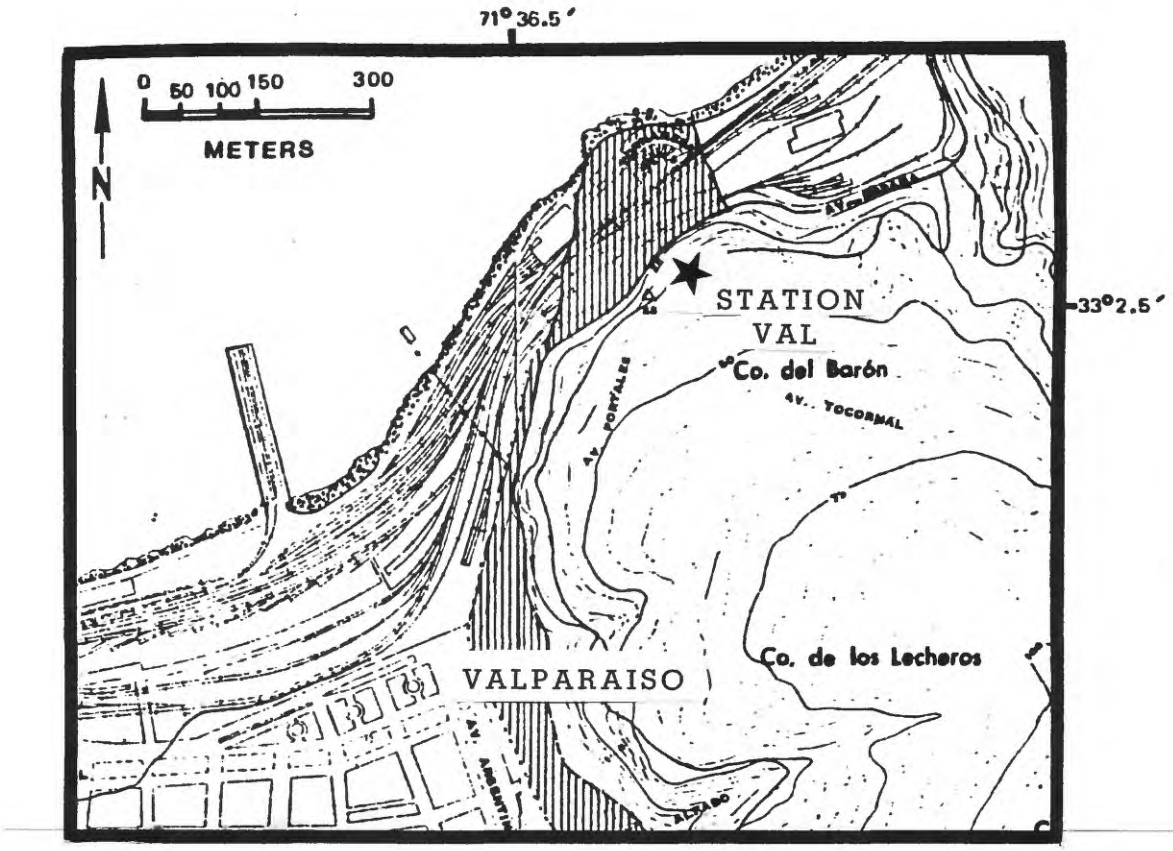

Figure 15. Location of reference station VAL--a granite and amphiobolite gneiss site (Figure adopted from Algermissen, 1985).

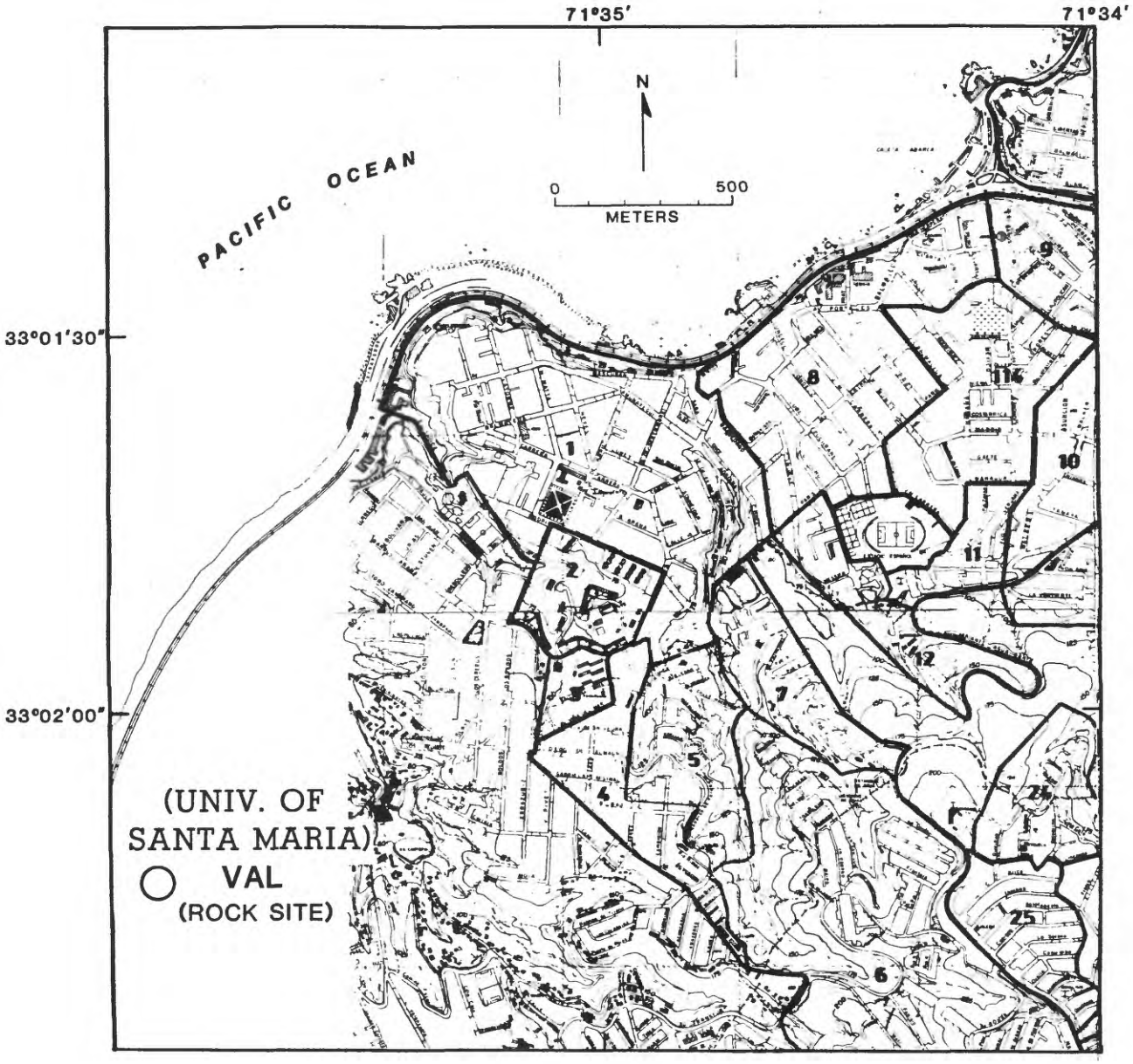

Figure 16. Location of reference station VAL.

Figure 17. Reference station VAL located at a vault within the University of Santa Maria (Valparaiso) Campus. This is the same location as the SMA station of the Chilean Strong Motion Accelerograph Network.

Figure 18. Reference station MUN at the basement of the Municipality Building in Viña del Mar. The building is found on alluvial deposits.

DEPLOYMENT OF INSTRUMENTS FOR "VIÑA" EXPERIMENT

The selection of specific sites for site response studies in Viña del Mar was greatly facilitated by the use of preliminary damage concentration maps compiled by the Municipality (Balbontin and others, 1985). Based on these maps, various stations were established on sandy, alluvial, and granitic sites. The reference station, VAL, established at the beginning of the previous experiment at Canal Beagle was kept as such (Figures 15-17). The locations of the stations in Viña del Mar and Renecá are depicted in Figures 19-21. For security reasons and protection against weather conditions, the instruments were located at basements or ground floors of structures.

The sand sites consisted of the ocean front areas where Edificio Acapulco and Edificio H'Angoroa (the two taller strutures that were severely damaged during the main event) (Wyllie, and others, 1985 and Celebi, 1985) as well as Edificio de Miramar (one of the undamaged four 22 story reinforced concrete structures with triangular shape in plan) are located. Stations EAC, HAN, and TRA were sited in the basements of Edificios Acapulco, H'Angoroa, and de Miramar, respectively. In addition, another site was occupied near the site of Edificio El Faro (the eight-story building in Renecá that tilted and was later dynamited).

The alluvial sites were the Municipality Building (MUN), Edificio Libertidad de Chile (ELC), Edificio Emparté (FMP) and the Church Building (CHU). The firmer decomposed granite and granite sites were one of the four towers of the Quinto Claude Complex (22 stories, block 2) (QCL), the Sietes Hermanas (HER) and Santa Ynez (YNE) (2075 at 24 Norte).

More detailed particulars of all stations in the Viña experiment are summarized in Table 2 along with reference figures.

STATION SCHEDULING, INSTRUMENT POSITIONING AND ADJUSTMENTS AND FIELD PLAYBACK

In general, instruments at established stations were relocated to other locations (new stations) only after making sure that a sufficient number of events were recorded at several of the stations. Thus, comparisons of motions (or transfer functions) at one station with respect to another could be made. However, in a couple of cases (*e.g.*, station CBG at Canal Beagle), the instruments were relocated even though no events were recorded to provide qualita-

tive comparison. In certain situations the instruments were relocated even though no events were recorded and results from another similar station (station CBA) could be used. A general schedule of the location of GEOS recording systems is shown in Table 3. General views of the instruments used (GEOS recorder, batteries, and transducers) are seen in Figure 29.

The velocity and acceleration sensors were always leveled. The horizontal components were aligned to true north direction using a compass.

Instrument gains were set generally at 36 dB for velocity sensors with the expectation of recording aftershocks in the magnitude 3 to 5 range. Gains for acceleration sensors were set generally at 12 dB for possible aftershocks greater than magnitude 5. These gains proved to be suitable after examination of the initial aftershock data on the GEOS analog playback oscillograph utilized in conjunction with a visicorder. In many instances, the events played back on the visicorder showed the amplification expected between the accelerograms obtained from different stations.

REFERENCES

Balbontin, H., and others, 1985, Daños Viviendas Sismo 1985, Direccion de Planificacion y Asesoria Urbana, Municipalidad Viña del Mar.

Celebi, M., 1985, Preliminary field trip report on Chile Earthquake of March 3, 1985: *Report to Earthquake Engineering Research Institute* (April 1985).

Wyllie, L., and others, 1985, Chile Report (to be published by *Earthquake Engineering Research Institute).*

TABLE 2
VIÑA EXPERIMENT STATIONS
(General Layout Seen in Figures 19 and 20)

Station	Description	Reference Figure
Sand Site Stations on Level Ground:		
EAC	At the lower level of the two-level basement of the 15 story reinforced concrete shear wall building whose plan is "fishbone shaped" (Edificio Acapulco). The structure was severely damaged during the main event. The building sits on the sand beach of Avenue San Martin.	19, 21, 22
HAN	At the lower level of the two-level basement of the 15 story reinforced concrete shear wall structure (Edificio H'Angoroa), severely damaged during the main event. The building is next to Edificio Acapulco on the sand beach of Avenue San Martin.	19, 21, 23
TRA	At the lower level of the two-level basement (garage) of the 21 story (not including basements) reinforced concrete structure (Edificio de Miramar) which was not structurally damaged during the main event. The building is one of 4 similar structures alongside Avenue San Martin. (Four more stations were located in this building as part of other experiments to be reported separately.)	19, 24
REN	This site was specifically chosen to study site response on the sandy hills of Reneca´. The specific station chosen on the ground floor of a single story building was in the immediate vicinity of Edificio El Faro which was severely damaged and tilted during the main event and as a consequence was later dynamited.	20, 25
Alluvial Stations on Level Ground:		
MUN	Same as previous experiment (See Table 1).	18, 19
ELC	Edificio Libertido Centro. (at 570 Libertido Street), 14 stories including 1 floor of basement. A reinforced concrete frame structure, suffering very minor damage during the main event. The location is on alluvial ground.	19, 26

TABLE 2 (Continued)
VIÑA EXPERIMENT STATION

Station	Description	Reference Figure
EMP	Edificio Emparte´ on 15 Norte Street. Block C4 of 19 similar social housing apartments. 5 story reinforced concrete framed building. The building is on level alluvial ground. Four of the 19 buildings were damaged.	19, 27
CHU	Espiritu Santo Church at the intersection of Llay Llay and Caucha Streets. Masonry structure on alluvial site. Severely damaged. Buildings around this church including a children's hospital (Hospital de Niños) also damaged.	19, 28
Rock Sites on Hills:		
QCL	Block 2 of the 22 story (plus two story basement) Quinta Claude structure (reinforced concrete frame with core shear wall). These structures were built on granitic rock and suffered negligible damage.	19, 29
HER	In the basement of one of the Sietes Hermanas Buildings (4-10 stories) which suffered minor structural damage during the main event. Most of the external stairways giving access to the structures from the exterior or access between buildings were damaged. The site is decomposed granite on a hill.	19, 30
YNE	One of two 5 story reinforced concrete framed structures (with brick infill walls) located on hill at 24 Norte Street off Avenue Santa Ynes. Minor damage during the main event. Instrument located in basement. The site is granite or decomposed granite.	19, 31
Reference Rock Site:		
VAL	Same as Table 1.	15-17

TABLE 3

RECORDER DEPLOYMENT SCHEDULE AT STATIONS

(Date and Stations-Installation Times (GMT) of some stations are indicated)

Recording Unit	7/27/85 Julian: 208	7/28/85 209	7/29/85 210	7/30/85 211	7/31/85 212	8/1/85 213	8/2/85 214	8/3/85 215	8/4/85 216	8/5/85 217	8/6/85 218	8/7/85 219	8/8/85 220
GEOS 19	(VAL) 14:03 GMT	(this station was operated continuously) ————											)+
GEOS 17	(MUN) 14:40 GMT					(HAN) 20:20:03	(REN)			(TRD)			)+ Santiago
GEOS 23	(CBA) 17:22 GMT				(EMP) 15:48 GMT					(TRB)			)+ Santiago
GEOS 3	(CBB) 18:30 GMT				(HER) 16:50 GMT				(MUN) 15:56	————			)+
GEOS 13		(CBC) 18:48 GMT		(ELC) 21:19						(TRC)			)+ Santiago
GEOS 15		(CBD) 19:14 GMT		(QCL) (21:00 GMT)					(CHU)	To Cartegena			)+
GEOS 12		(CBE) 19:43 GMT		(EAC) 21:39						(TRE)			)+ Santiago
GEOS 25		(CBF)		(CBG) 17:30 GMT	(YNE) 20:11 GMT				(TRA)				)+ Santiago

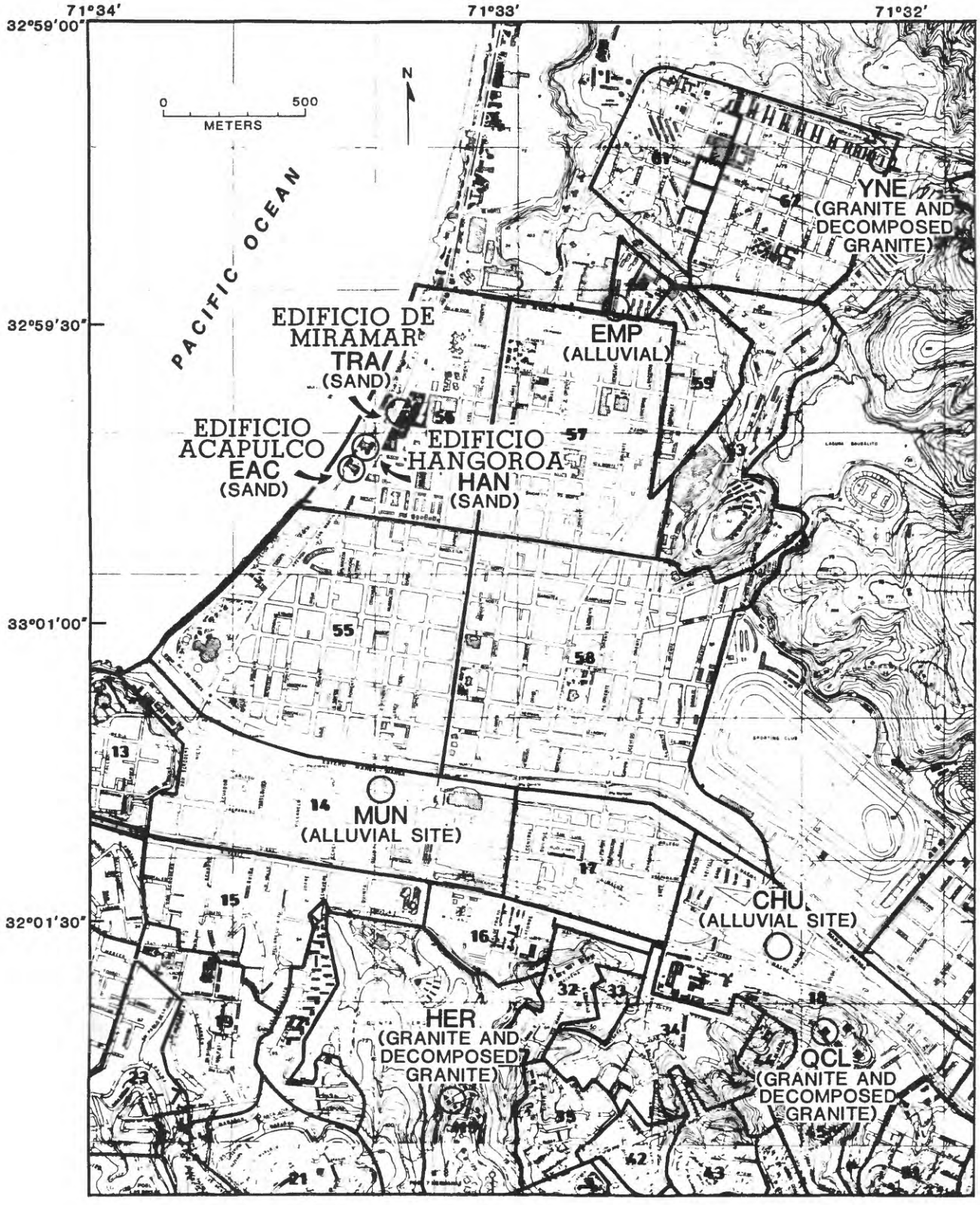

Figure 19. Location of stations in Viña del Mar.

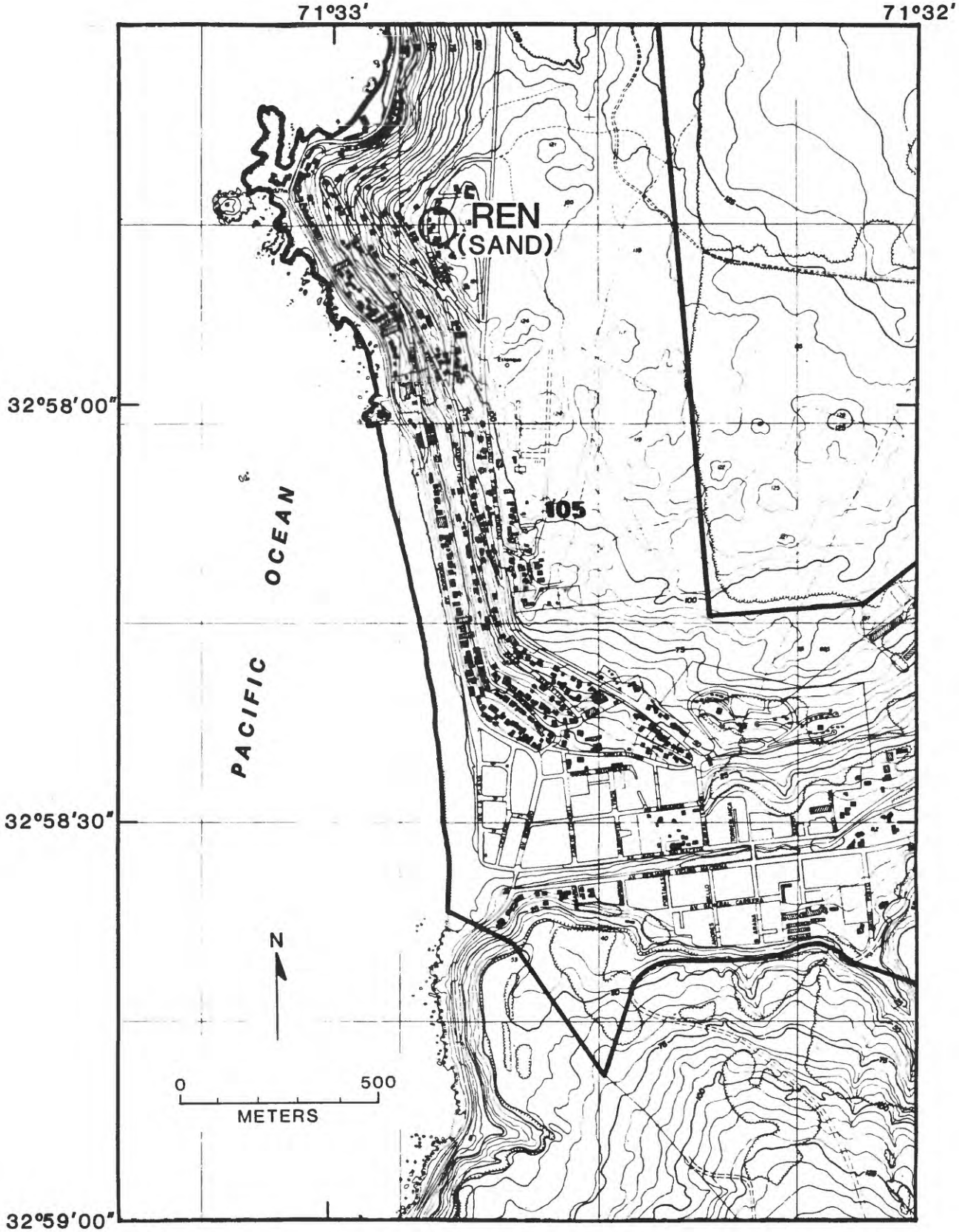

Figure 20. Location of station REN in Reneca. Latitudes and longitudes, as well as a general scale is shown.

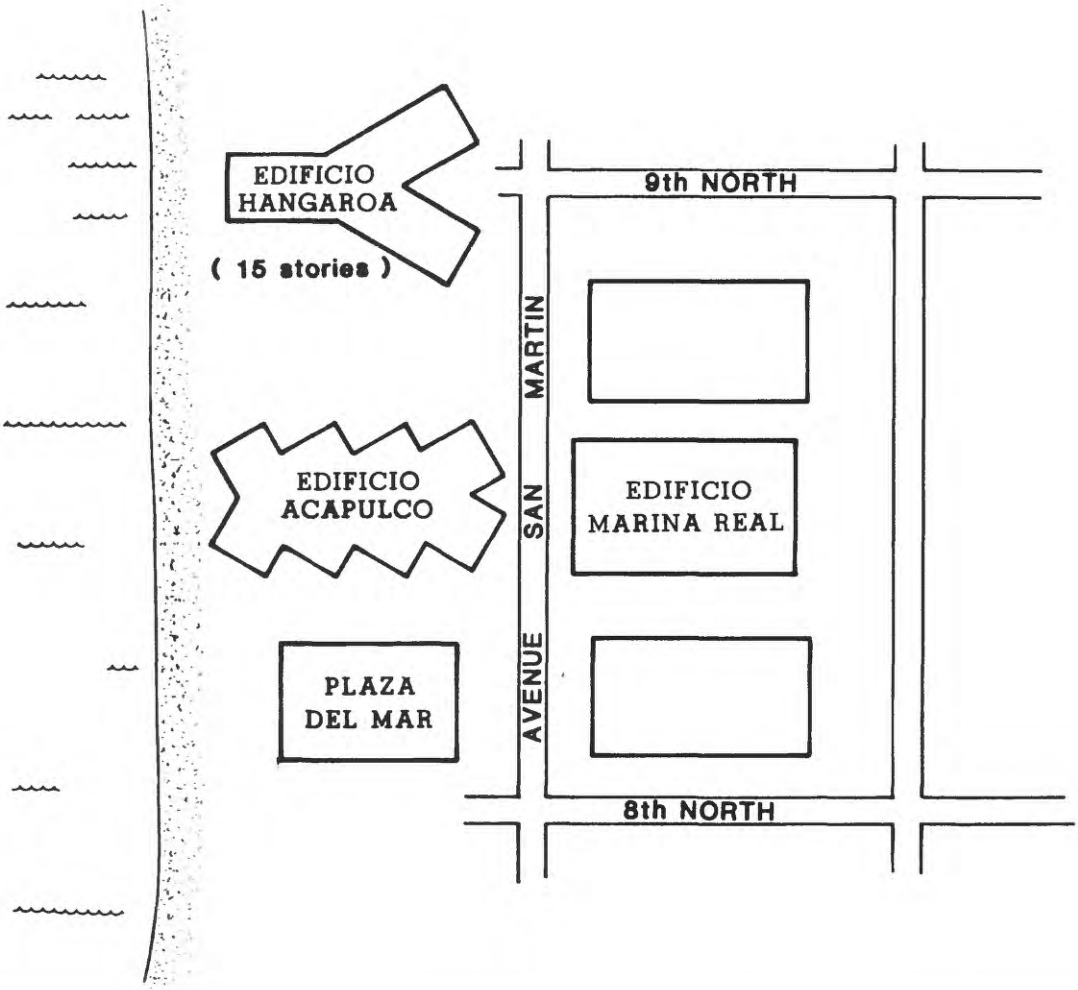

Figure 21. Locations of Edificio Acapulco and Edificio H'Angaroa severely damaged modern engineered buildings, on Avenue San Martin.

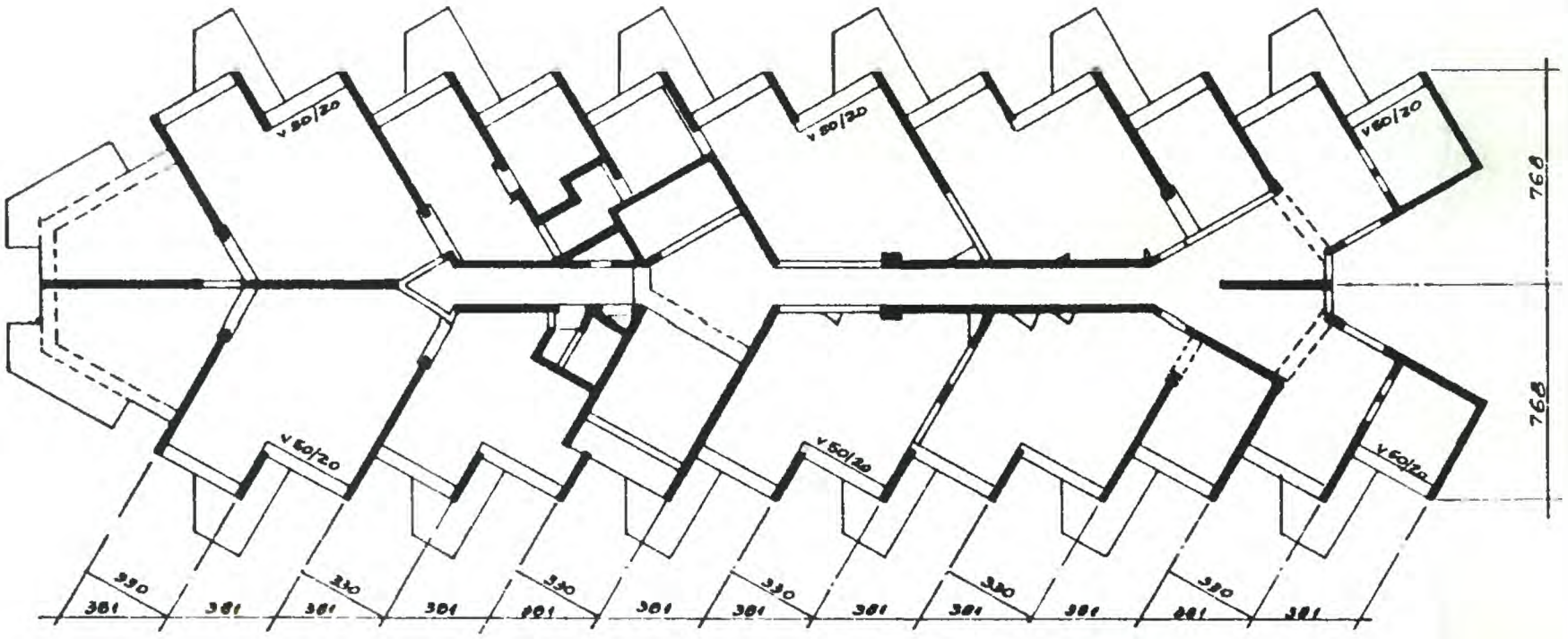

NOTAS: - ESTA PLANTA ES VÁLIDA PARA 2°, 3°, 4°, 5° y 6° PISOS
- MUROS ESPESOR = 20 cm
- LOSAS ESPESOR = 12 cm

PLAN VIEW

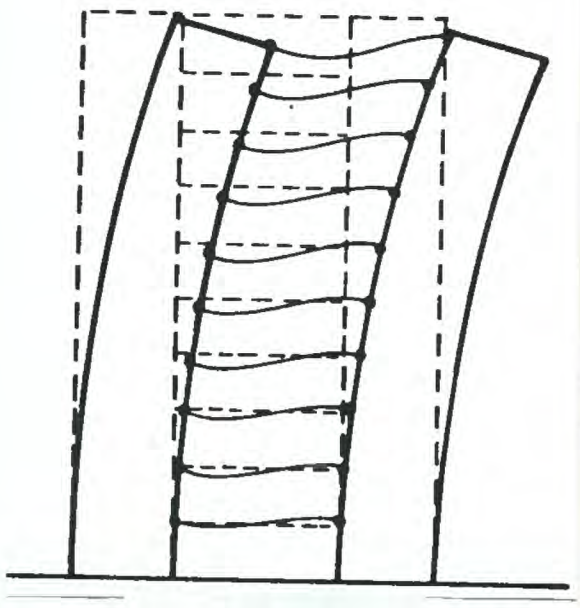

BEHAVIOUR

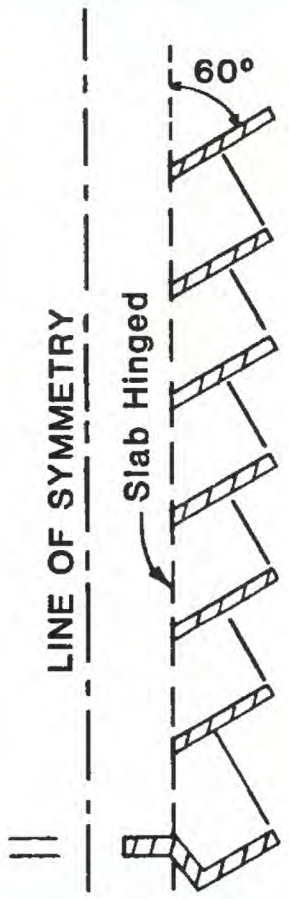

DAMAGE PATTERN

Figure 22. Plan view, qualitative damage pattern and view of the extensive damage to the exterior shear wall of Edificio Acapulco--station EAC. (Plan view of the building is provided by Prof. P. Bonelli).

EDIFICIO HANGAROA

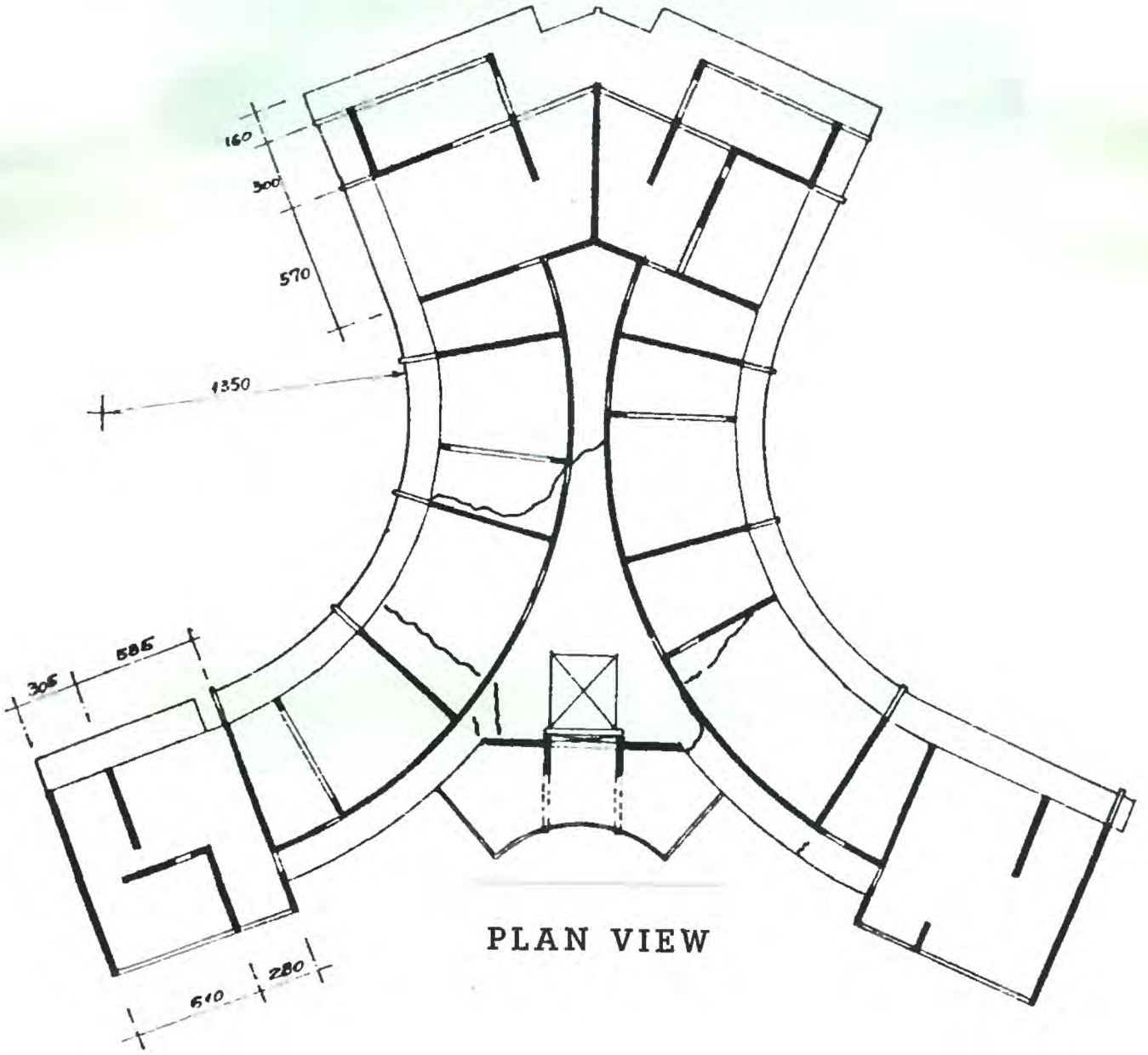

PLAN VIEW

Figure 23. Plan view, qualitative damage pattern and general view of Edificio H'Angoroa--station HAN. The slabs and shear walls cracked extensively from top to ground floor. (Plan view of the building provided by Prof. P. Bonelli).

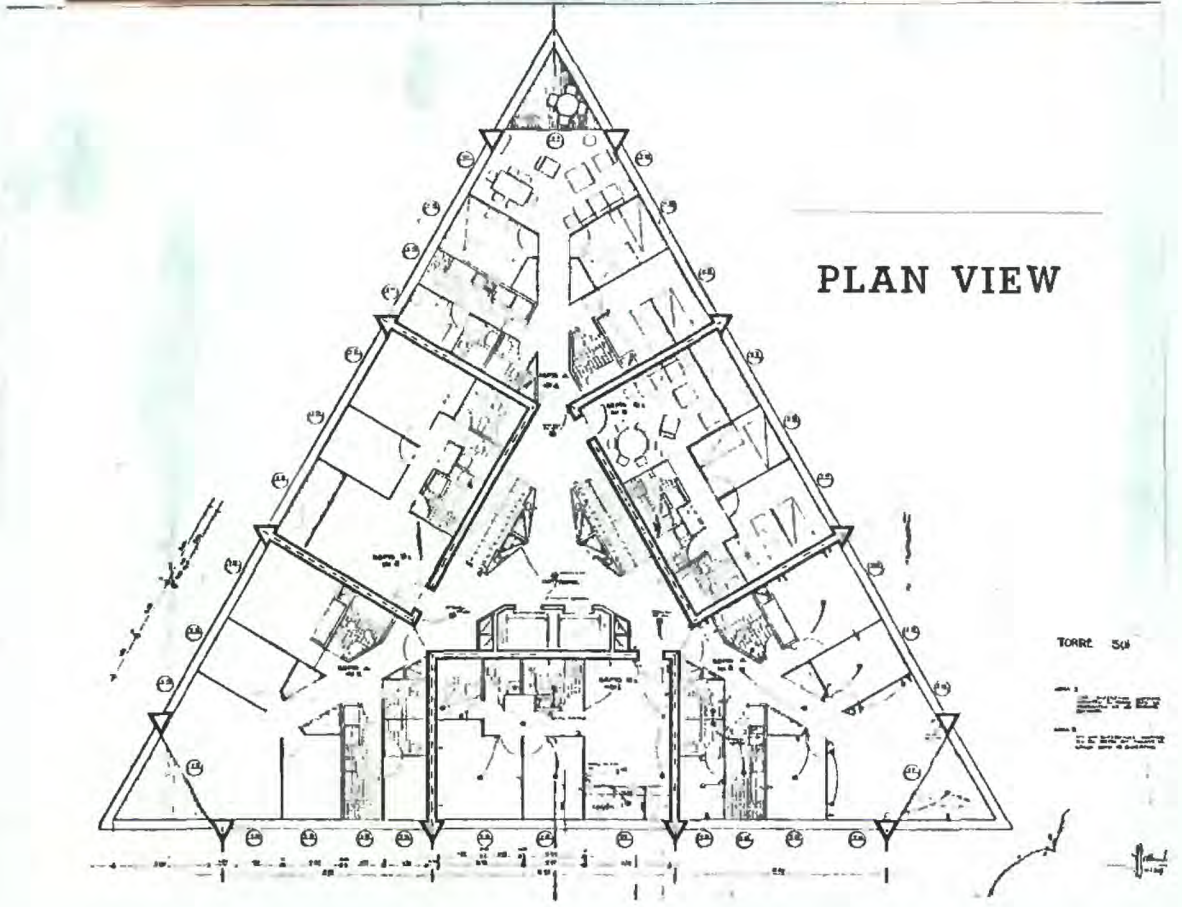

Figure 24. General and plan views of Edificio de Miramar, one of the several twenty-two story buildings that survived the main event without damage.

EDIFICIO EL FARO

Figure 25. General view of Edificio El Faro (on sand dune hills of Renecá) after the main event. The building was later dynamited. Station REN was sited on ground floor of a single story building immediately adjacent to Edificio El Faro.

Figure 26. General view of Edificio Libertidad de Chile (Station ELC).

Figure 27. Edifico Emparte (Station EMP)--one of nine similar buildings that suffered moderate damage during the main event.

Figure 28. Church building on the left (station CHU), Hospital de Niños next to it (on the right top) and single story masonry structures in the same vicinity (on the right bottom). All these structures were moderately damaged during the main event.

Figure 29. Two of the four twenty-two story reinforced concrete Quinte Claude buildings with shear walls (station QCL was sited at the basement of block 2 at the right). These buildings, situated on decomposed granite hills, suffered no damage.

Figure 30. Two of the several reinforced concrete shear wall Sietes Hermanos buildings situated on decomposed granite hills. Station HER was sited in the basement of one of these buildings. During the main event, the sky-walkways and stairs suffered extensively.

Figure 31. One of the two buildings on decomposed granite hills of Avenue Ste. Ynez. Station YNE was located in the basement of this building (minor damage during main event).

Figure 32. General view of GEOS recorder, batteries and sensors at a particular site and check being performed to determine whether events have been recorded.

DATA PROCESSING AND CALCULATION OF SPECTRAL RATIOS

by

John C. Watson and Charles S. Mueller

This section constitutes a description of the procedures used for processing the extensive set of digital strong motion recordings obtained from aftershocks following the May 3, 1985 Chile earthquake (M_S=7.8). Two overlapping studies conducted during late July and early August of 1985 resulted in 40 DC300XL data cartridges from 18 stations recorded on wide dynamic range GEOS instruments (Borcherdt and others, 1984). Each GEOS operated in trigger mode, simultaneously recording six channels of ground motion at 200 samples-per-second-per-channel; namely, three-components of ground acceleration (Kinemetrics FBA-13 force balance accelerometer) and three components of velocity (Mark Products L-22 geophone). The FBA's were recorded at relatively low gain in order to obtain unclipped recordings of large ground motions while the geophones were recorded at higher gain. The combination allowed high signal-to-noise recordings over a range of ground motion amplitude to be obtained. No clipped records were observed. Each GEOS clock was set once at installation using a portable master clock; therafter clock corrections were obtained approximately once every twenty-four hours when the sites were visited for tape changes. Other GEOS parameters are described elsewhere in this report.

Data cartridges were returned to Menlo Park for processing. During playback, the computer directory structure (and the subsequent magtape archival structure) was organized by increasing trigger-time. Data cartridges were played-back with a Tandberg TDC3000 digital cartridge recorder onto a PDP11/70 minicomputer. The software interface is the FORTRAN program RDGEOS written by Gary Maxwell of the USGS, Menlo Park. The data were demultiplexed and stored, one trace per file, in blocked binary format. Each file name consists of 13 characters following the USGS Branch of Engineering Seismology and Geology filename convention:

character 1-3 — Julian day
character 4-5 -- hour
character 6-7 — minute
character 8 -- seconds (A = 0-3, B = 3-6, C = 6-9,..., T = 57-60)
character 9 — motion (1-3 = acceleration, 4-6 = velocity)
character 10 -- period (.)
character 11-13 -- station-instrument identifier.

Each file consists of two header blocks which contain relevent field and playback parameters followed by data blocks.

Figures 1 and 2 are plots of all trigger times versus Julian day for the Canal Beagle and Viña del Mar studies, respectively. With the files on disk two archival tapes were made and all seismograms were plotted for preliminary seismic interpretation. The data set was then winnowed so that single-station triggers were excluded. Considering the overall network configuration, a twenty second sliding window was chosen in order to select common-event triggers. The winnowed data set was then copied to the VAX-11/750 minicomputer for more detailed seismic analysis. Tables 1 and 2 list aftershocks recorded at two or more stations for the Canal Beagle and Viña del Mar studies, respectively. The three-letter station-instrument codes appear in the first row and the origin times of events appear in the first column. If a station recorded an event, character 8 of the filename (the trigger-time seconds character, a useful file identifier) appears in the table. Of 355 triggers from nine stations during the Canal Beagle study (including stations VAL and MUN, which are common to both studies), 29 were earthquakes recorded at two or more stations, 11 at four or more stations, and six events at six or more stations. Of 491 triggers recorded from 11 stations during the Viña del Mar study (including stations VAL and MUN) 27 were earthquakes recorded at two or more stations, seven at four or more stations, and two at six or more stations.

Plots of vertical and horizontal (N-S and E-W) components of velocity for all events recorded at two or more stations were made. Velocity records generally provide better results; therefore, only velocity seismograms are plotted herein (acceleration time histories are currently being studied and processed by the editor of this report). These plots of velocity seismograms and related spectra are provided in Appendices A and B for the Canal Beagle and Viña experiments, respectively. Indexing of events, and descriptions of the plots are also provided in these Appendices. In the plots, a positive amplitude for the vertical ground motion corresponds to upward motion, and for the horizontal ground motions, positive amplitudes correspond to northward and eastward motions for the N-S (H=0) and E-W (H=90) directions, respectively.

In order to characterize the site-dependence of ground motion in the Canal Beagle and Viña experiments, spectra and spectral ratios were calculated from whole-record waveforms. For recordings made at closely-spaced sites

(relative to the focal distance), spectral ratios tend to deemphasize common source and whole-path wave-propagation effects, and emphasize local wave-propagation differences. The experiments described in this report were so designed.

To calculate amplitude spectra, waveforms were windowed (to insure equal-length numerator and denominator and not to isolate phases), DC corrected, tapered (10% cosine front and back), padded with zeros to an integral power-of-2 number of points, and fast-Fourier transformed. Spectra were not corrected for instrument or anti-alias-filter response; these effects are assumed to be common to all instruments to the level of detail considered here and, therefore, to cancel in spectral ratios. Spectra were smoothed with a running triangle (width ~ 0.5 Hz) prior to obtaining ratios. All spectra are plotted up to 30 Hz and signal-to-noise is generally adequate in this band for the best recorded events (Figure 3).

Fourier amplitude spectra and spectral ratios accompanied by windowed time series are provided in Appendices A and B for the Canal Beagle and Viña experiments, respectively.

REFERENCE

Borcherdt, R.D., Fletcher, J.B., Jensen, E.G., Maxwell, G.L., Cranswick, E., VanSchaack, J.R., Warrick, R.E., 1984. A General Earthquake Observation System (GEOS), submitted to *Bulletin, Seismological Society of America*.

TABLE 1.—Events recorded on two or more stations (Canal Beagle Experiment)

WHERE OUTPUT, TBACK= 5.0, TAHEAD= 20.0. 2 RECORDS TO DECLARE AN EVENT.

	VAL	MUN	CBA	CBB	CBC	CBD	CBE	CBF	CBG
2090350A			A	A					
2091701R		D							
2091723G		G	I						
20918491		J			I				
2091915C		C				H			
2091919H		L				H			
2091921F		F				K			
2092020F	F	F							
2100011G	G			H			H	H	
21006525	S		S	S	S		S	S	
2100710G			G	G	G		G	G	
2100711H	H		I	I	I			I	
2101029N				N	N				
2101044E				E	E				
21014481	I			J				J	
2101536A	B				A			A	
2101609N	N		N	N	N		N	N	
2101816B	B		B	B	B		B	B	
2101919H	H			H	H		H	H	
2101926C	C				R			P	
2102023L	L			L					
2110059P	P		P	P	P		P	P	
2110337D	D			D	D			D	
2110602A					A			A	
2110933S	S	S	S	S	S	S	S	S	
2111026B			F	B					
2111208R	R	R	R	R	R	R	R	R	
2111221Q	Q				Q				
2111630M				S				M	

TABLE 2.—Events recorded on two or more stations (Viña Experiment)

WHERE OUTPUT, TBACK= 5.0, TAHEAD= 20.0. 2 RECORDS TO DECLARE AN EVENT.

	VAL	MUN	QCL	ELC	EAC	HAN	EMP	HER	YNE	REN	CHU	TRA
2091701R		D										
2092020F	F	F										
2110933S	S	S										
2111208R	R	R										
2121822L	L							L				
2130430P	P							P	P			
2130851S	A						S					
2131743M	M		M					M	M			
2140256D	D							D				
2141457M	M							M				
2141800J	J								J			
2150204N	N		S		O			N	N	N		
2150337K	K		K				K	K	K			
2160018M	M							M				
2160054H	I							J	H			
2160125Q	Q								Q			
2160336H				H						M		
2160447Q	Q							Q	Q	Q		
2160536L	N									L		
2160657J	L			J			J	J	J	J		
2161006F	F							G	F	F		
2161857F	F	G			G					G		G
2191002F	F	G										G
2191110K	K	L										L
22006060	C	P										
2220853E	E	E										
2231300L	L	L										

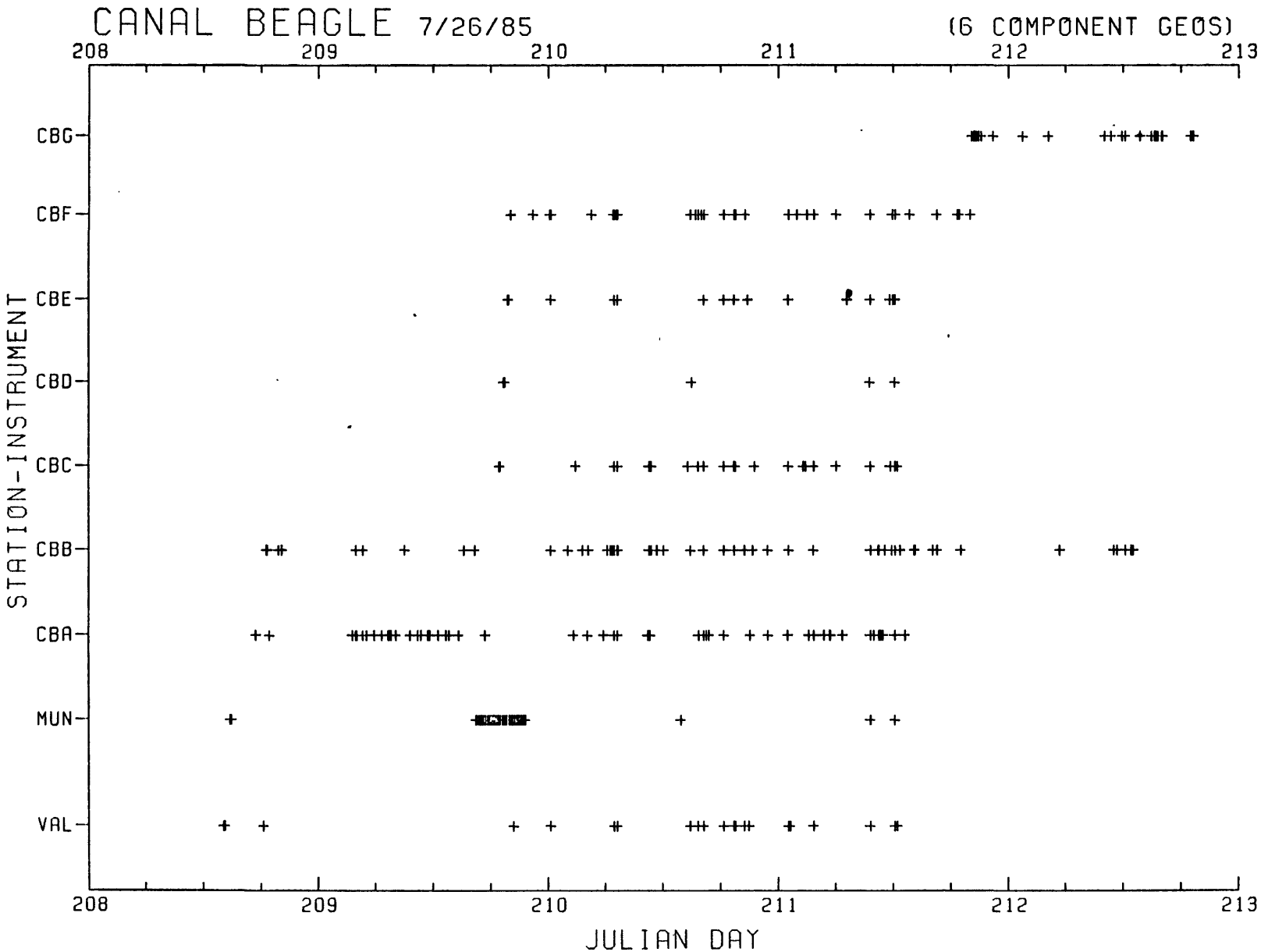

Figure 1. Recording vs. time plot (Canal Beagle Experiment). (Each "+" represents a trigger)

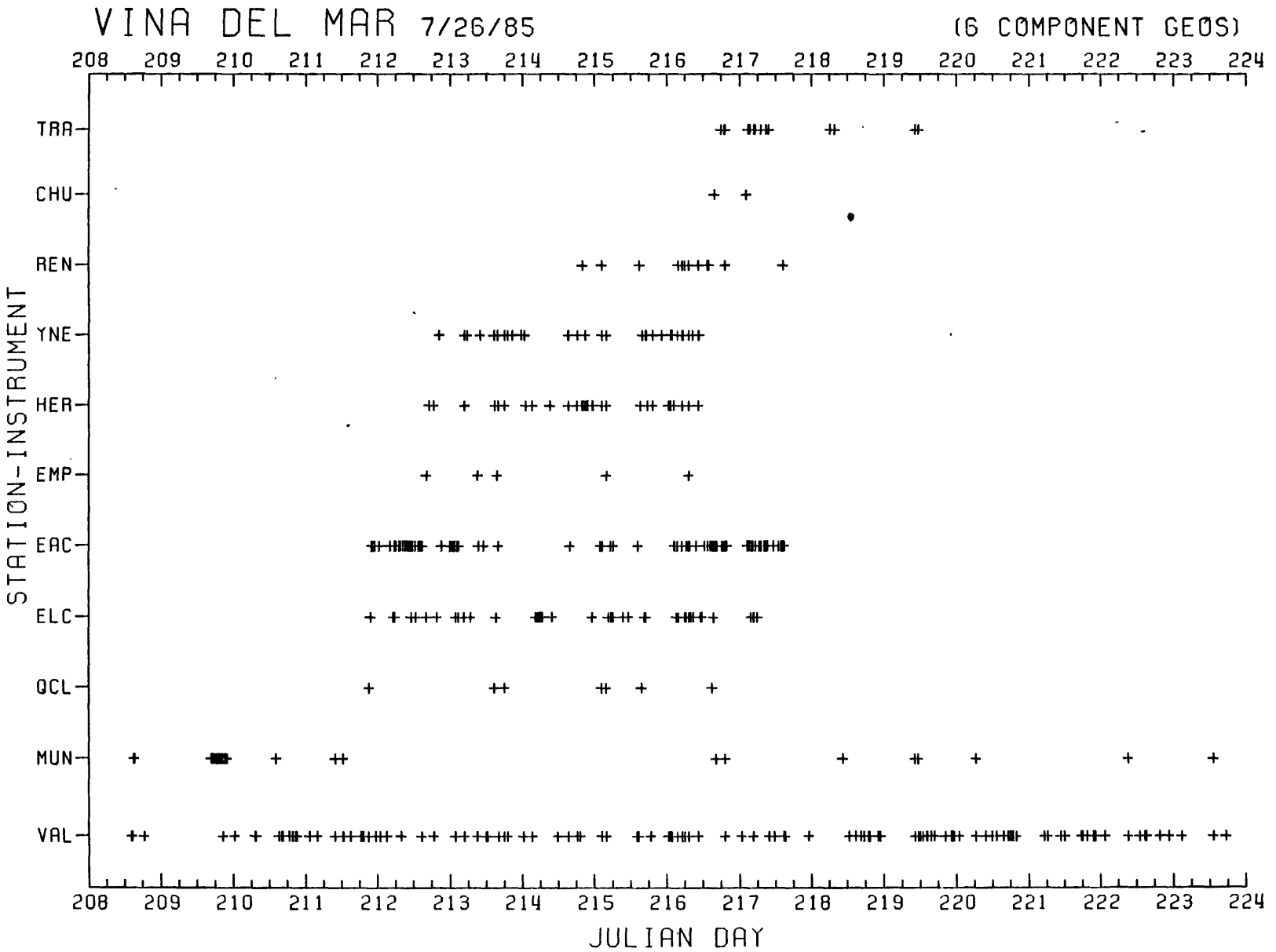

Figure 2. Recording vs. time plot (Viña Experiment) (Each "+" represents a trigger)

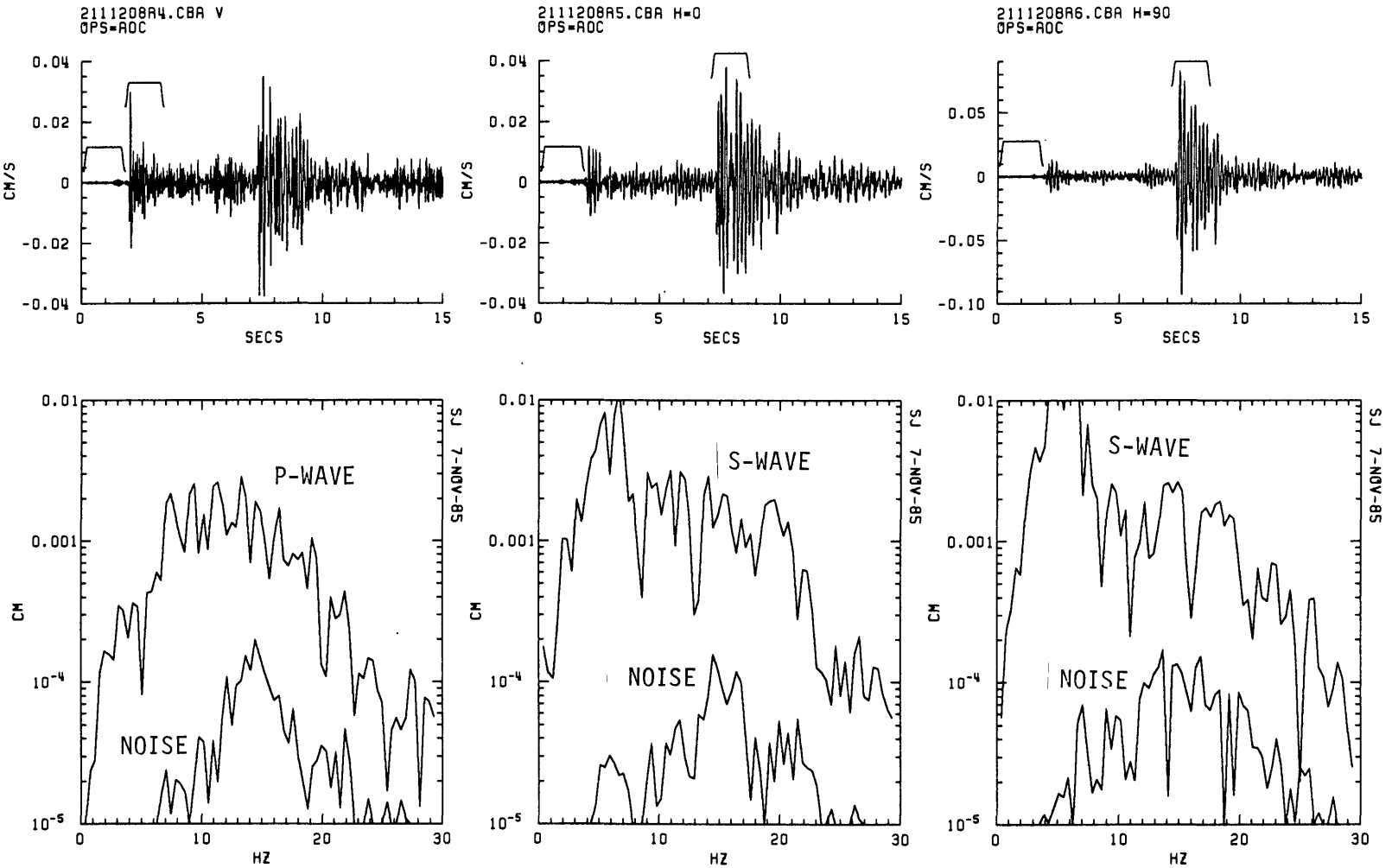

Figure 3. Spectral signal-noise comparison for a typical three component recording (event 211208 at station CBA).

PRELIMINARY ANALYSES OF RESULTS, CONCLUSIONS AND RECOMMENDATIONS

M. Celebi

The seismograms, Fourier amplitude spectra, and spectral ratios presented in Appendices A and B constitute a significant percentage of the processed data from the Canal Beagle and Viña experiments, respectively. At the time of preparation of this report, the epicentral distances, magnitudes, and other relevant information of events presented herein were not yet available from the Geophysical Institute of the University of Chile in Santiago. However, even without this information and because the stations established were close to one another (as compared to epicentral distances), for each one of the events, the velocity seismograms (presented in Appendices A and B) obtained from different stations visually depict the degree of overall amplification of motions at one site relative to another.

Although this data set is currently being analyzed for other purposes, in this section the spectral ratios obtained from velocity seismograms are examined more closely with respect to amplification at specific sites. By this method, it is intended to distinguish between the topographical and geological amplification at different sites.

In order to draw conclusions related to practical engineering and to correlate the results with the damage distribution at Canal Beagle and Viña del Mar, selected spectral ratios corresponding to pairs of stations presented in Appendices A and B have been replotted for frequencies 0-10 Hz and with a standard format. The main reason why spectral ratios are replotted for 0-10 Hz is to show the amplification within a frequency range (0-10 Hz) that is applicable for most structures. In obtaining the spectral ratios, standard 25-second windows were applied to velocity seismograms if the records were 25 seconds or longer; otherwise, the length of the shorter seismogram was used for both records of the pair for which the spectral ratio is calculated. If spectral ratios between pairs of stations are available, for more than one event, the spectral ratios are superimposed to study the repeatability of the relative response at that pair of sites. All spectral ratio plots are smoothed with a triangular weighting function of 0.25 Hz width.

TOPOGRAPHICAL AMPLIFICATION AT CANAL BEAGLE

In Figures 1-3 the spectral ratios of three different events for stations CBA/VAL are presented for vertical and horizontal (N-S and E-W) components,

respectively. These ratios are representative of only geological effects (ignoring distances and source parameters of the three events) and therefore represent the geological transfer function T_G:

$$T_G = \frac{A_{G2}(\omega)}{A_{G1}(\omega)}$$

where $A_{Gi}(\omega)$ is the Fourier amplitude spectrum at site i.

The transfer function justifications have been discussed in detail by Rogers and others (1984).

To provide a better comparison, the spectral ratios for stations CBA/VAL of all three events are superimposed in Figure 4 for the vertical and horizontal (N-S and E-W), respectively. These summary figures display distinctive resonance at approximately 6 to 7 Hz and amplification ratios ranging from 1 to a minimum of 2 for frequencies 4 to 7 Hz in the N-S and E-W directions and for frequencies 6-8 in the vertical direction.

The spectral ratios of the same three events (as in Figures 1-4) and their superimposed comparative ratios for stations CBB/CBA are presented in Figures 5 to 7 for the vertical and horizontal (N-S and E-W) components, respectively. The same is repeated for stations CBC/CBA in Figures 8-10. Similarly, spectral ratios from data available of only two events and their superimposed comparative ratios for stations CBE/CBA are presented in Figures 11 to 13 for vertical and horizontal (N-S and E-W) components, respectively. The same is repeated for stations CBF/CBA in Figures 14-16. In the case of station CBD sited on the top of the hill from which the ridges appear, the spectral ratios show considerable variation. During the main event of March 3, 1985, there was no damage inflicted on the single and two-story buildings on this hill, nor was there damage in the canyon where reference station CBA was established. The spectral ratios from the data available of only two events and their superimposed comparative ratios for stations CBD/CBA are presented in Figures 17-19 for the vertical and horizontal (N-S and E-W) components, respectively. For these two events, the spectral ratios do not indicate the repeatability of frequency dependent amplifications of motions observed in spectral ratios of other pairs of stations. Although some resonance (for both events) is apparent around 8 Hz, until further observations can be made at the pair of stations CBD and CBA, no credible amplification of motions at station

CBD as compared to motions at CBA can be claimed for frequencies between 0-10 Hz.

The significant amplification ratios are consistent and repeatable for multiple events, particularly for N-S and E-W directions of stations CBB, CBC, and CBF compared with station CBA. Therefore, it is concluded that with these spectral ratios the ridge effects are separated as topographical transfer function T_t:

$$T_t = \frac{A_{t2}(\omega)}{A_{t1}(\omega)}$$

where A_{ti} is the Fourier amplitude spectrum at site i.

Noting that stations CBB and CBC are on one ridge and station CBF is on another, the spectral ratios displayed in Figures 6, 7, 9, 10, 15, and 16 for N-S and E-W directions clearly indicate for different events resonance at frequencies that are in the range of the structures built on the ridges. On the other hand, the spectral ratio corresponding to station CBE (being at the junction of the ridge and the hill) does not show similarities to the other stations on the ridges.

GEOLOGICAL AMPLIFICATION AT VIÑA DEL MAR

Only selected spectral ratios are presented for most of the stations in Viña. Data from some of the stations are not presented since the particular events recorded at these stations do not provide a basis for comparison. In obtaining the spectral ratios, the distance and topographical effects are ignored as most of these stations are in close proximity to one another. Therefore, only geological effects are assumed to be exhibited.

SPECTRAL RATIOS AT SAND SITES

Spectral ratio plots for two separate events each as well as superimposed spectral ratios for stations EAC/VAL are presented in Figures 20-22 for the vertical and horizontal (N-S and E-W) components, respectively. The same is repeated for stations EAC/VAL (Figures 23-25) and for stations REN/VAL (Figures 26-28). Stations EAC (at Edificio Acapulco--a severely damaged build-

ing), TRA (undamaged building, triangular shaped in plan, in close proximity to Edificio Acapulco) and REN (on the hills of Reneca´ and near Edificio El Faro--the structure which tilted during the main event and was dynamited shortly after) were established to measure the amplification at the coastal zone. These figures display the repeated and significant degree of amplification at frequencies in the range of those structures (8-15 stories) where these stations were sited.

SPECTRAL RATIOS AT ALLUVIAL SITES

The only station on an alluvial site for which there is available data for several events is station MUN. The data from stations (*e.g.*, EMP and ELC) on other alluvial sites exhibit very high spectral ratios as compared to station VAL (rock site) because of the low amplitude and high frequency noise mixed with the data from station VAL for the corresponding event. Therefore the plots for the spectral ratios for stations MUN/VAL only corresponding to two different events and their superimposed plots are presented in Figures 29-31 for vertical and horizontal (N-S and E-W) components, respectively.

SPECTRAL RATIOS AT ROCK SITES

Spectral ratios from one event only for each one of the comparative stations QCL/VAL, HER/VAL and YNF/VAL, are provided in Figures 32-34, respectively. Each figure depicts the spectral ratios of motions in vertical and horizontal (N-S and E-W) components for the stations indicated.

CONCLUSIONS

The data set presented herein allow the following conclusions to be made:

- The data from Canal Beagle comprise essentially the first set of data from a dense array deployed at a heavily populated region with ridges and provides an opportunity to distinguish topographical effects from others, and to correlate these effects with damage patterns.
- For several events, the seismograms obtained from different stations and plotted with the same scale presented in Appendices A and B clearly depict the degree of overall amplification of motions at various stations as compared to the rock station or at any one station relative to any other station.

- It has been shown by use of the spectral ratios that there is significant geological and topographical amplification at the ridges of Canal Beagle as compared with the rock site (VAL).
- It has been shown that there is significant topographical amplification at the ridges of Canal Beagle compared with the canyons of Canal Beagle. The frequency dependent topographical amplification ratios of motions at the ridges range from 1 to a minimum of 2 or 3 for most frequencies in the ranges of structures built on them.
- The spectral ratios for different sites at Viña del Mar depict clearly the frequency-dependent geological amplification at sand, alluvial, and firmer sites (QCL, HER, YNE) as compared to the reference rock station (VAL).

RECOMMENDATIONS FOR FUTURE WORK

- Engineering application of these results should be derived and incorporated into local microzonation maps.
- Limited data has been obtained from alluvial sites in Viña del Mar. In the future, additional data should be obtained at alluvial sites in Viña del Mar.
- The work should be extended to Valparaiso where there is similar geological detail and damage correlation.
- The work presented herein should be further substantiated by theoretical studies involving wave propagation.
- In order to pursue the above, reliable soil layer stratification information is necessary. This necessitates soil logs.
- Further work to quantify statistically engineering amplification factors is warranted. Mean spectral ratios will be obtained for those stations where multiple-event data are available.
- Throughout this report only velocity seismograms have been used. The acceleration seismograms are currently being studied to obtain response spectra and Fourier spectral ratios and to compare these with spectral ratios from velocity seismograms.
- Information on epicentral coordinates, magnitudes, and depths of the aftershocks recorded in these experiments was not available during the preparation of this report. This information is essential to pursue further seismological studies. Further work to obtain epicentral dis-

tances from S-P times is currently in progress and these will be compared with actual data of epicentral coordinates to be obtained from the Geophysical Institute of the University of Chile.

REFERENCE

Rogers, A.M., Borcherdt, R.D., Covington, P.A., and Perkins, D.M., 1984, A comparative ground response study near Los Angeles using recordings of Nevada nuclear tests and the 1971 San Fernando earthquake: *Bulletin, Seismological Society of America*, **74**, No. 5, pp. 1925-1949.

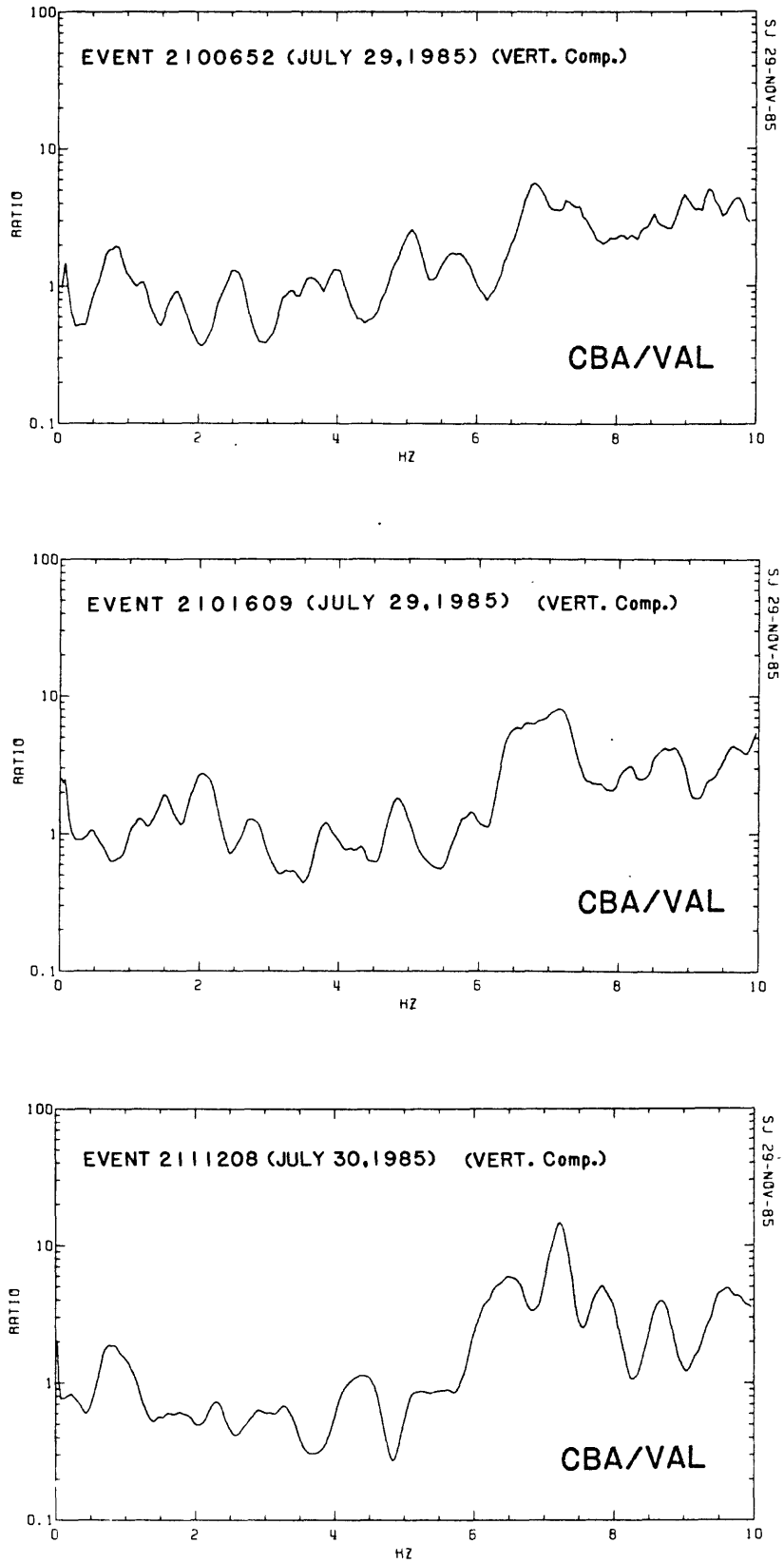

Figure 1. Spectral ratios of three different events, respectively (vertical components) for stations CBA/VAL (Plots are log-linear for frequencies 0-10 Hz).

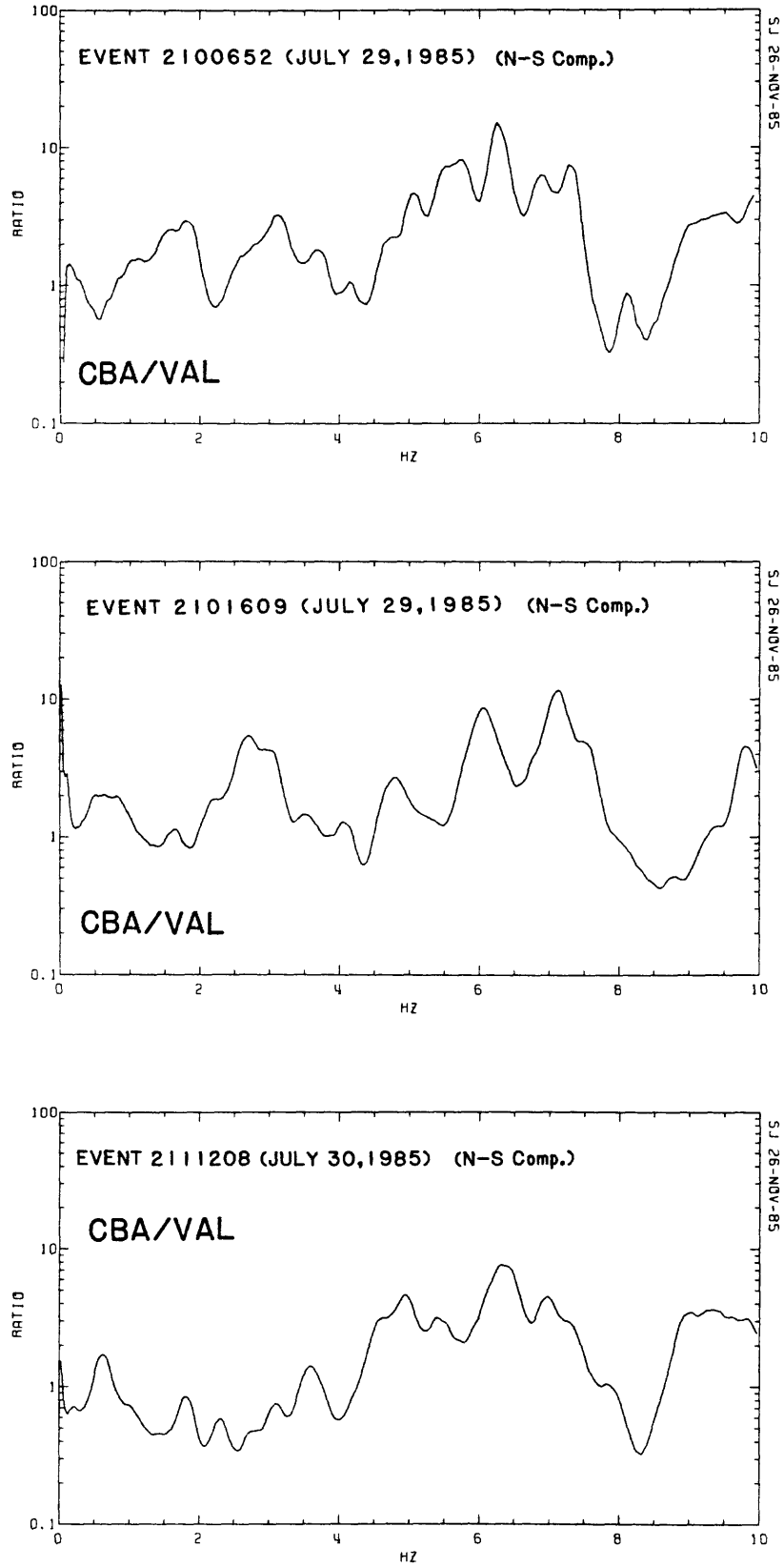

Figure 2. Spectral ratios of three different events, respectively (N-S components) for stations CBA/VAL.

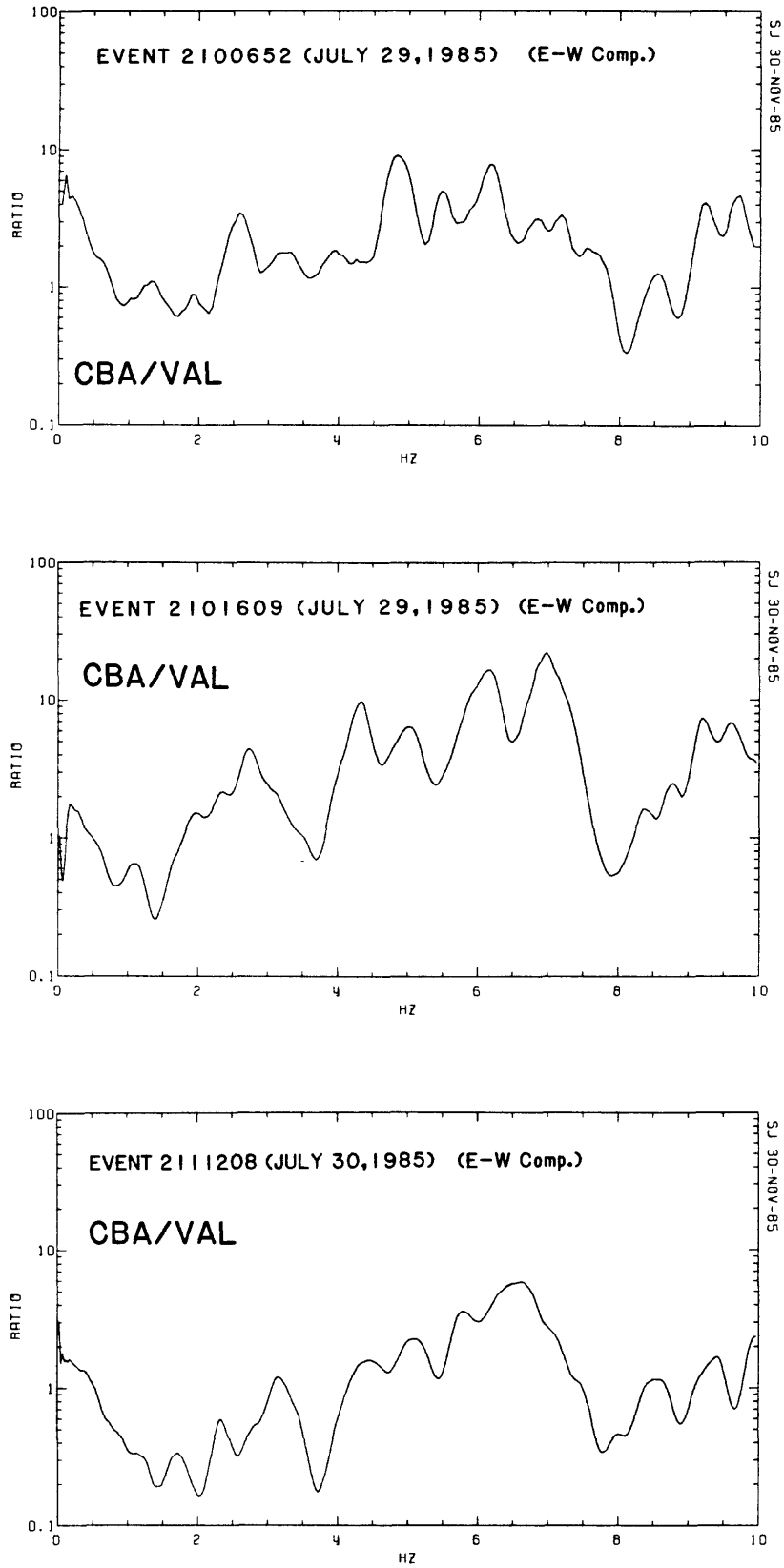

Figure 3. Spectral ratios of three different events, respectively (E-W components) for stations CBA/VAL.

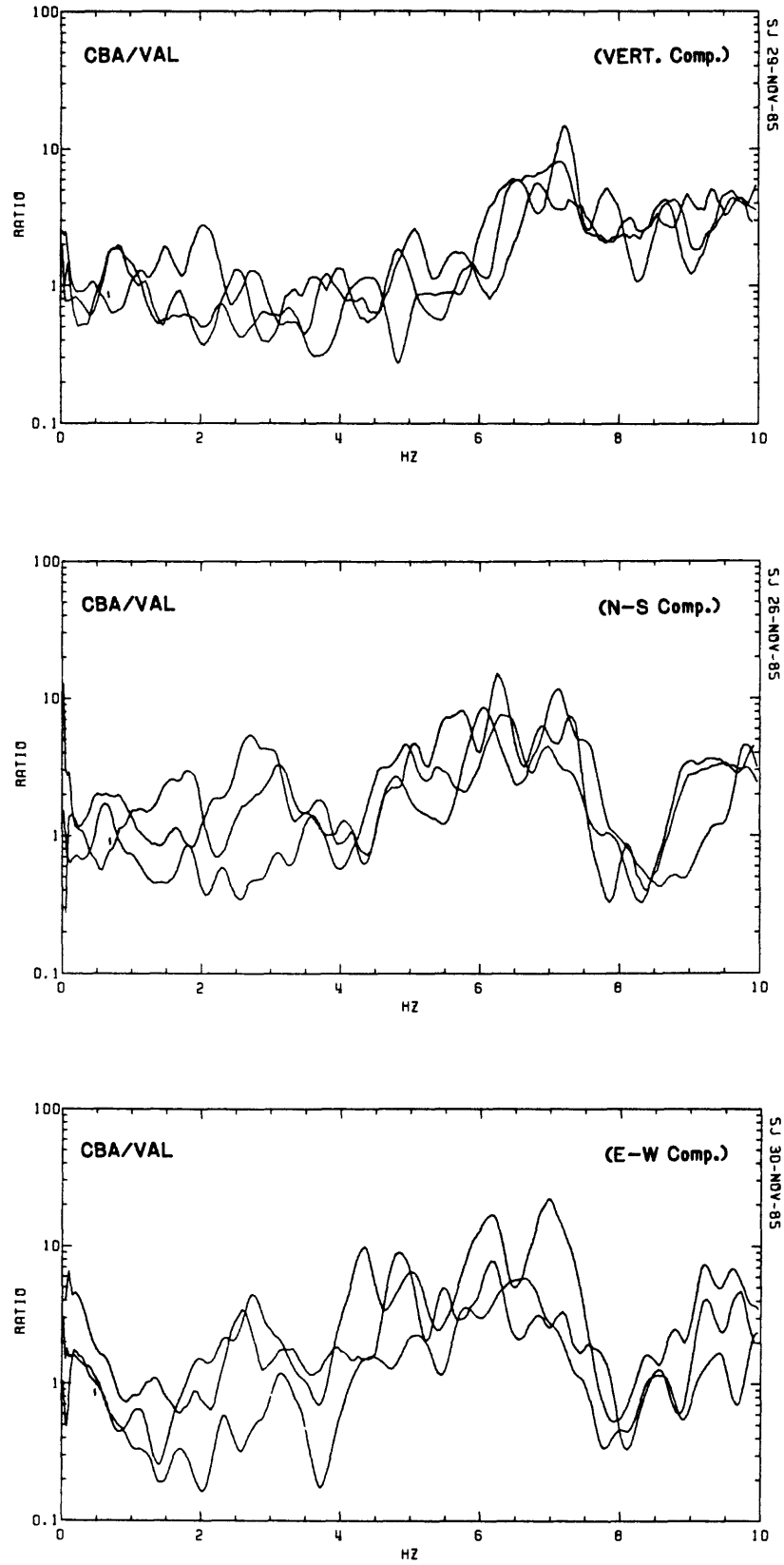

Figure 4. Superimposed spectral ratios of three different events for vertical and horizontal (N-S and E-W) components, respectively, for stations CBA/VAL.

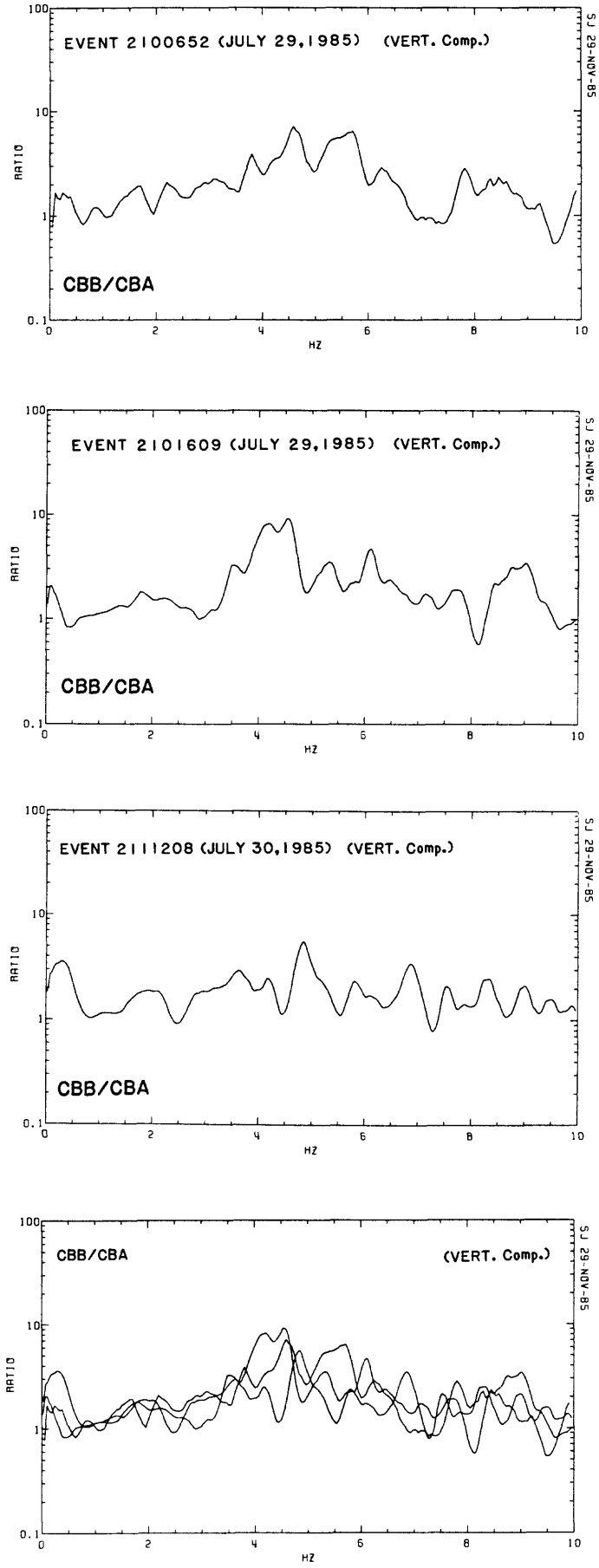

Figure 5. Spectral ratios of three different events, respectively, and their superimposed plot (vertical components) for stations CBB/CBA.

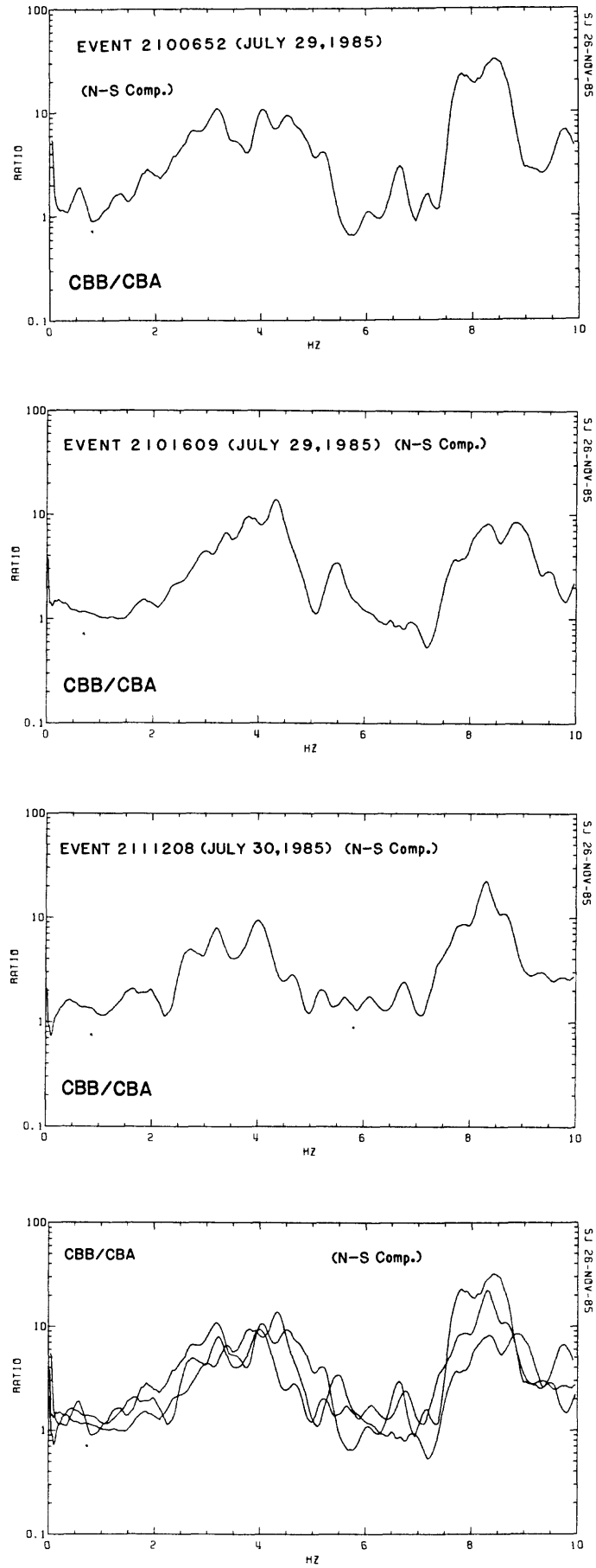

Figure 6. Spectral ratios of three different events, respectively, and their superimposed plot (N-S components) for stations CBB/CBA.

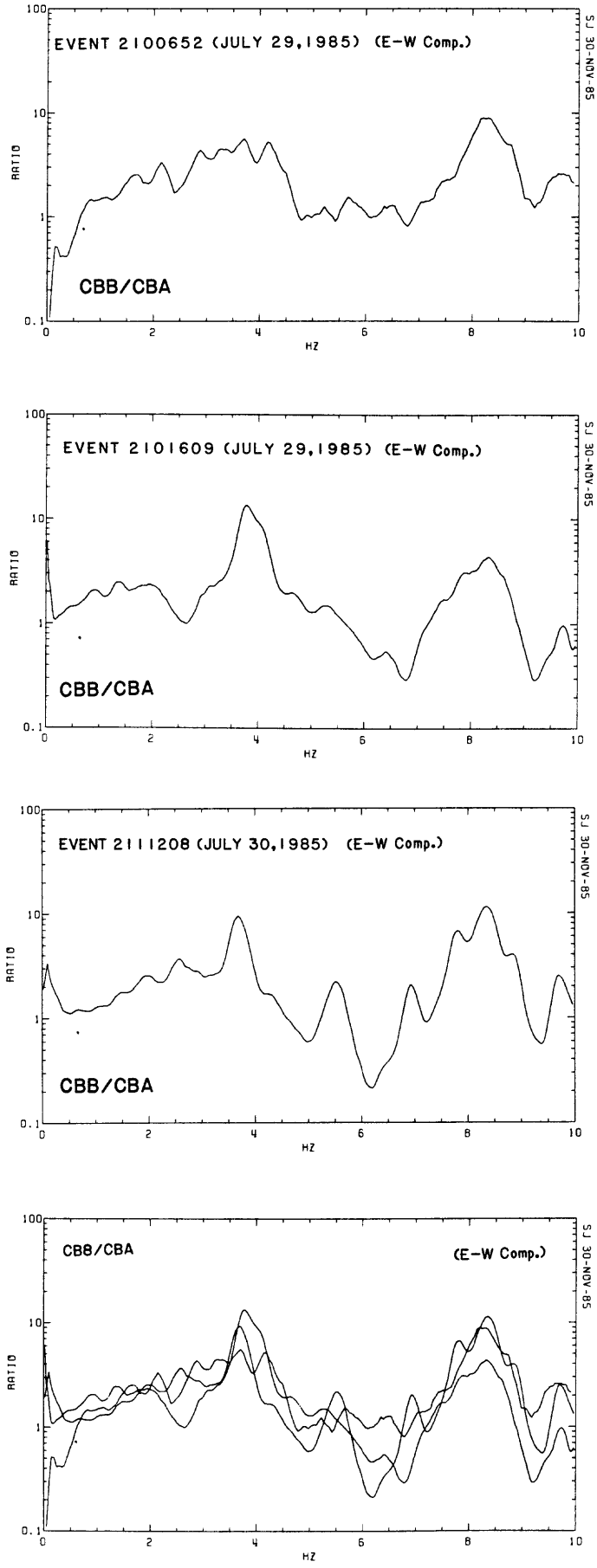

Figure 7. Spectral ratios of three different events, respectively, and their superimposed plot (E-W components) for stations CBB/CBA.

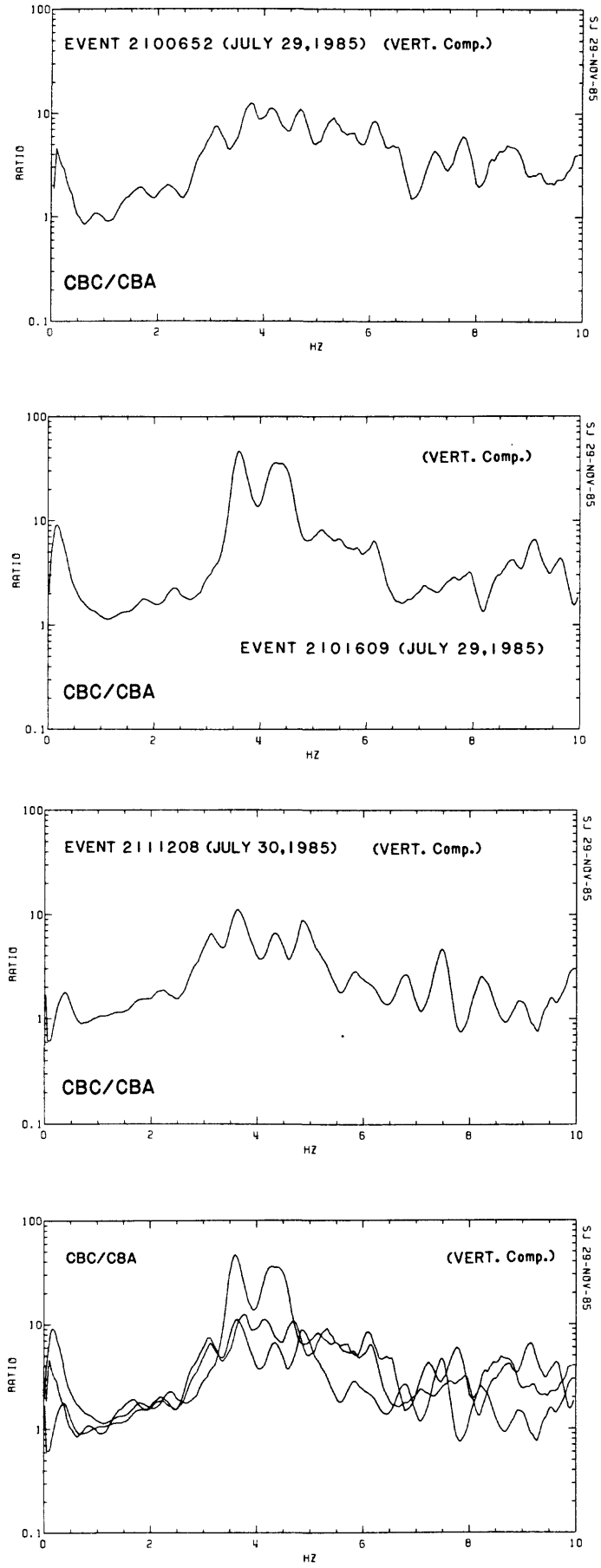

Figure 8. Spectral ratios of three different events, respectively, and their superimposed plot (vertical components) for stations CBC/CBA.

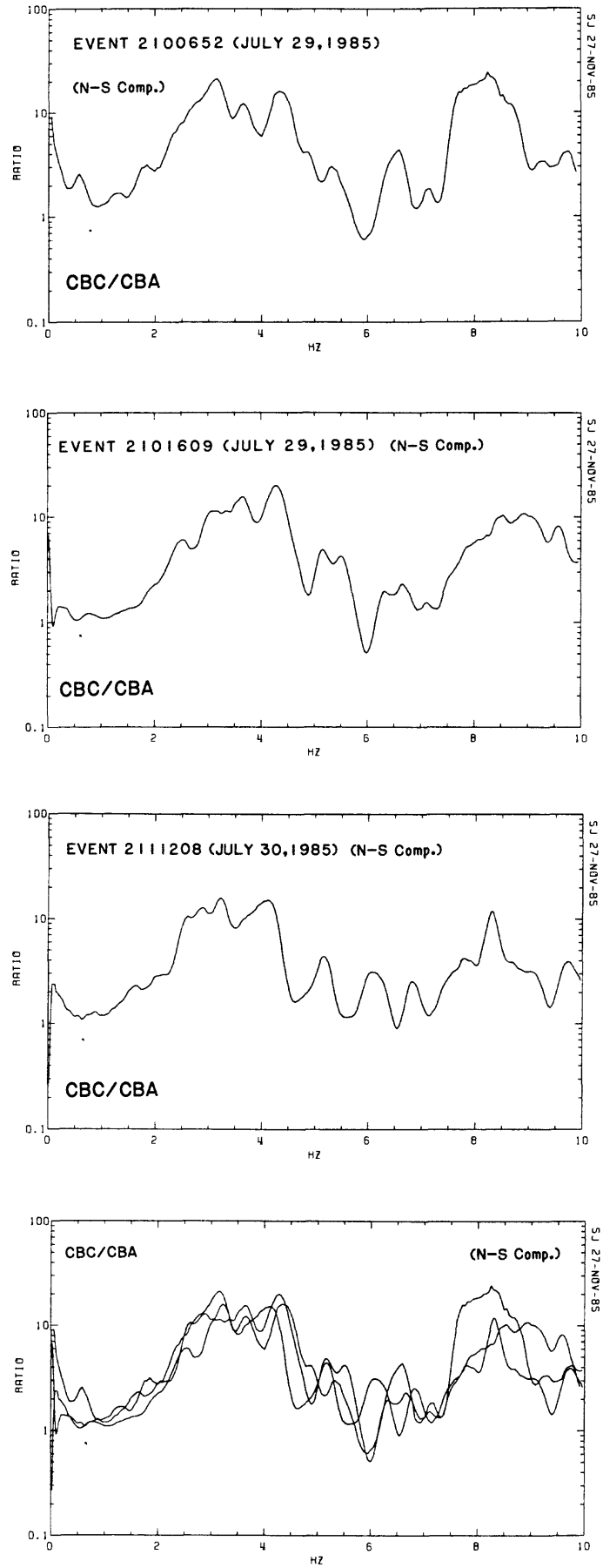

Figure 9. Spectral ratios of three different events, respectively, and their superimposed plot (N-S components) for stations CBC/CBA.

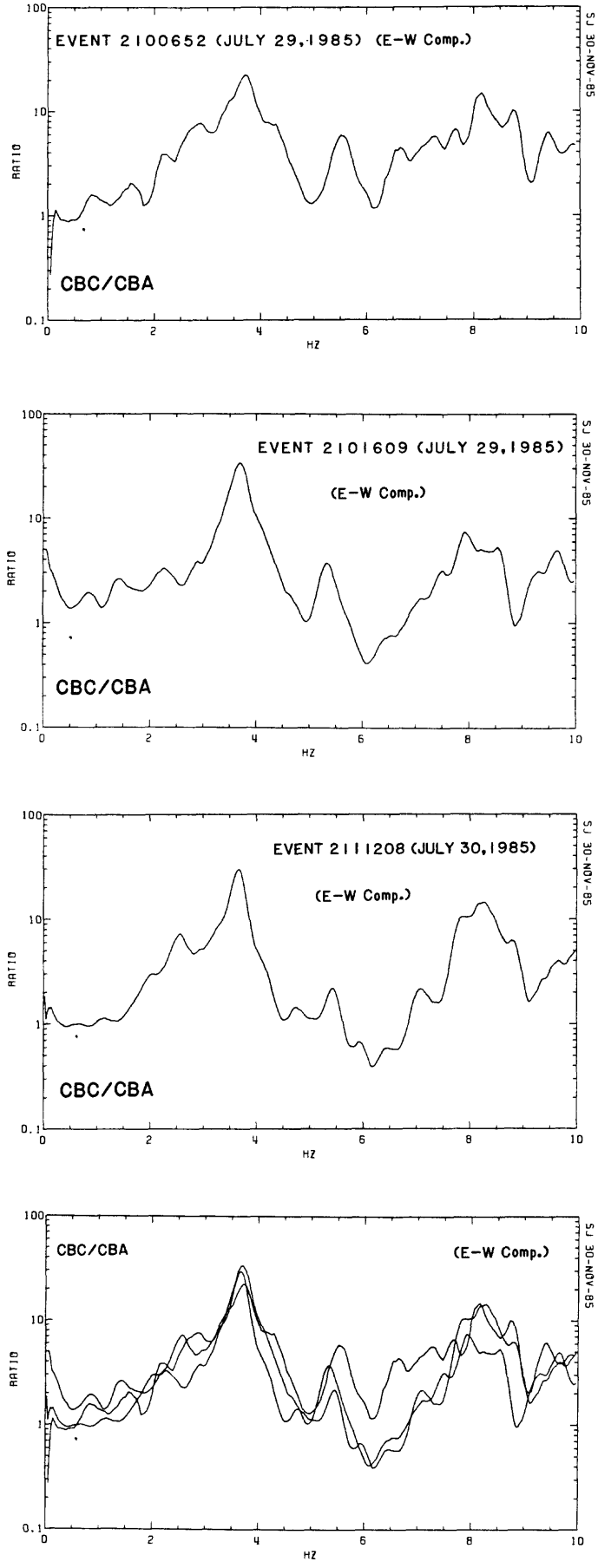

Figure 10. Spectral ratios of two different events, respectively, and their superimposed plot (E-W components) for stations CBC/CBA.

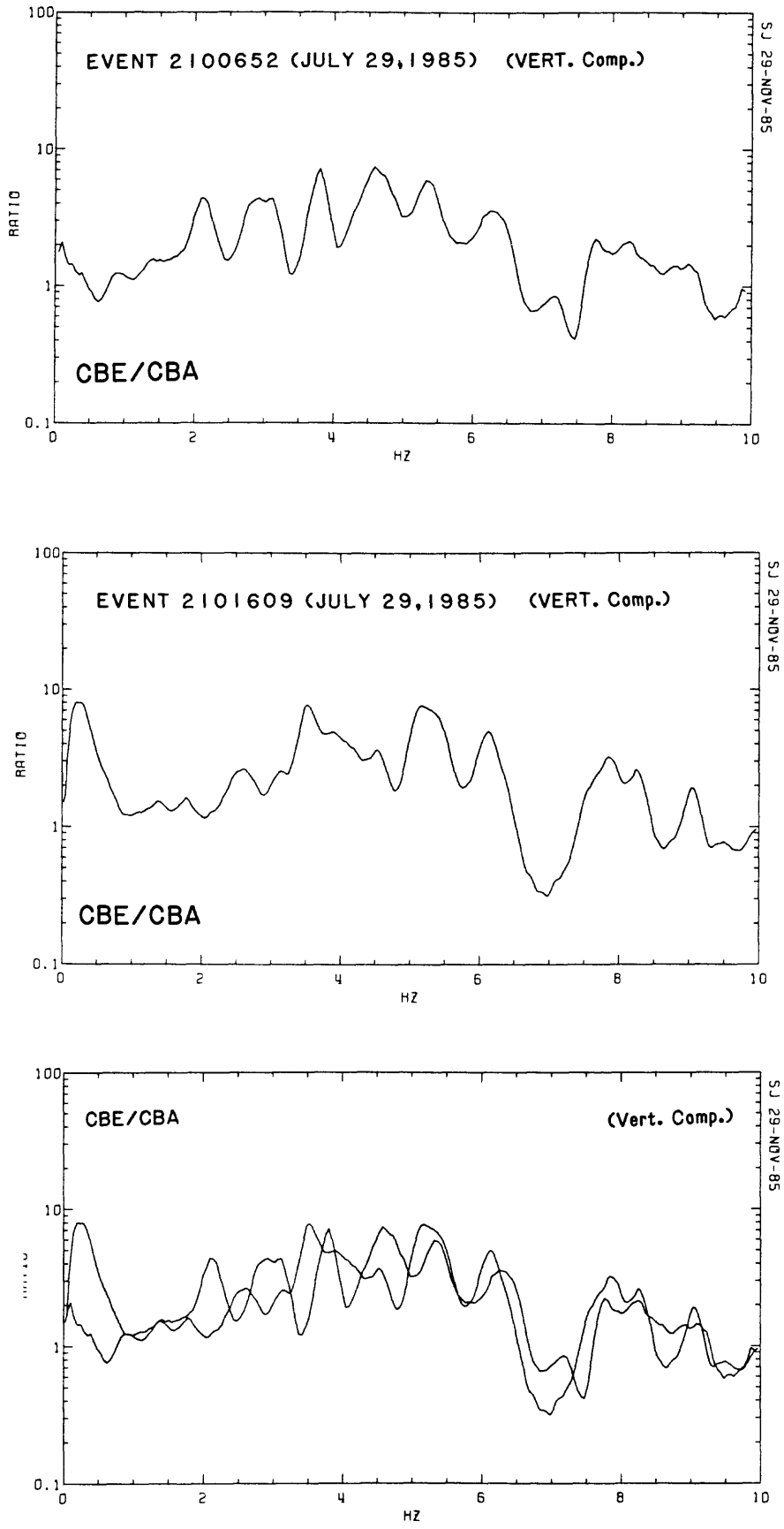

Figure 11. Spectral ratios of two different events, respectively, and their superimposed plot (vertical components) for stations CBE/CBA.

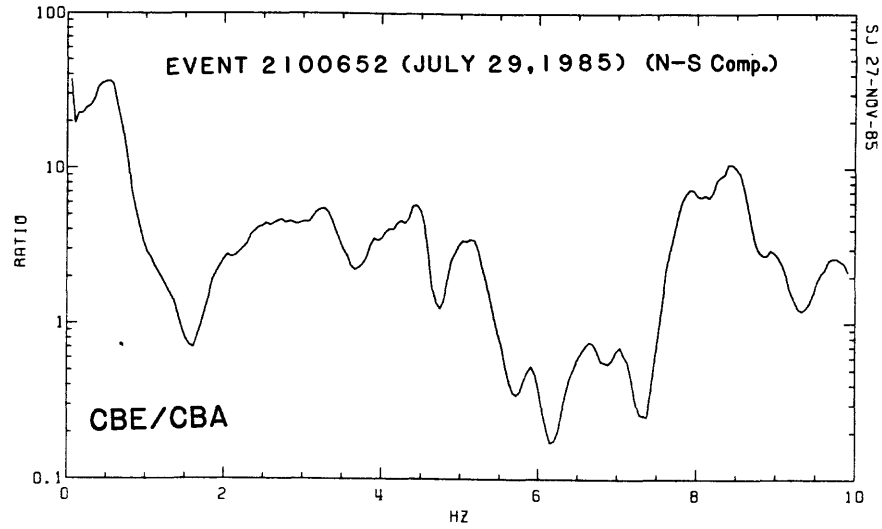

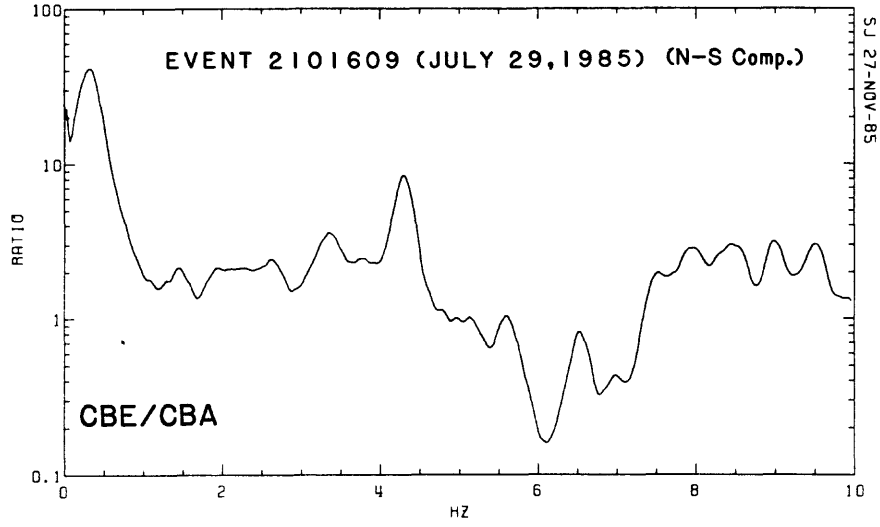

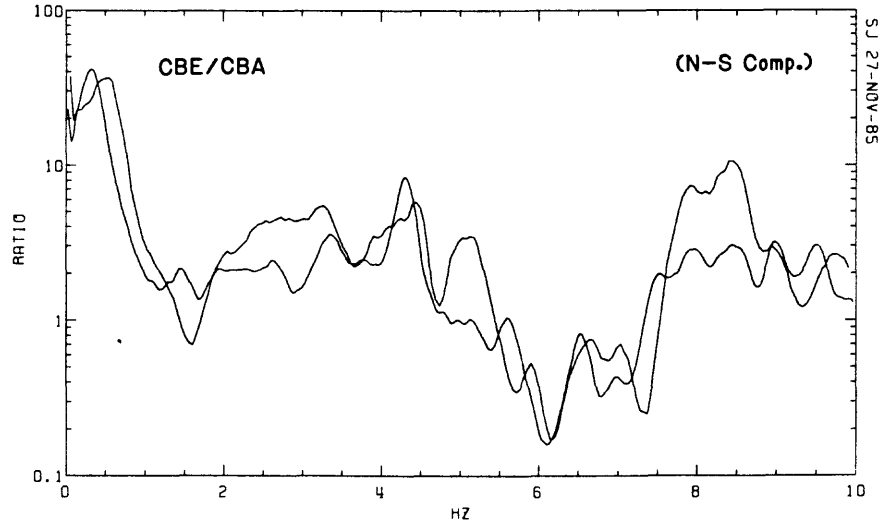

Figure 12. Spectral ratios of two different events, respectively, and their superimposed plot (N-S components) for stations CBE/CBA.

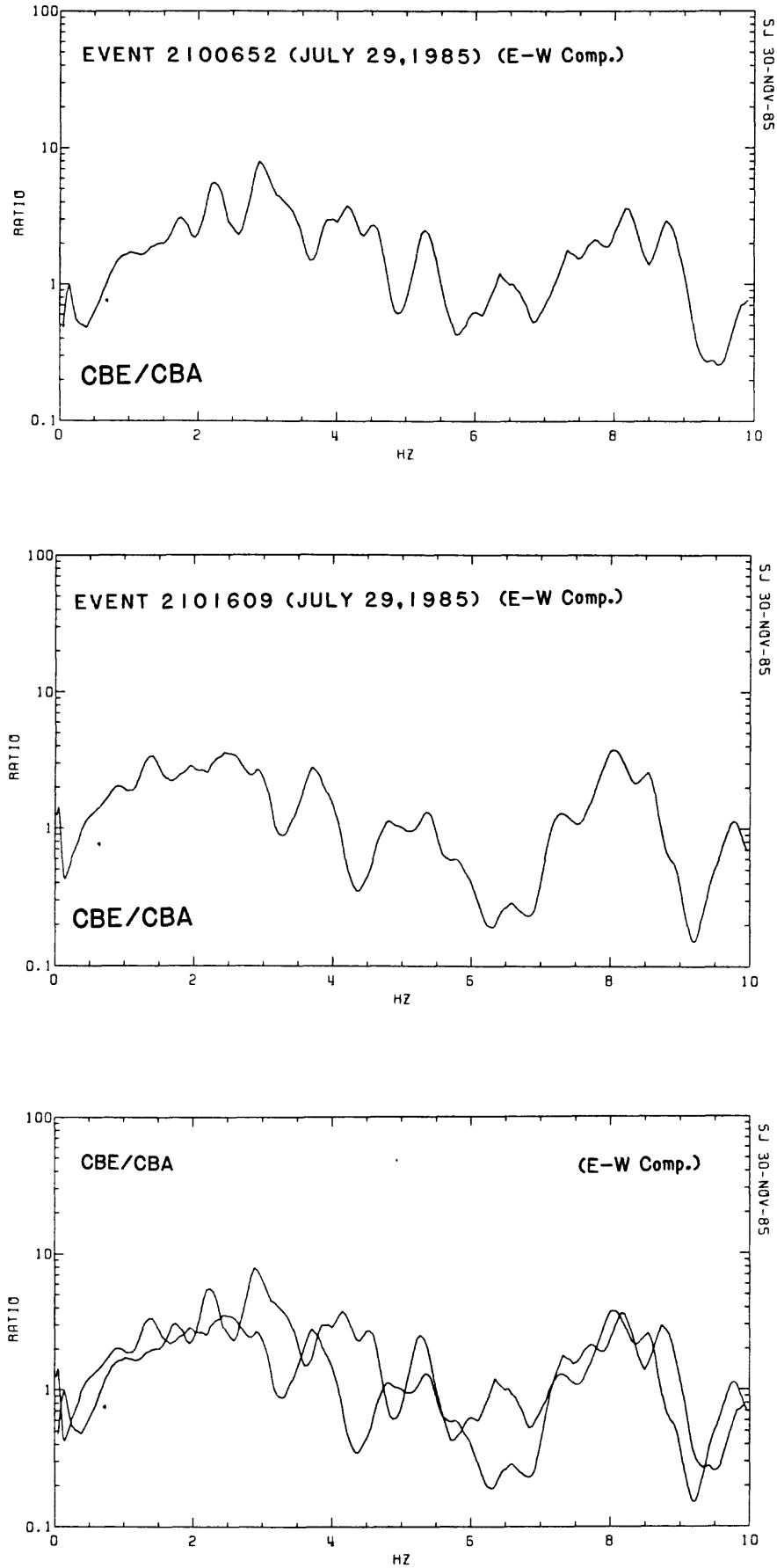

Figure 13. Spectral ratios of two different events, respectively, and their superimposed plot (E-W components) for stations CBE/CBA.

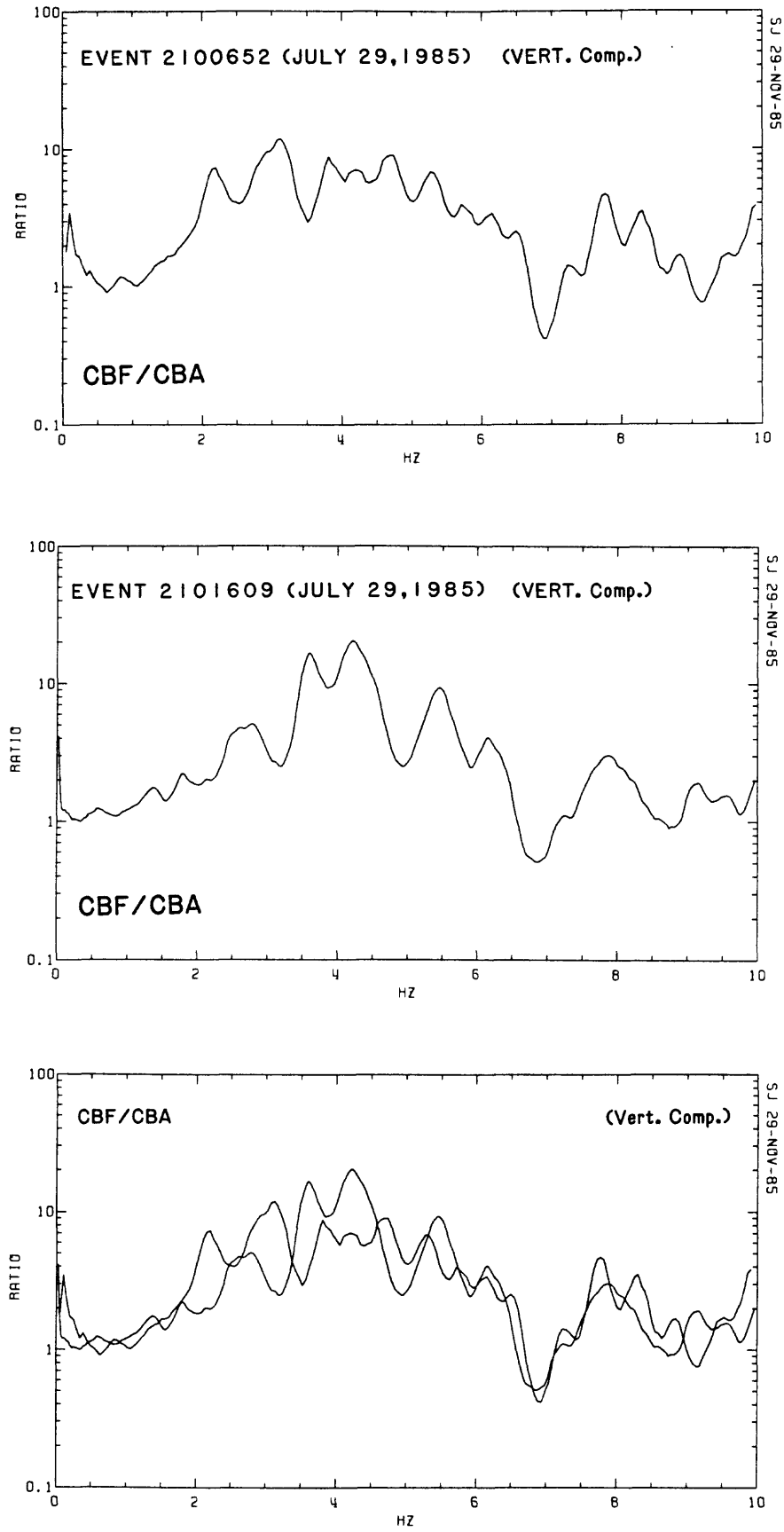

Figure 14. Spectral ratios of two different events, respectively, and their superimposed plot (vertical components) for stations CBF/CBA.

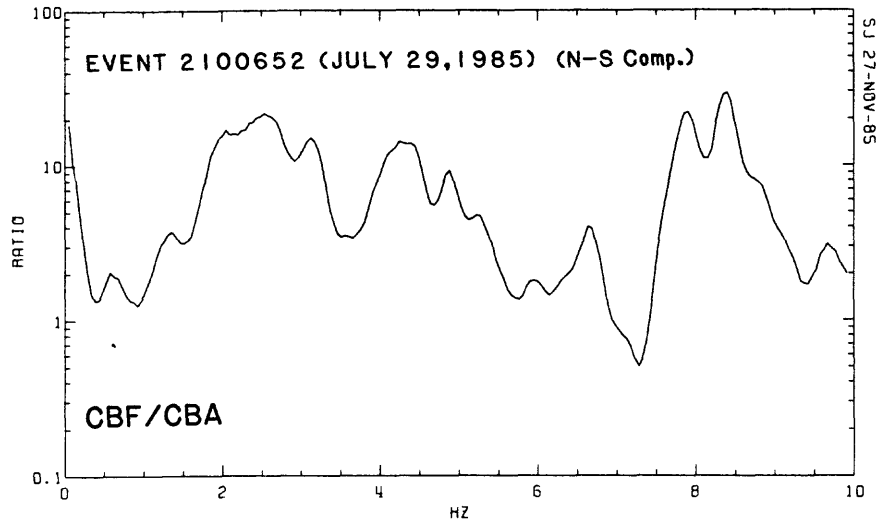

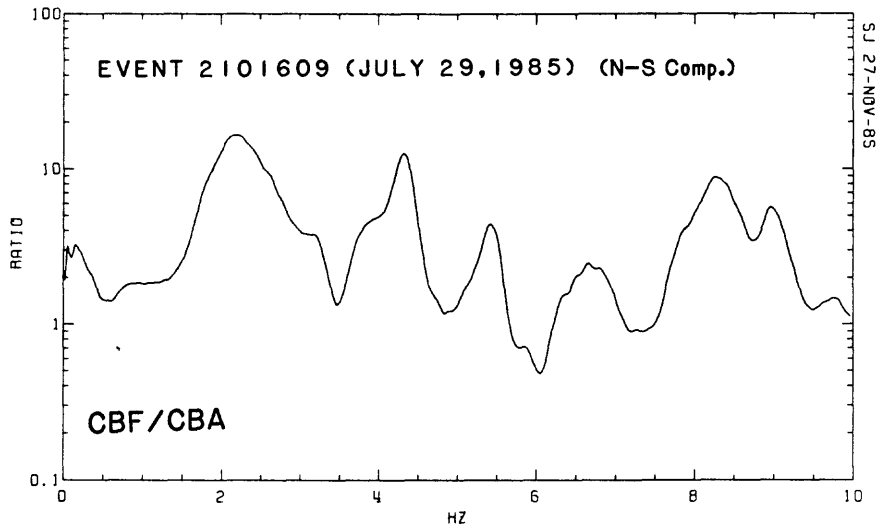

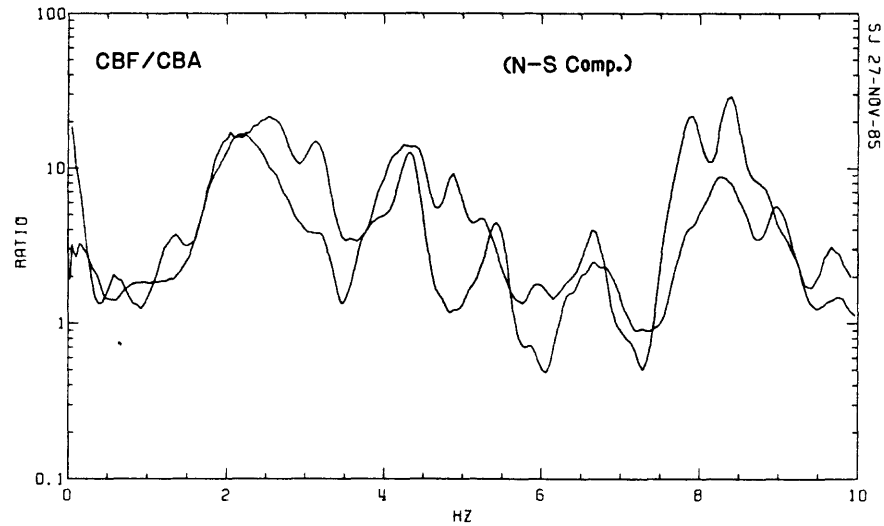

Figure 15. Spectral ratios of two different events, respectively, and their superimposed plot (N-S components) for stations CBF/CBA.

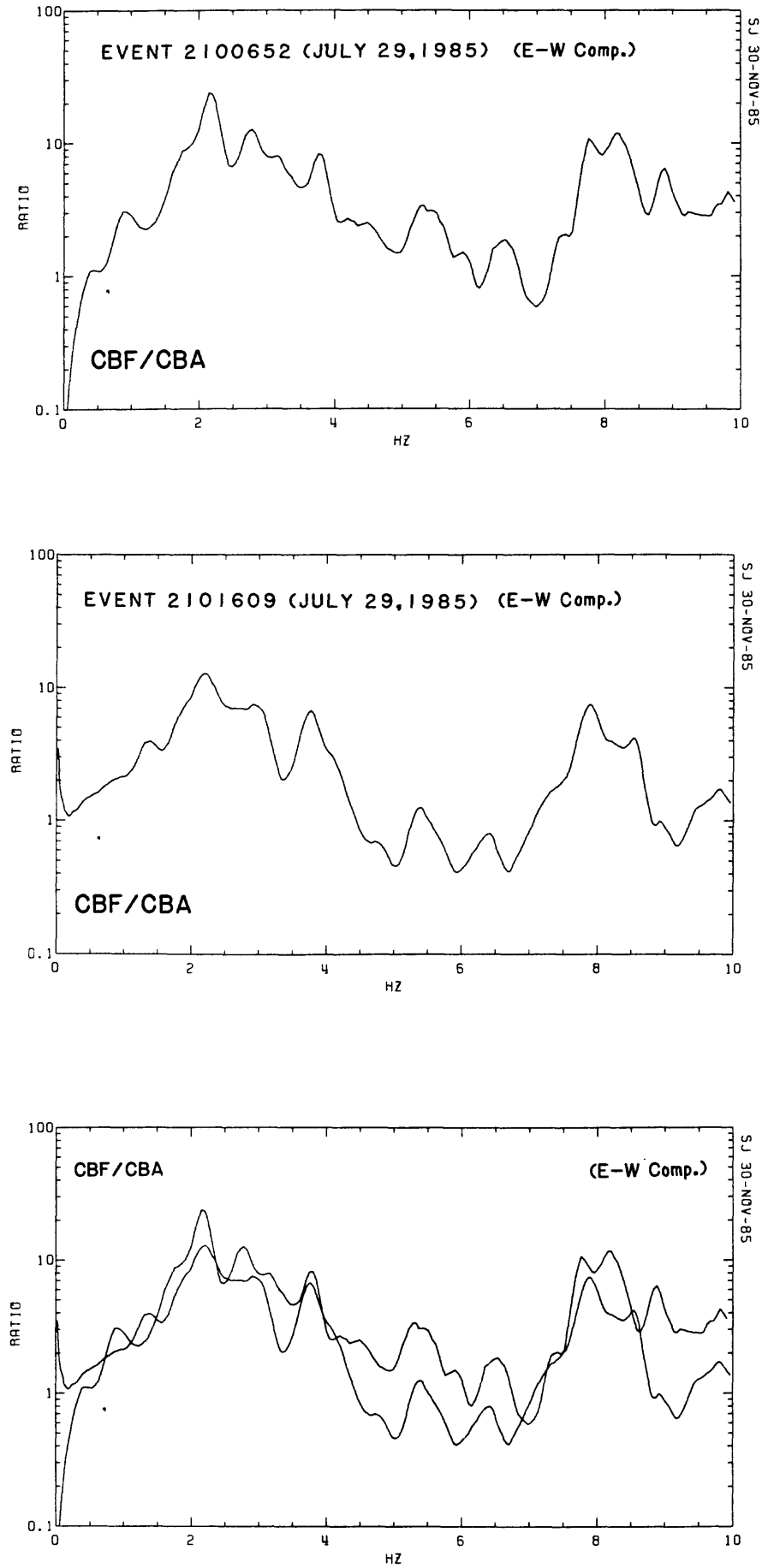

Figure 16. Spectral ratios of two different events, respectively, and their superimposed plot (E-W components) for stations CBF/CBA.

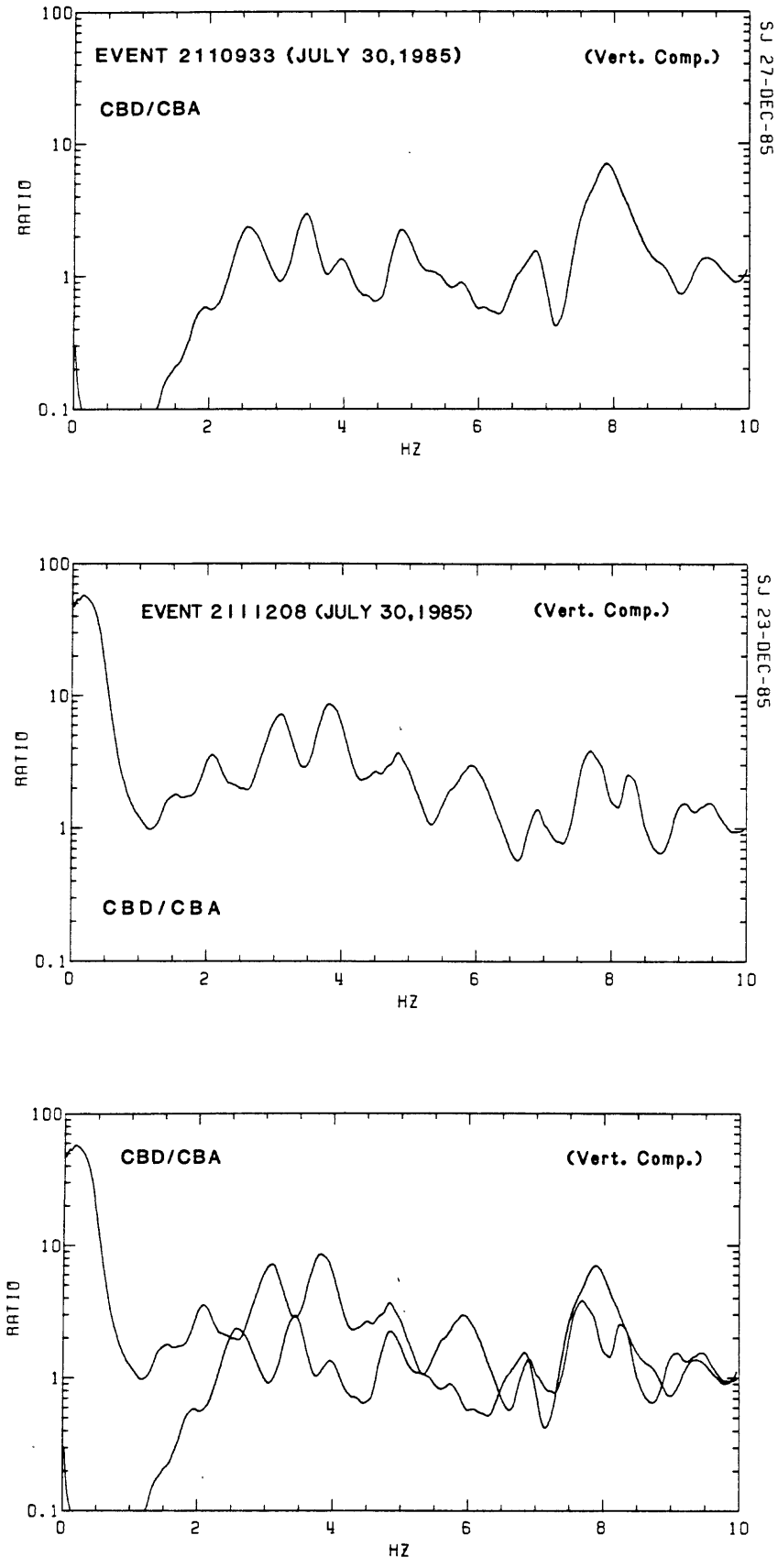

Figure 17. Spectral ratios of two different events, respectively, and their superimposed plot (vertical components) for stations CBD/CBA.

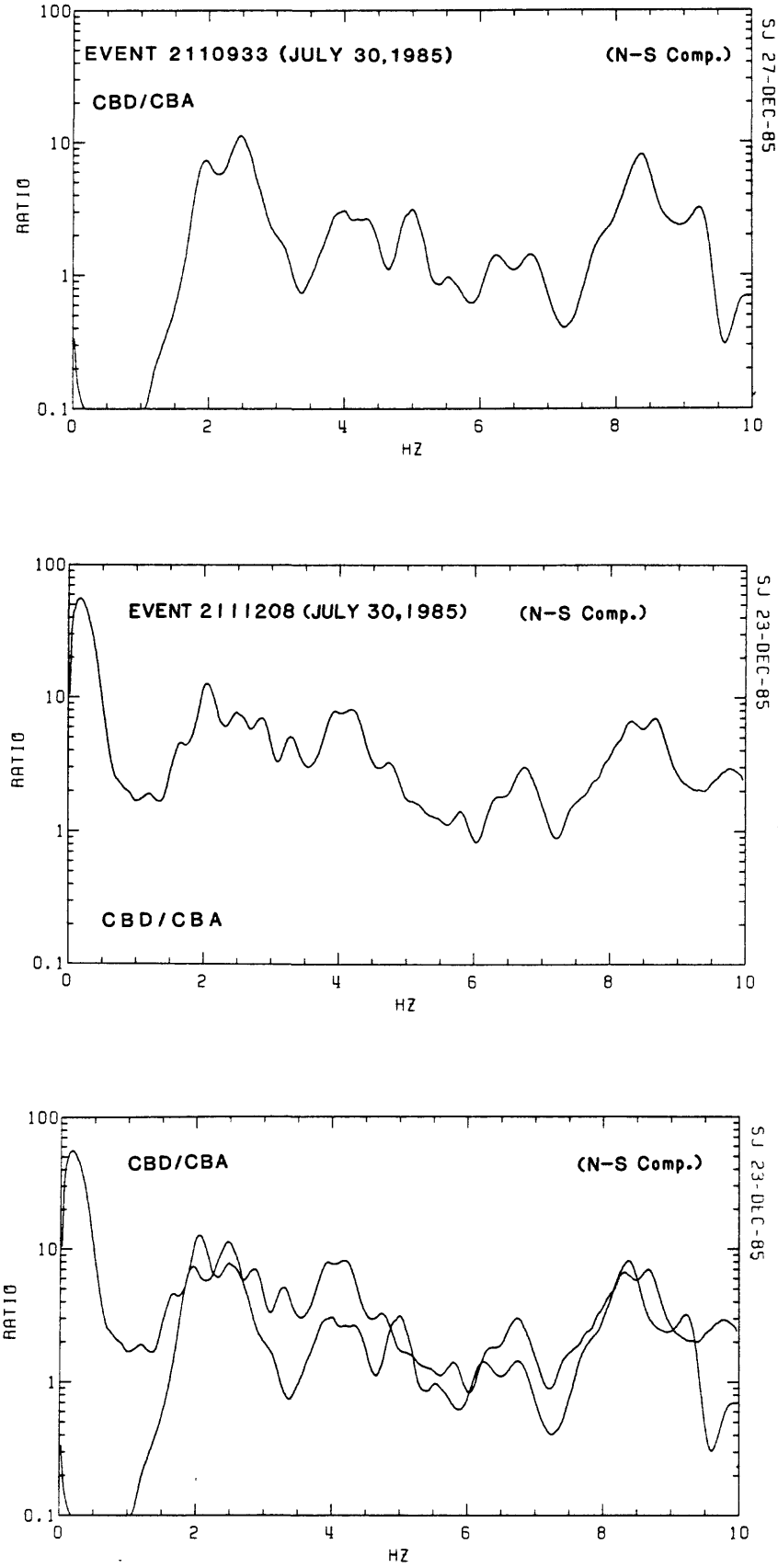

Figure 18. Spectral ratios of two different events, respectively, and their superimposed plot (N-S components) for stations CBD/CBA.

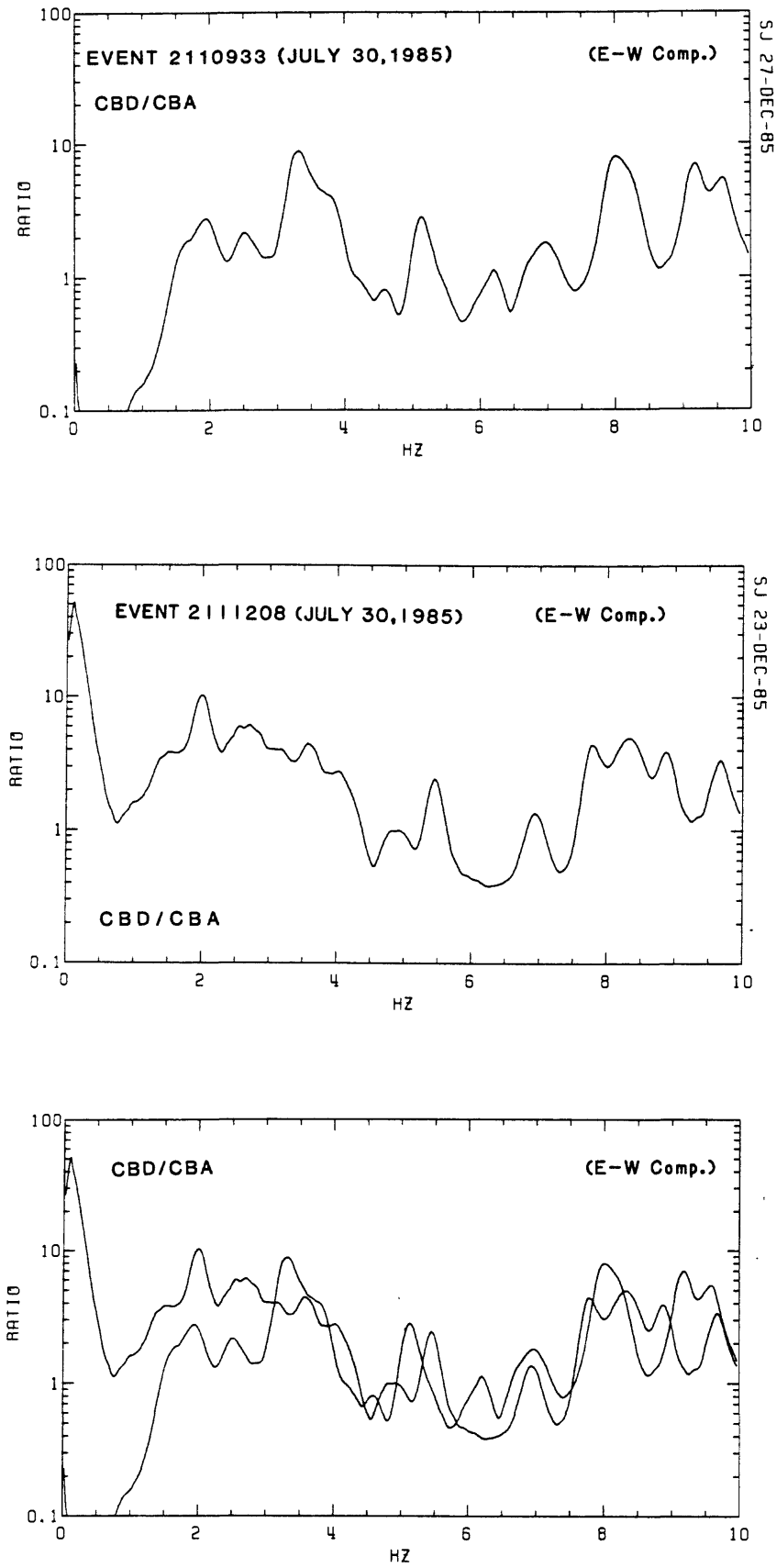

Figure 19. Spectral ratios of two different events, respectively, and their superimposed plot (E-W components) for stations CBD/CBA.

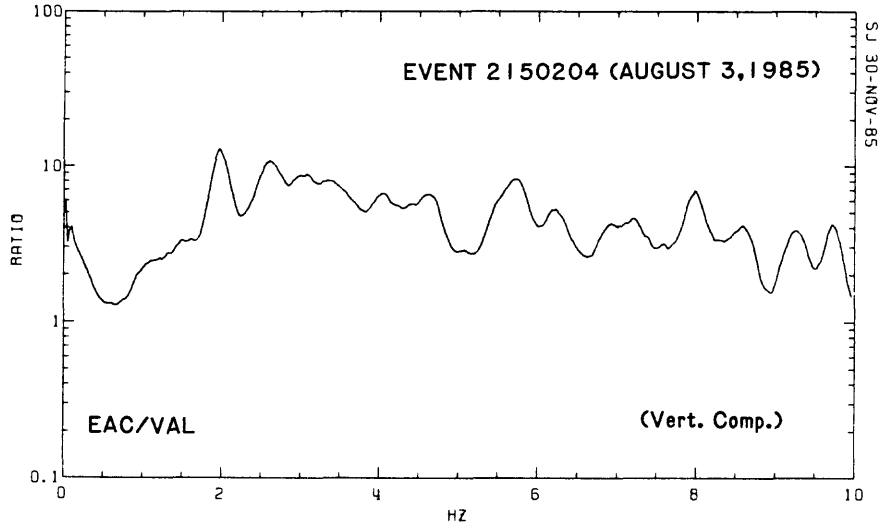

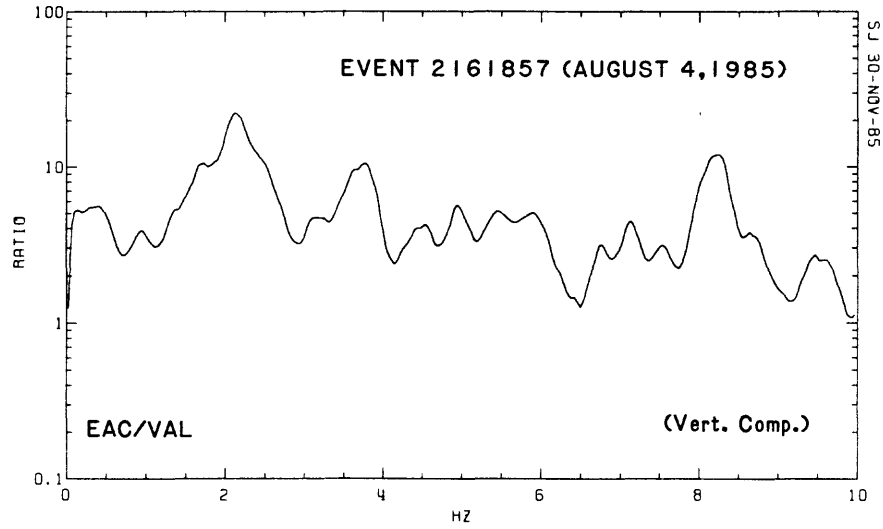

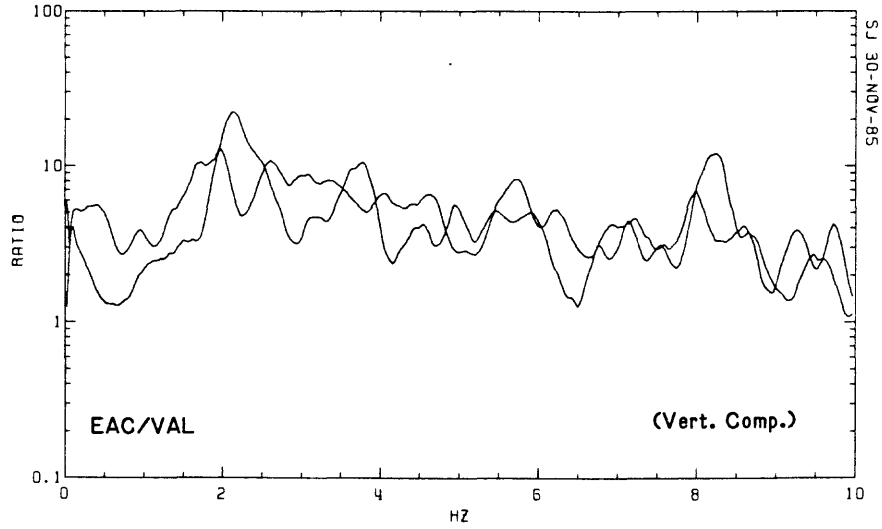

Figure 20. Spectral ratios of two different events, respectively, and their superimposed plot (vertical components) for stations EAC/VAL.

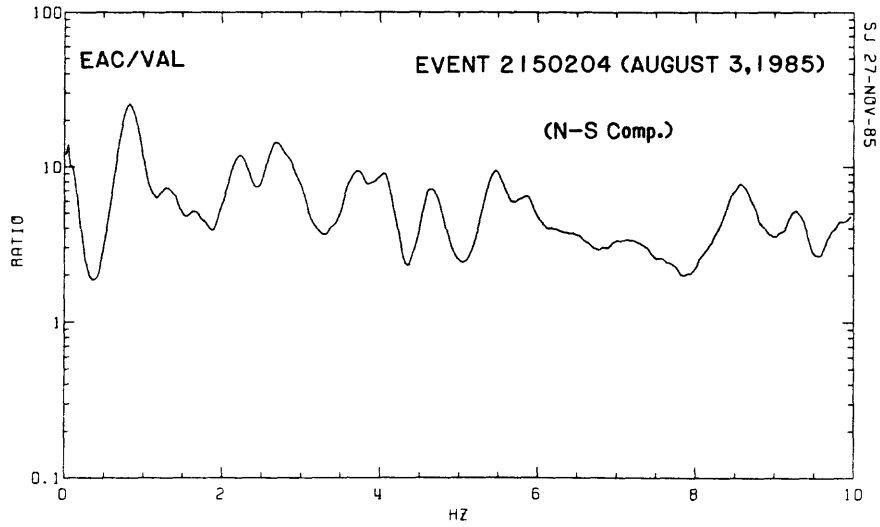

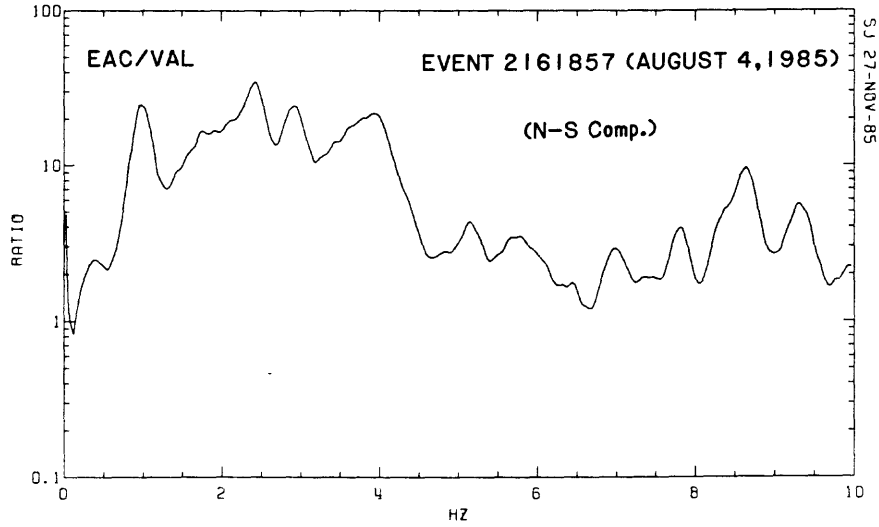

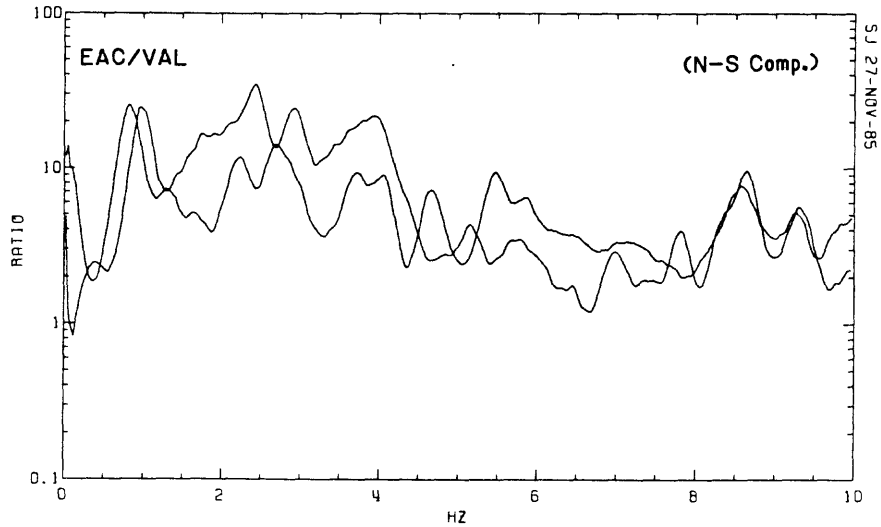

Figure 21. Spectral ratios of two different events, respectively, and their superimposed plot (N-S components) for stations EAC/VAL.

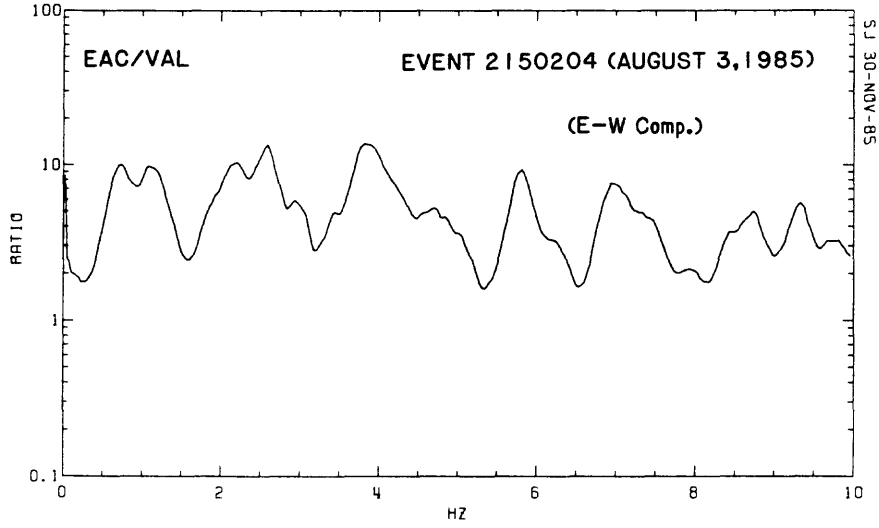

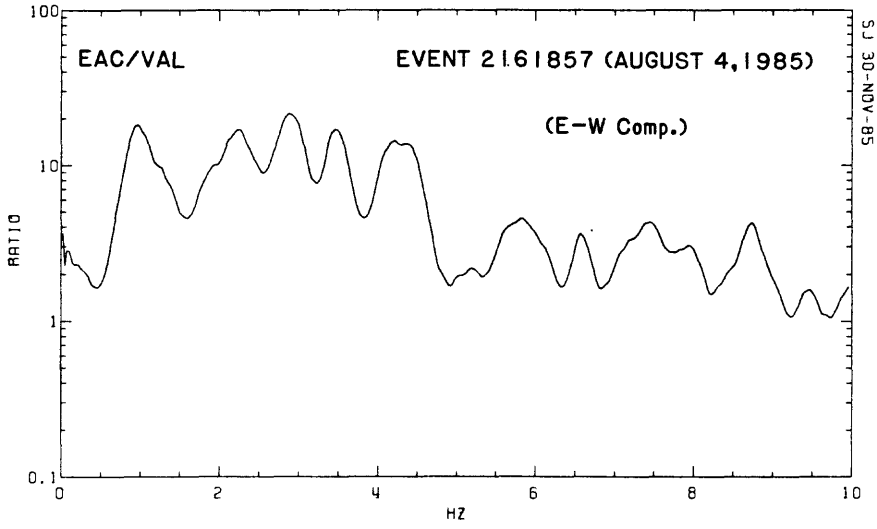

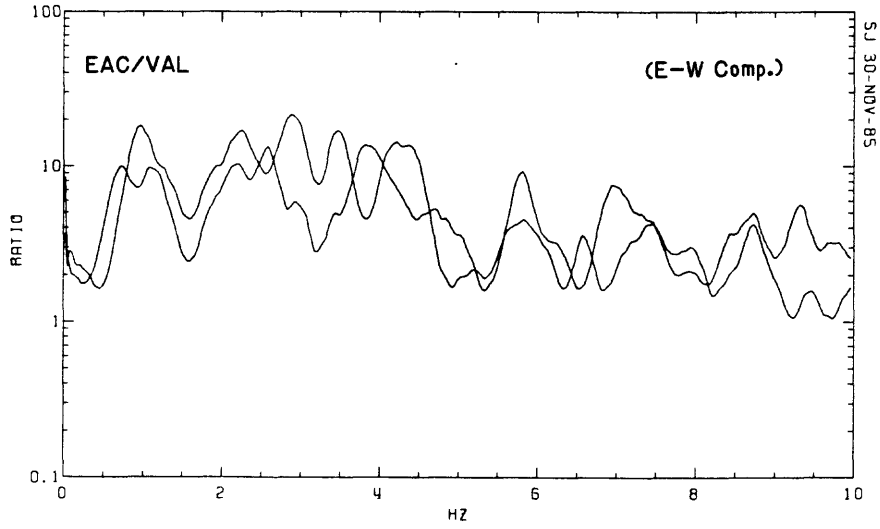

Figure 22. Spectral ratios of two different events, respectively, and their superimposed plot (E-W components) for stations EAC/VAL.

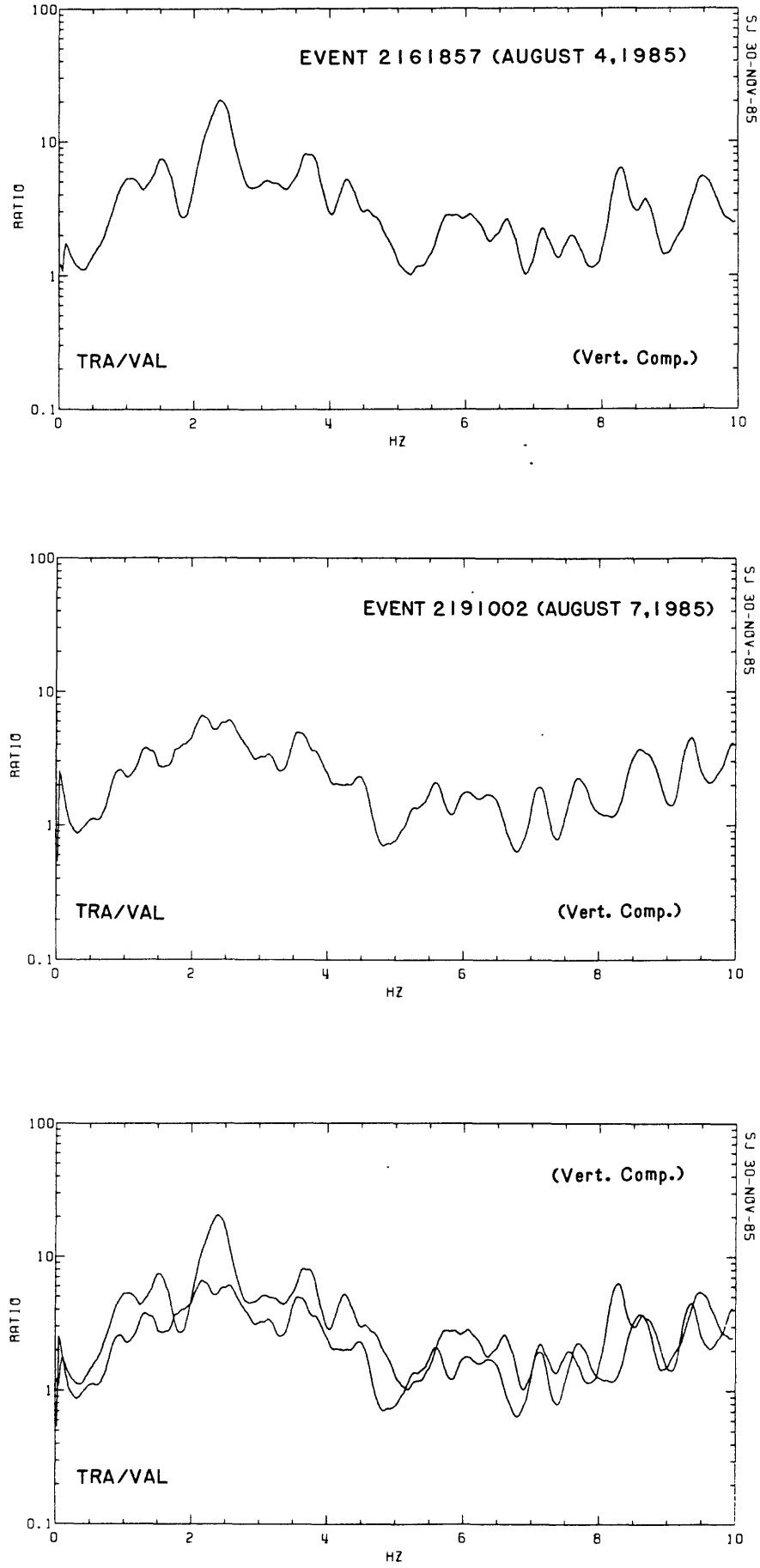

Figure 23. Spectral ratios of two different events, respectively, and their superimposed plot (vertical components) for stations TRA/VAL.

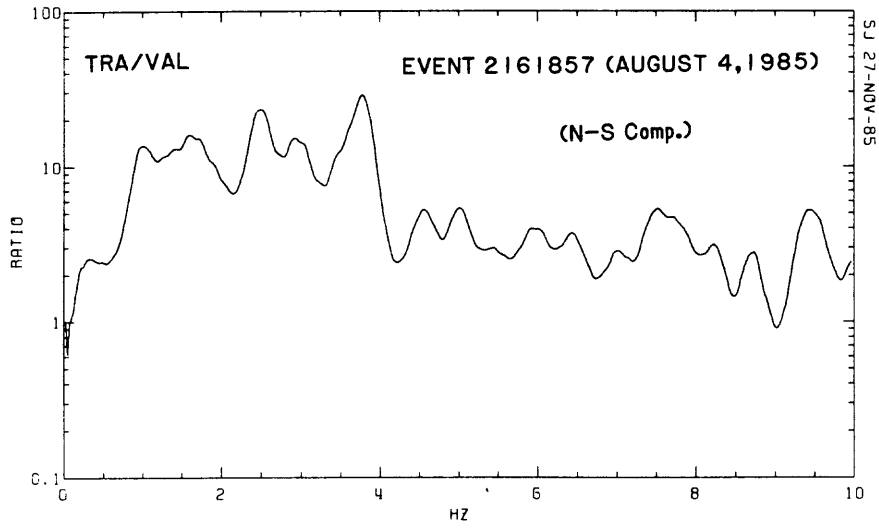

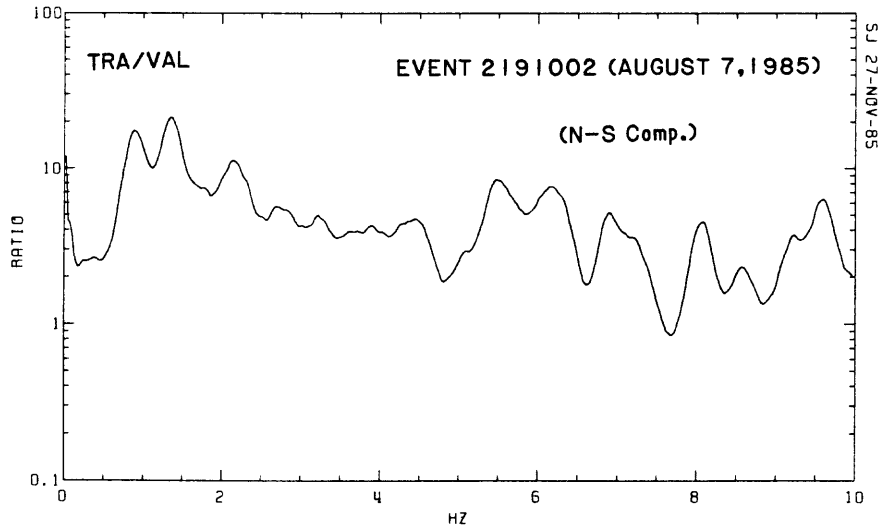

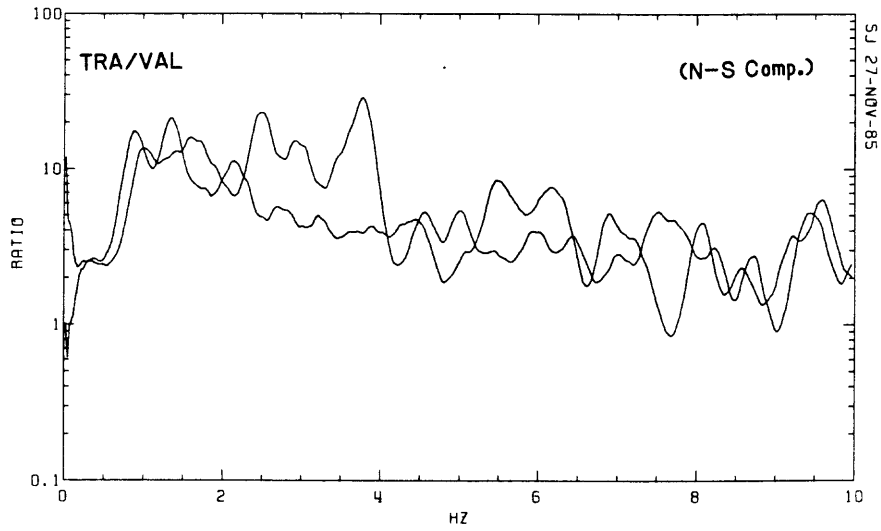

Figure 24. Spectral ratios of two different events, respectively, and their superimposed plot (N-S components) for stations TRA/VAL.

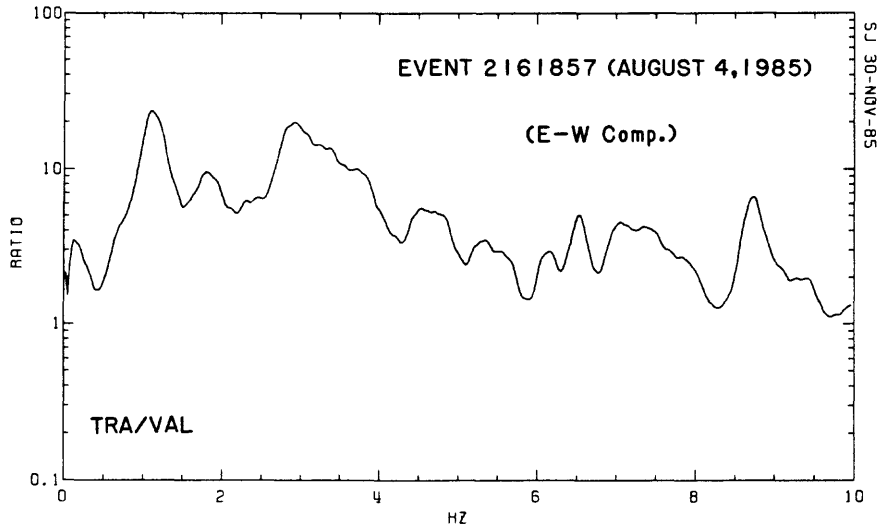

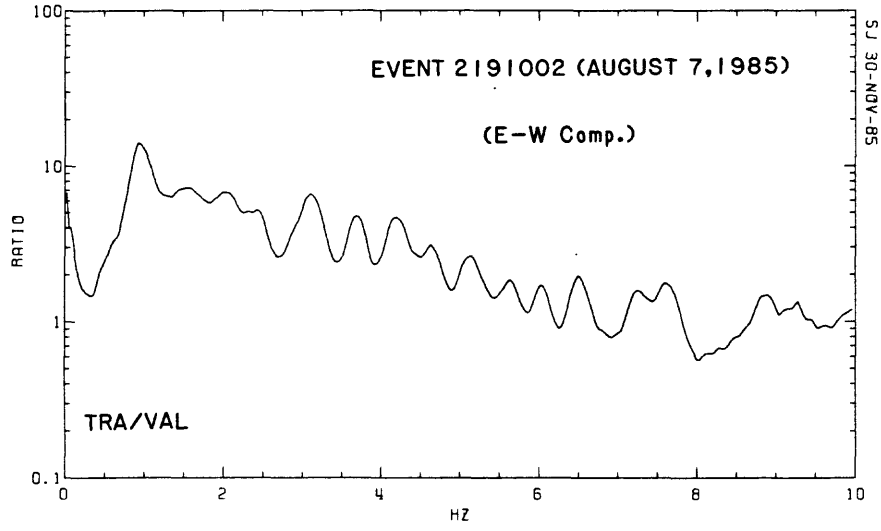

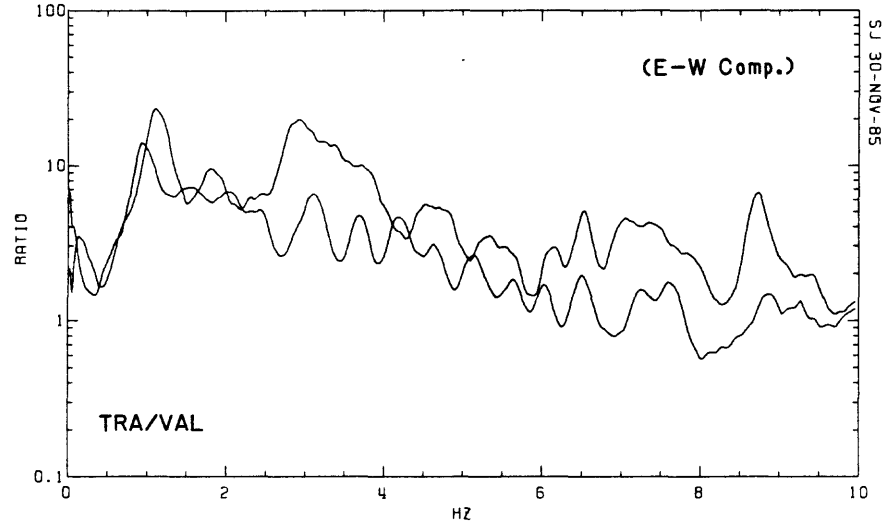

Figure 25. Spectral ratios of two different events, respectively, and their superimposed plot (E-W components) for stations TRA/VAL.

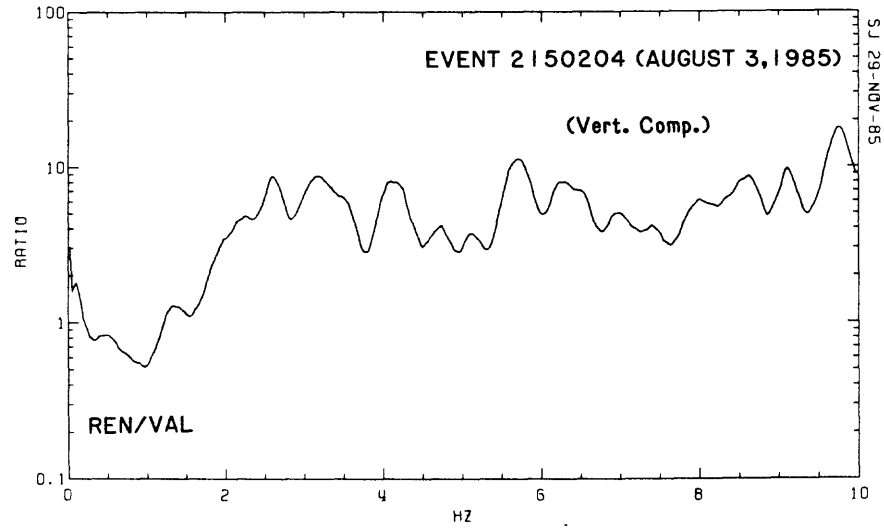

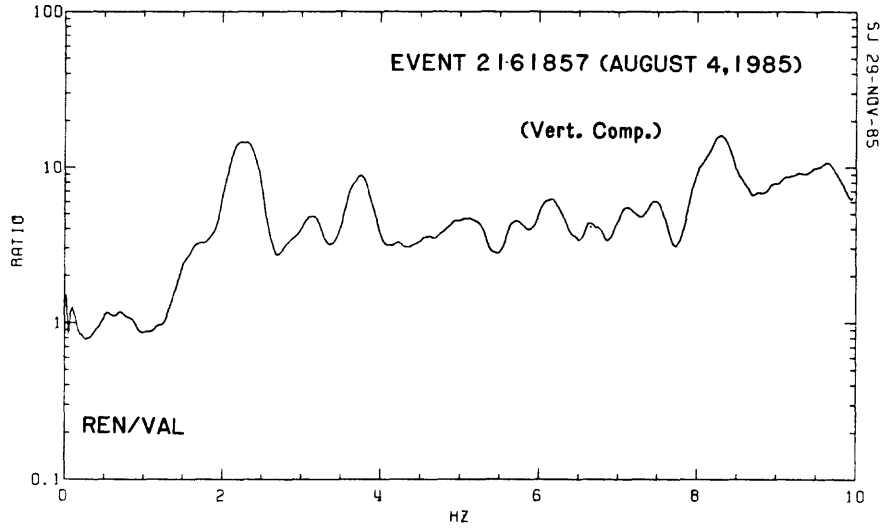

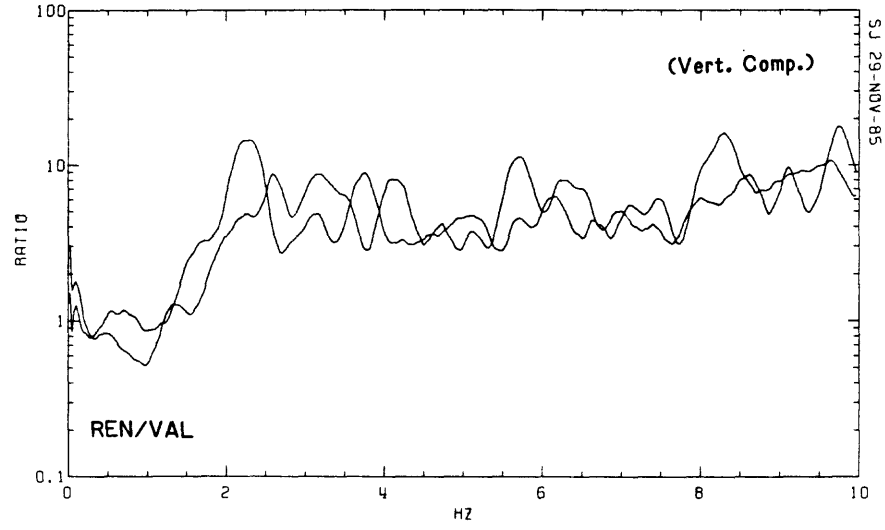

Figure 26. Spectral ratios of two different events, respectively, and their superimposed plot (vertical components) for stations REN/VAL.

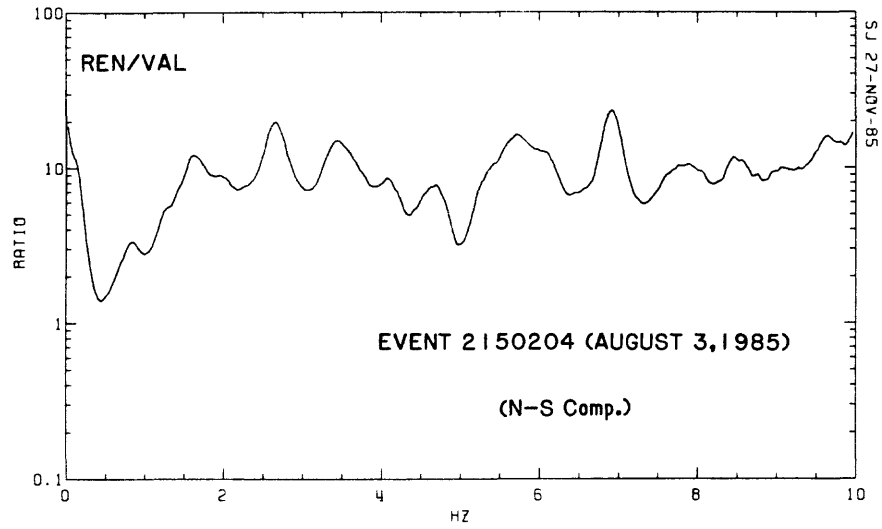

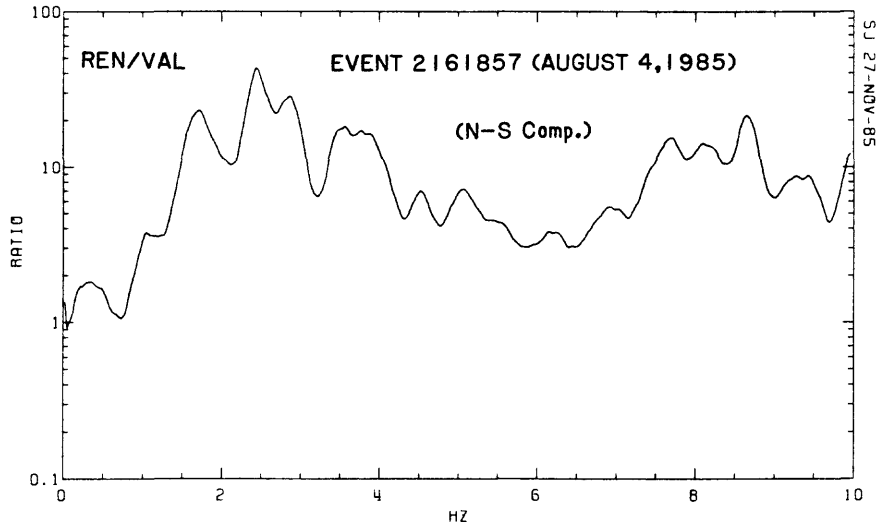

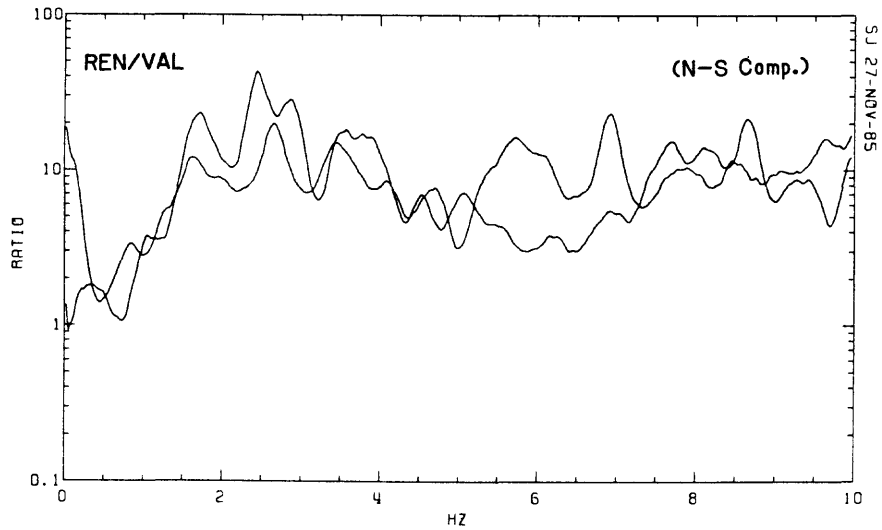

Figure 27. Spectral ratios of two different events, respectively, and their superimposed plot (N-S components) for stations REN/VAL.

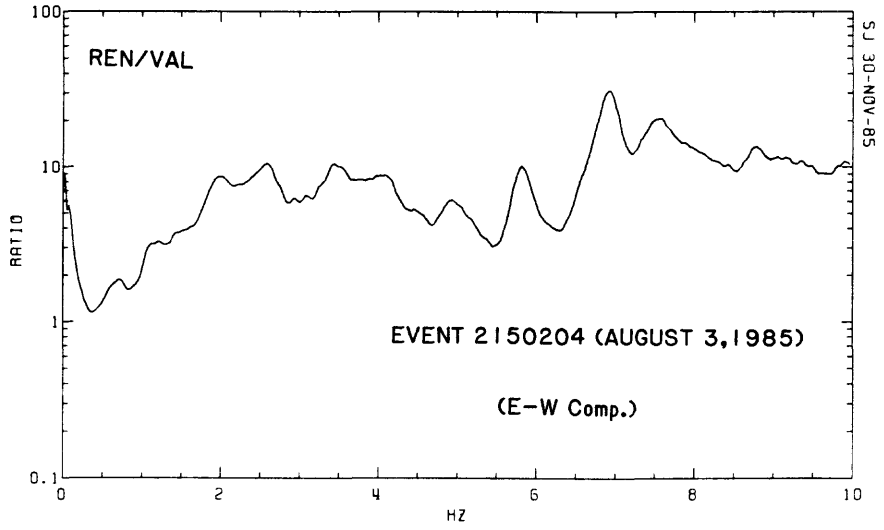

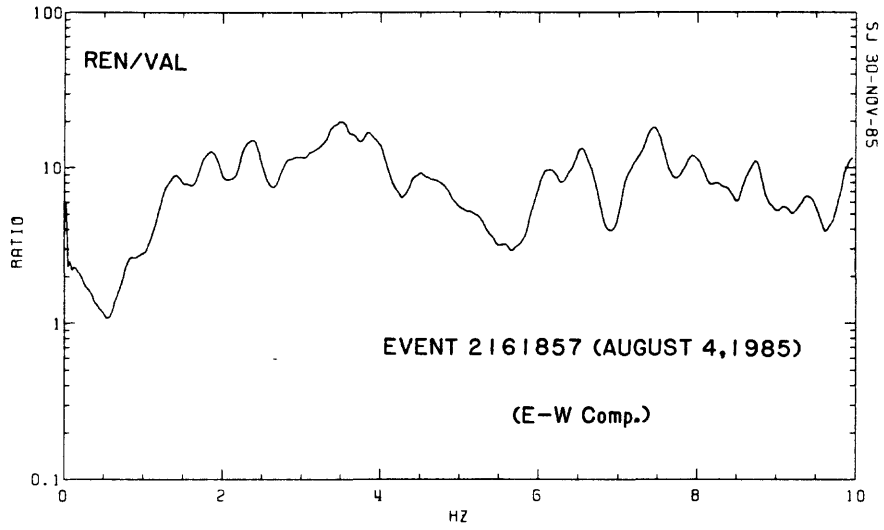

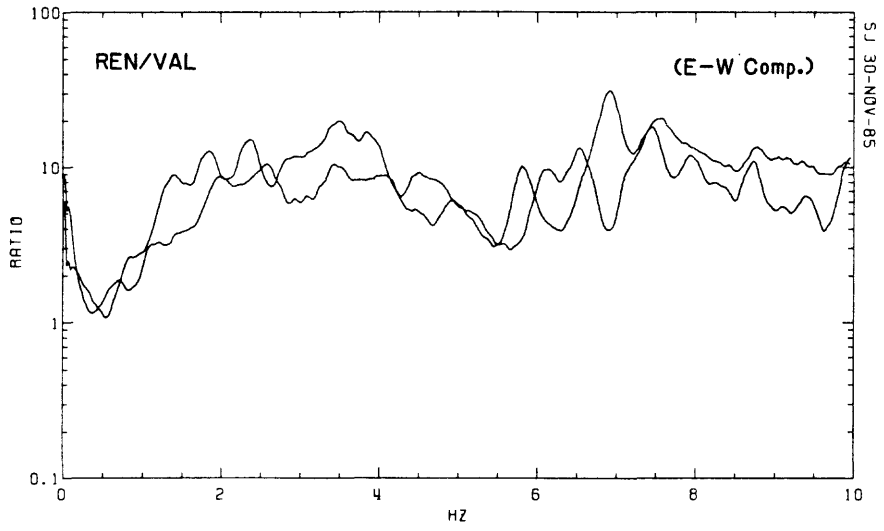

Figure 28. Spectral ratios of two different events, respectively, and their superimposed plot (E-W components) for stations REN/VAL.

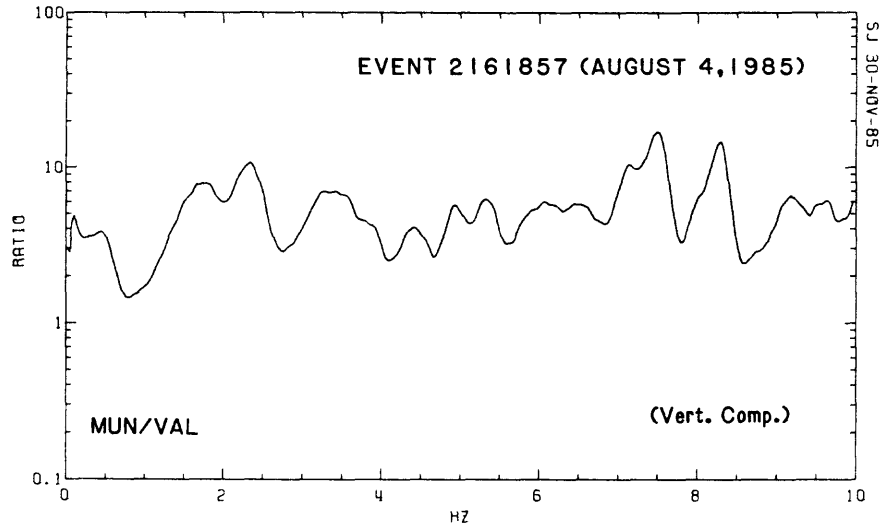

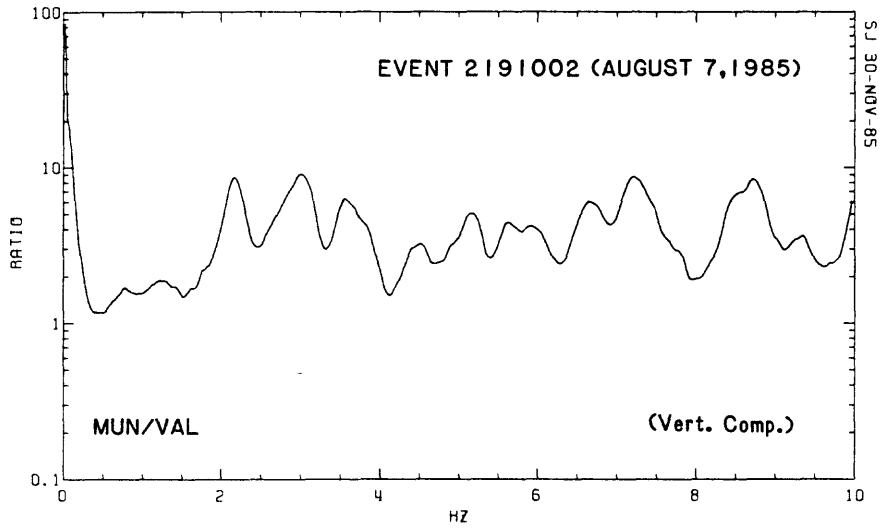

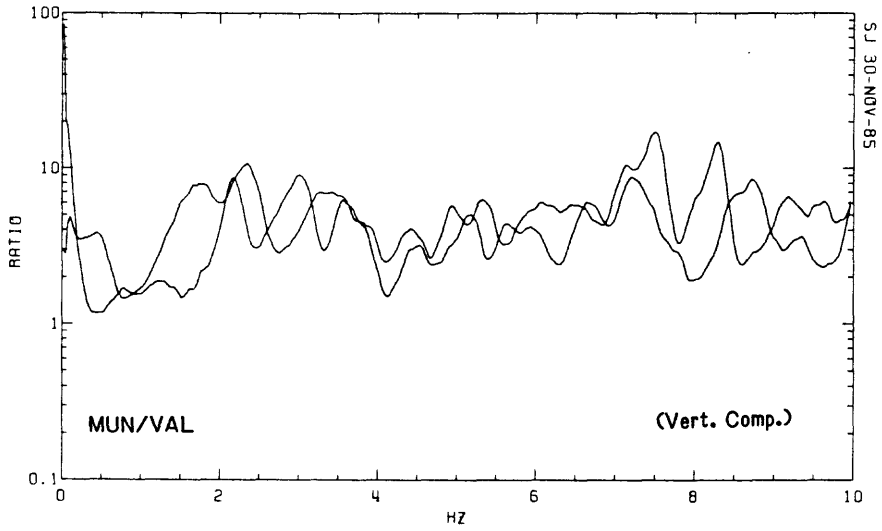

Figure 29. Spectral ratios of two different events, respectively, and their superimposed plot (vertical components) for stations MUN/VAL.

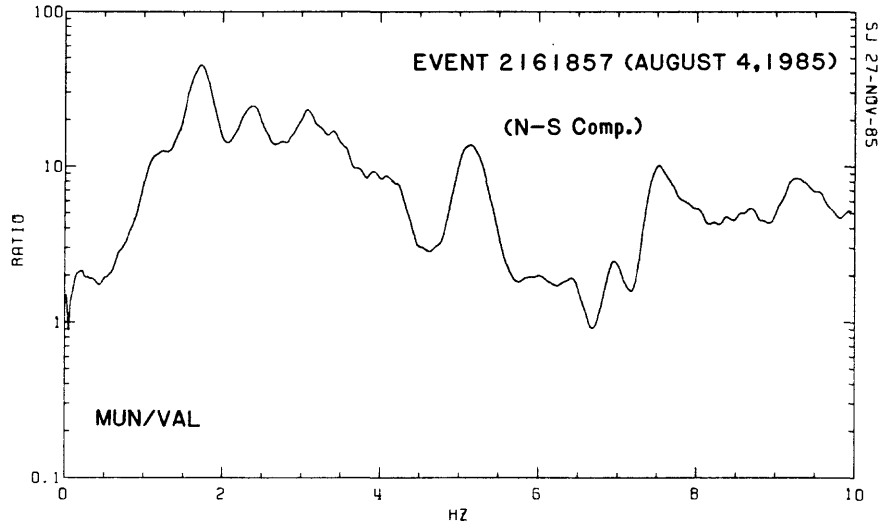

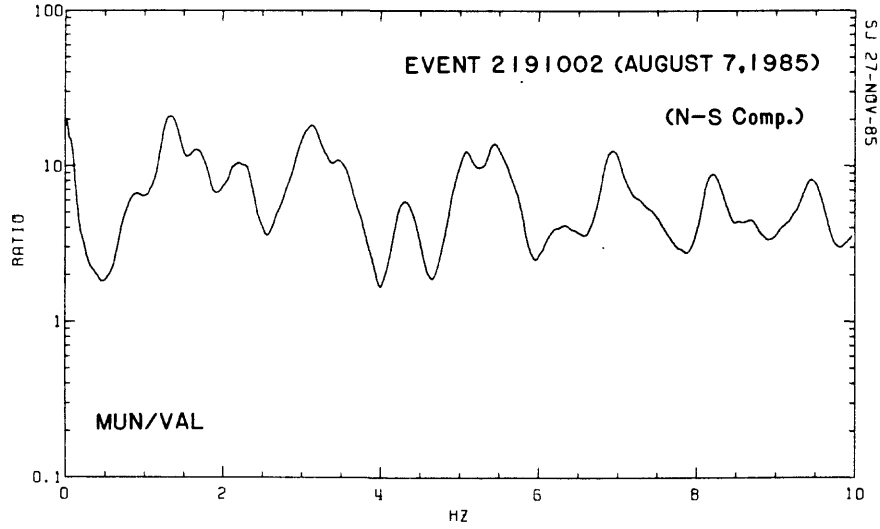

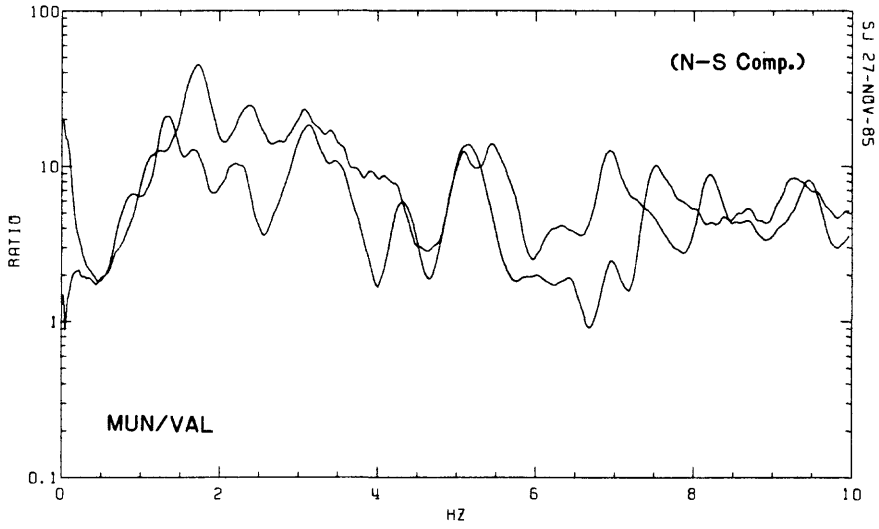

Figure 30. Spectral ratios of two different events, respectively, and their superimposed plot (N-S components) for stations MUN/VAL.

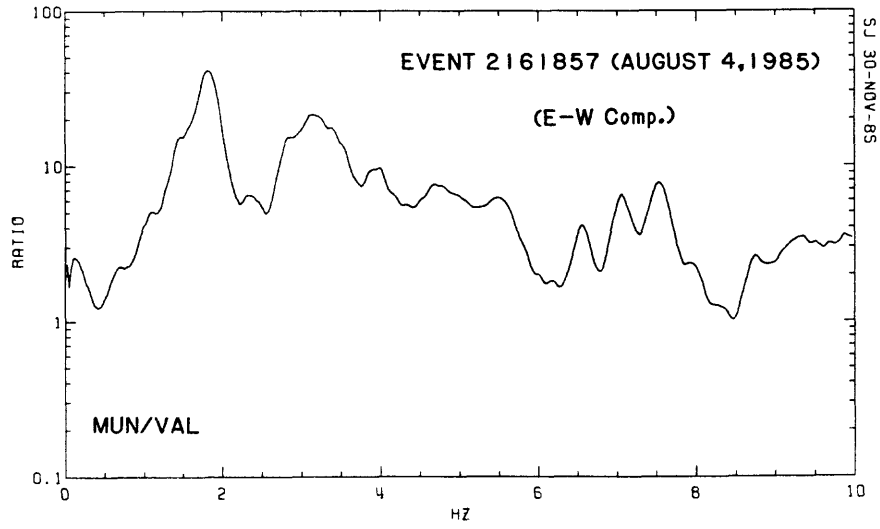

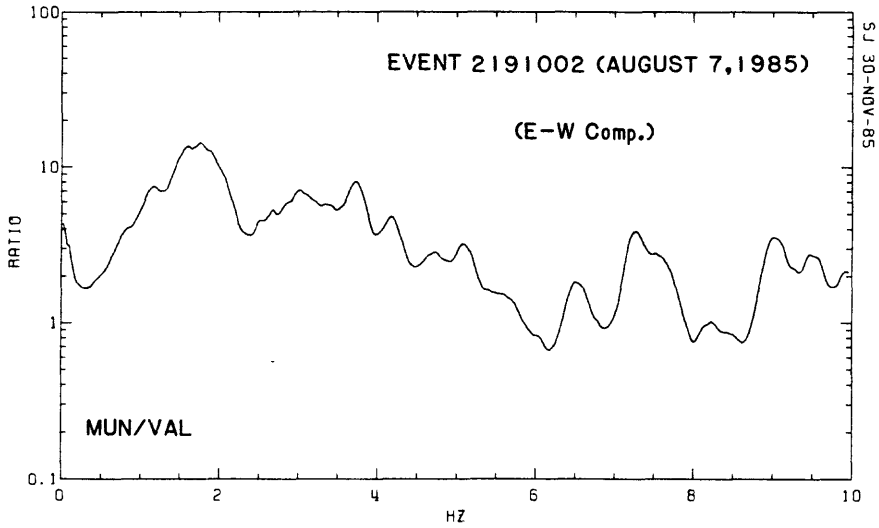

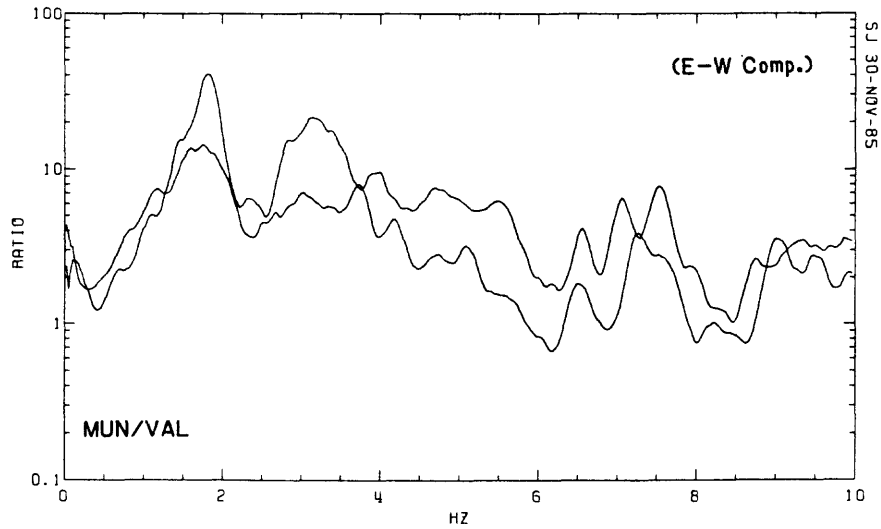

Figure 31. Spectral ratios of two different events, respectively, and their superimposed plot (E-W components) for stations MUN/VAL.

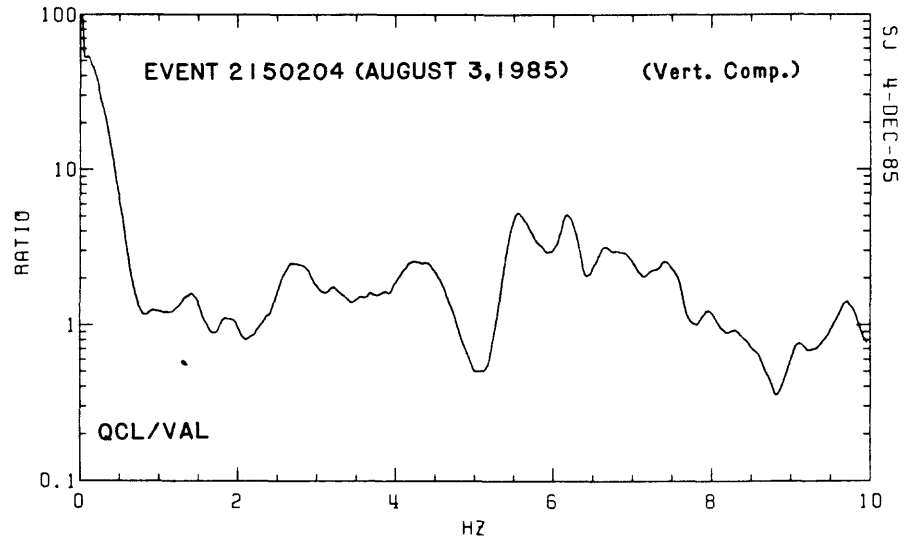

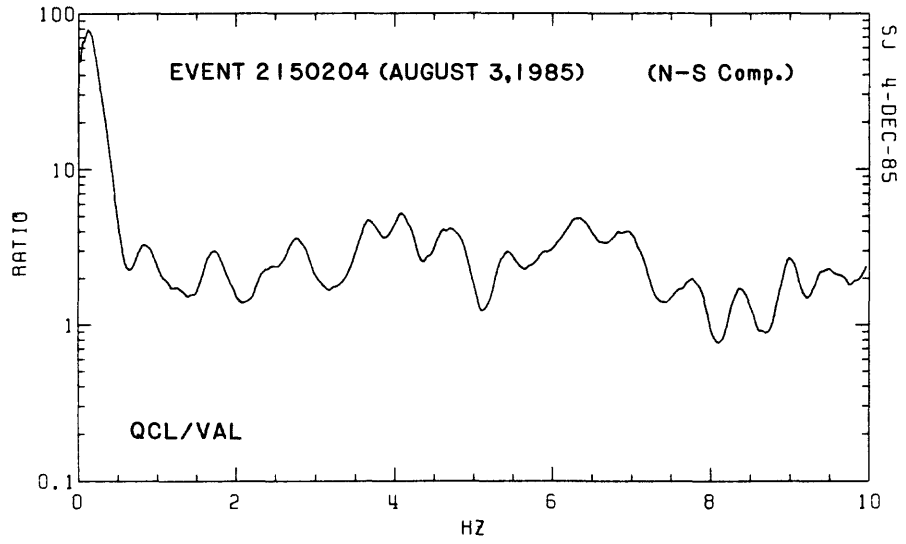

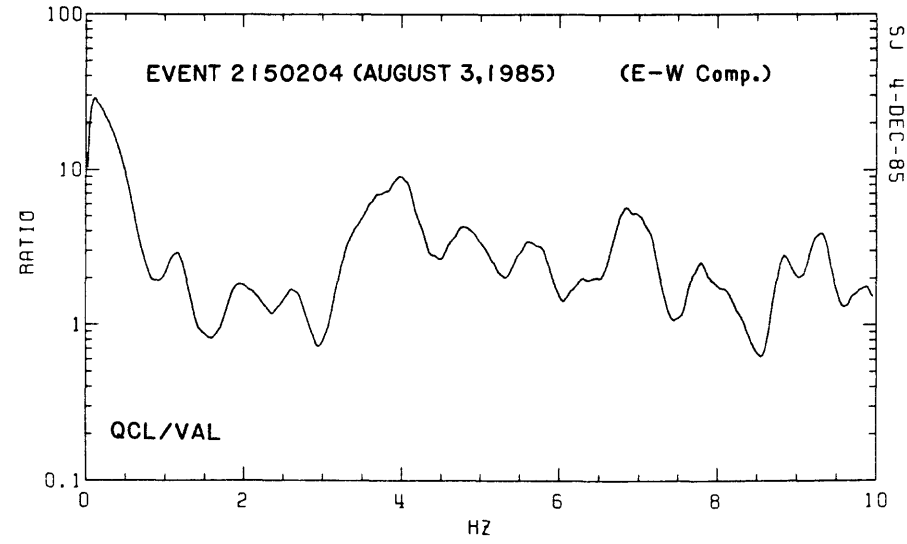

Figure 32. Spectral ratios of one event for vertical and horizontal (N-S and E-W) components, respectively, for stations QCL/VAL.

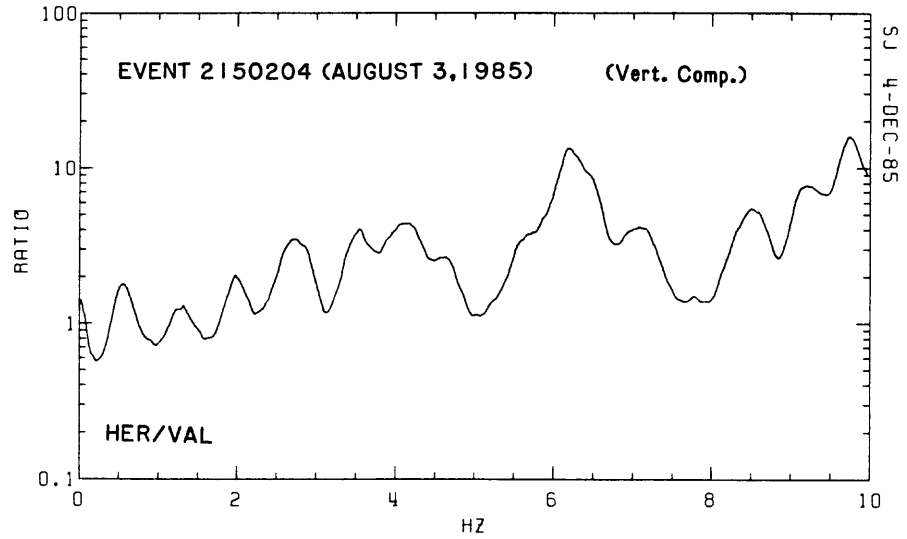

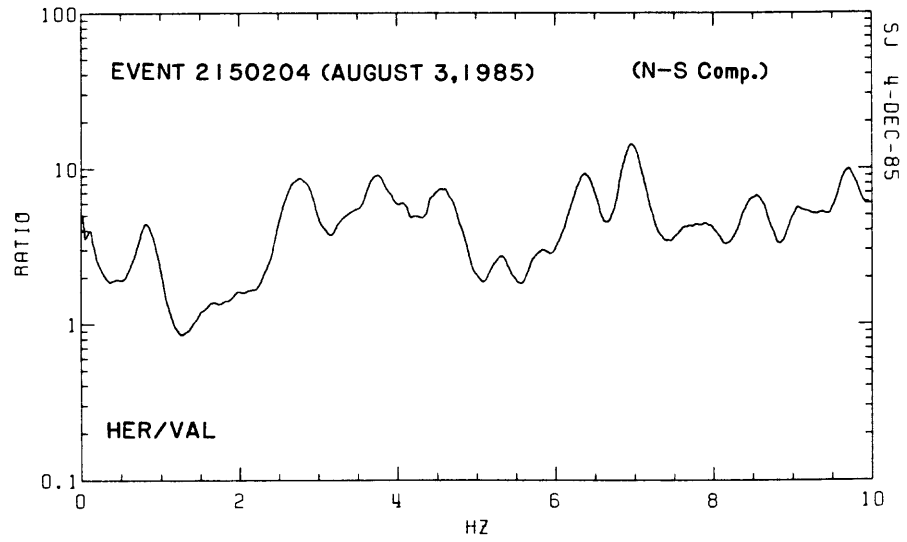

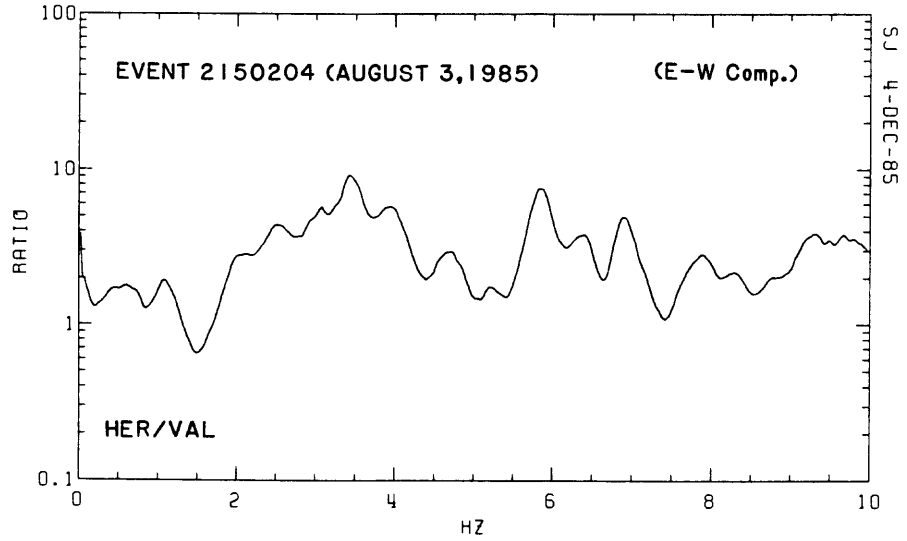

Figure 33. Spectral ratios of one event for vertical and horizontal (N-S and E-W) components, respectively, for stations HER/VAL.

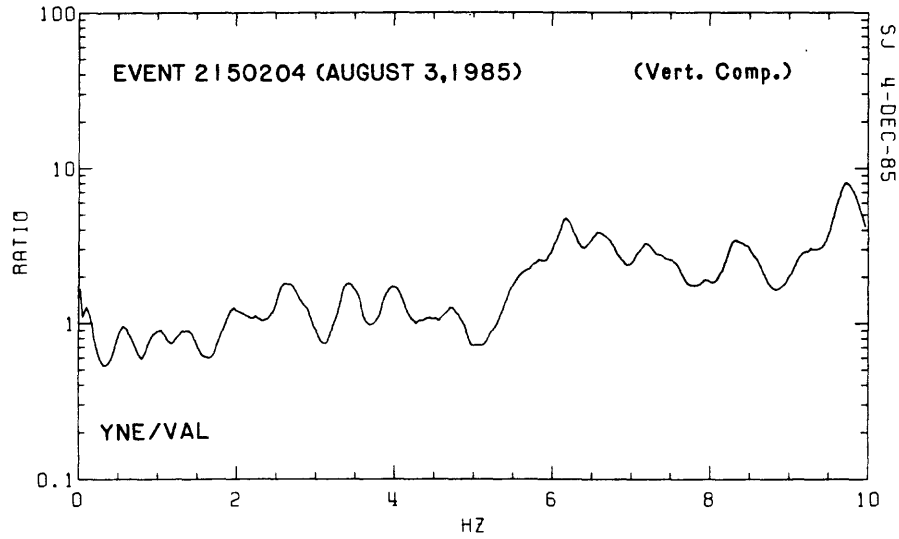

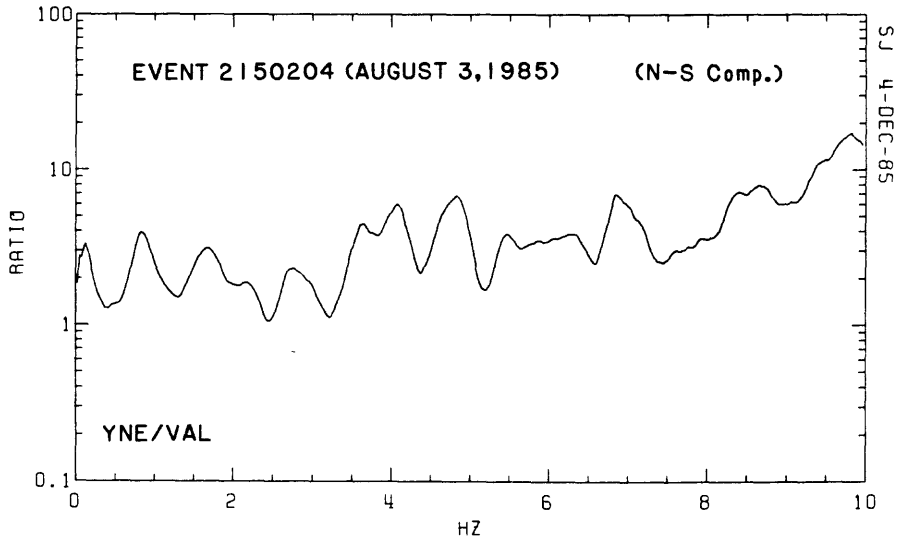

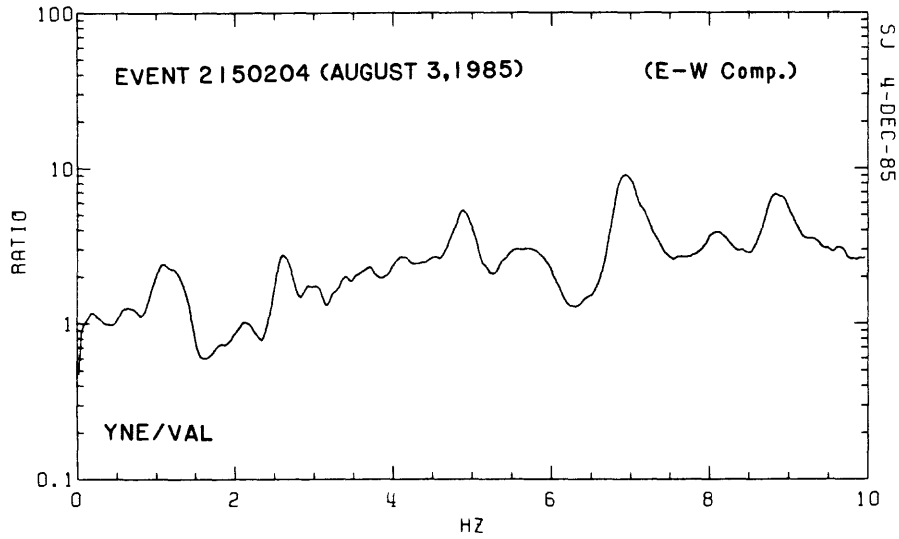

Figure 34. Spectral ratios of one event for vertical and horizontal (N-S and E-W) components, respectively, for stations YNE/VAL.

APPENDIX A
CANAL BEAGLE EXPERIMENT
SEISMOGRAMS, FOURIER AMPLITUDE SPECTRA, AND SPECTRAL RATIOS

The objective of this appendix is to provide in a compact format the seismograms, Fourier amplitude spectra and spectral ratios related to Canal Beagle experiment only. Selected plots of data processed by C. Mueller and J. Watson are presented herein.

The plots are organized as follows:

Event	Type of Plot	Figure(s)
2100652	Seismograms	A1-A3
	Fourier amplitude spectra	A4-A9
	Spectral ratios	A10-18
2101609	Seismograms	A19-A21
	Fourier amplitude spectra	A22-A27
	Spectral ratios	A28-A36
2110933	Seismograms	A37-A39
	Fourier amplitude spectra	A40-A45
	Spectral ratios	A46-A50
2111208	Seismograms	A51-A53
	Fourier Amplitude Spectra	A54-A60
	Spectral Ratios	A61-A70

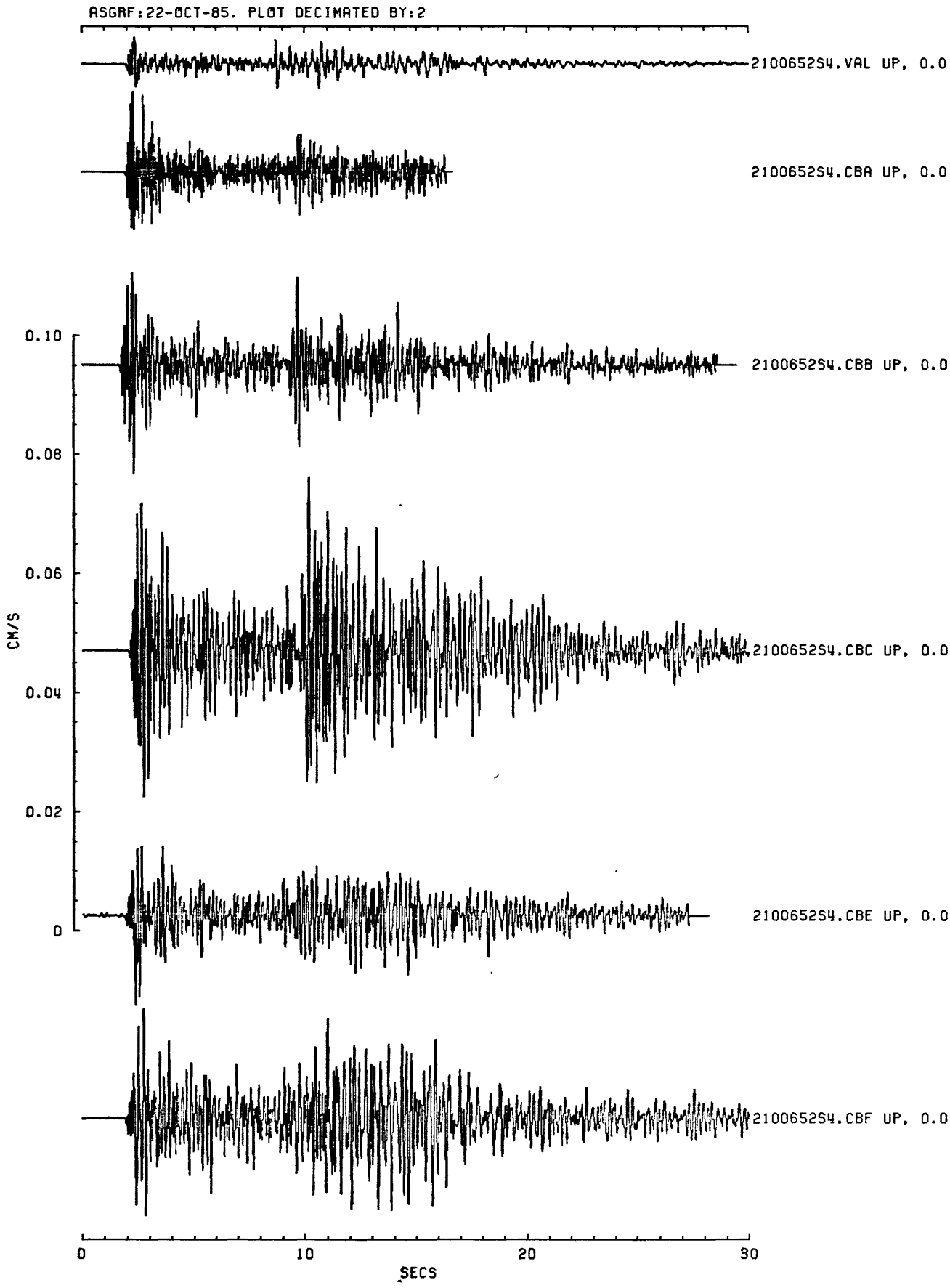

Figure A1. Scaled seismograms for event 2100652S (vertical components).

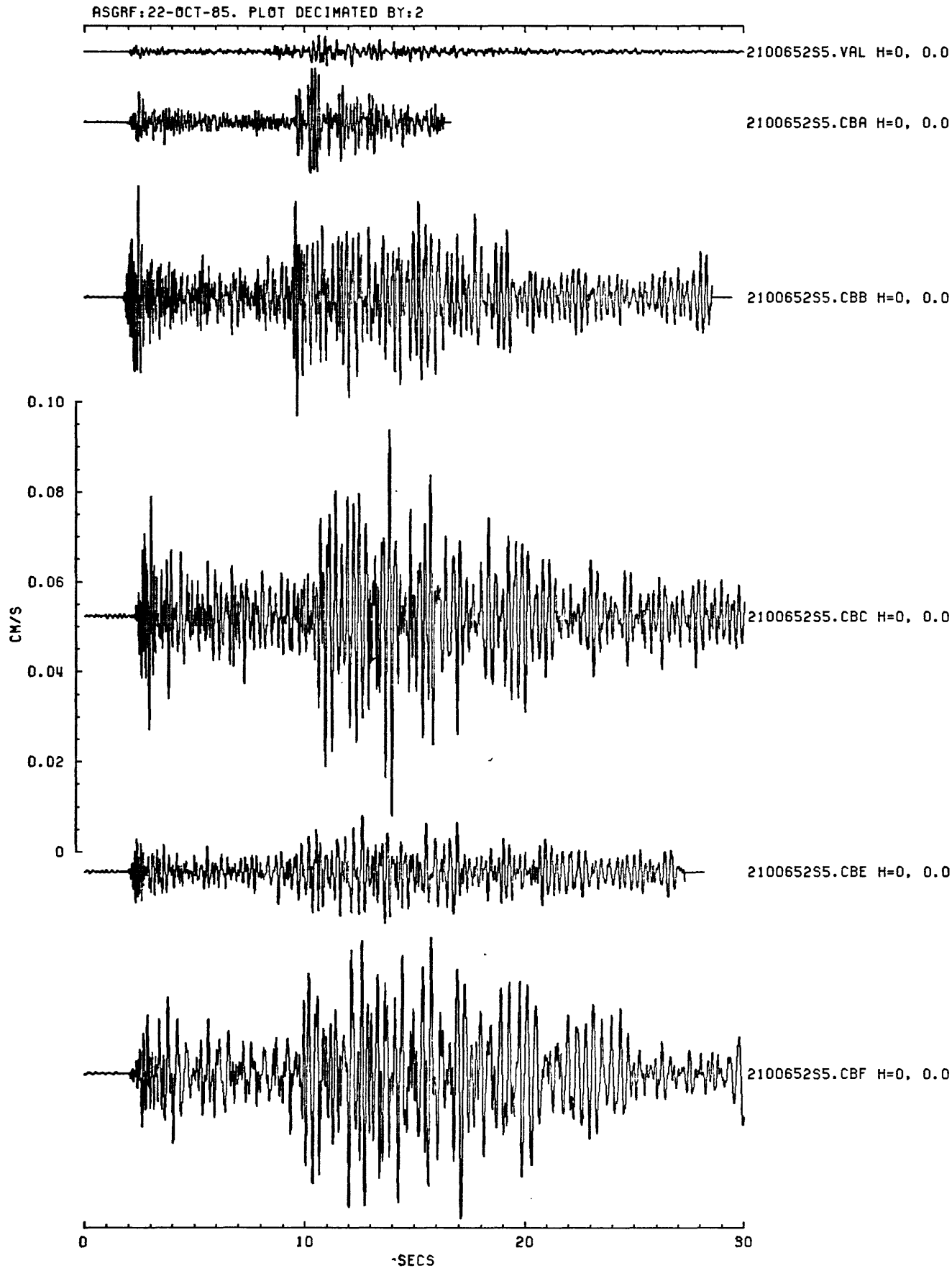

Figure A2. Scaled seismograms for event 2100652S (N-S components).

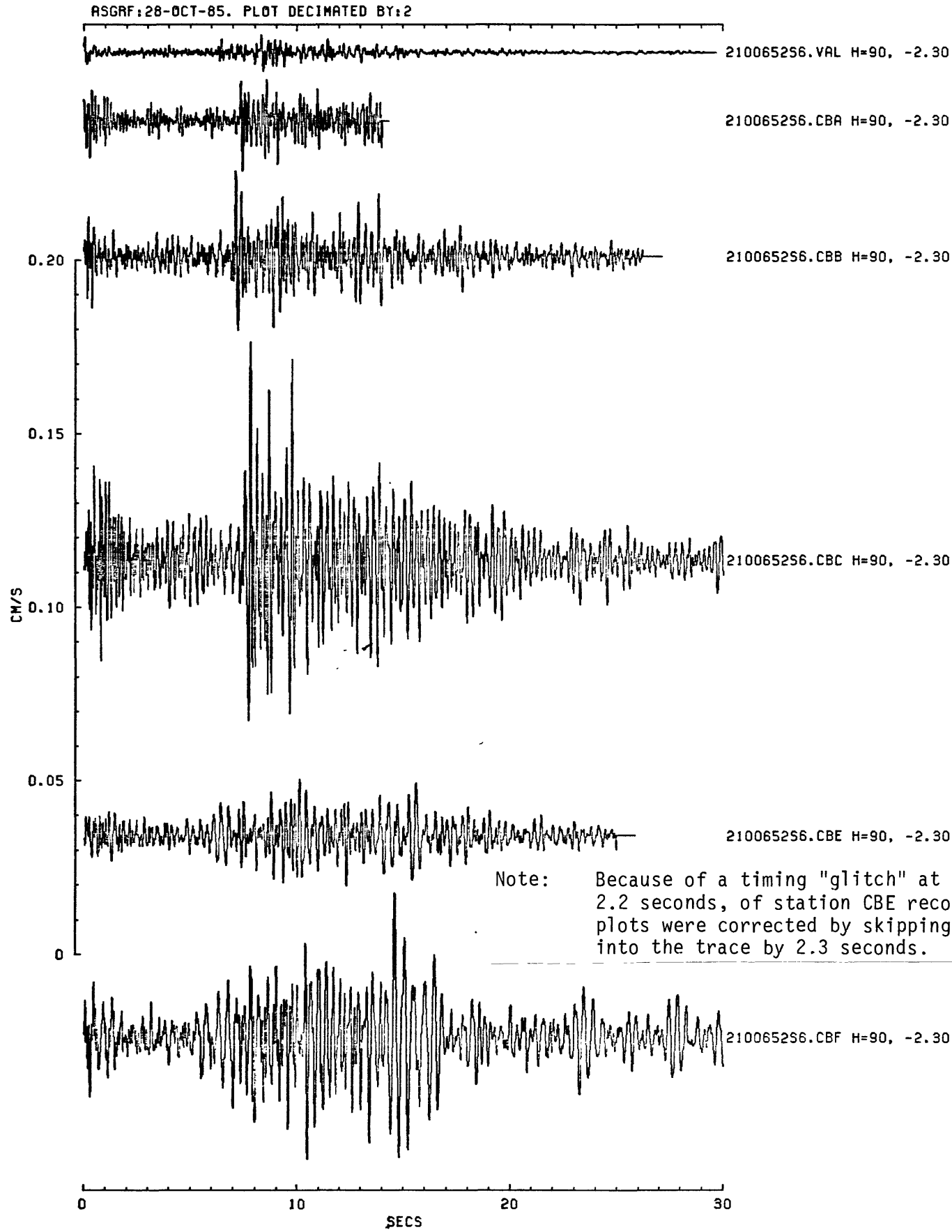

Note: Because of a timing "glitch" at 2.2 seconds, of station CBE records, plots were corrected by skipping into the trace by 2.3 seconds.

Figure A3. Scaled seismograms for event 2100652S (E-W components).

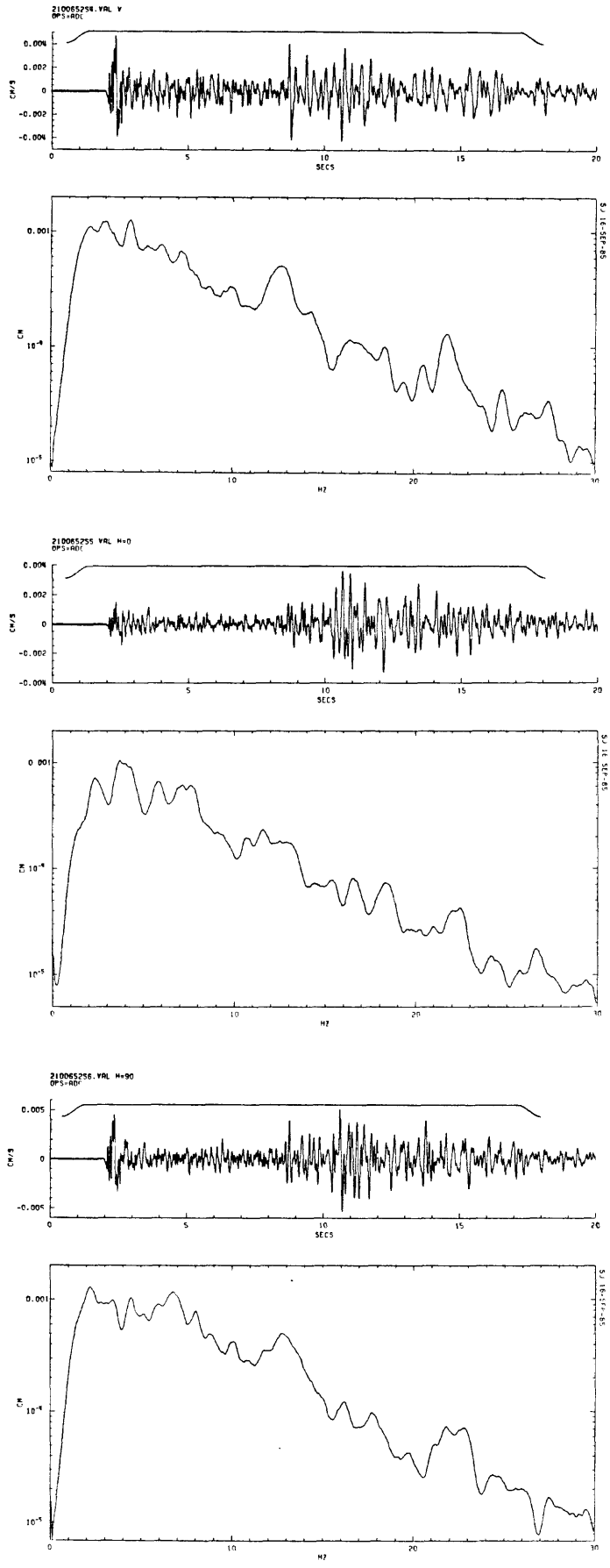

Figure A4. Time series and Fourier amplitude spectra of event on July 29, 1985 (Julian 210) at 06:52 for the vertical, horizontal (N-S and E-W) components, respectively, for station VAL.

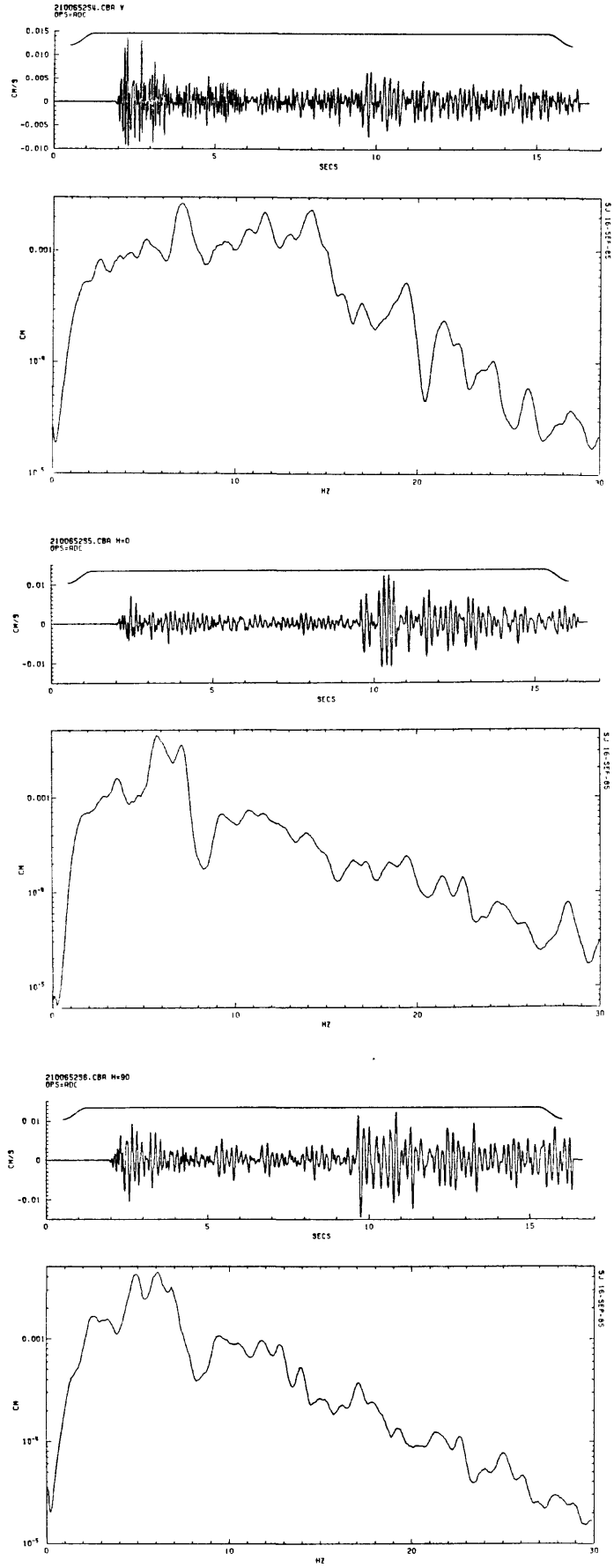

Figure A5. Time series and Fourier amplitude spectra of event on July 29, 1985 (Julian 210) at 06:52 for the vertical, horizontal (N-S and E-W) components, respectively, for station CBA.

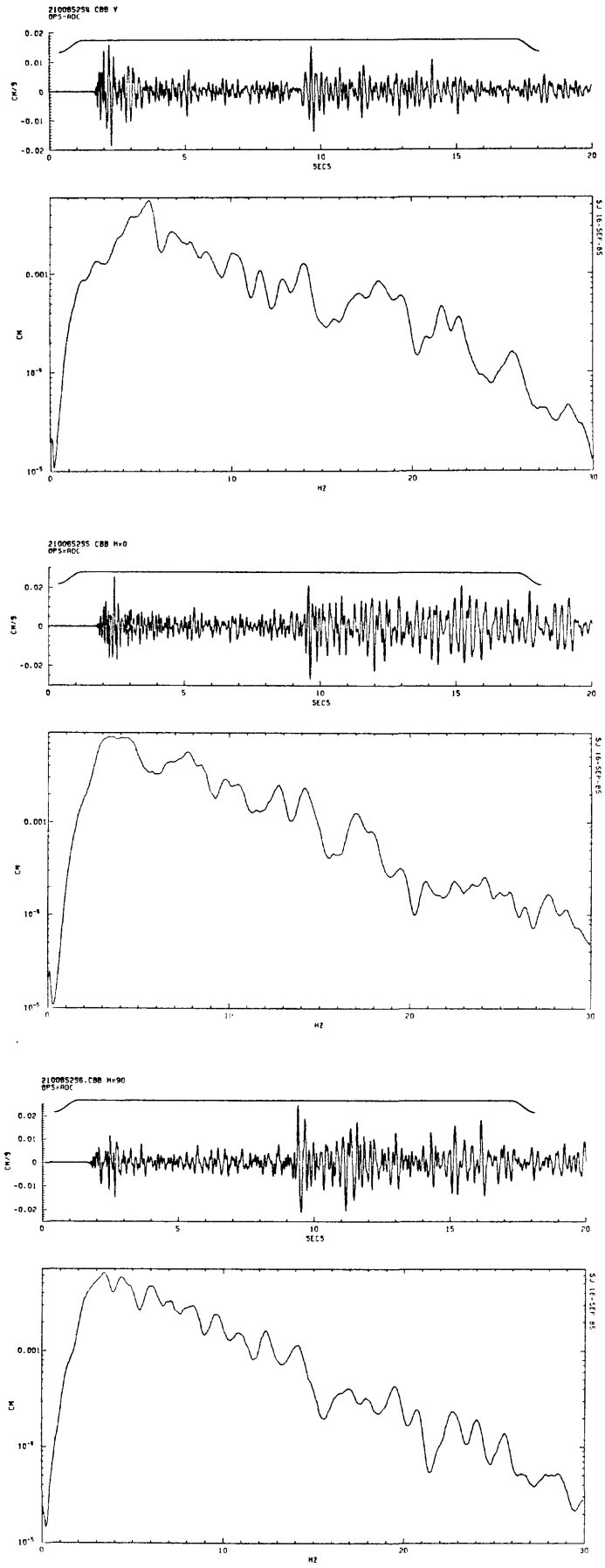

Figure A6. Time series and Fourier amplitude spectra of event on July 29, 1985 (Julian 210) at 06:52 for the vertical, horizontal (N-S and E-W) components, respectively, for station CBB.

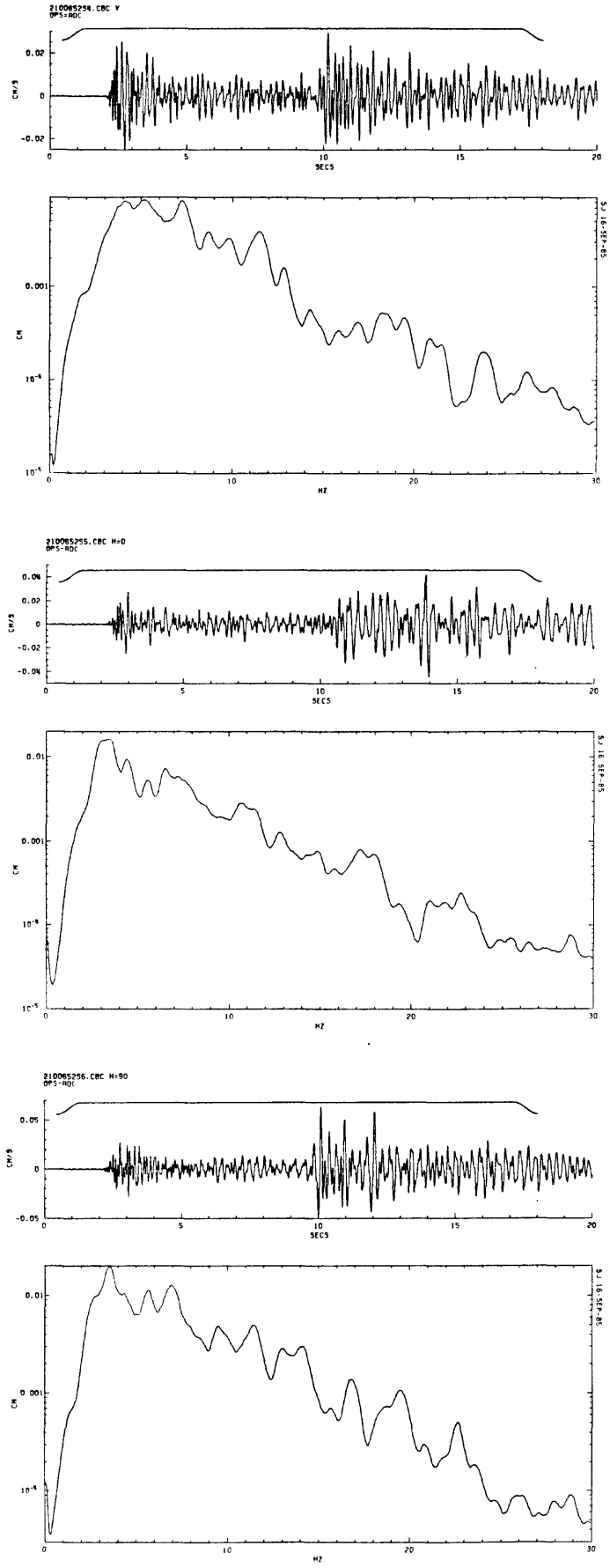

Figure A7. Time series and Fourier amplitude spectra of event on July 29, 1985 (Julian 210) at 06:52 for the vertical, horizontal (N-S and E-W) components, respectively, for station CBC.

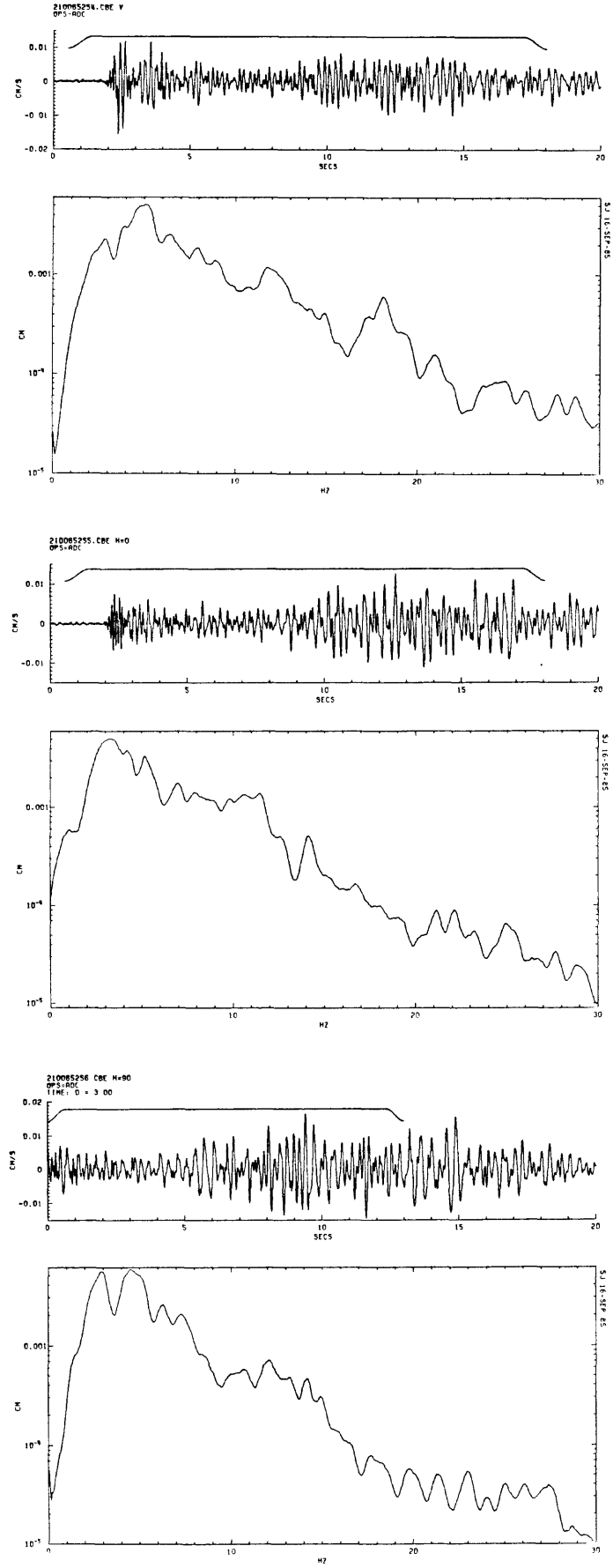

Figure A8. Time series and Fourier amplitude spectra of event on July 29, 1985 (Julian 210) at 06:52 for the vertical, horizontal (N-S and E-W) components, respectively, for station CBE.

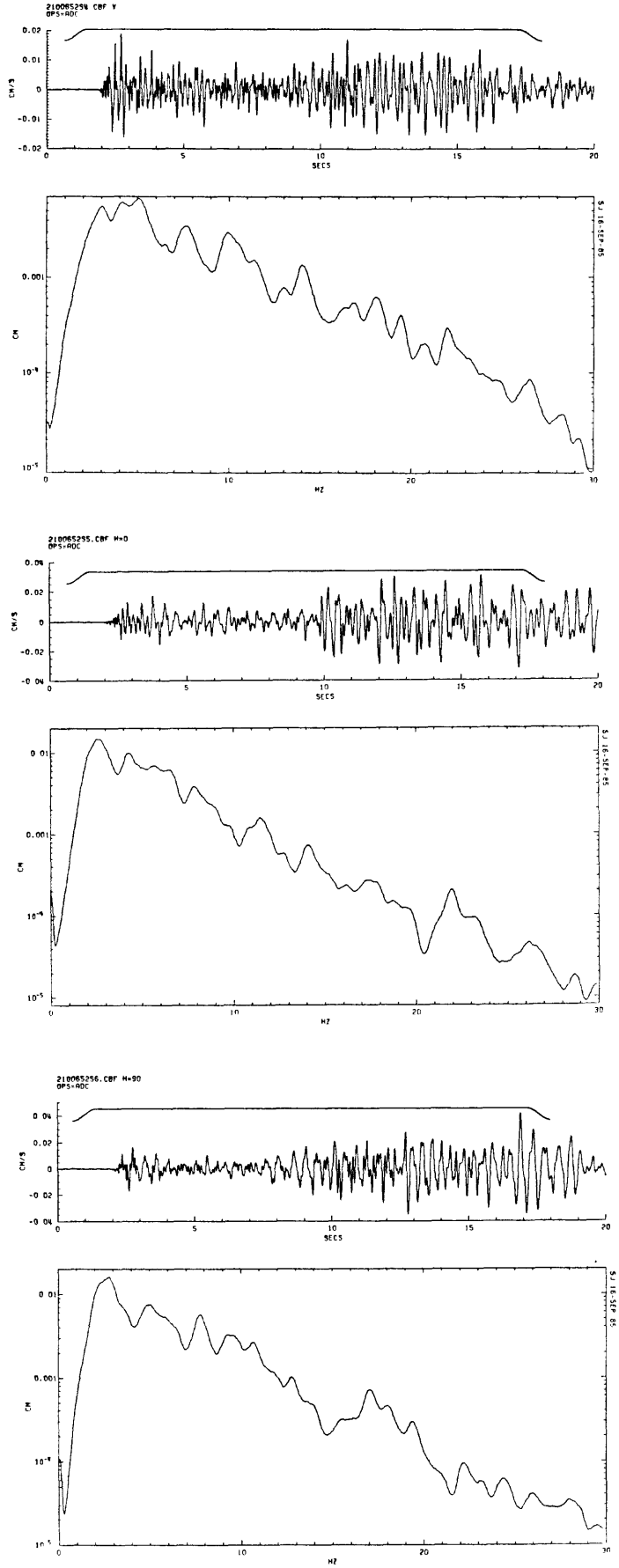

Figure A9. Time series and Fourier amplitude spectra of event on July 29, 1985 (Julian 210) at 06:52 for the vertical, horizontal (N-S and E-W) components, respectively, for station CBF.

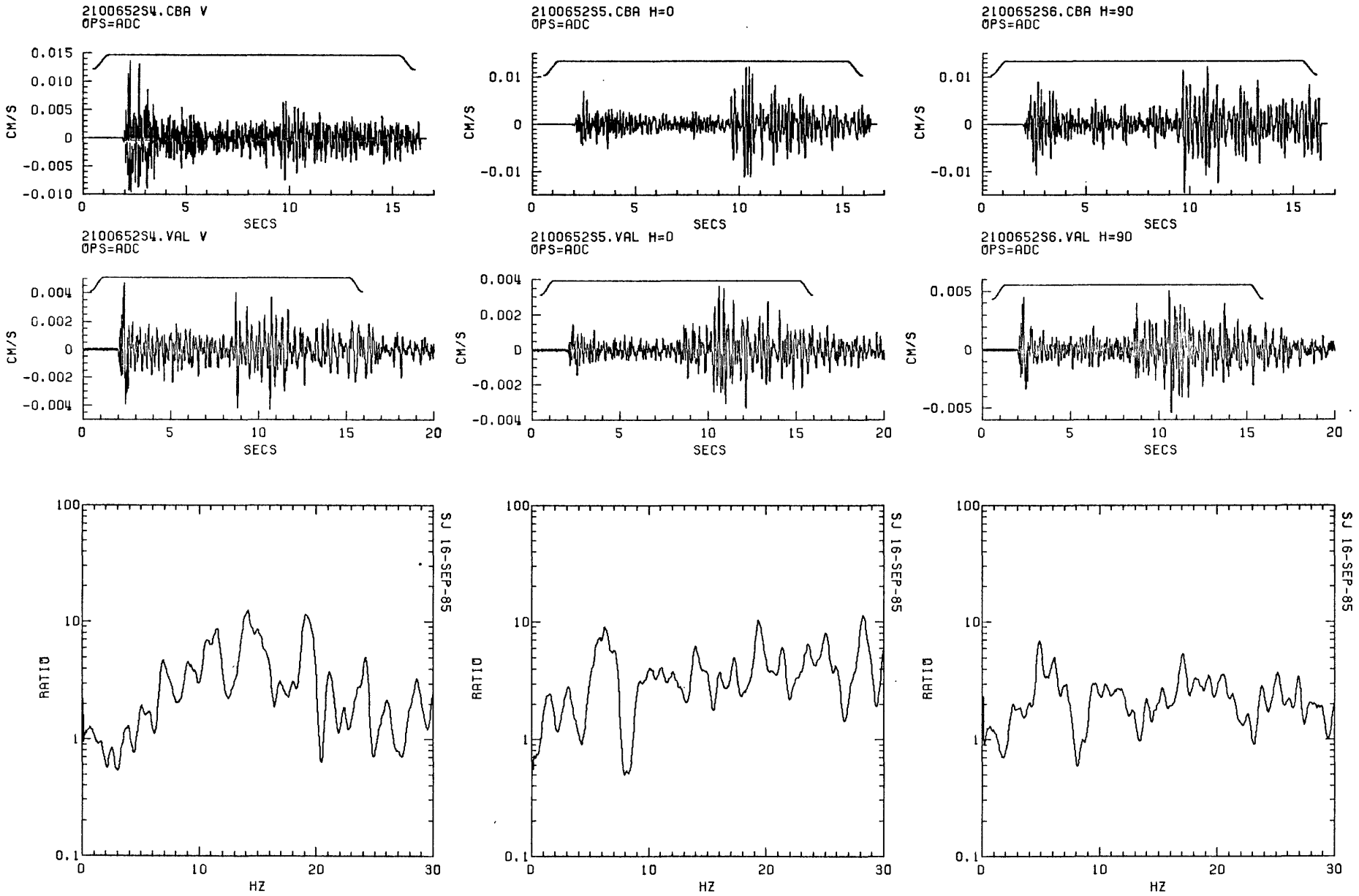

Figure A10. Scaled seismograms and spectral ratios of event on July 29, 1985 (Julian 210) at 06:52 for the vertical, horizontal (N-S and E-W) components, respectively, for station CBA/VAL.

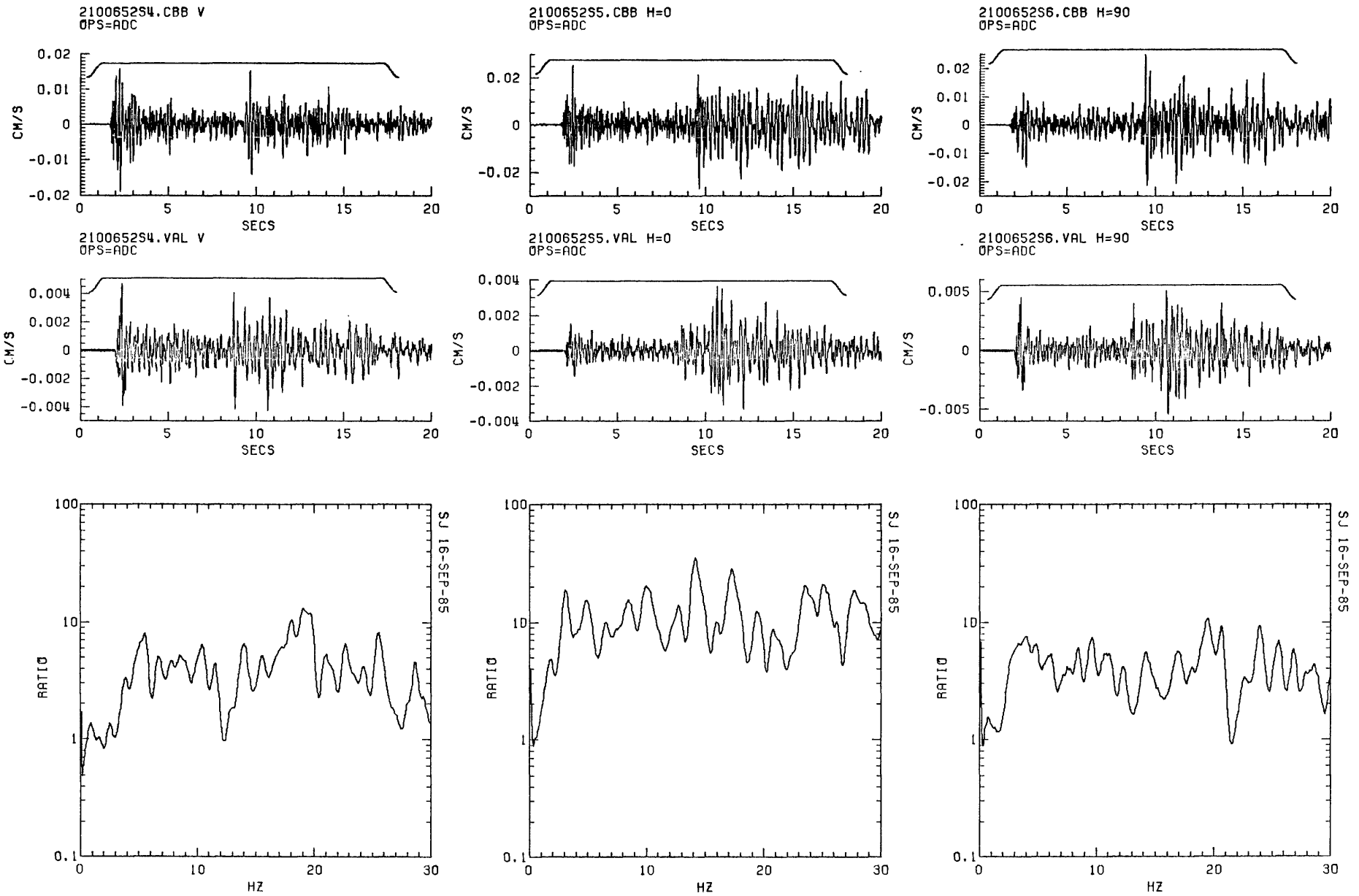

Figure A11. Scaled seismograms and spectral ratios of event on July 29, 1985 (Julian 210) at 06:52 for the vertical, horizontal (N-S and E-W) components, respectively, for station CBB/VAL.

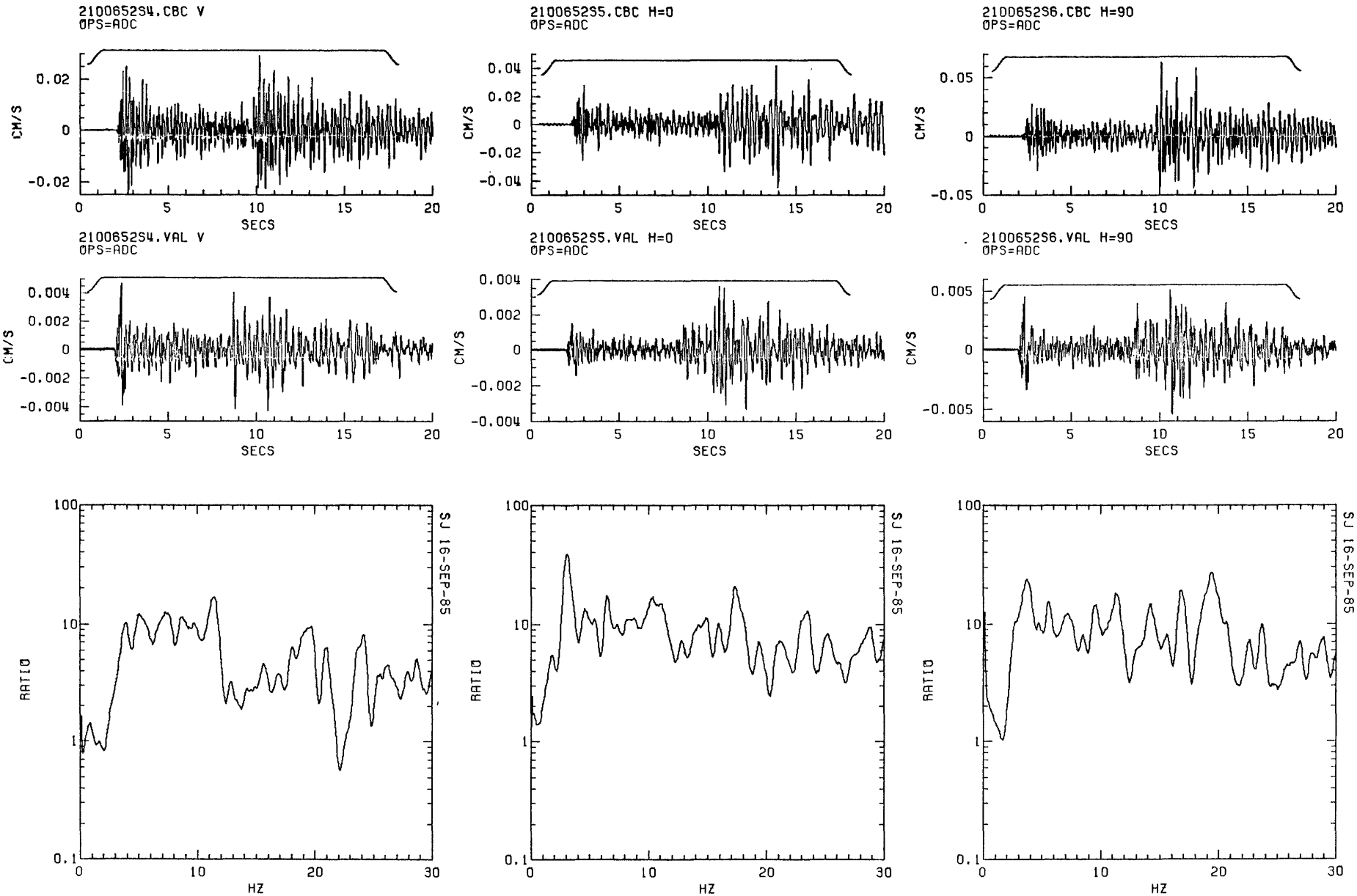

Figure A12. Scaled seismograms and spectral ratios of event on July 29, 1985 (Julian 210) at 06:52 for the vertical, horizontal (N-S and E-W) components, respectively, for station CBC/VAL.

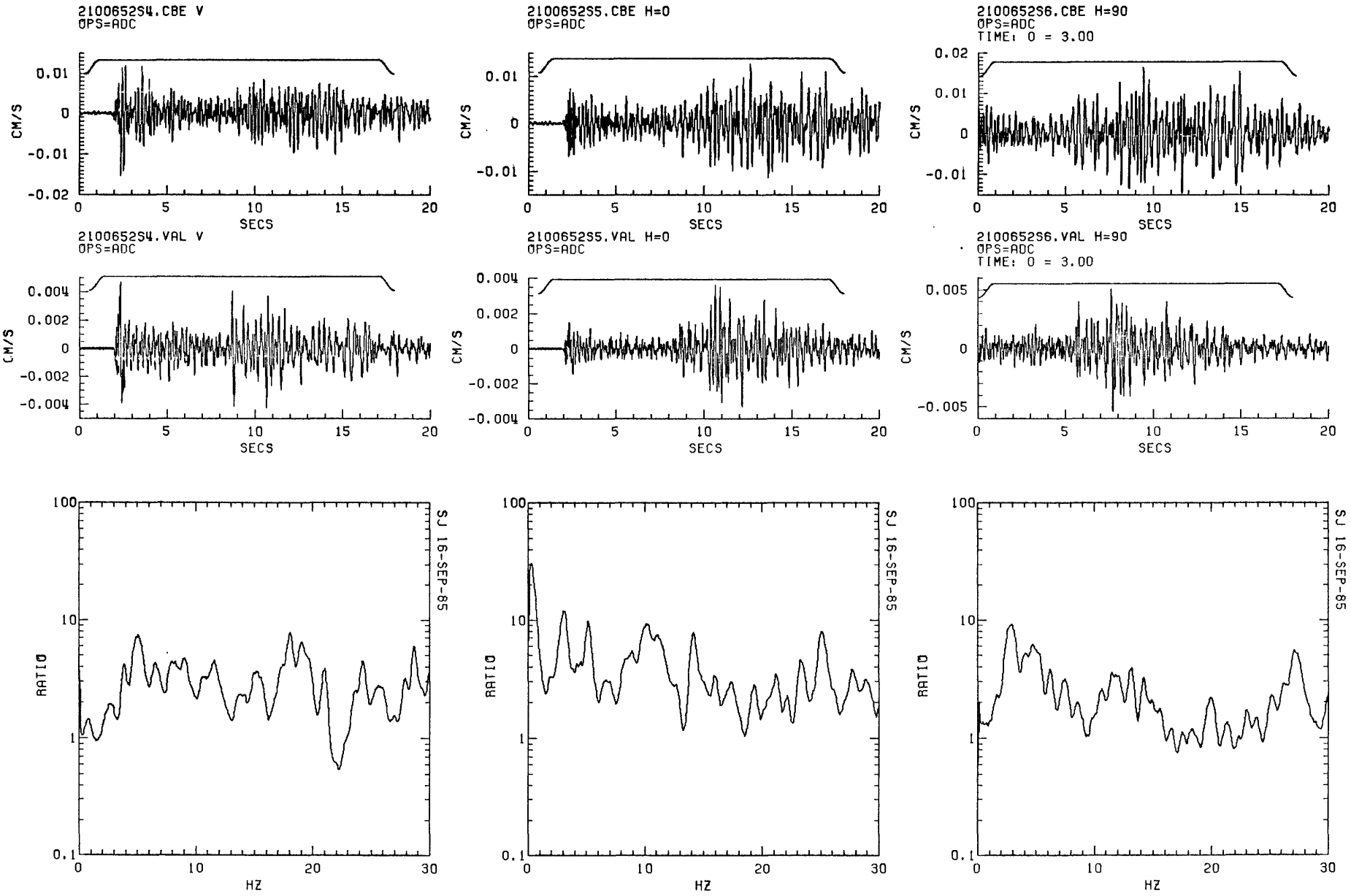

Figure A13. Scaled seismograms and spectral ratios of event on July 29, 1985 (Julian 210) at 06:52 for the vertical, horizontal (N-S and E-W) components, respectively, for station CBE/VAL.

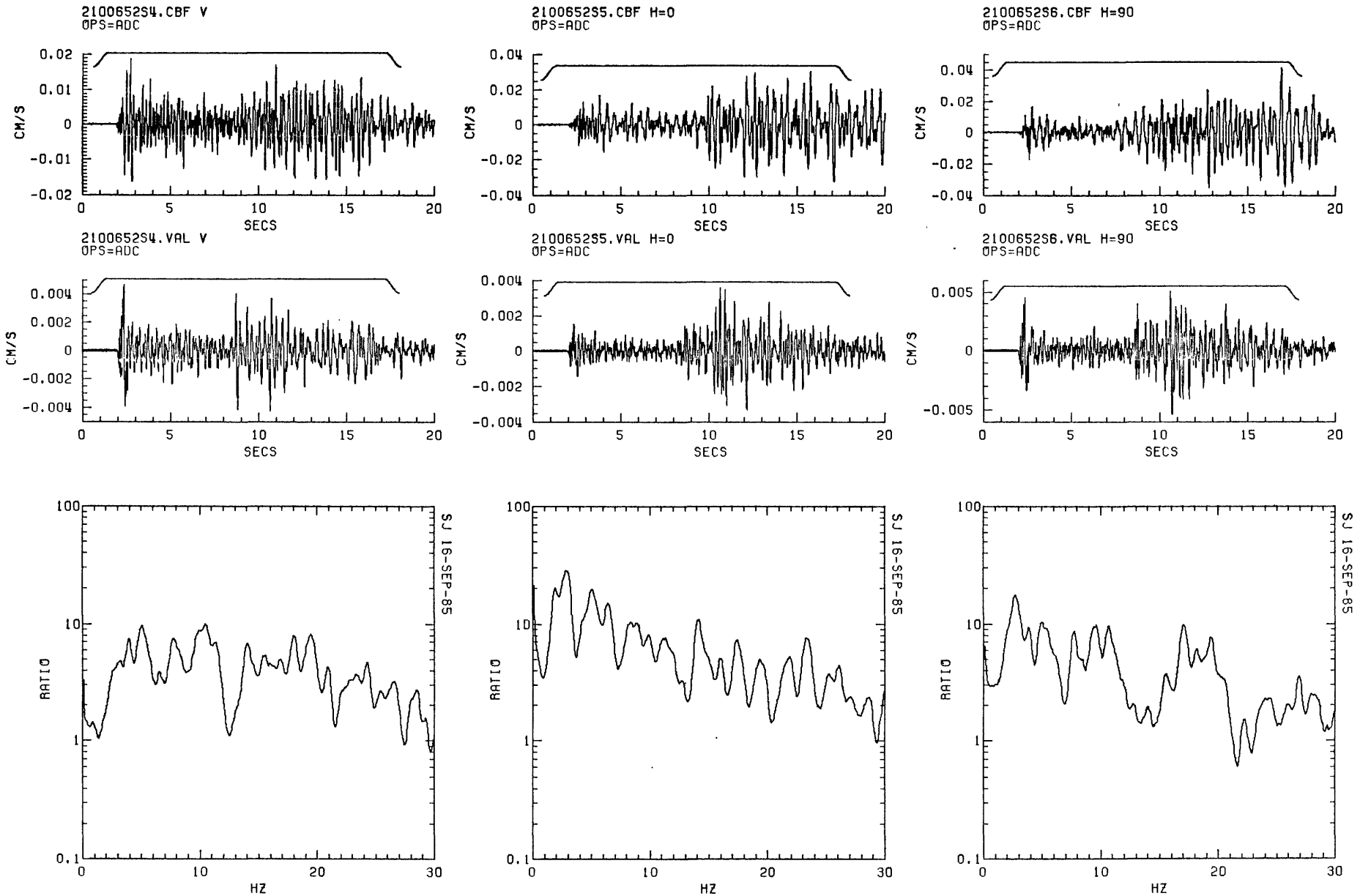

Figure A14. Scaled seismograms and spectral ratios of event on July 29, 1985 (Julian 210) at 06:52 for the vertical, horizontal (N-S and E-W) components, respectively, for station CBF/VAL.

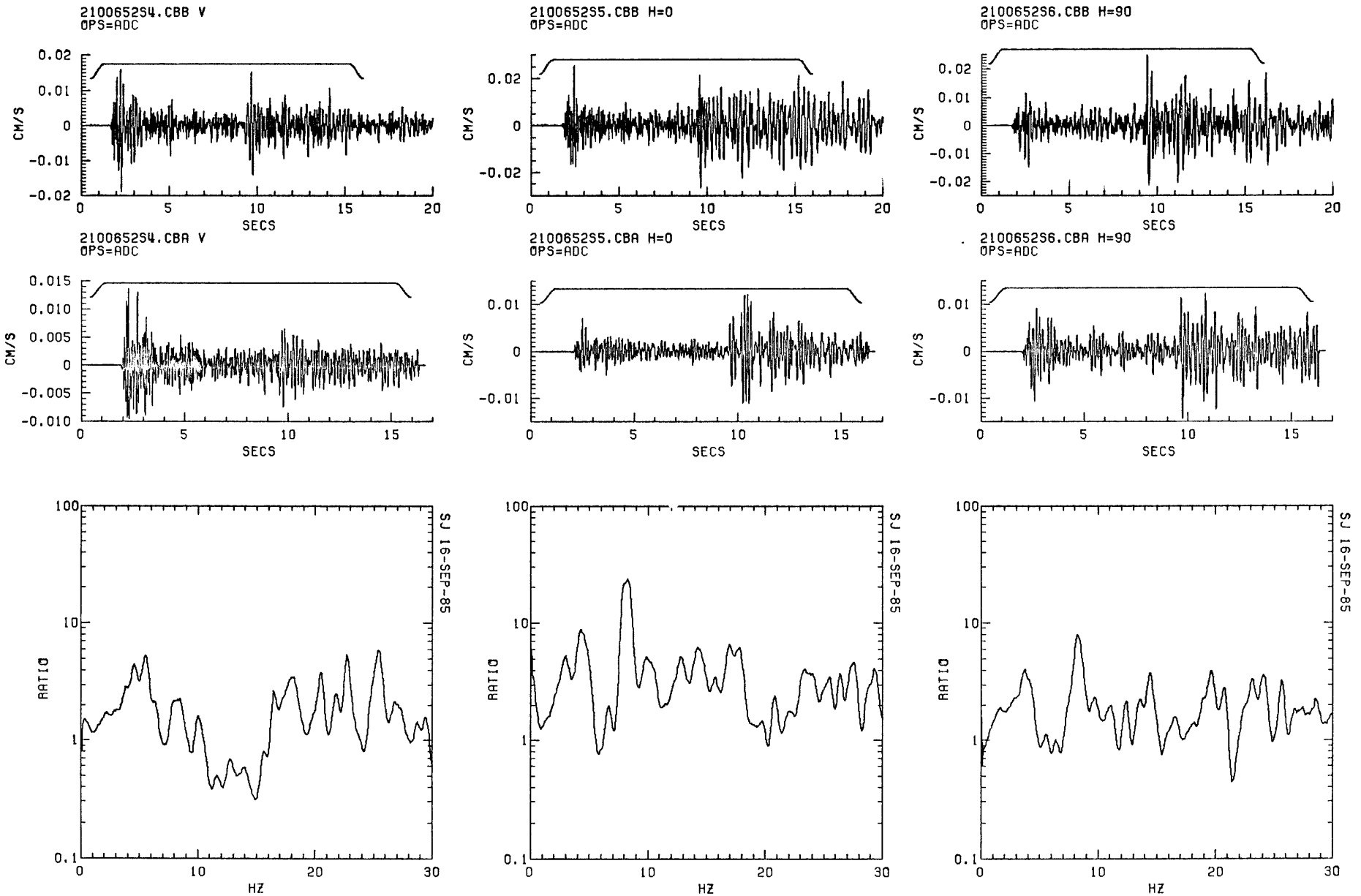

Figure A15. Scaled seismograms and spectral ratios of event on July 29, 1985 (Julian 210) at 06:52 for the vertical, horizontal (N-S and E-W) components, respectively, for station CBB/CBA.

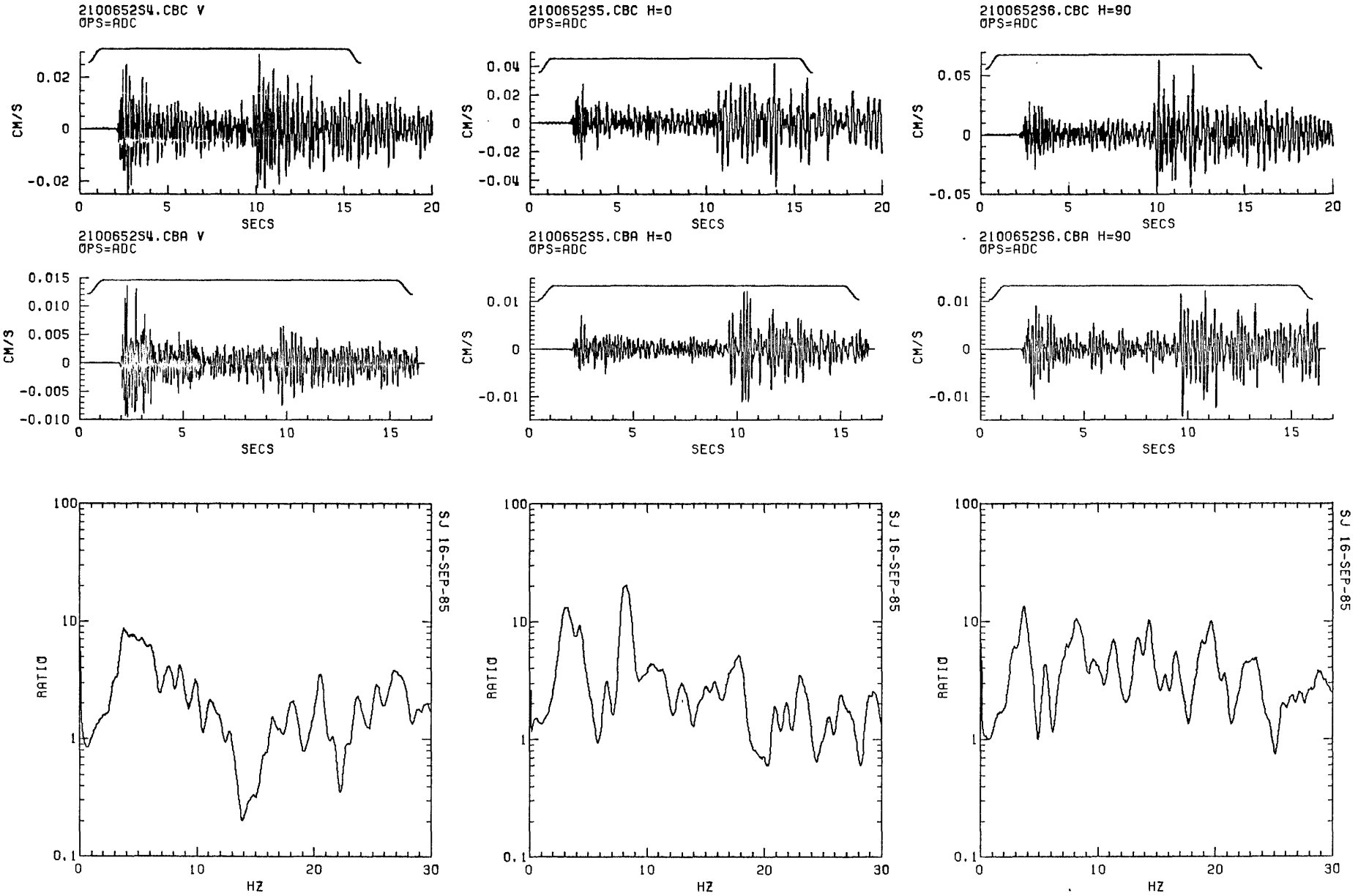

Figure A16. Scaled seismograms and spectral ratios of event on July 29, 1985 (Julian 210) at 06:52 for the vertical, horizontal (N-S and E-W) components, respectively, for station CBC/CBA.

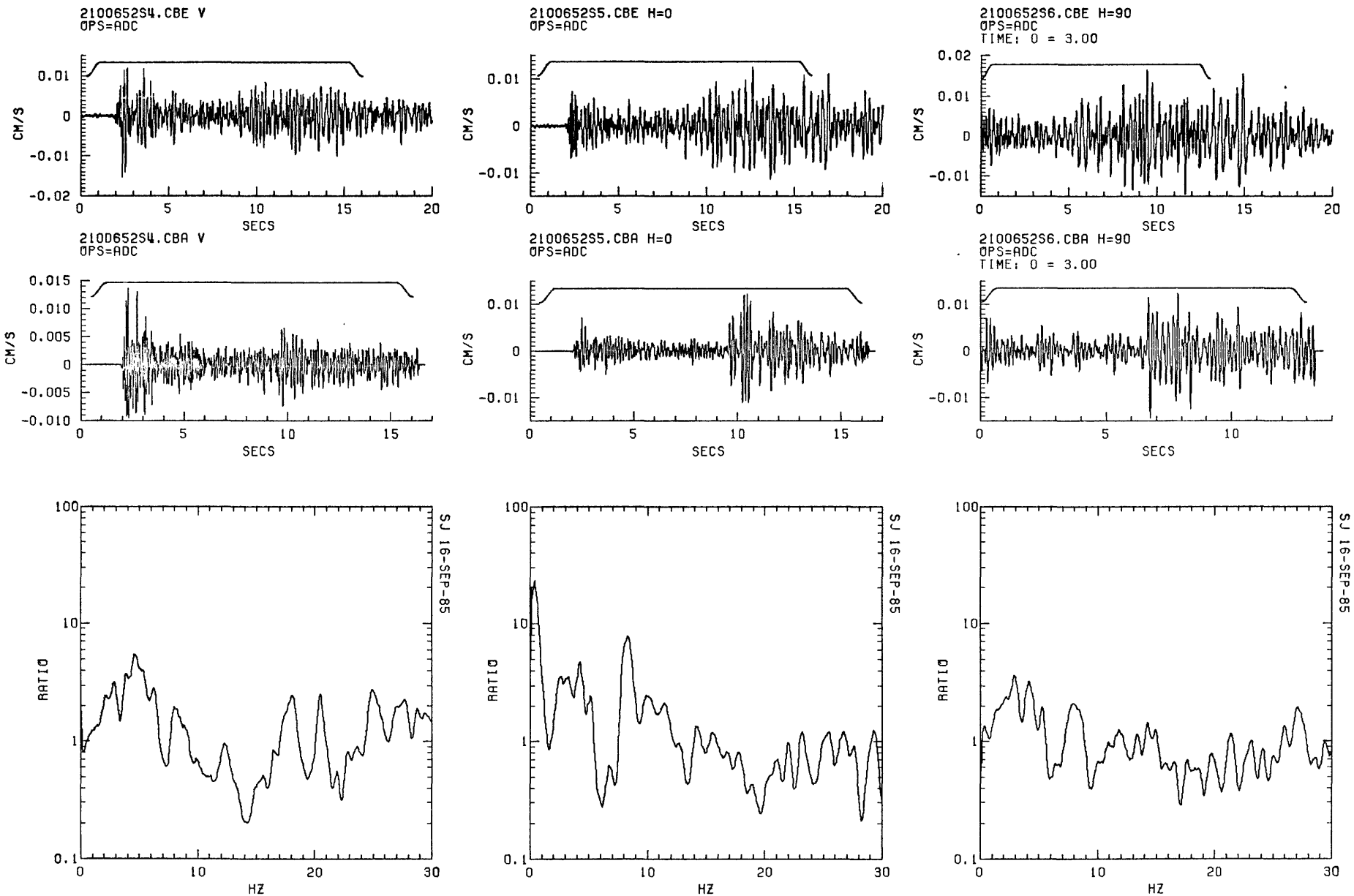

Figure A17. Scaled seismograms and spectral ratios of event on July 29, 1985 (Julian 210) at 06:52 for the vertical, horizontal (N-S and E-W) components, respectively, for station CBE/CBA.

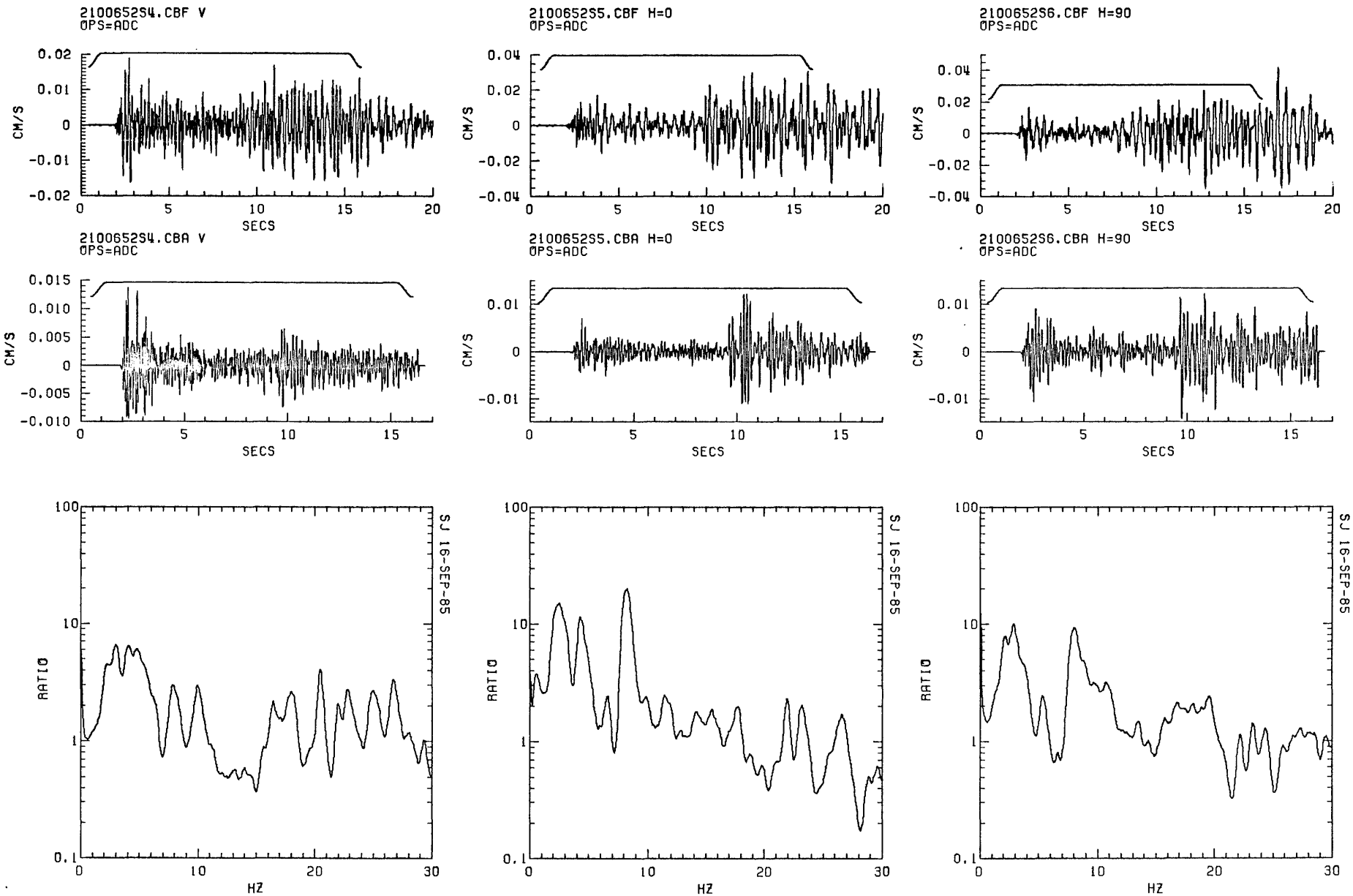

Figure A18. Scaled seismograms and spectral ratios of event on July 29, 1985 (Julian 210) at 06:52 for the vertical, horizontal (N-S and E-W) components, respectively, for station CBF/CBA.

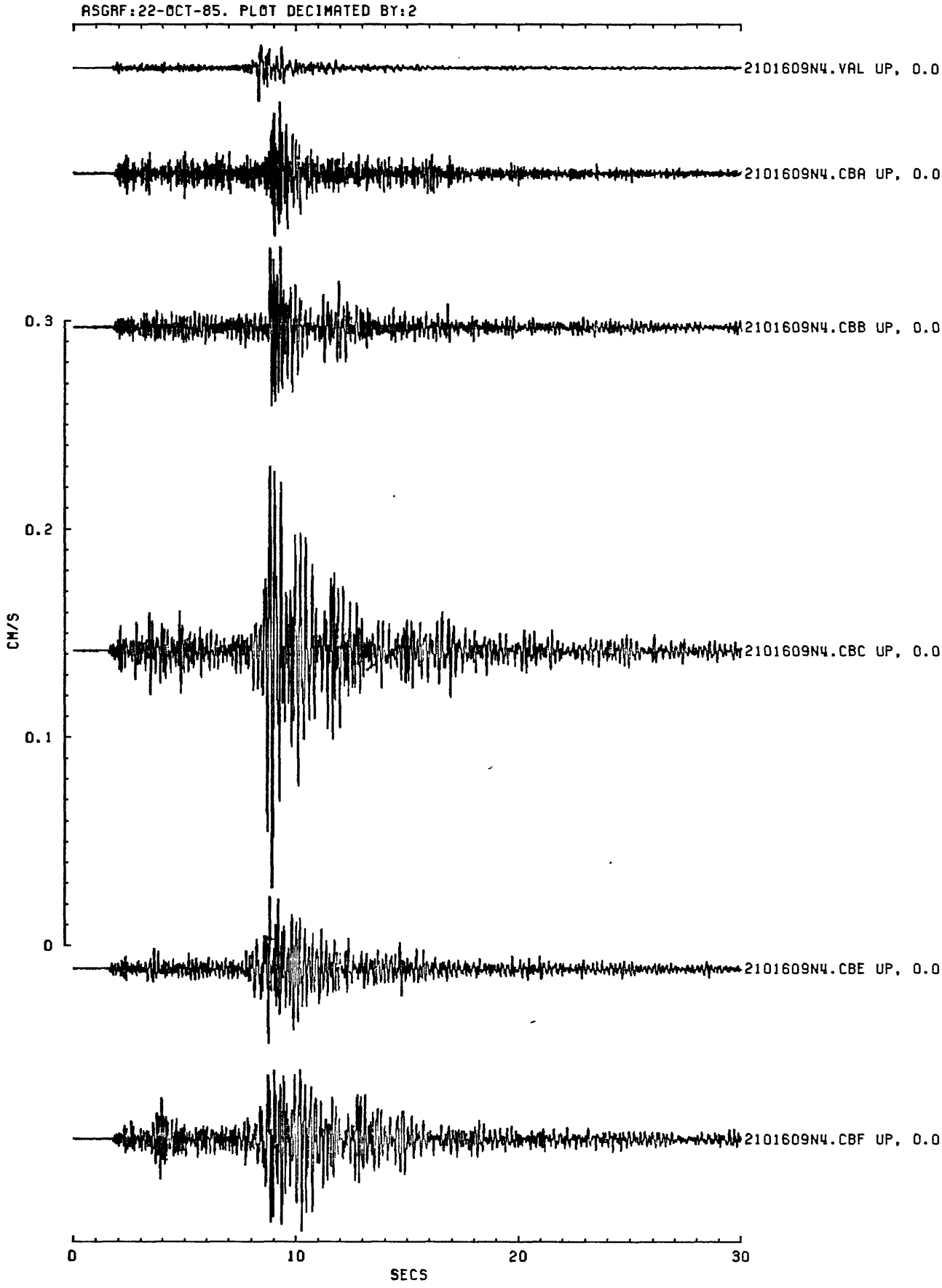

Figure A19. Scaled seismograms for event 2101609 (vertical components).

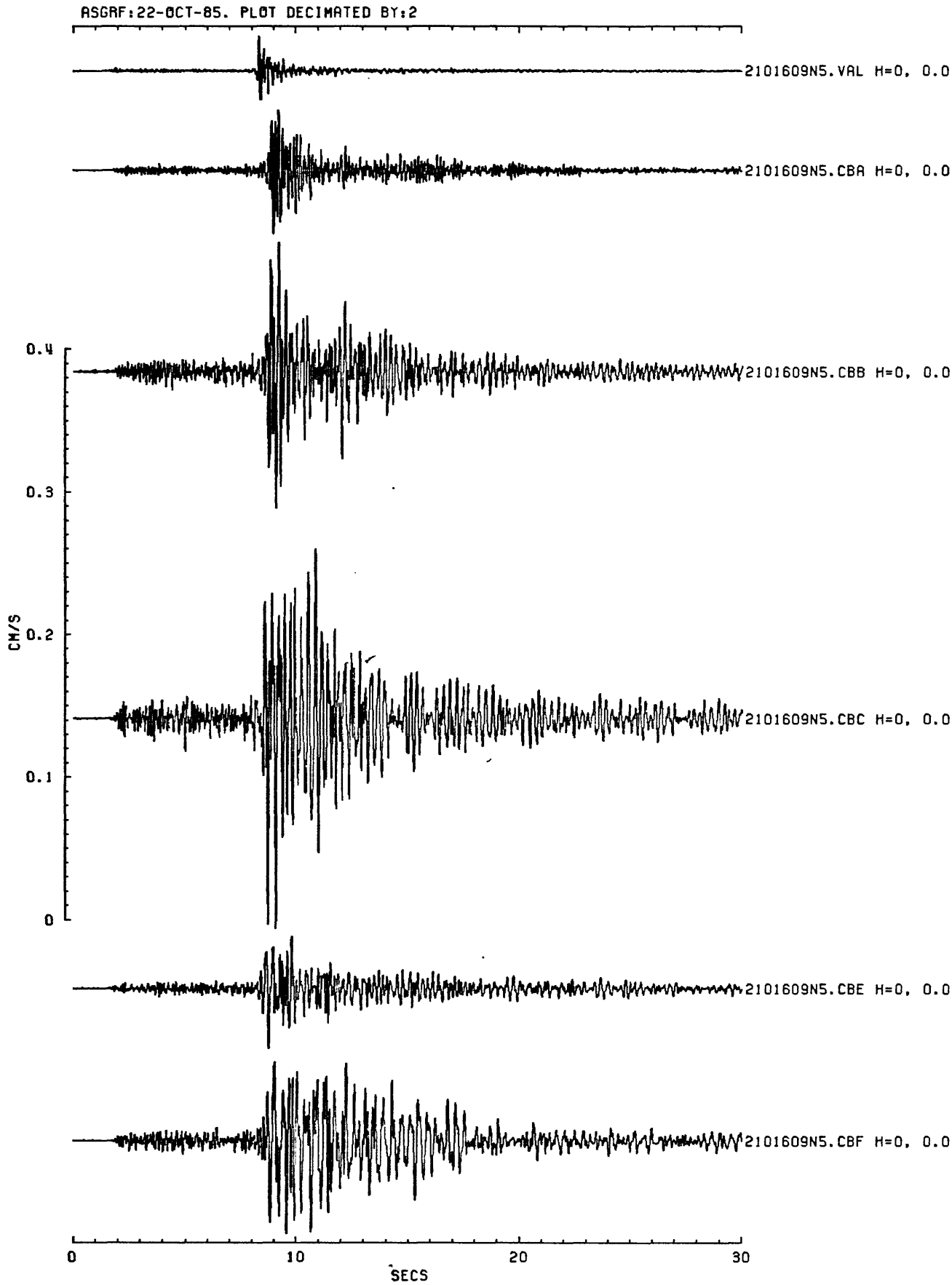

Figure A20. Scaled seismograms for event 2101609 (N-S components).

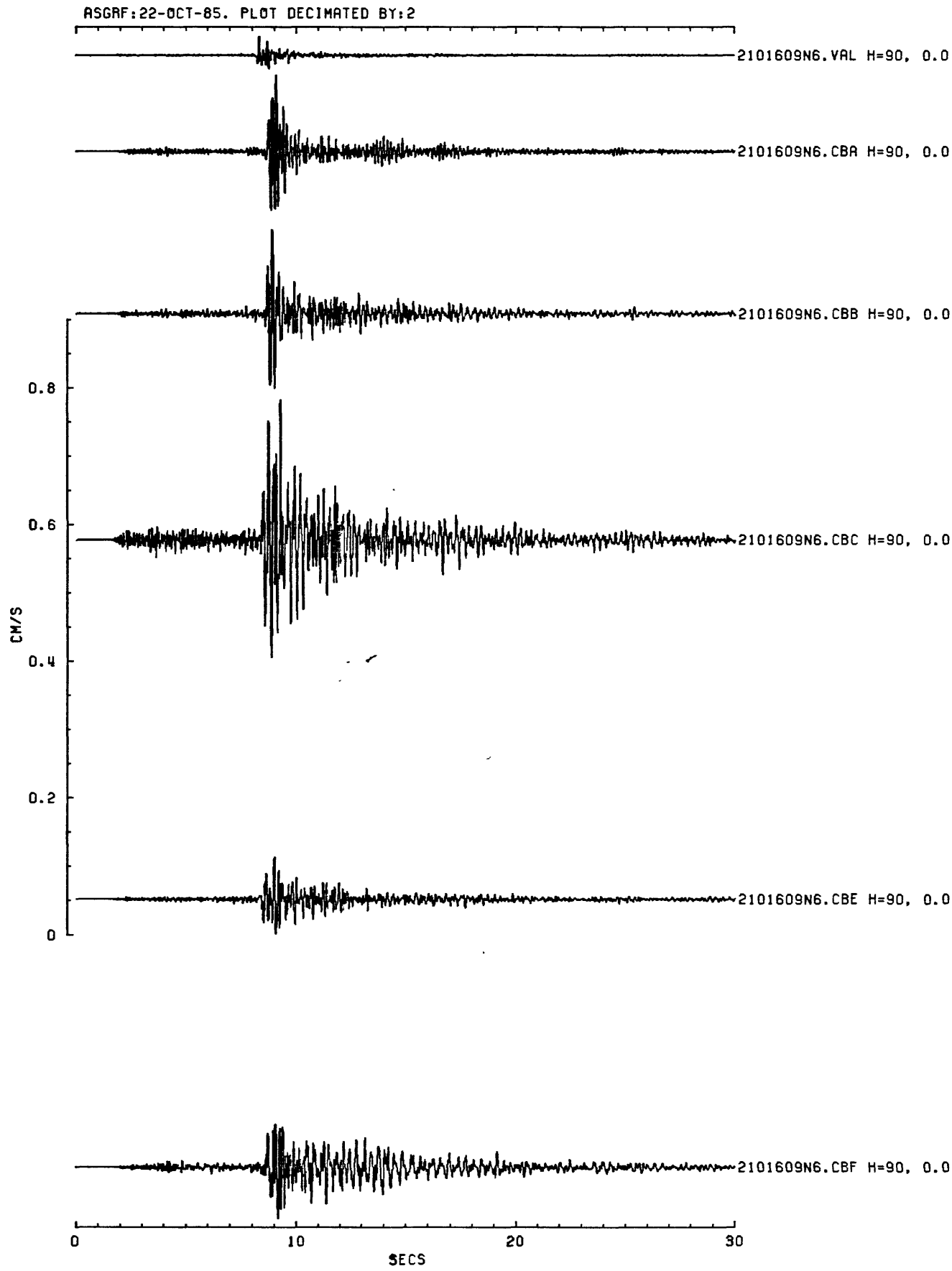

Figure A21. Scaled seismograms for event 2101609 (E-W components).

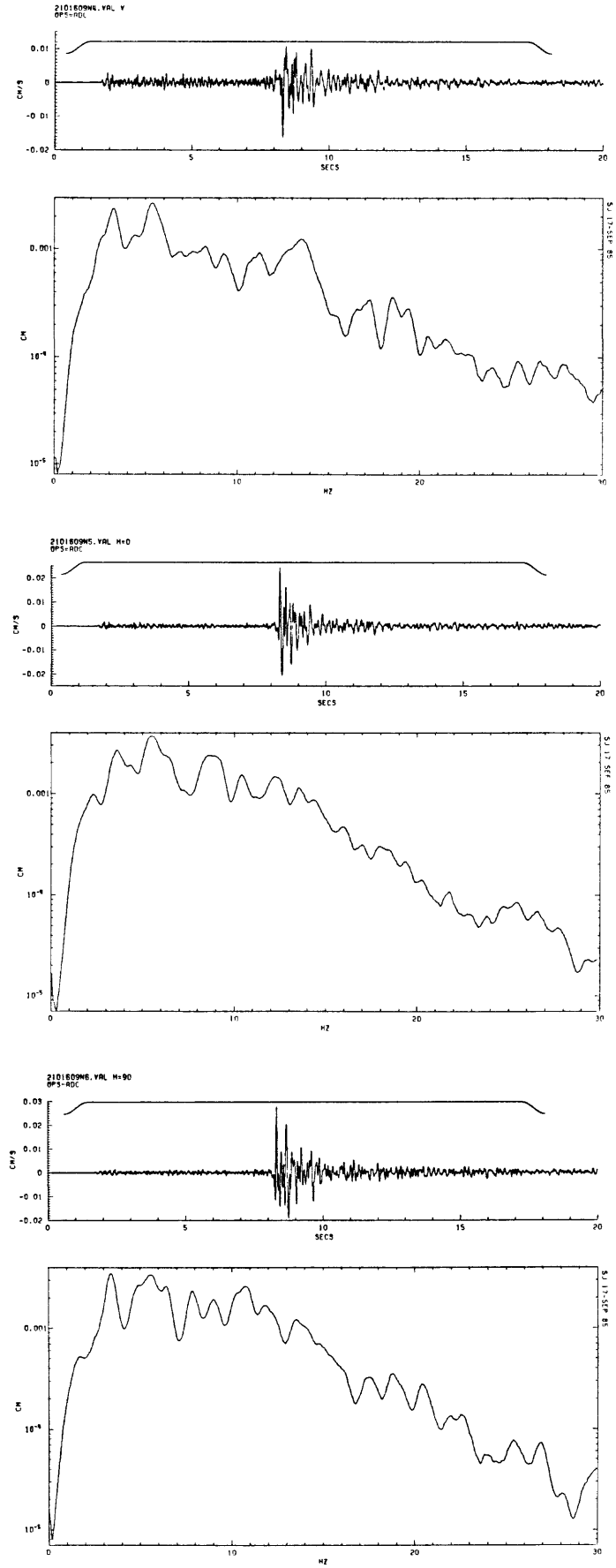

Figure A22. Time series and Fourier amplitude spectra of event on July 29, 1985 (Julian 210) at 16:09 for the vertical, horizontal (N-S and E-W) components, respectively, for station VAL.

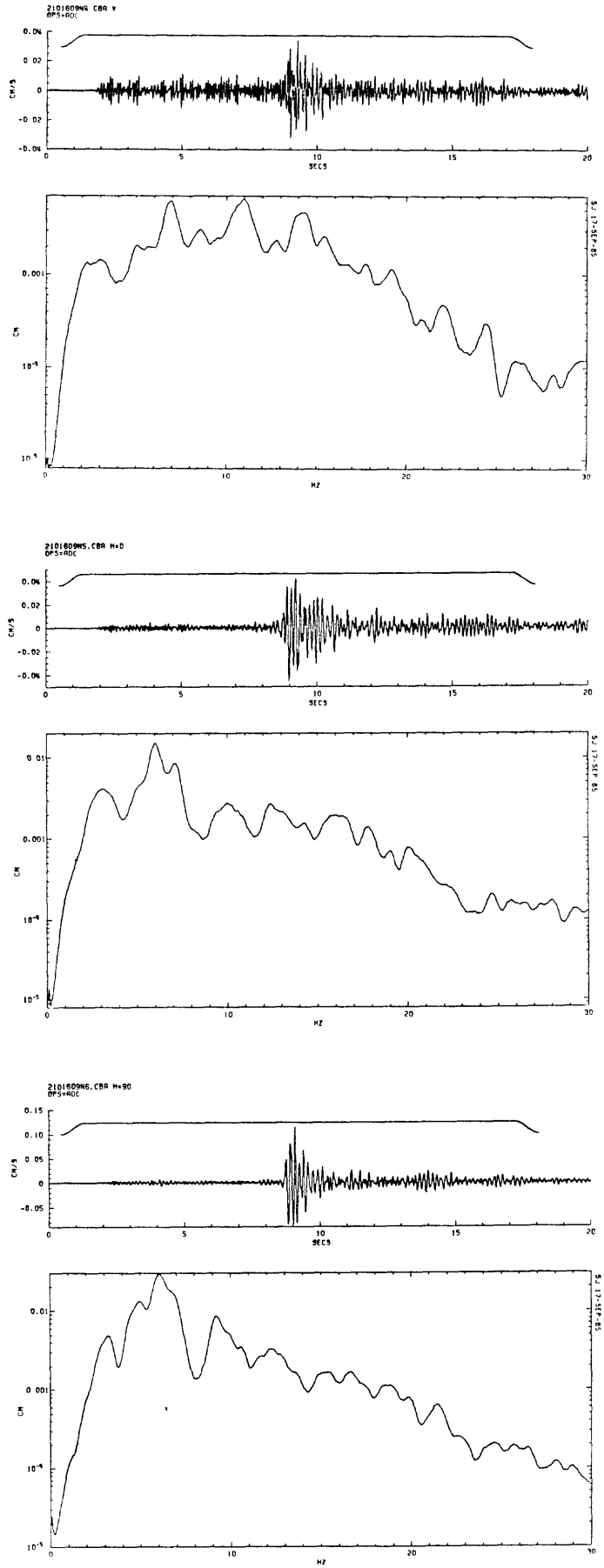

Figure A23. Time series and Fourier amplitude spectra of event on July 29, 1985 (Julian 210) at 16:09 for the vertical, horizontal (N-S and E-W) components, respectively, for station CBA.

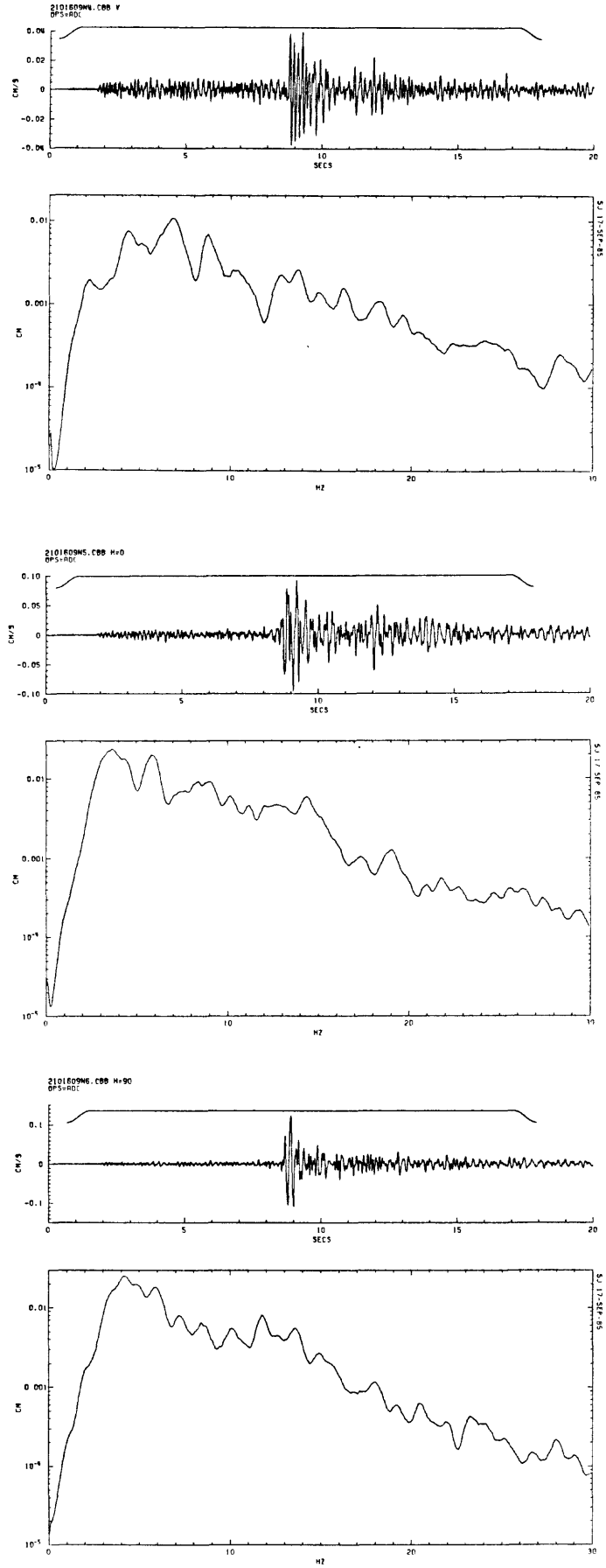

Figure A24. Time series and Fourier amplitude spectra of event on July 29, 1985 (Julian 210) at 16:09 for the vertical, horizontal (N-S and E-W) components, respectively, for station CBB.

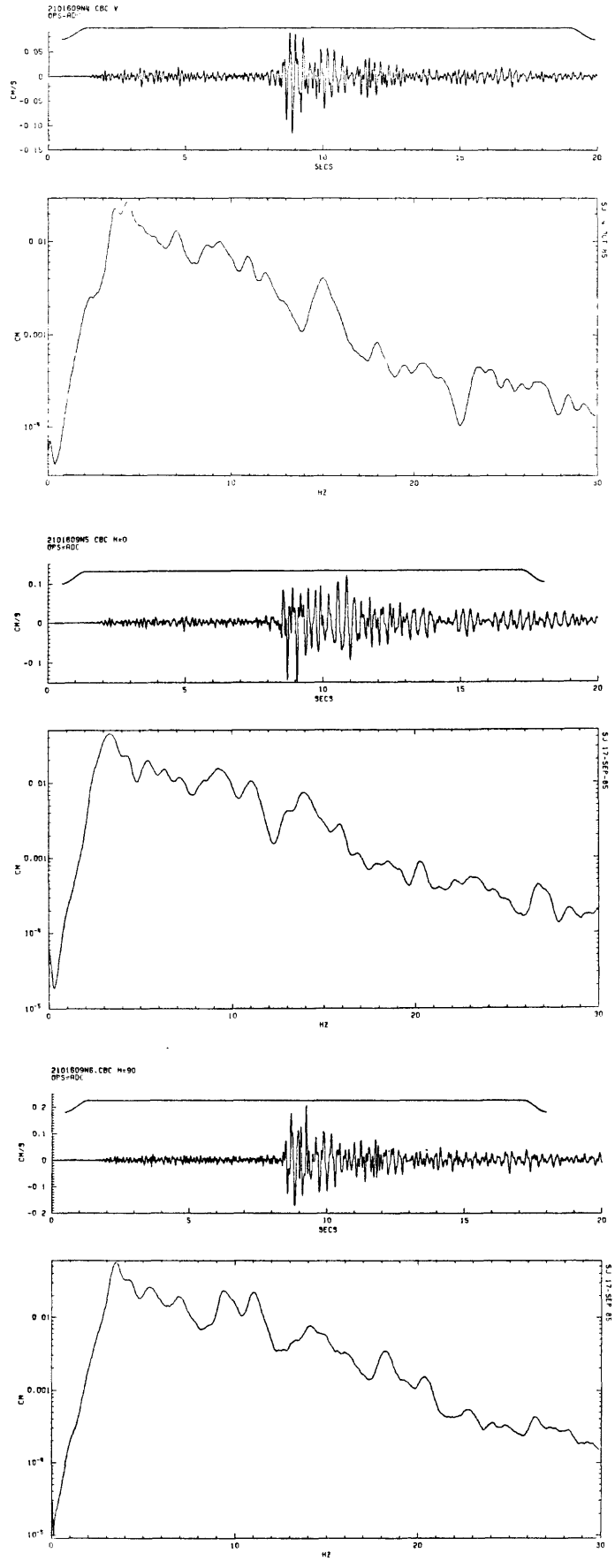

Figure A25. Time series and Fourier amplitude spectra of event on July 29, 1985 (Julian 210) at 16:09 for the vertical, horizontal (N-S and E-W) components, respectively, for station CBC.

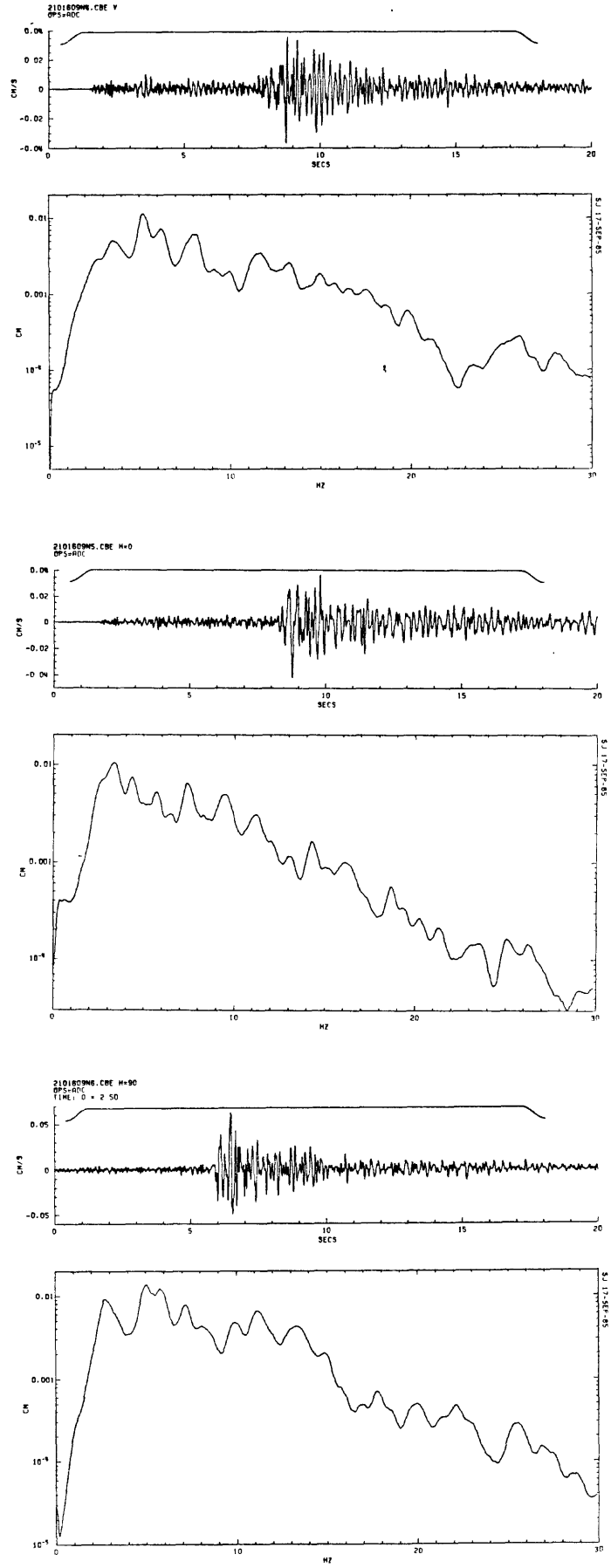

Figure A26. Time series and Fourier amplitude spectra of event on July 29, 1985 (Julian 210) at 16:09 for the vertical, horizontal (N-S and E-W) components, respectively, for station CBF.

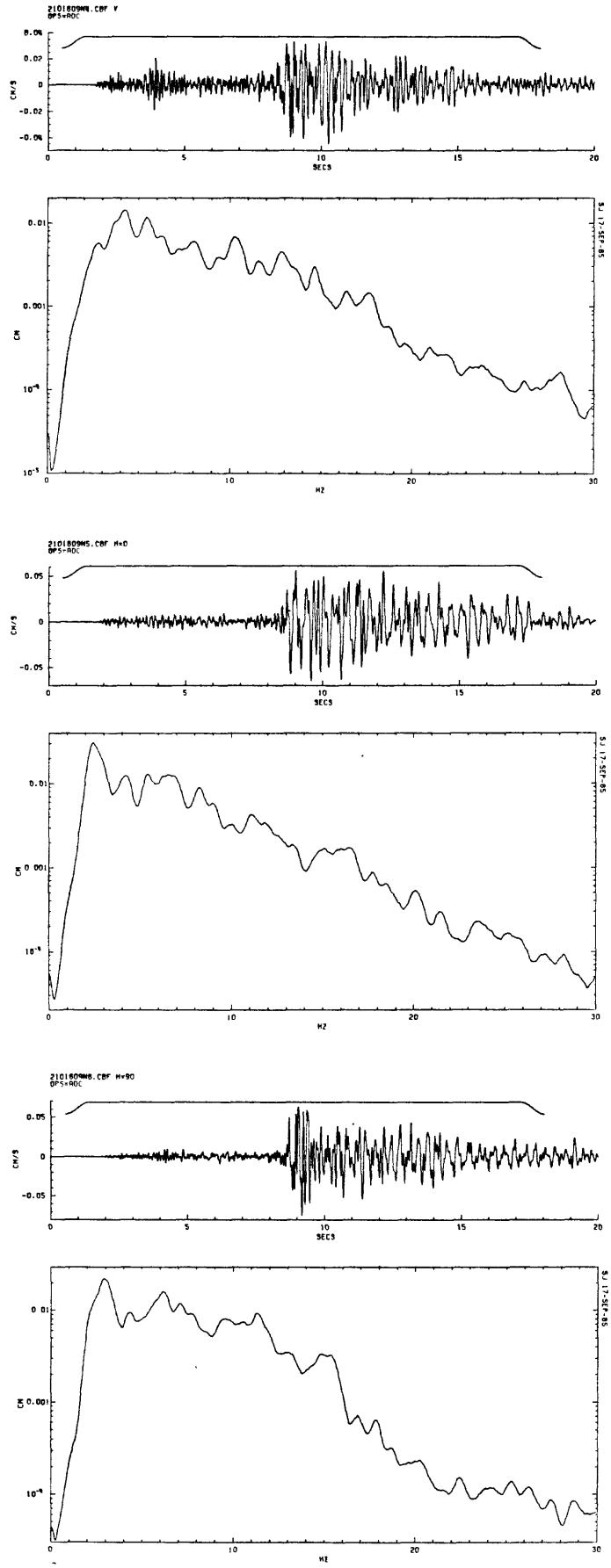

Figure A27. Time series and Fourier amplitude spectra of event on July 29, 1985 (Julian 210) at 16:09 for the vertical, horizontal (N-S and E-W) components, respectively, for station CBF.

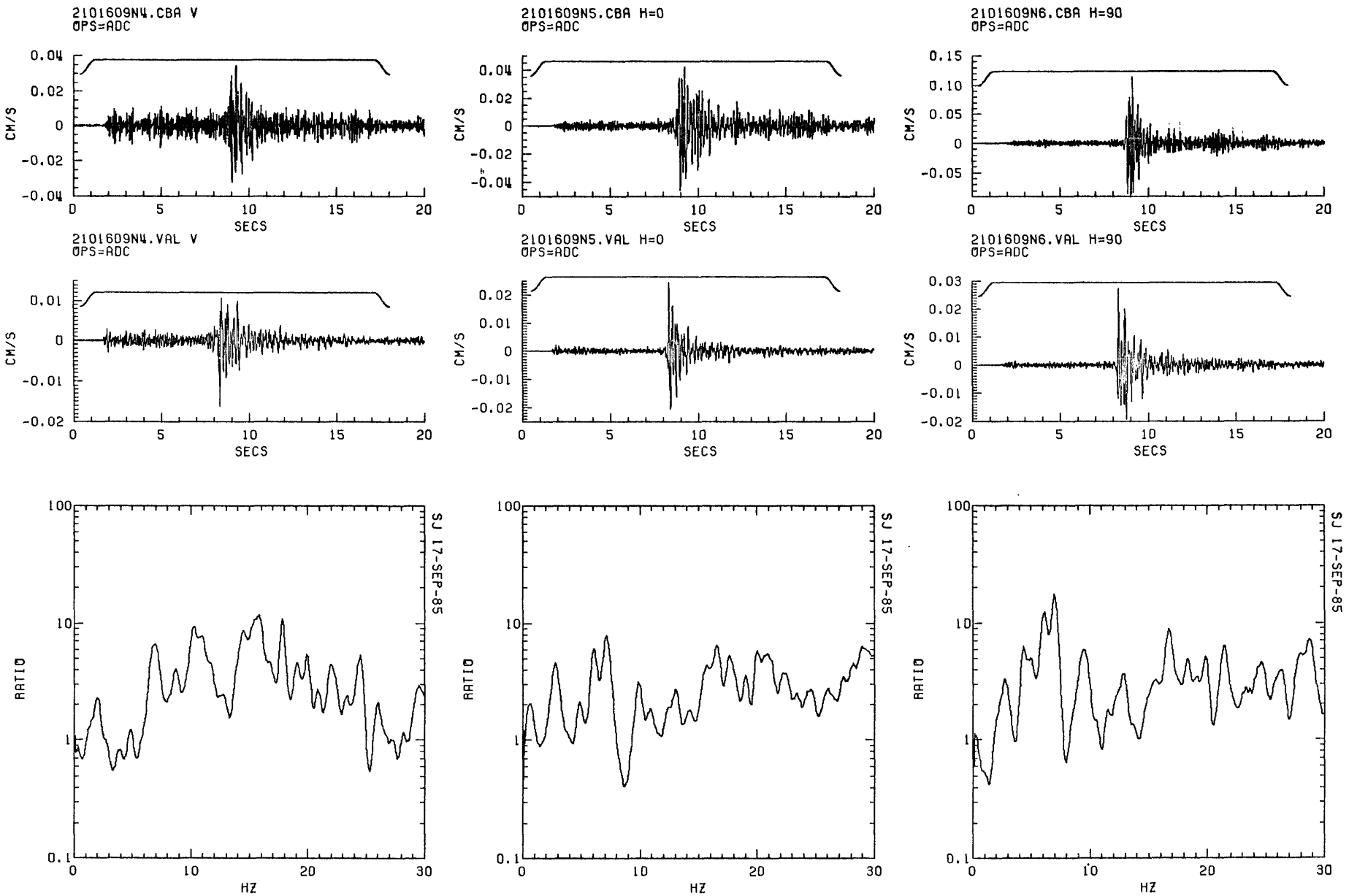

Figure A28. Scaled seismograms and spectral ratios of event on July 29, 1985 (Julian 210) at 16:09 for the vertical and horizontal (N-S and E-W) components, respectively, for stations CBA/VAL.

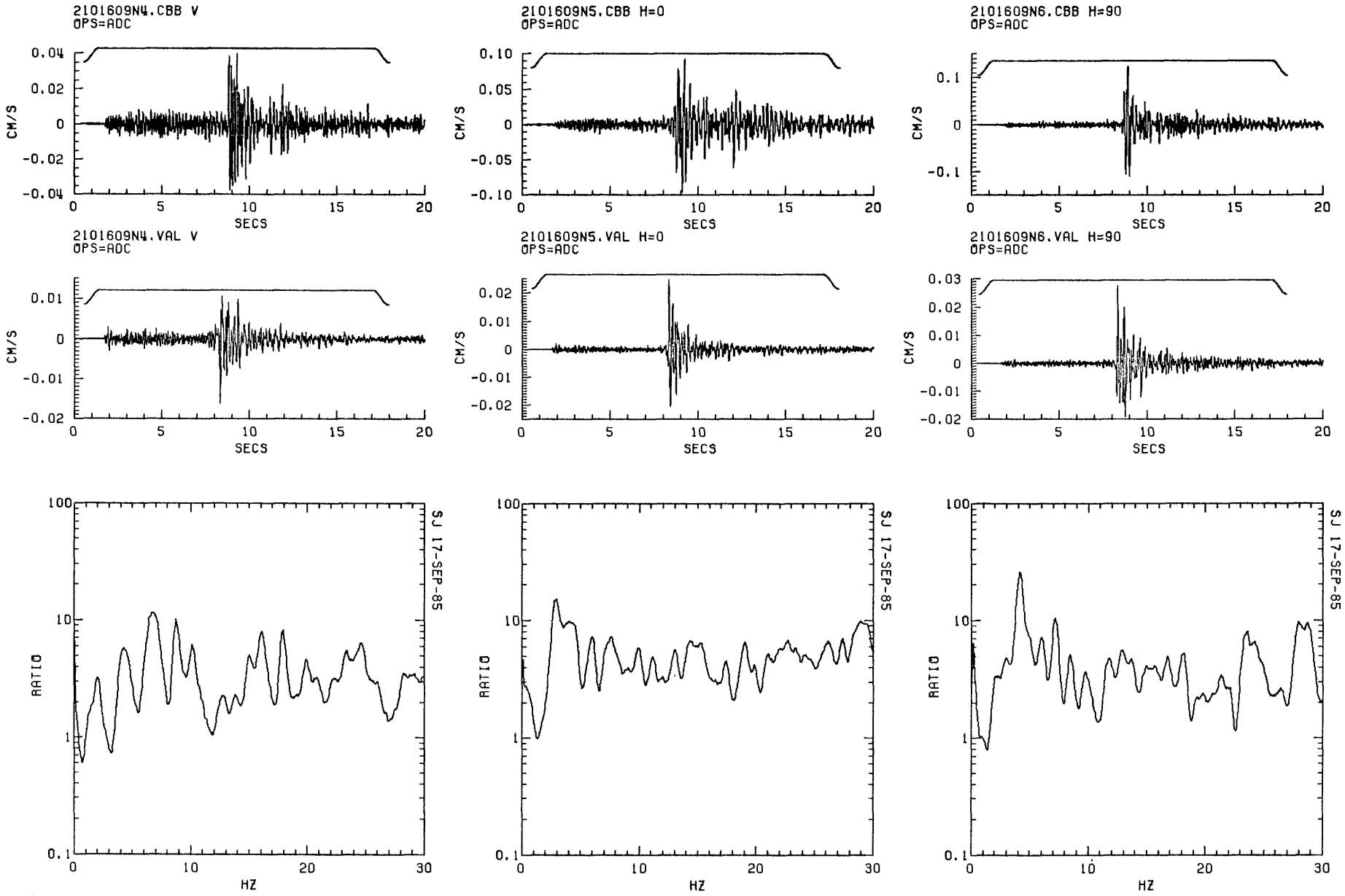

Figure A29. Scaled seismograms and spectral ratios of event on July 29, 1985 (Julian 210) at 16:09 for the vertical and horizontal (N-S and E-W) components, respectively, for stations CBB/VAL.

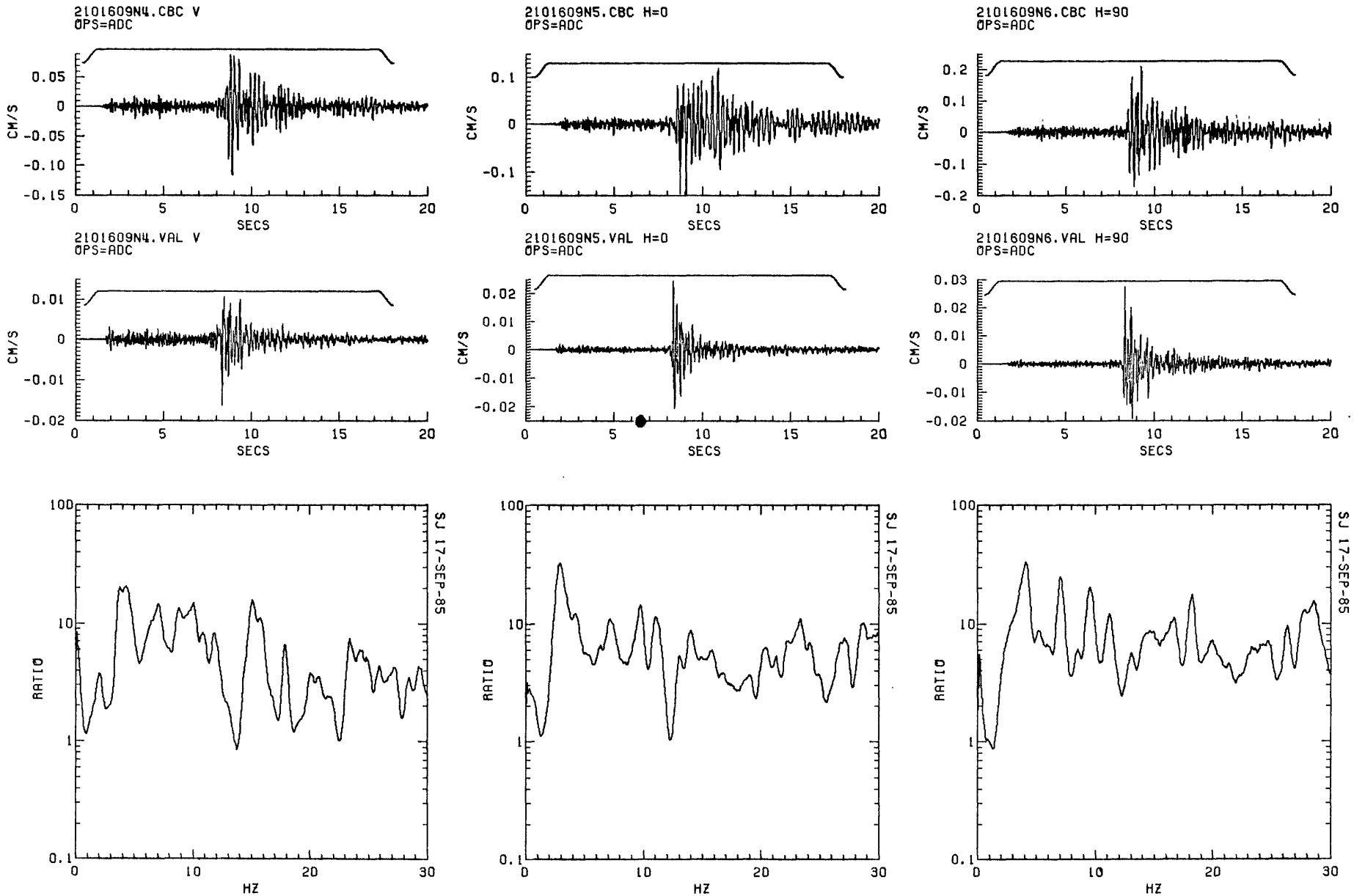

Figure A30. Scaled seismograms and spectral ratios of event on July 29, 1985 (Julian 210) at 16:09 for the vertical and horizontal (N-S and E-W) components, respectively, for stations CBC/VAL.

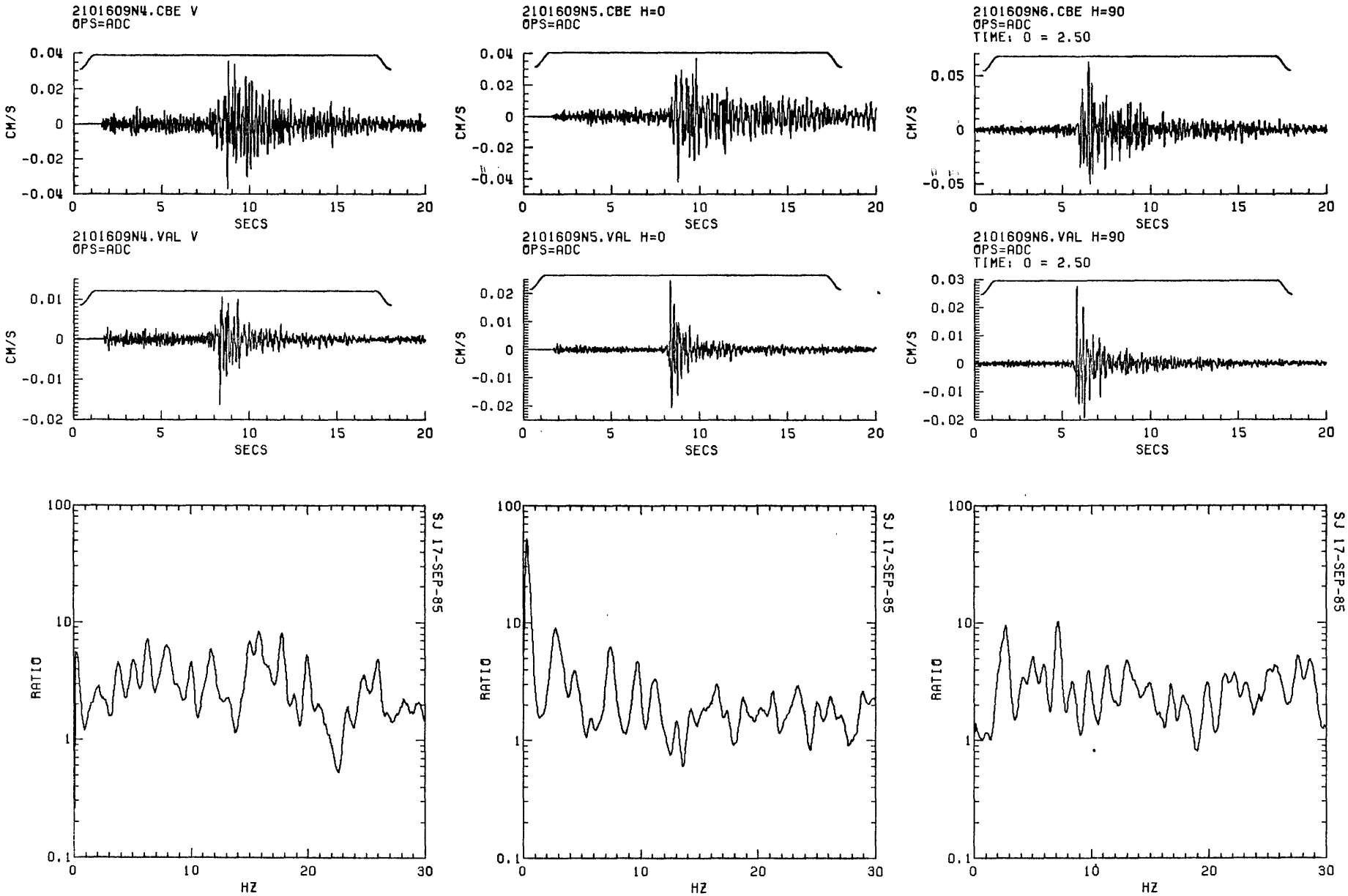

Figure A31. Scaled seismograms and spectral ratios of event on July 29, 1985 (Julian 210) at 16:09 for the vertical and horizontal (N-S and E-W) components, respectively, for stations CBE/VAL.

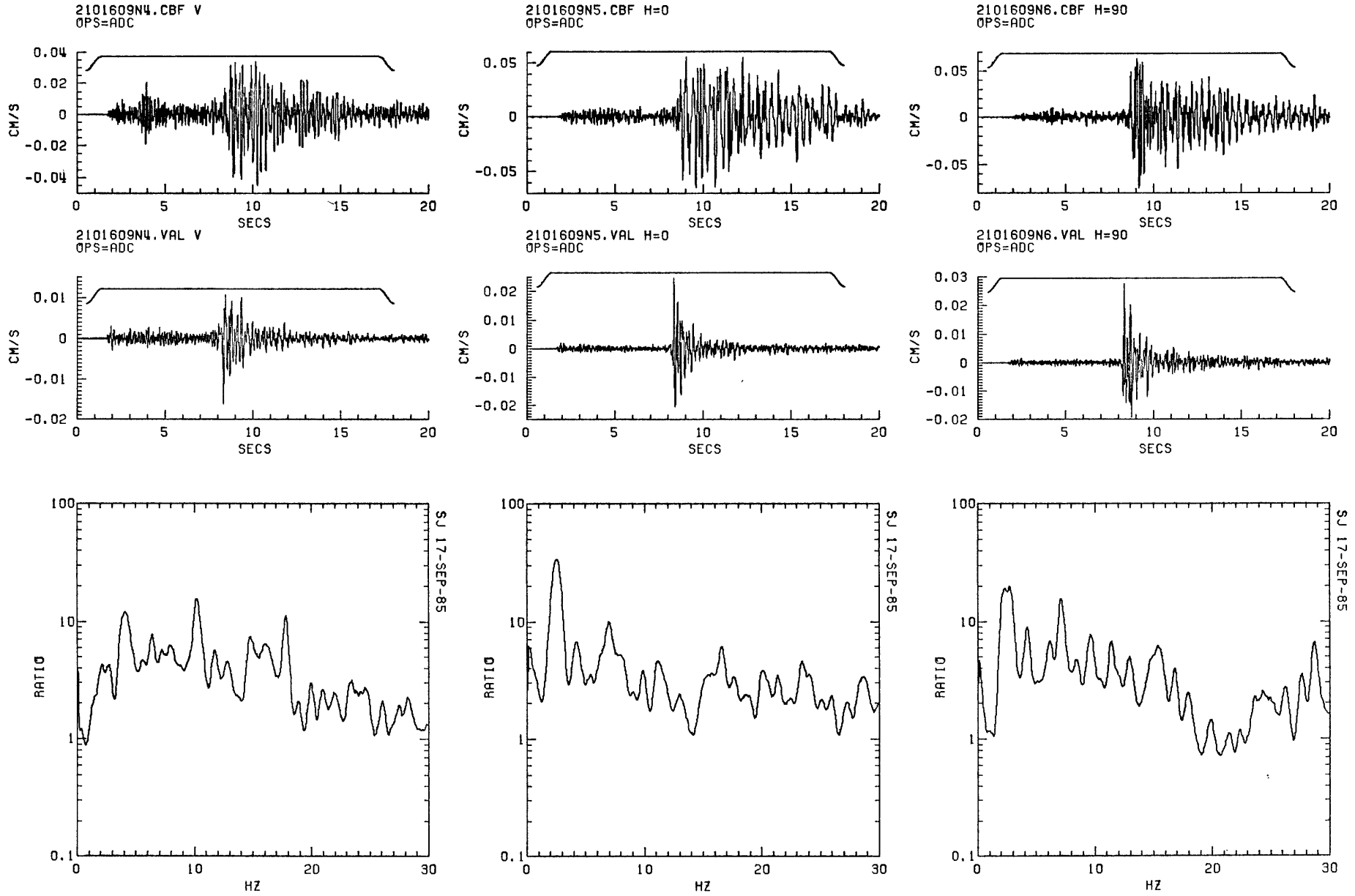

Figure A32. Scaled seismograms and spectral ratios of event on July 29, 1985 (Julian 210) at 16:09 for the vertical and horizontal (N-S and E-W) components, respectively, for stations CBF/VAL.

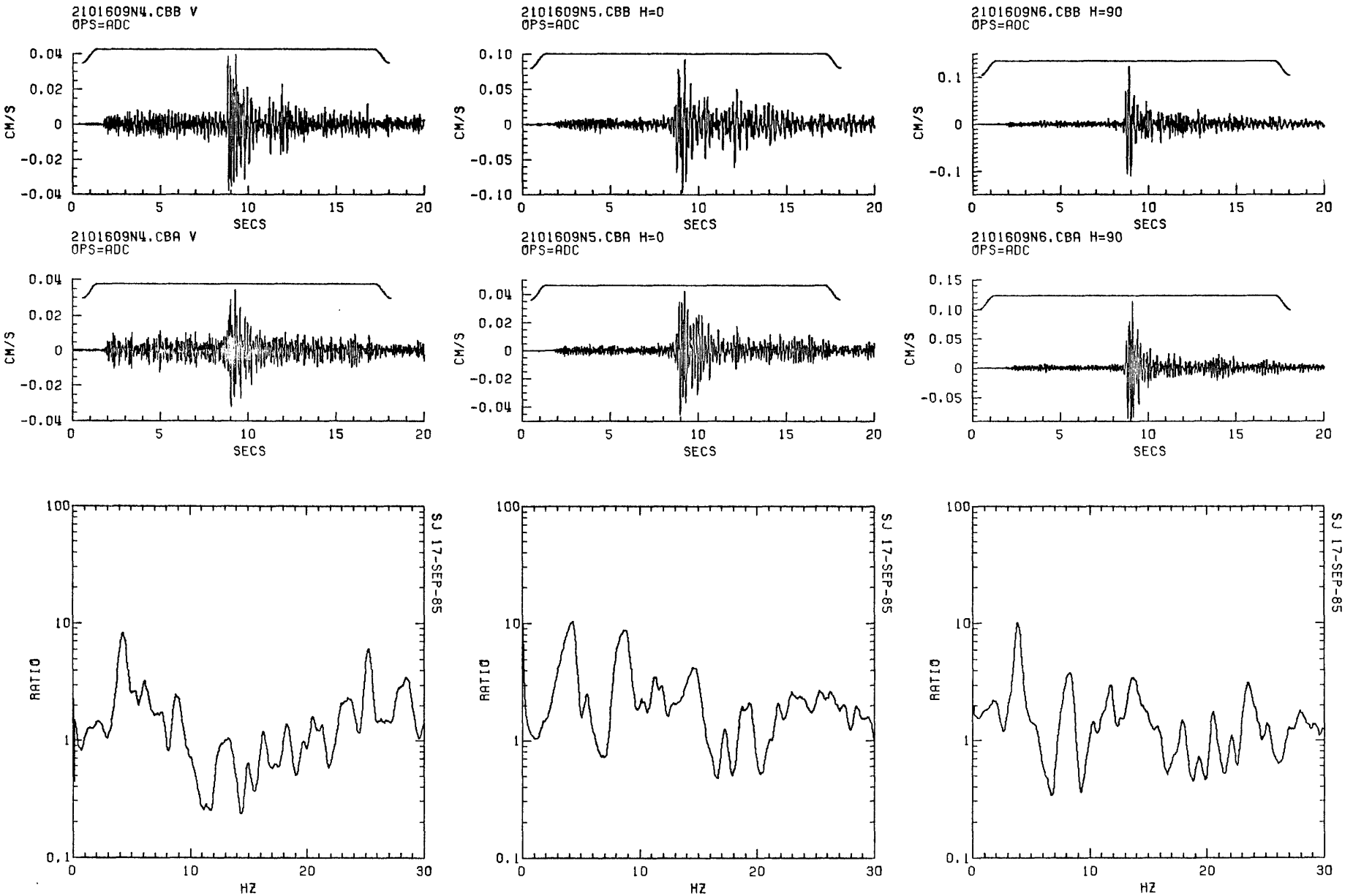

Figure A33. Scaled seismograms and spectral ratios of event on July 29, 1985 (Julian 210) at 16:09 for the vertical and horizontal (N-S and E-W) components, respectively, for stations CBB/CBA.

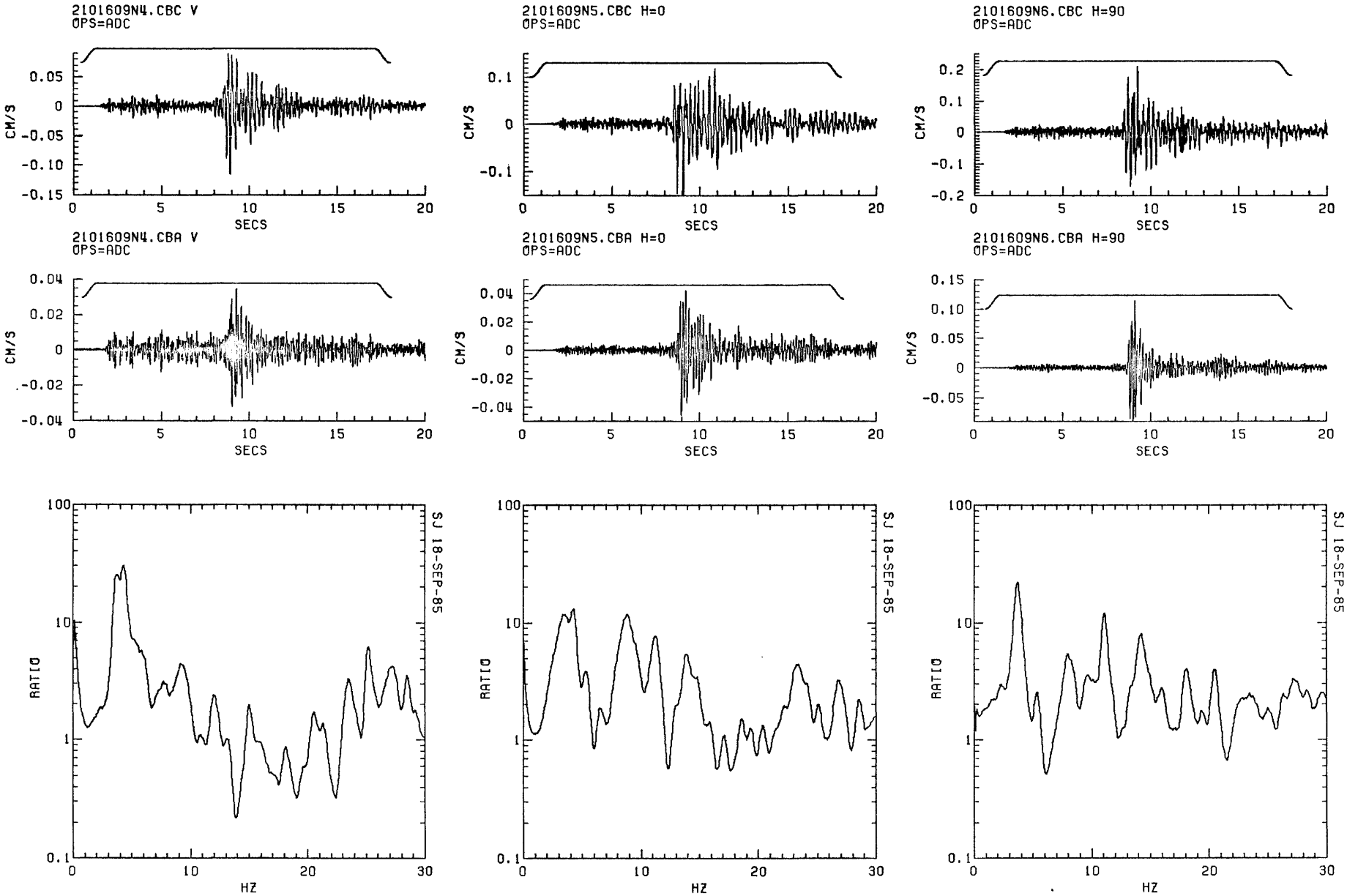

Figure A34. Scaled seismograms and spectral ratios of event on July 29, 1985 (Julian 210) at 16:09 for the vertical and horizontal (N-S and E-W) components, respectively, for stations CBC/CBA.

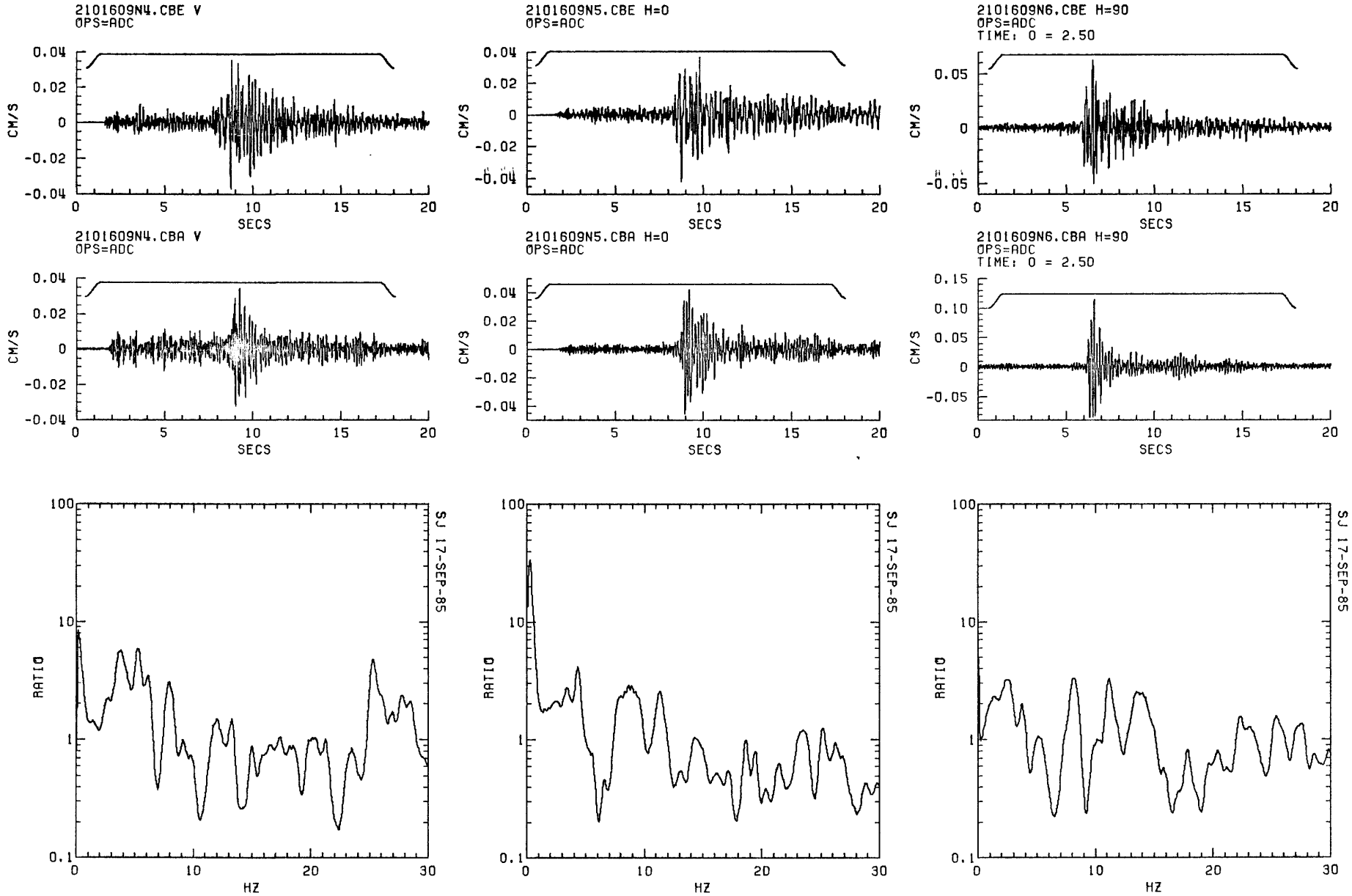

Figure A35. Scaled seismograms and spectral ratios of event on July 29, 1985 (Julian 210) at 16:09 for the vertical and horizontal (N-S and E-W) components, respectively, for stations CBE/CBA.

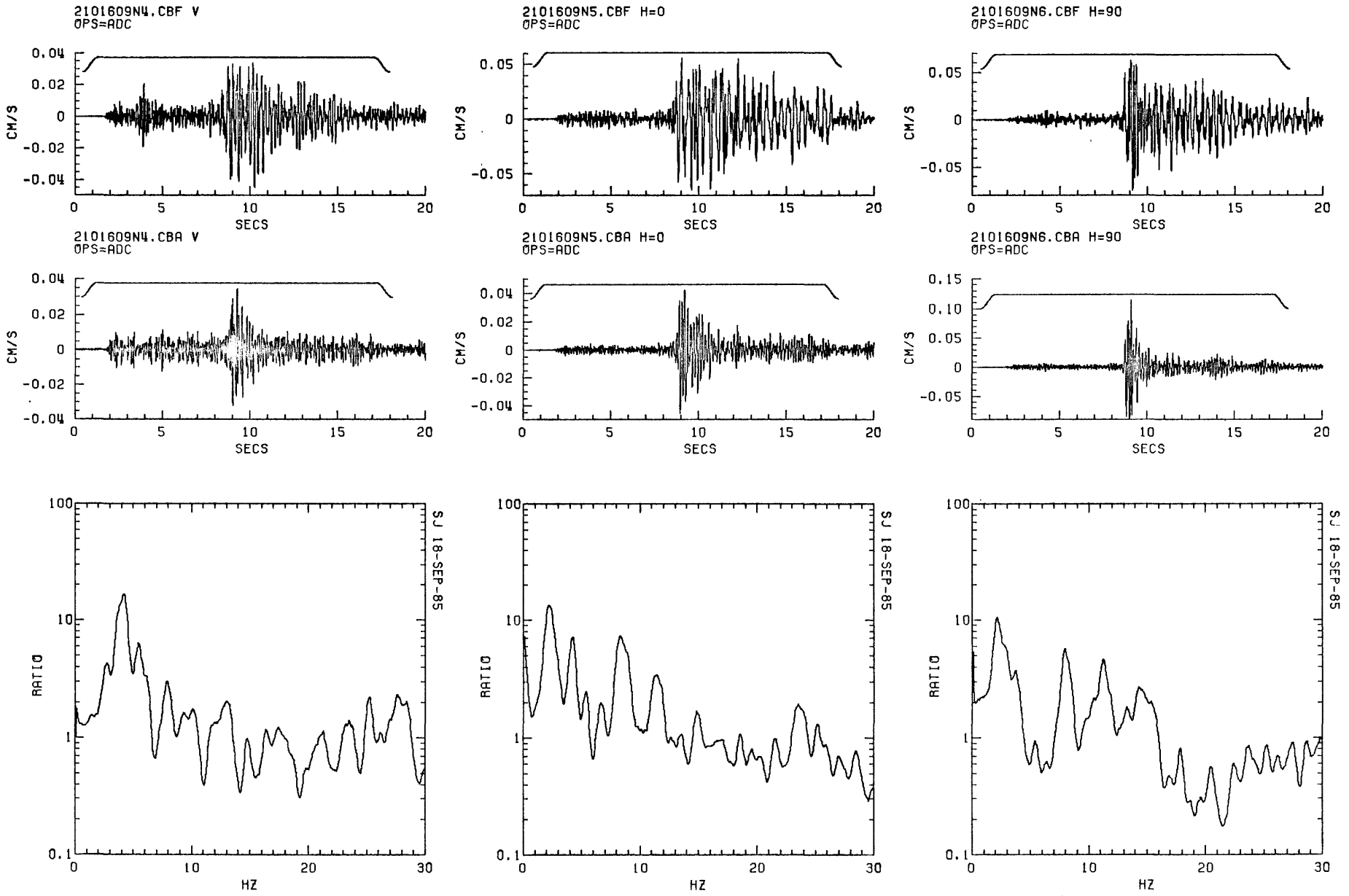

Figure A36. Scaled seismograms and spectral ratios of event on July 29, 1985 (Julian 210) at 16:09 for the vertical and horizontal (N-S and E-W) components, respectively, for stations CBF/CBA.

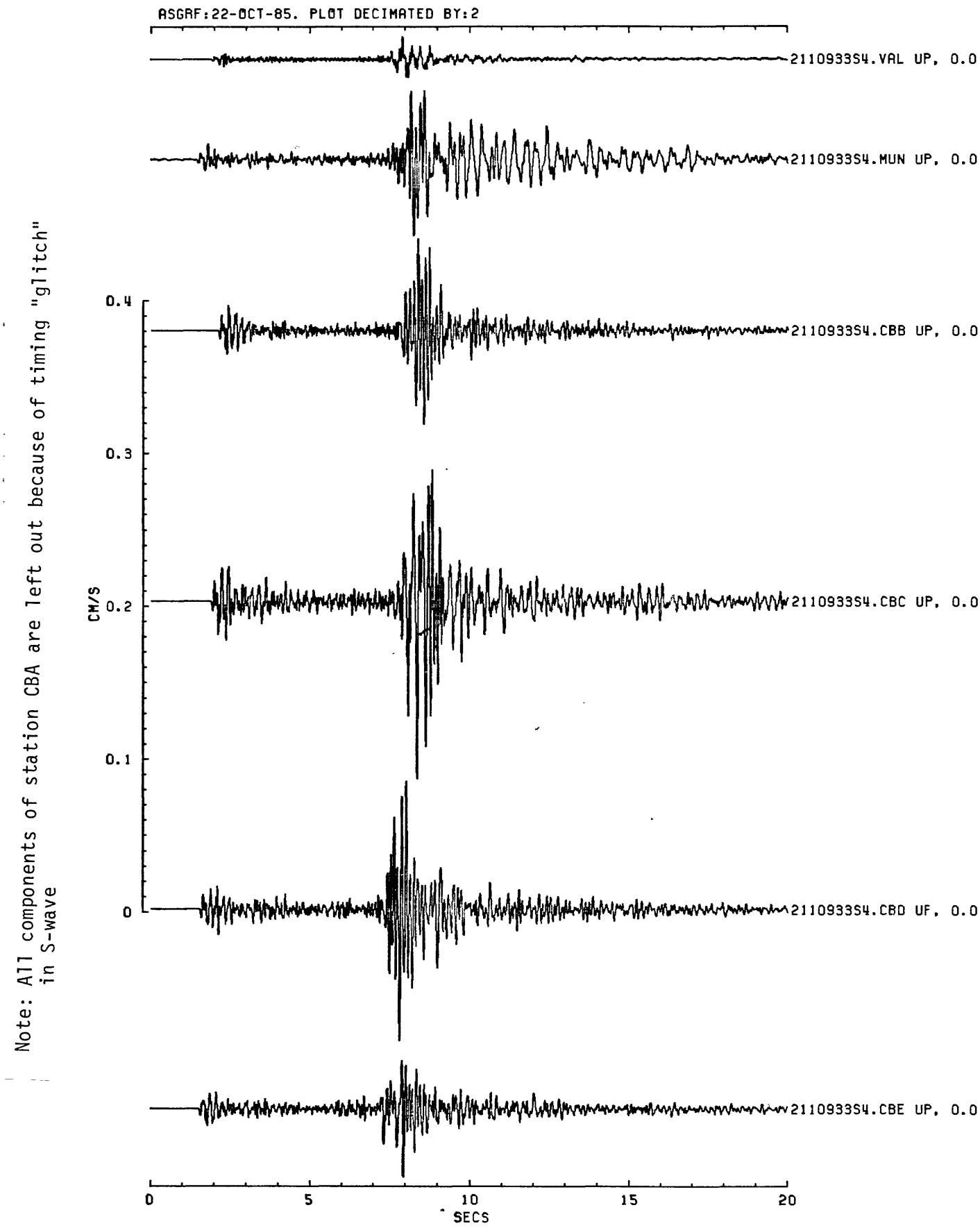

Figure A37. Scaled seismograms for event 2110933 (vertical components).

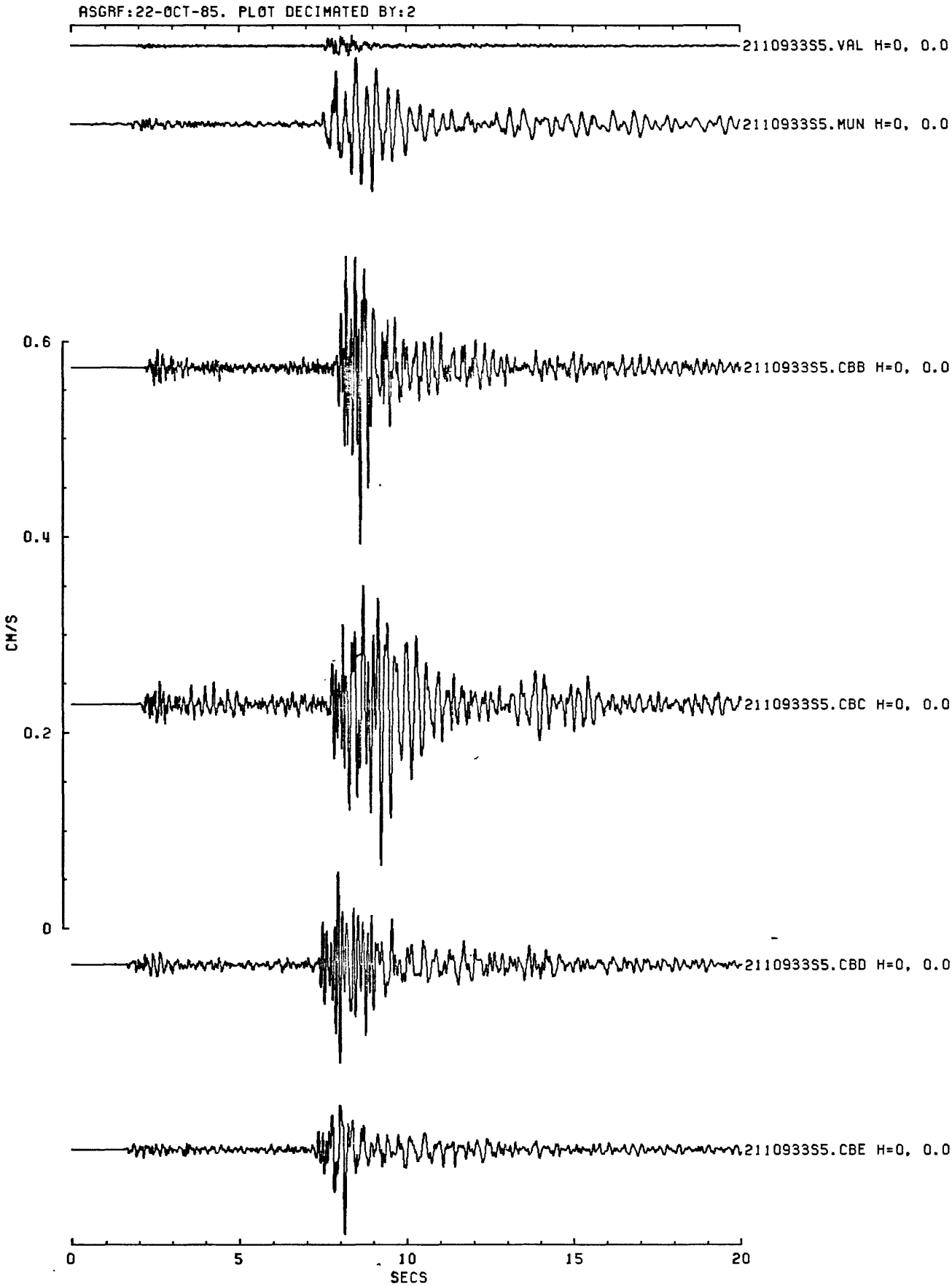

Figure A38. Scaled seismograms for event 2110933 (N-S components).

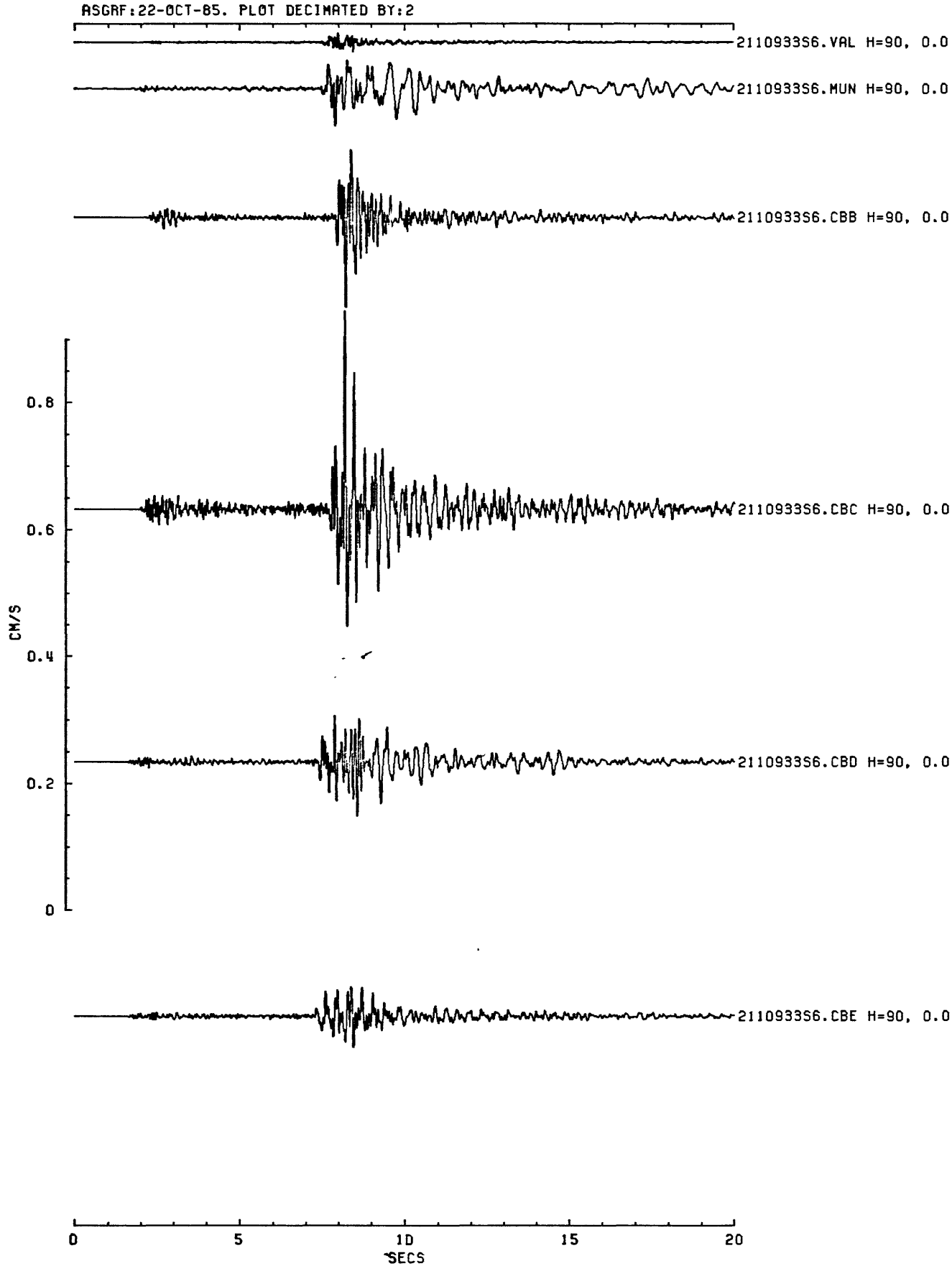

Figure A39. Scaled seismograms for event 2110933 (E-W components).

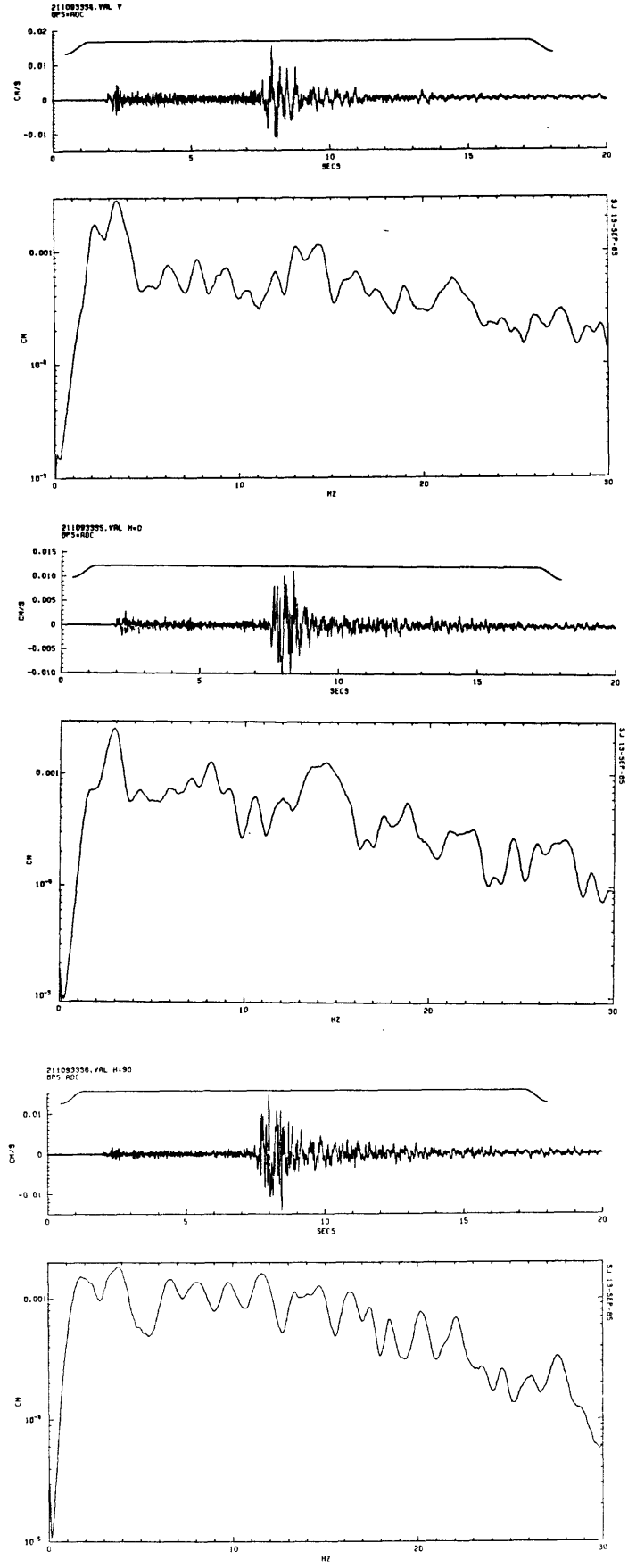

Figure A40. Time series and Fourier amplitude spectra of event on July 30, 1985 (Julian 211) at 09:33 for the vertical, horizontal (N-S and E-W) components, respectively, for stations VAL.

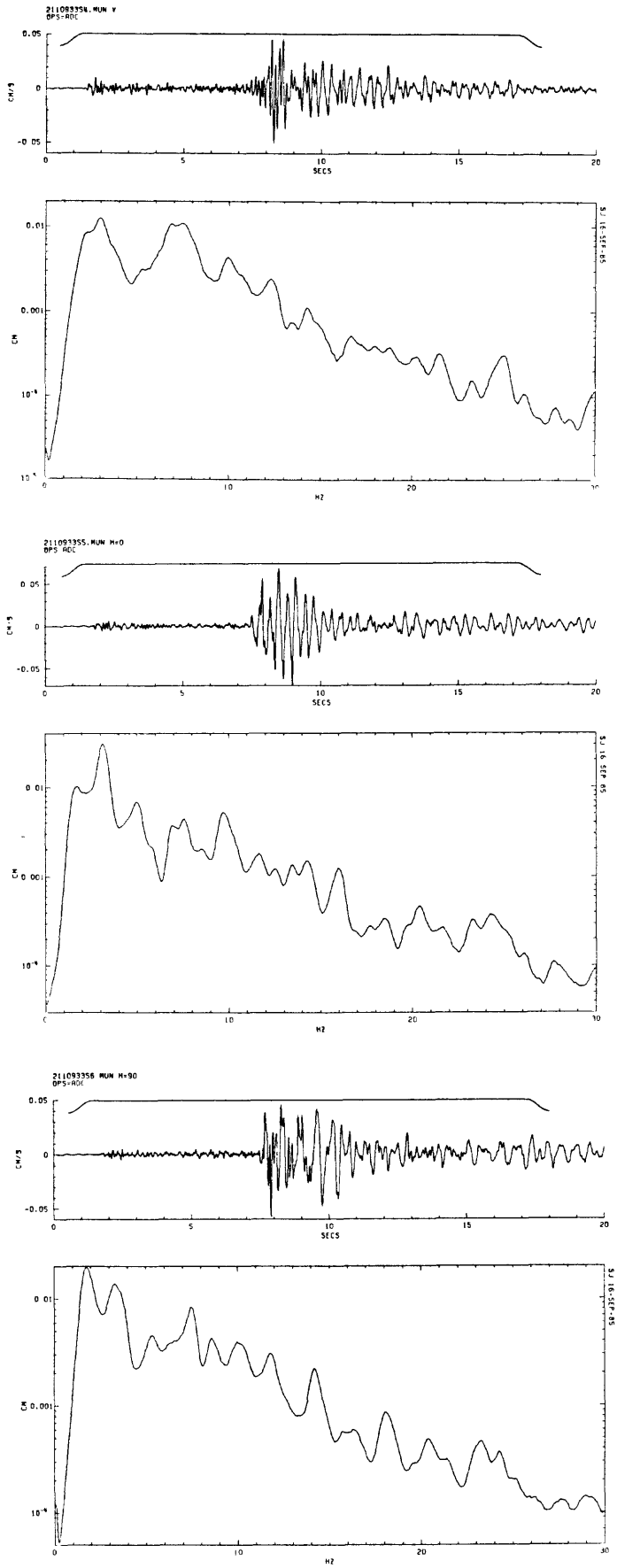

Figure A41. Time series and Fourier amplitude spectra of event on July 30, 1985 (Julian 211) at 09:33 for the vertical, horizontal (N-S and E-W) components, respectively, for stations MUN.

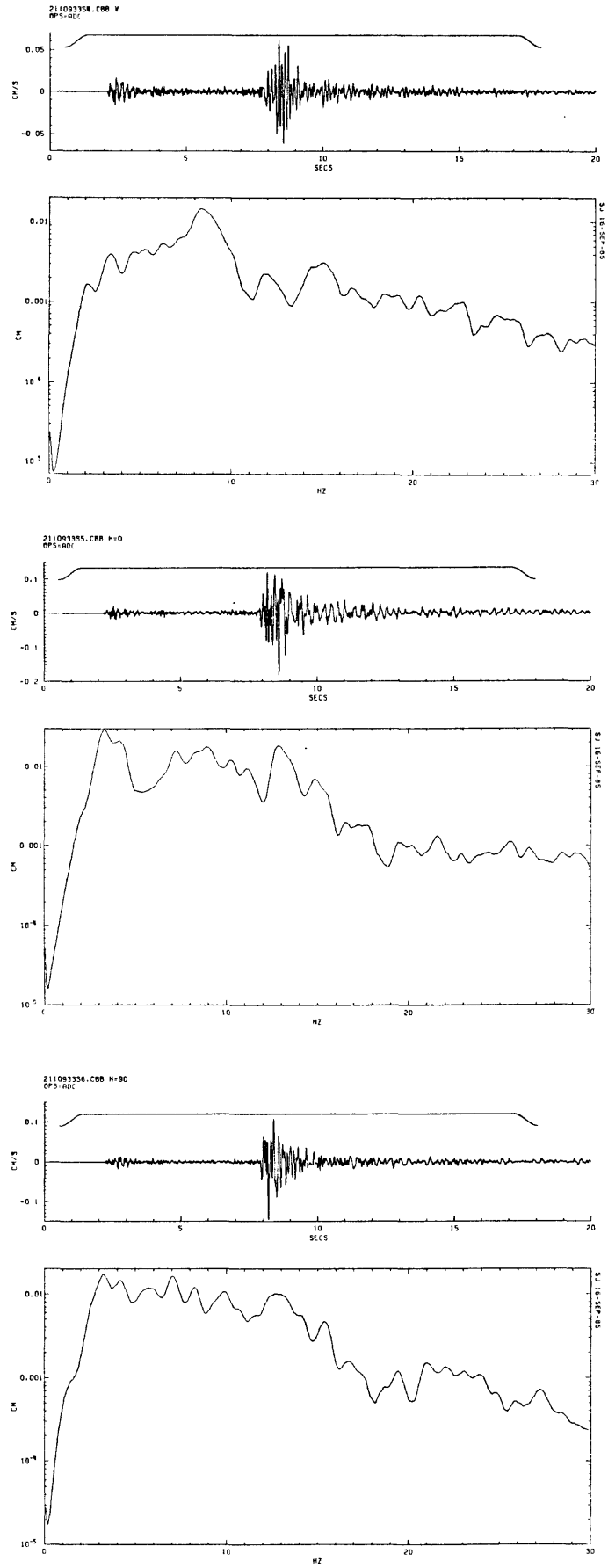

Figure A42. Time series and Fourier amplitude spectra of event on July 30, 1985 (Julian 211) at 09:33 for the vertical, horizontal (N-S and E-W) components, respectively, for stations CBB.

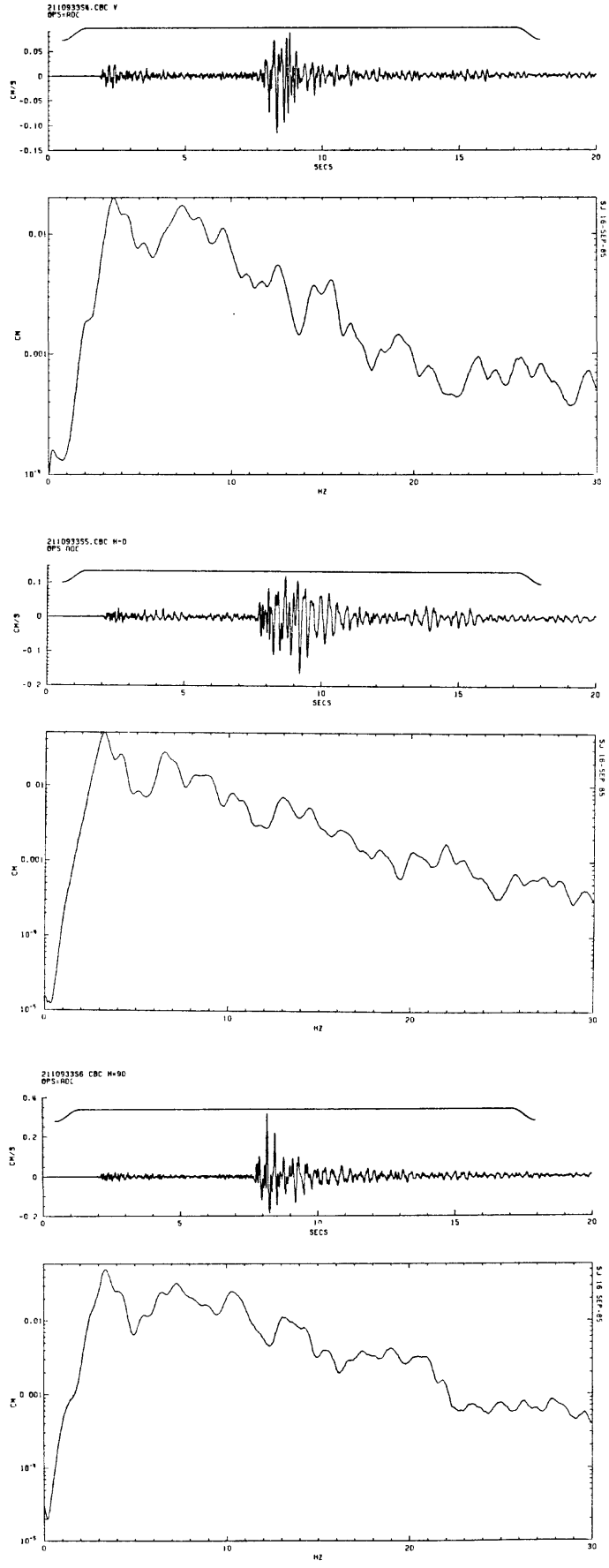

Figure A43. Time series and Fourier amplitude spectra of event on July 30, 1985 (Julian 211) at 09:33 for the vertical, horizontal (N-S and E-W) components, respectively, for stations CBC.

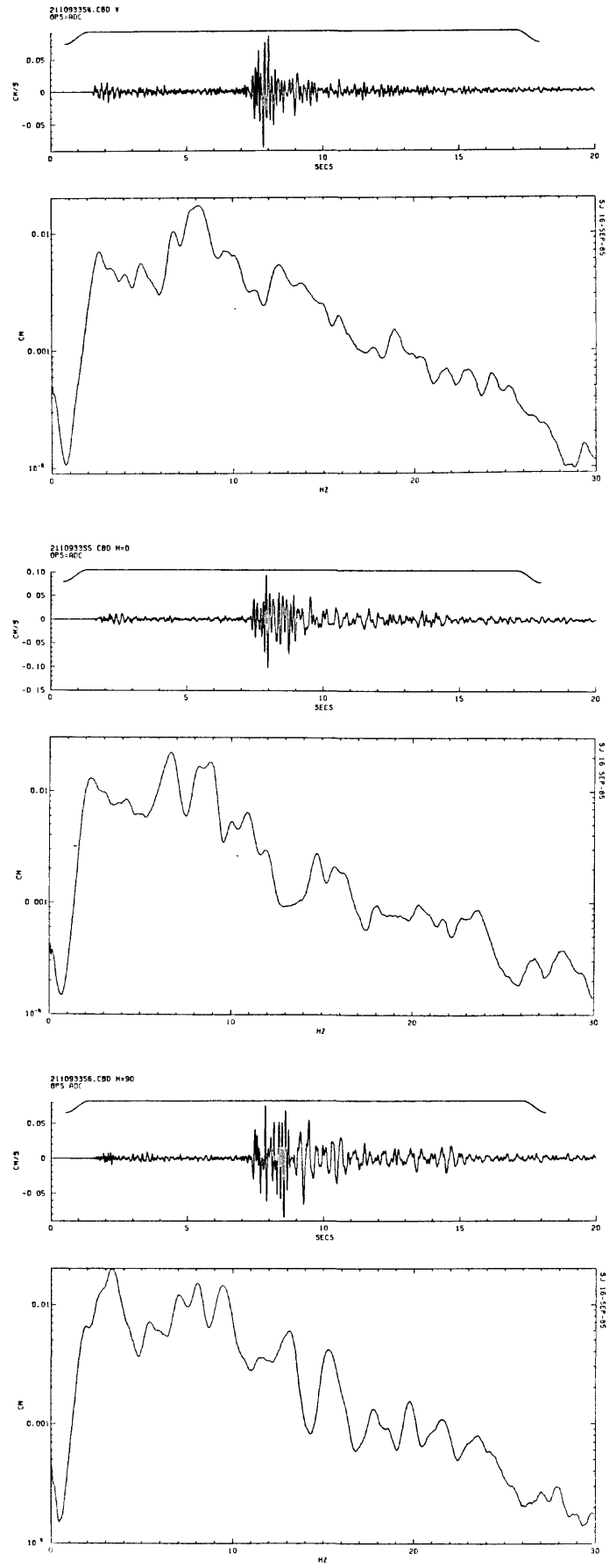

Figure A44. Time series and Fourier amplitude spectra of event on July 30, 1985 (Julian 211) at 09:33 for the vertical, horizontal (N-S and E-W) components, respectively, for stations CBD.

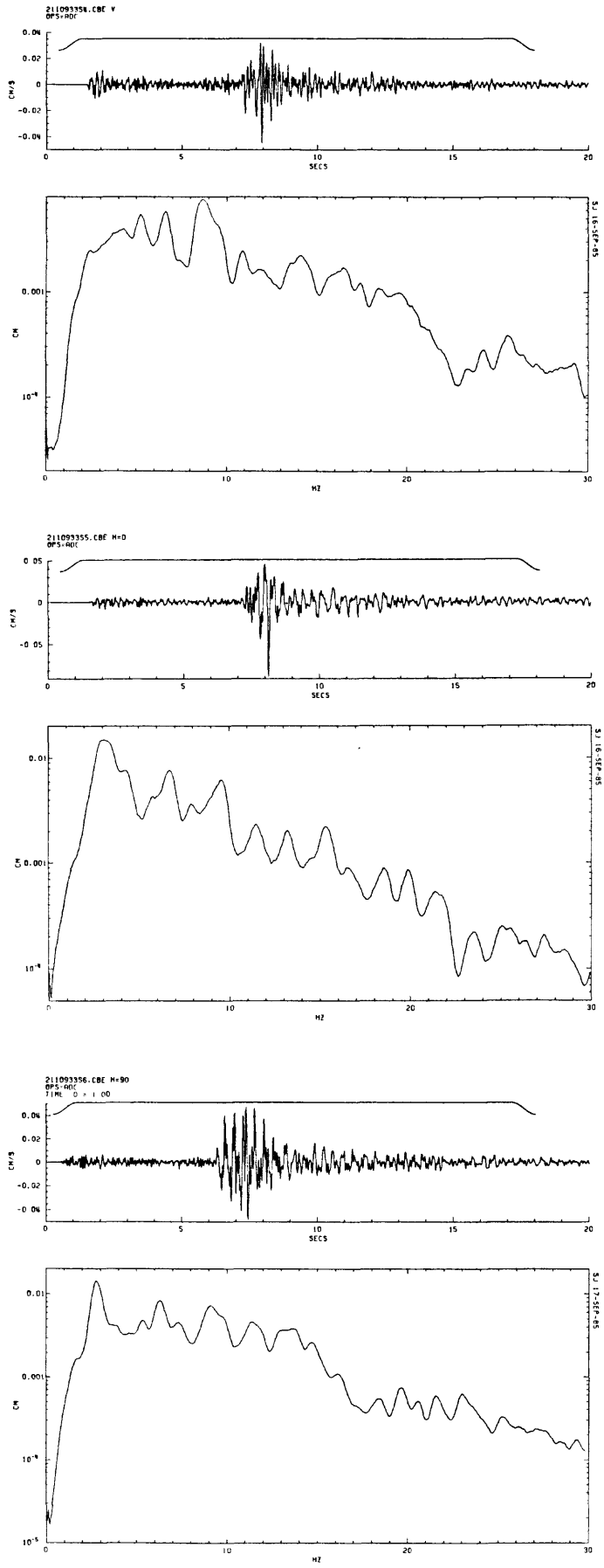

Figure A45. Time series and Fourier amplitude spectra of event on July 30, 1985 (Julian 211) at 09:33 for the vertical, horizontal (N-S and E-W) components, respectively, for stations CBE.

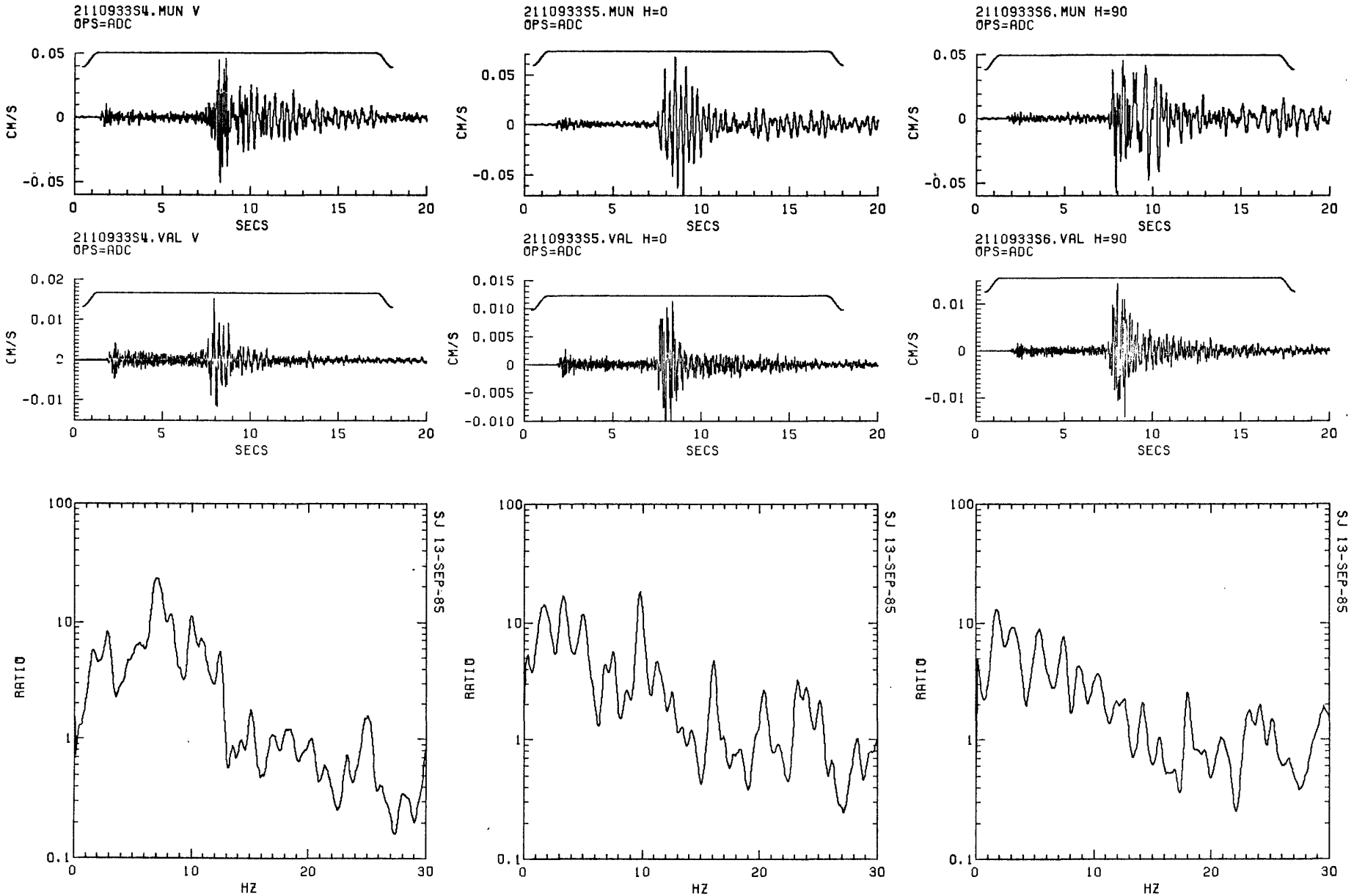

Figure A46. Scaled seismograms and spectral ratios of event on July 30, 1985 (Julian 211) at 09:33 for the vertical, horizontal (N-S and E-W) components, respectively, of stations MUN/VAL.

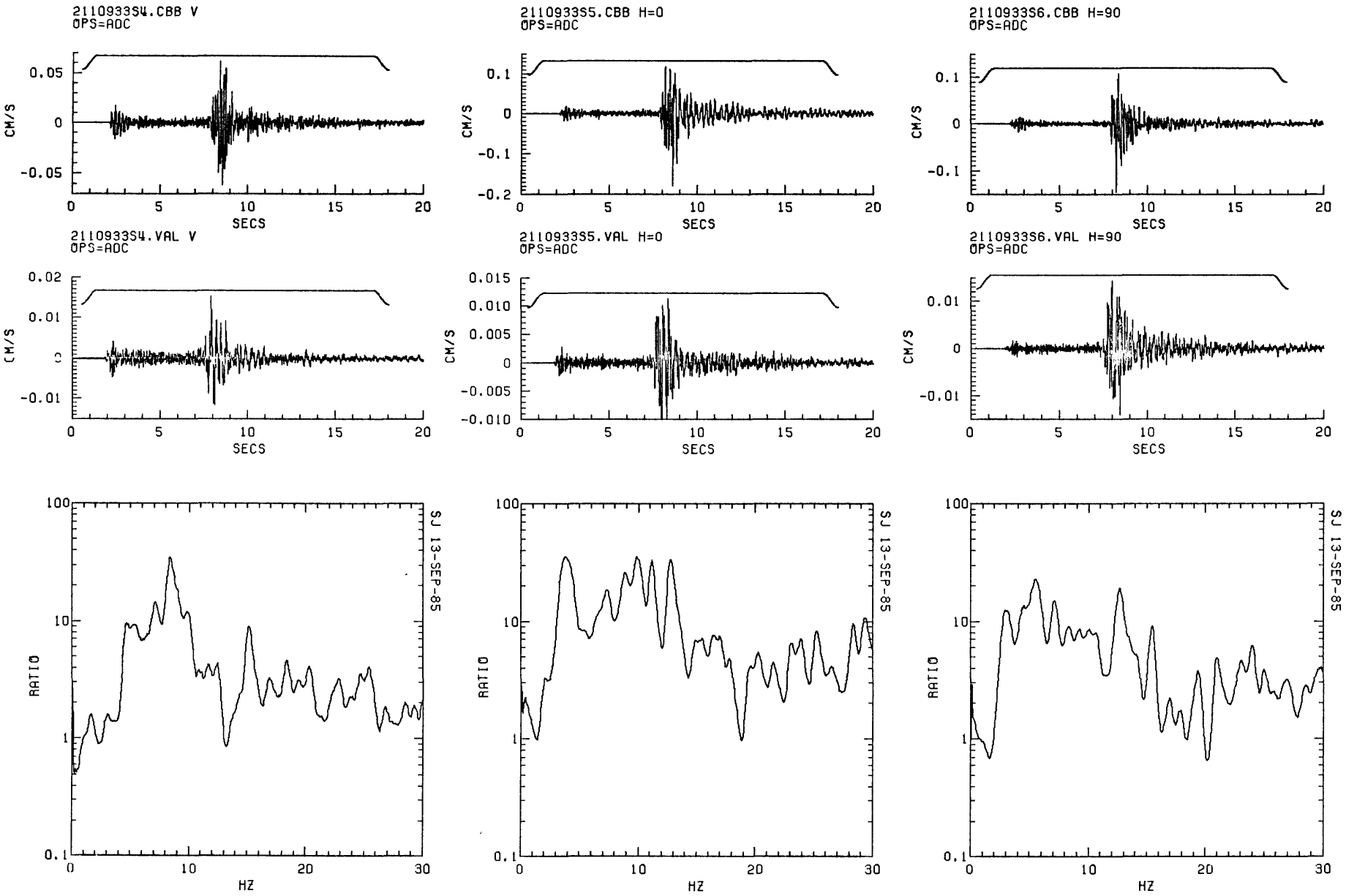

Figure A47. Scaled seismograms and spectral ratios of event on July 30, 1985 (Julian 211) at 09:33 for the vertical, horizontal (N-S and E-W) components, respectively, of stations CBB/VAL.

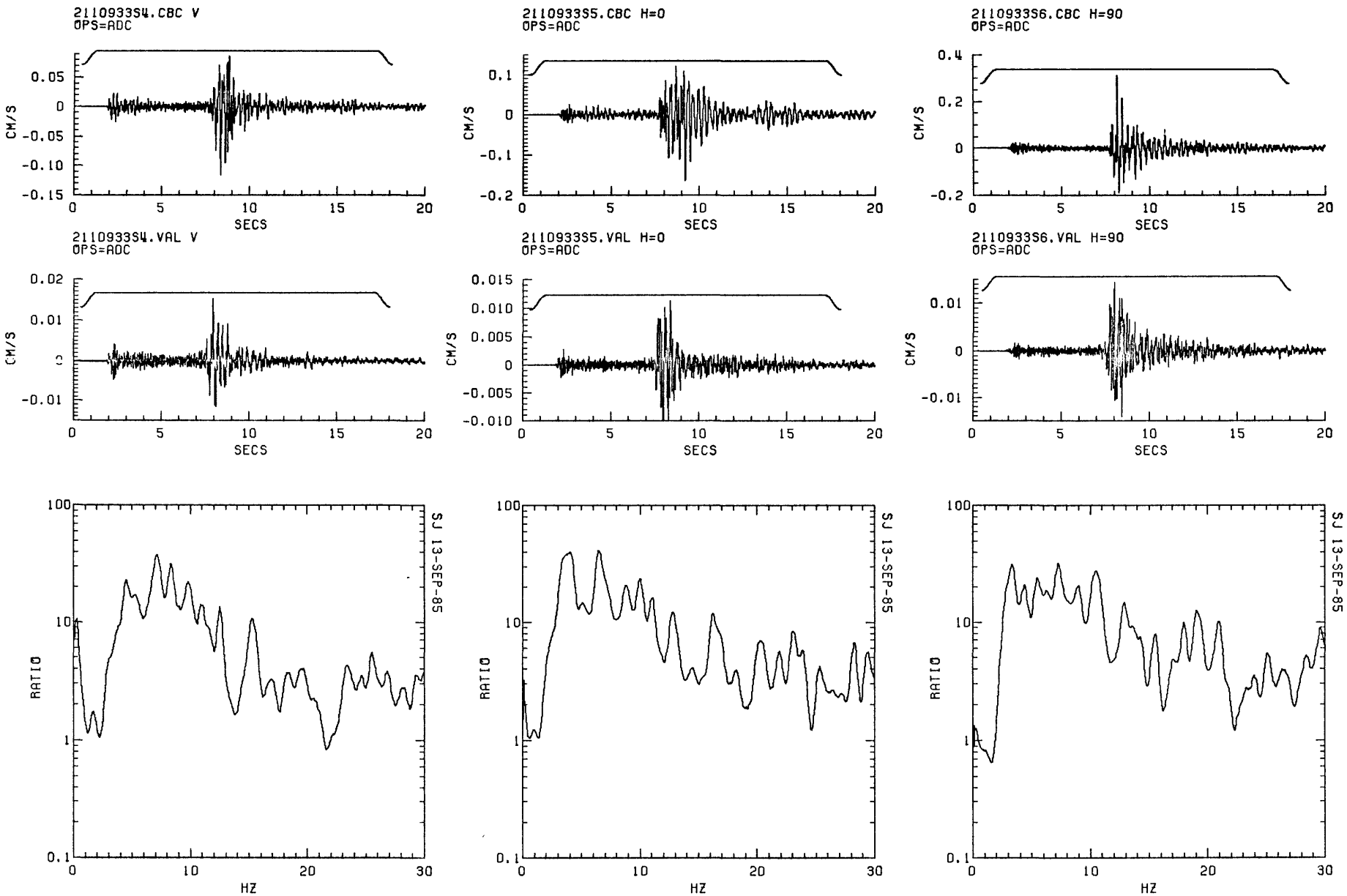

Figure A48. Scaled seismograms and spectral ratios of event on July 30, 1985 (Julian 211) at 09:33 for the vertical, horizontal (N-S and E-W) components, respectively, of stations CBC/VAL.

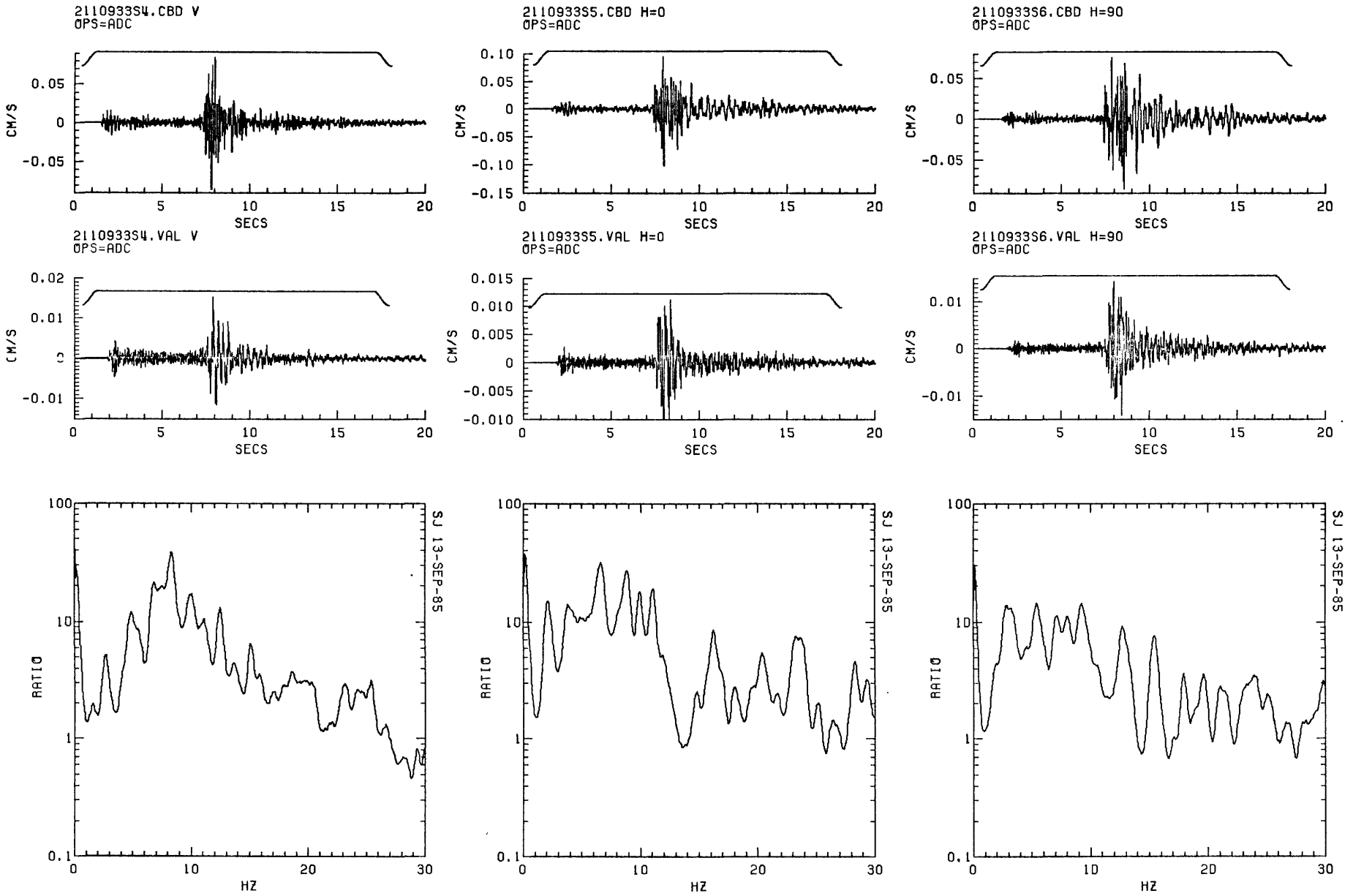

Figure A49. Scaled seismograms and spectral ratios of event on July 30, 1985 (Julian 211) at 09:33 for the vertical, horizontal (N-S and E-W) components, respectively, of stations CBD/VAL.

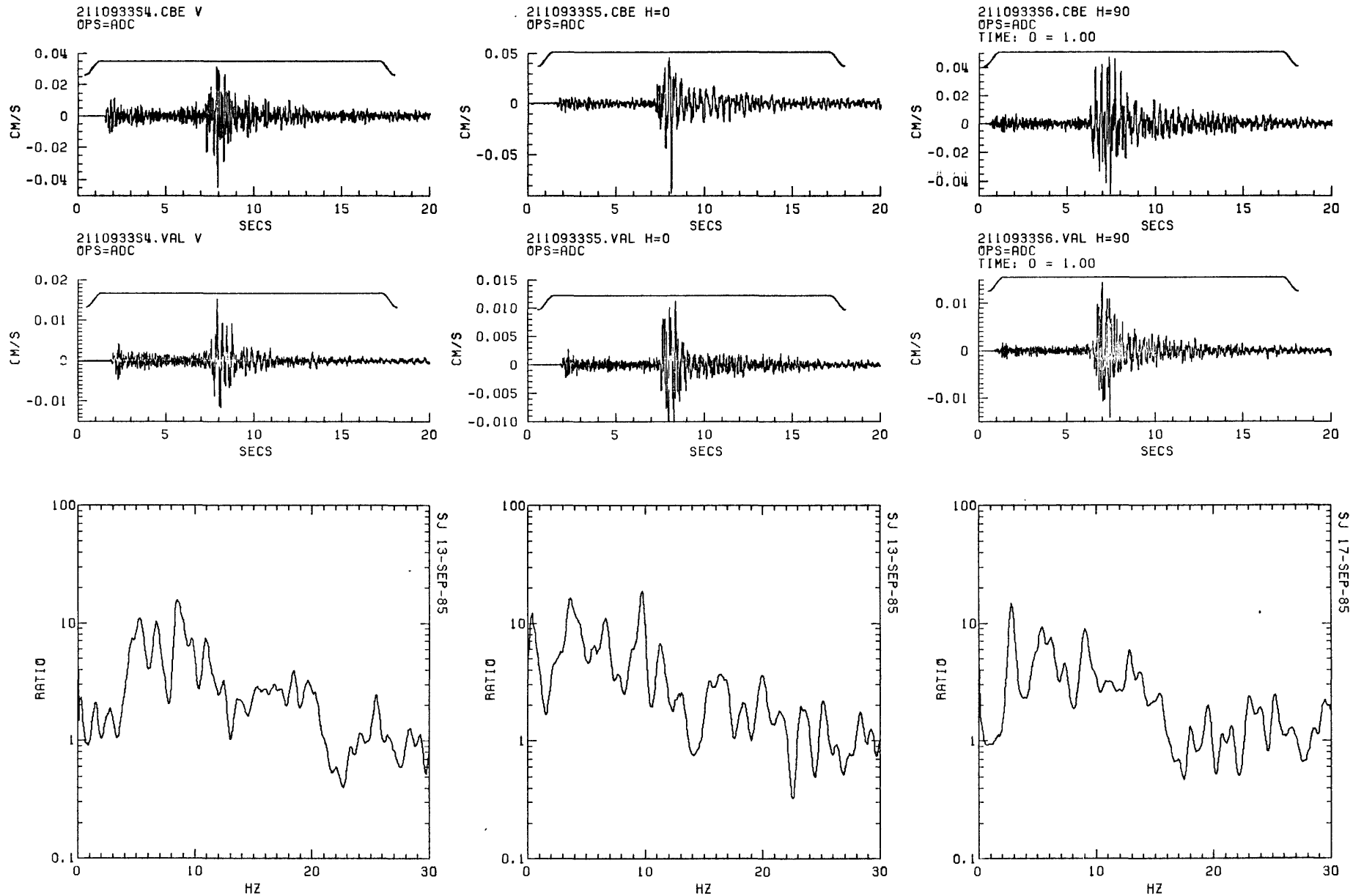

Figure A50. Scaled seismograms and spectral ratios of event on July 30, 1985 (Julian 211) at 09:33 for the vertical, horizontal (N-S and E-W) components, respectively, of stations CBE/VAL.

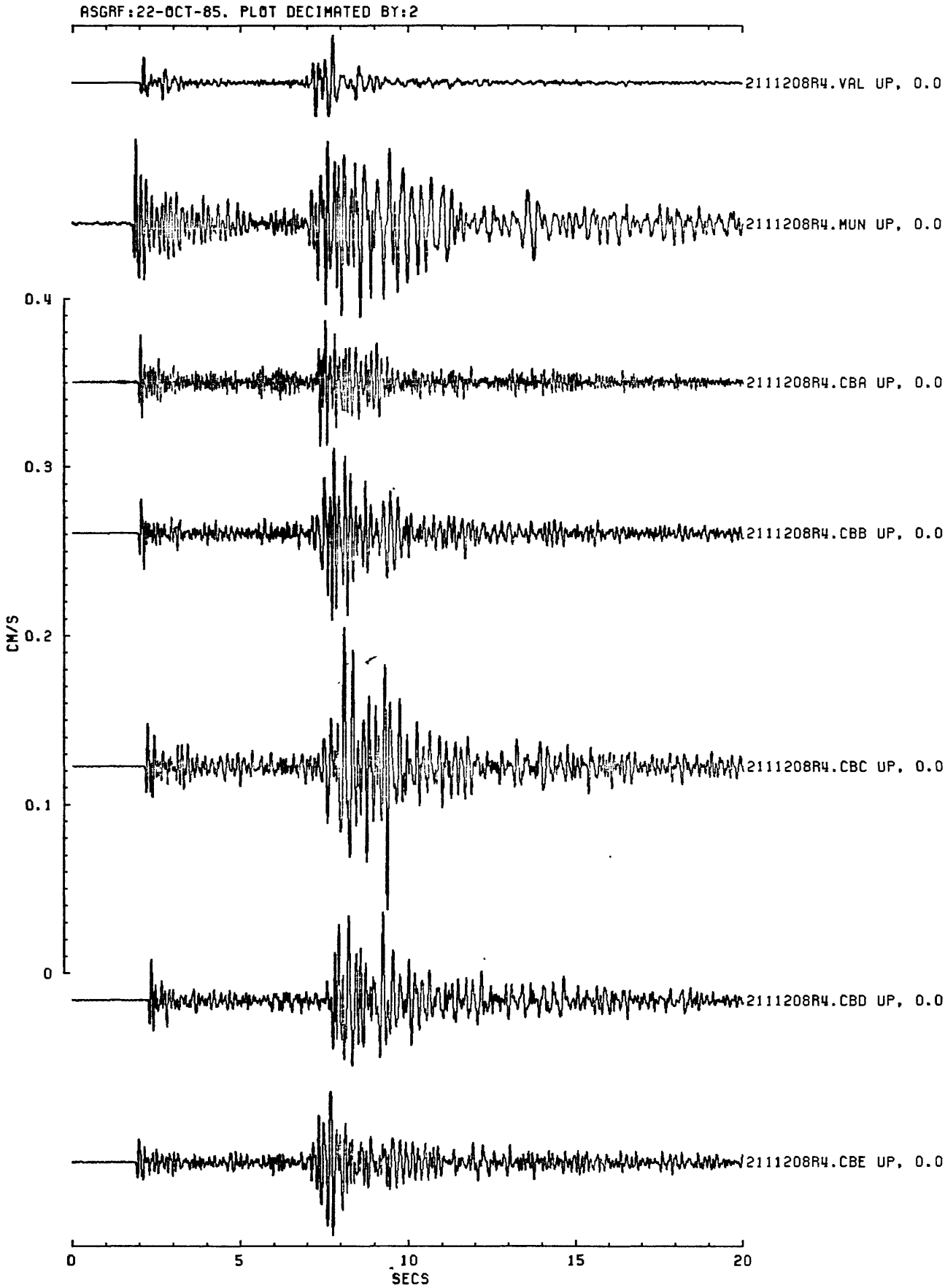

Figure A51. Scaled seismograms for event 2111208 (vertical components).

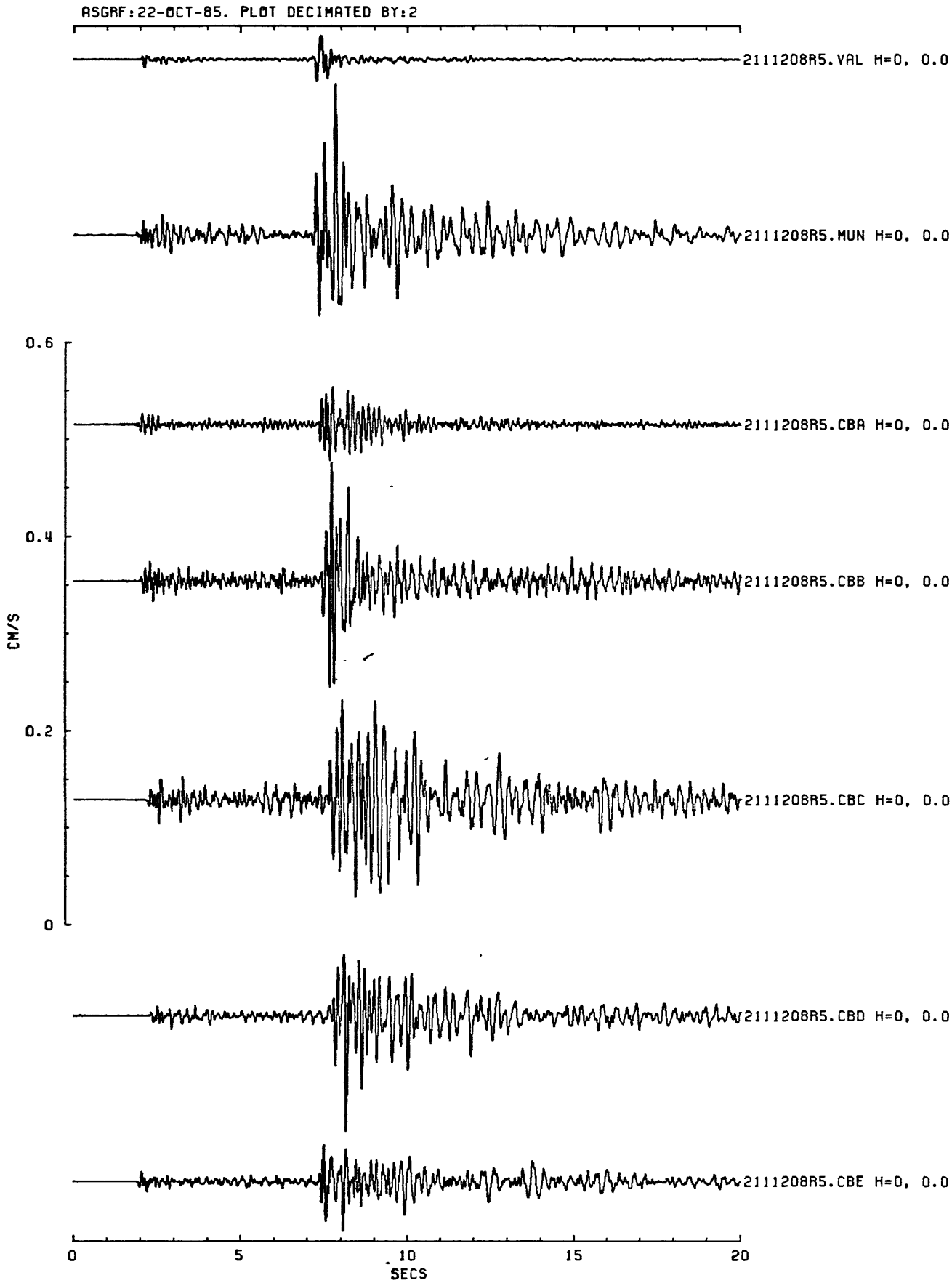

Figure A52. Scaled seismograms for event 2111208 (N-S components).

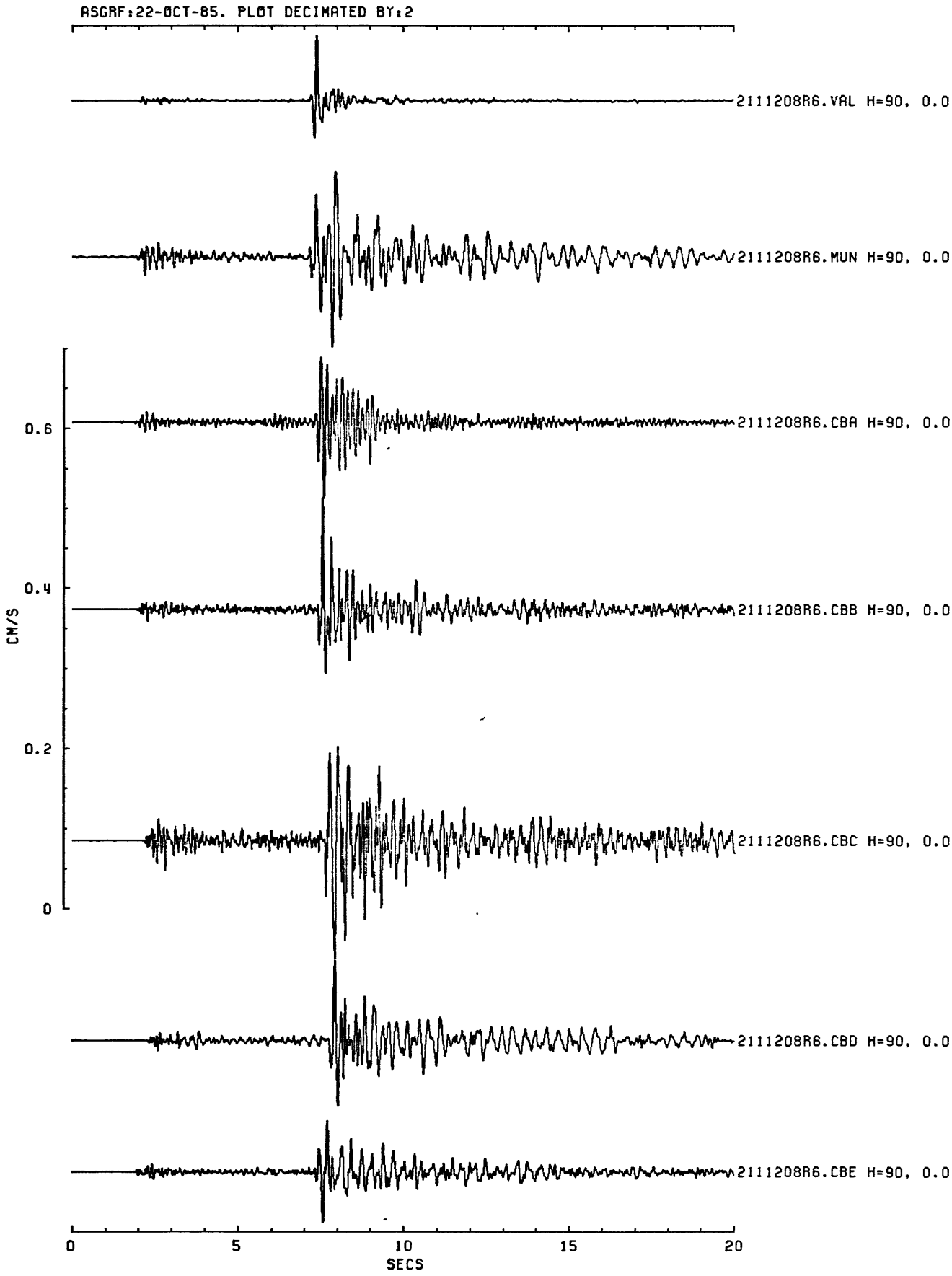

Figure A53. Scaled seismograms for event 2111208 (E-W components).

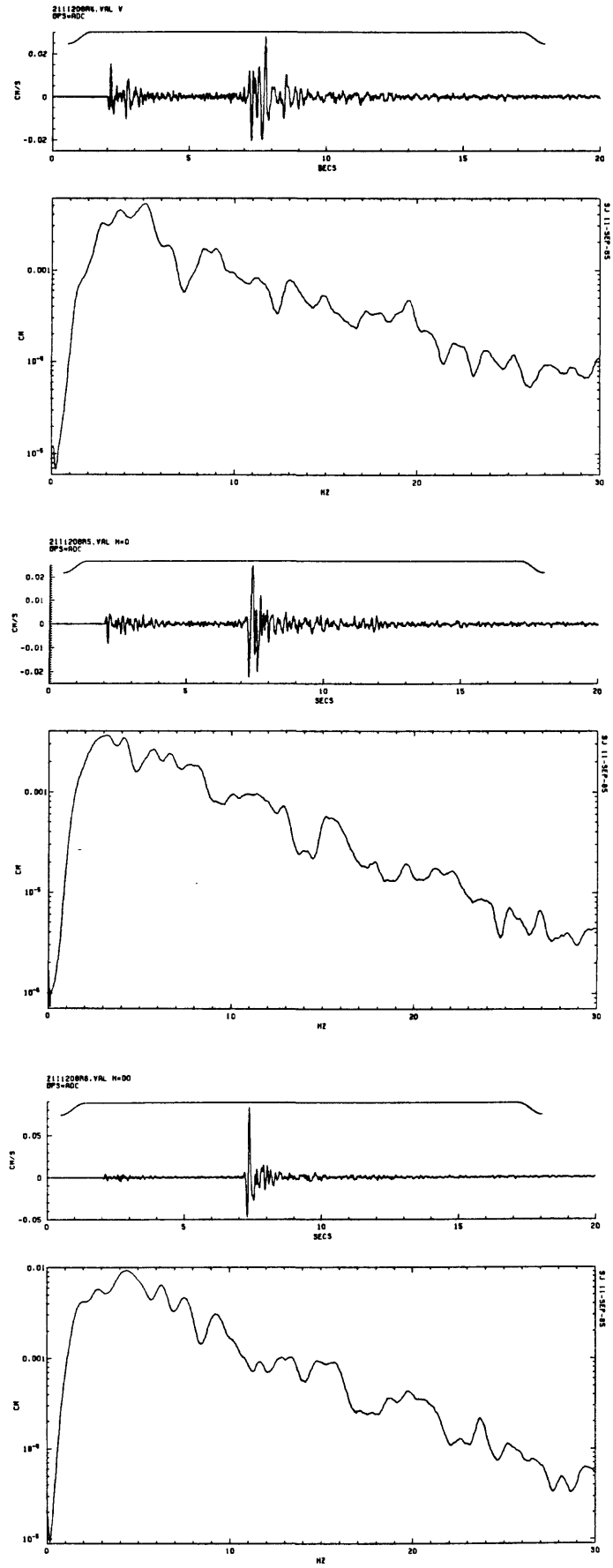

Figure A54. Time series and Fourier amplitude spectra of event on July 30, 1985 (Julian 211) at 12:08 for the vertical, horizontal (N-S and E-W) components, respectively, for station VAL.

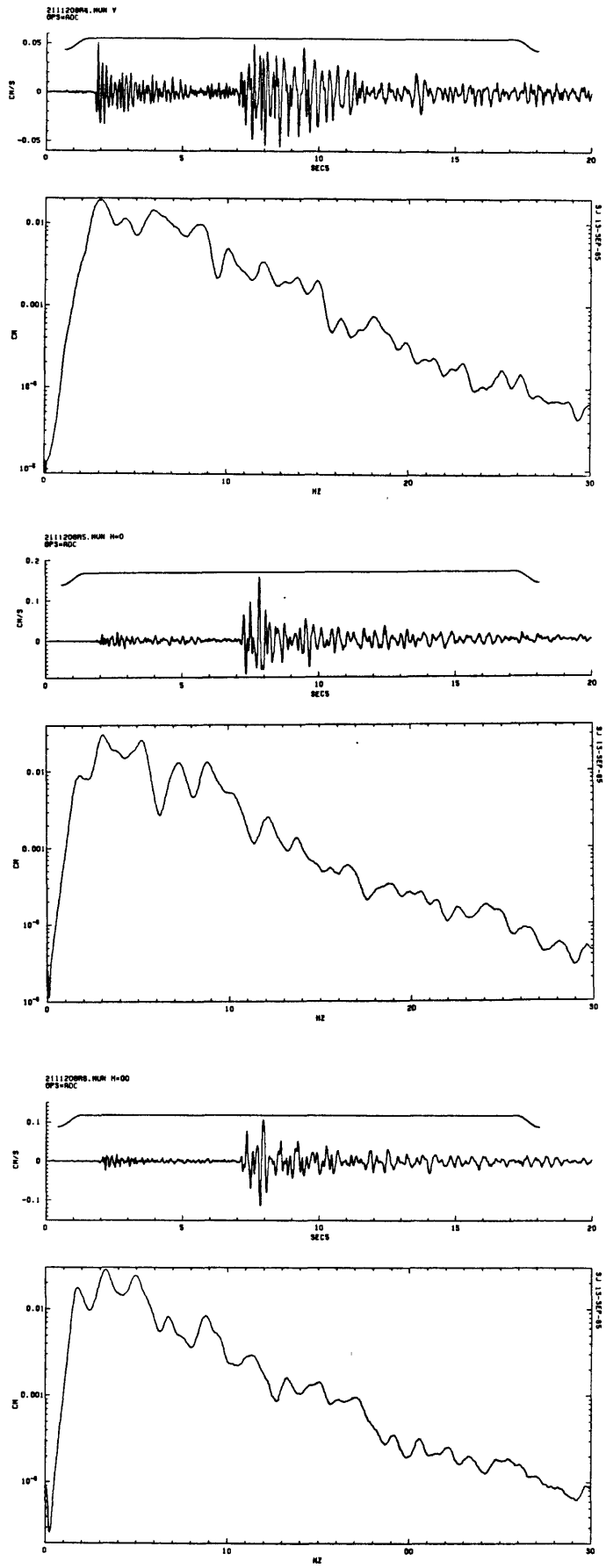

Figure A55. Time series and Fourier amplitude spectra of event on July 30, 1985 (Julian 211) at 12:08 for the vertical, horizontal (N-S and E-W) components, respectively, for station MUN.

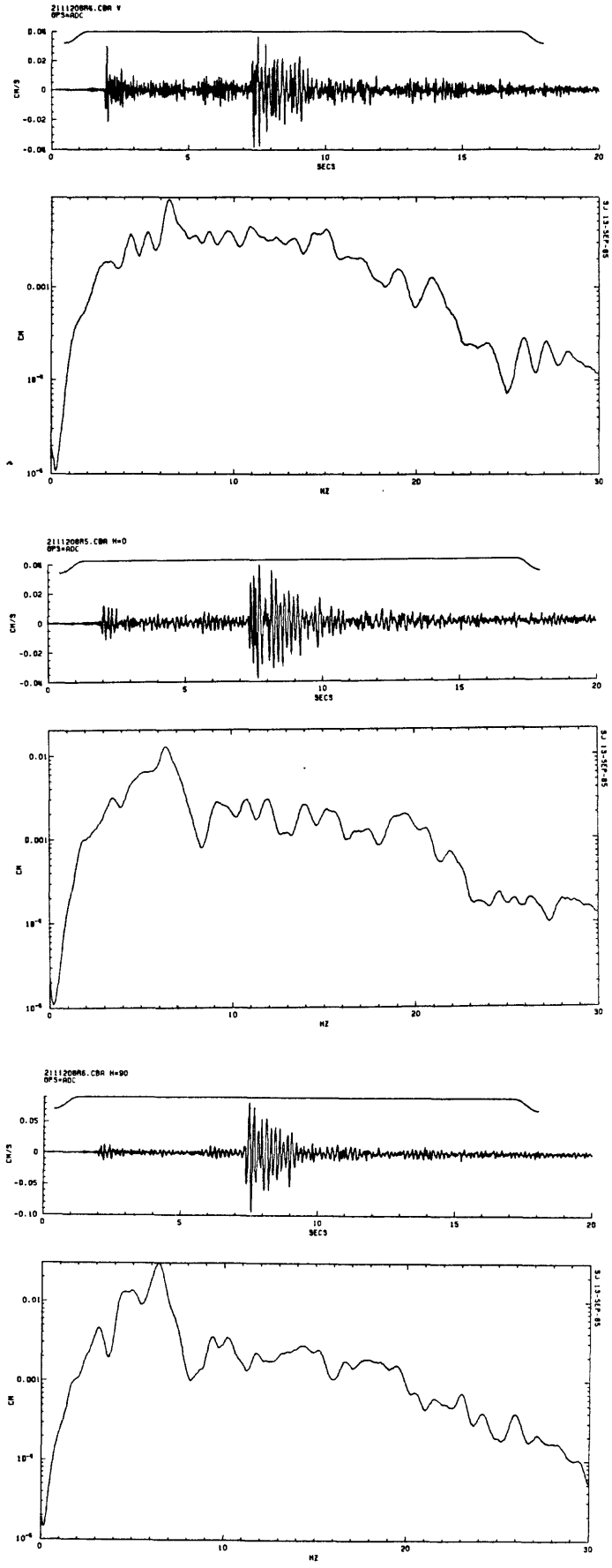

Figure A56. Time series and Fourier amplitude spectra of event on July 30, 1985 (Julian 211) at 12:08 for the vertical, horizontal (N-S and E-W) components, respectively, for station CBA.

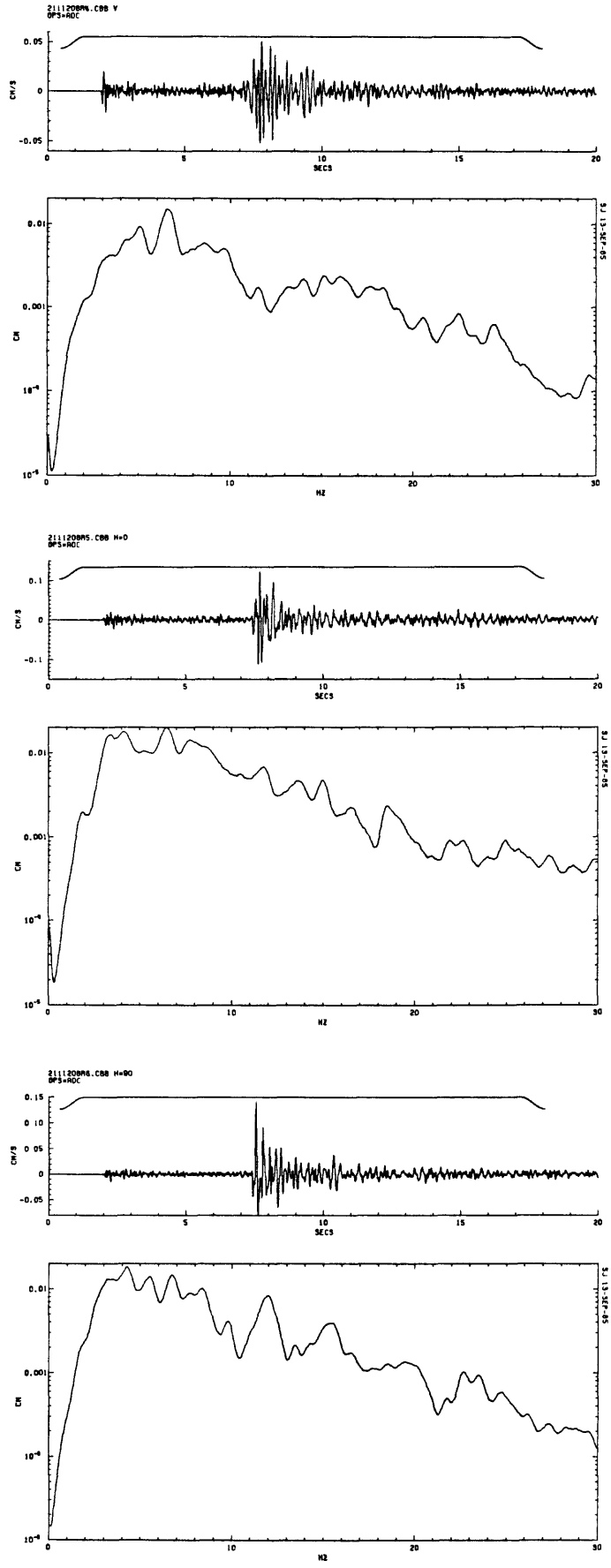

Figure A57. Time series and Fourier amplitude spectra of event on July 30, 1985 (Julian 211) at 12:08 for the vertical, horizontal (N-S and E-W) components, respectively, for station CBB.

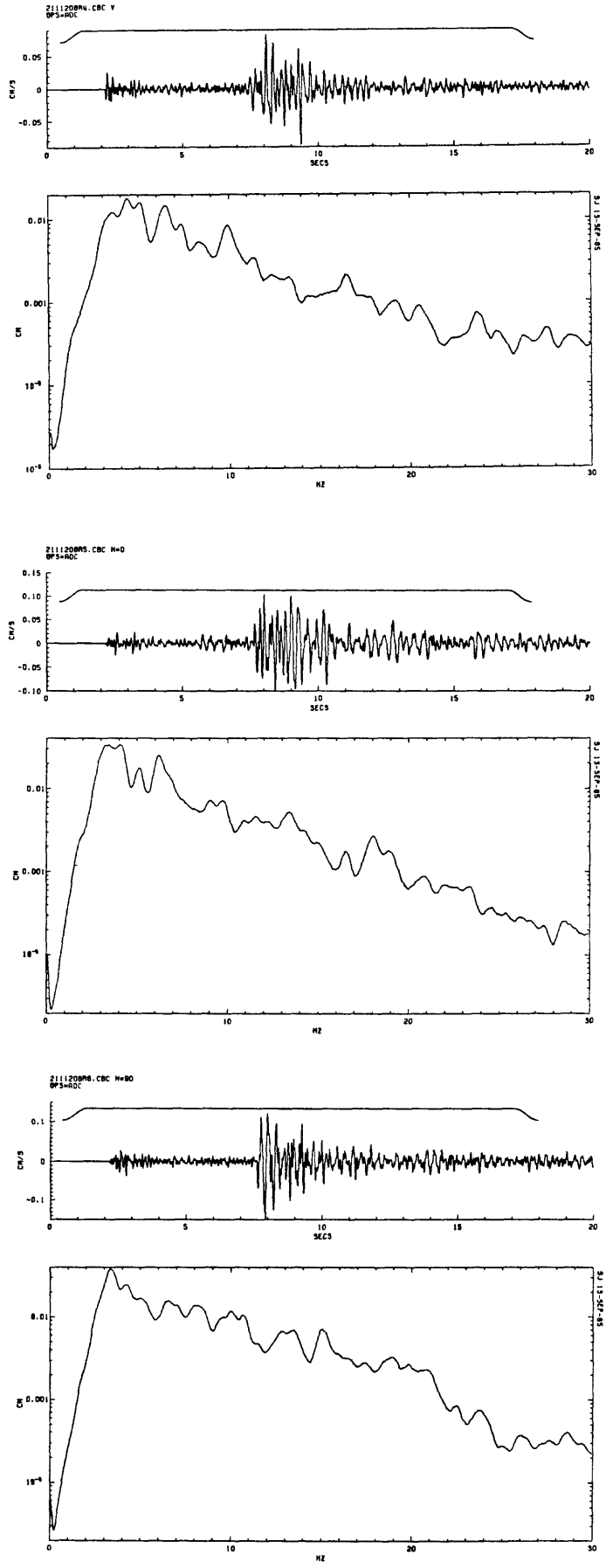

Figure A58. Time series and Fourier amplitude spectra of event on July 30, 1985 (Julian 211) at 12:08 for the vertical, horizontal (N-S and E-W) components, respectively, for station CBC.

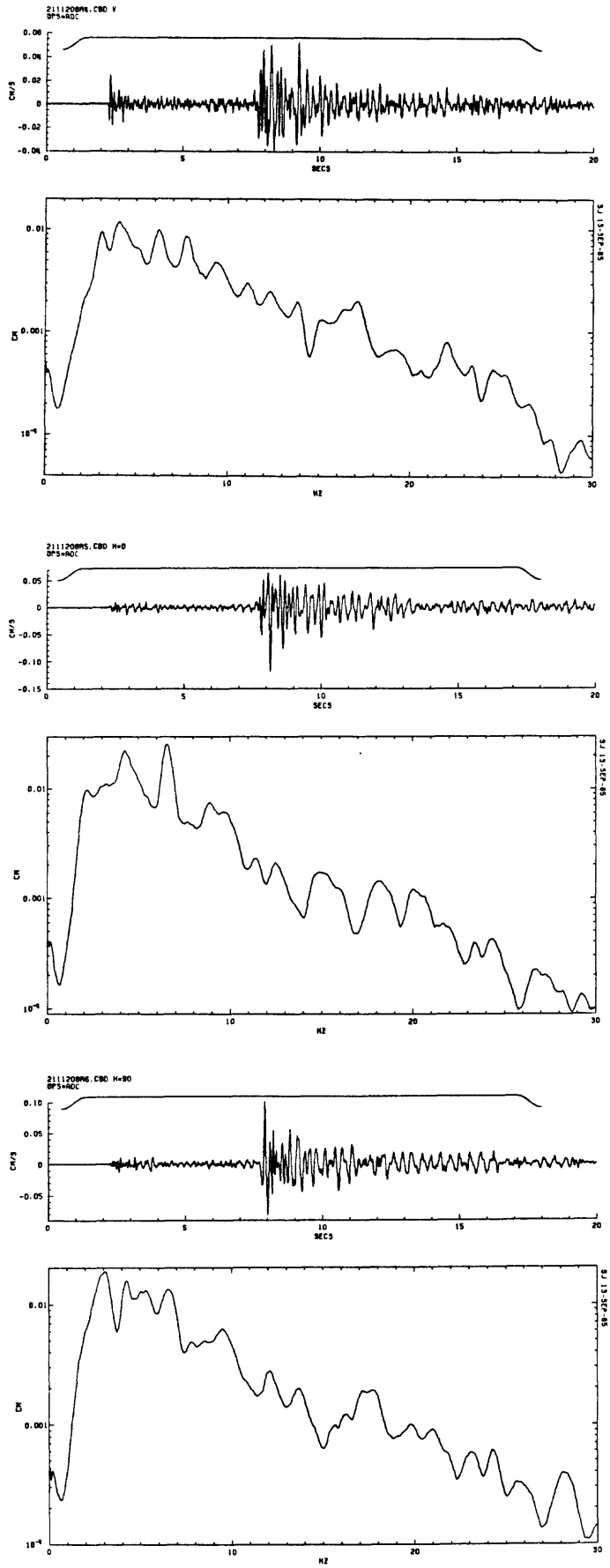

Figure A59. Time series and Fourier amplitude spectra of event on July 30, 1985 (Julian 211) at 12:08 for the vertical, horizontal (N-S and E-W) components, respectively, for station CBD.

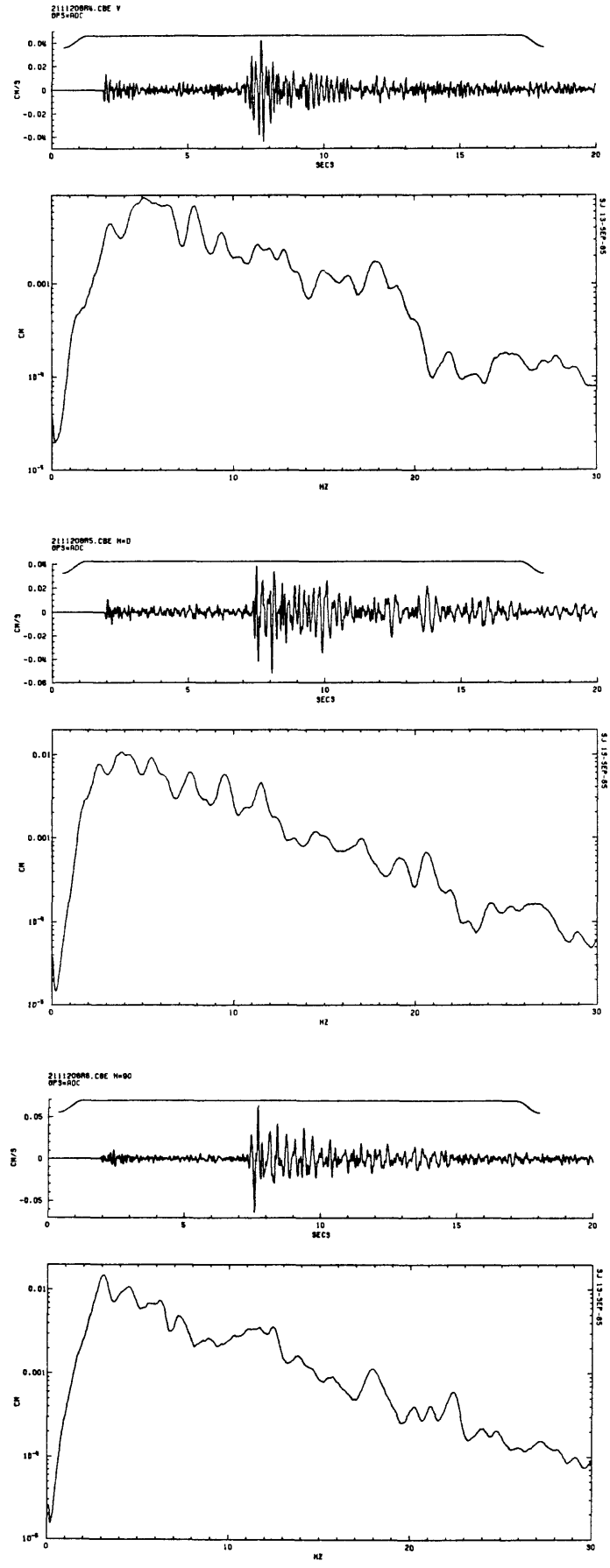

Figure A60. Time series and Fourier amplitude spectra of event on July 30, 1985 (Julian 211) at 12:08 for the vertical, horizontal (N-S and E-W) components, respectively, for station CBF.

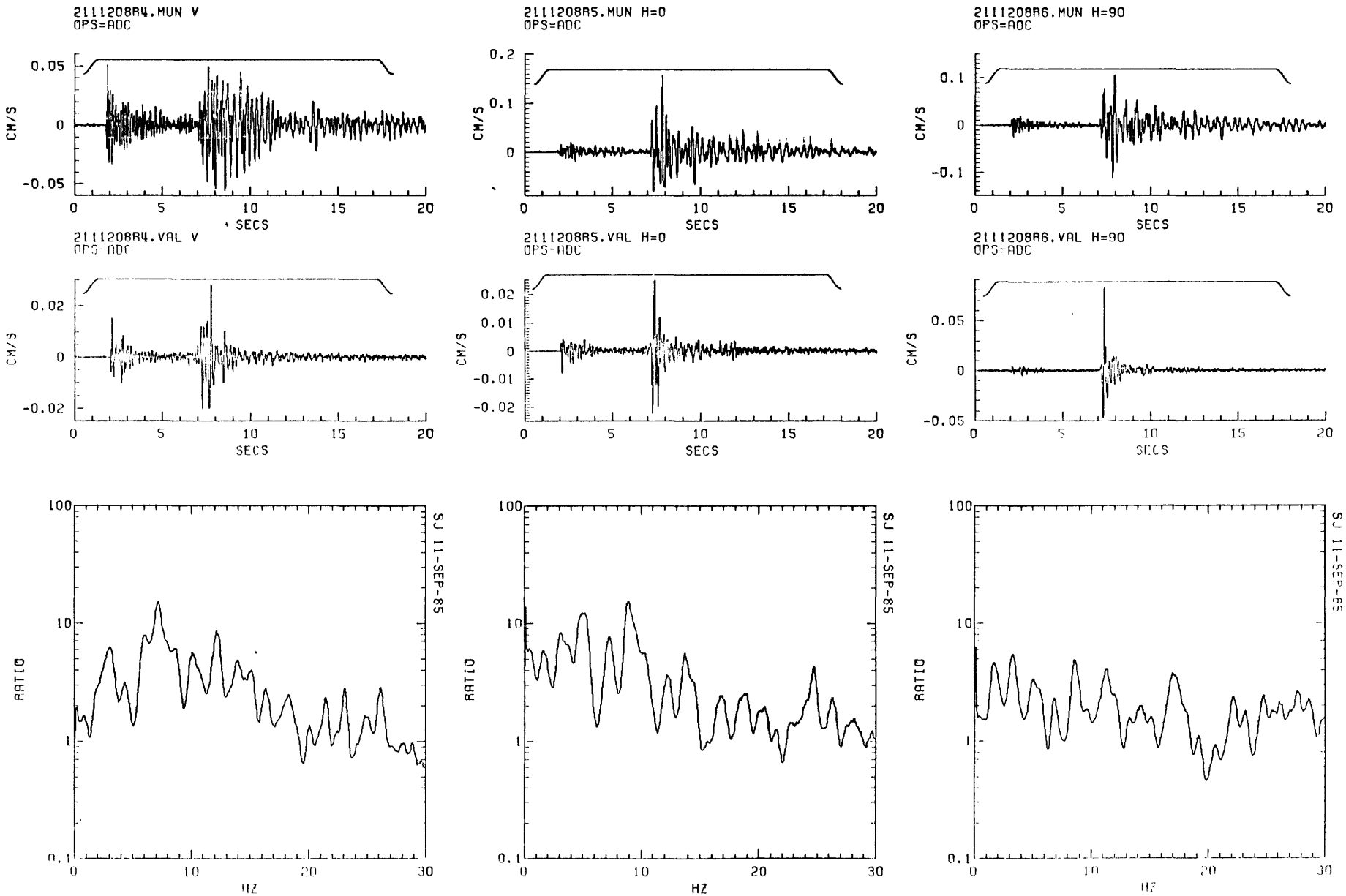

Figure A61. Scaled seismograms and spectral ratios of event on July 29, 1985 (Julian 211) at 12:08 for the vertical, horizontal (N-S and E-W) components, respectively, of stations MUN/VAL.

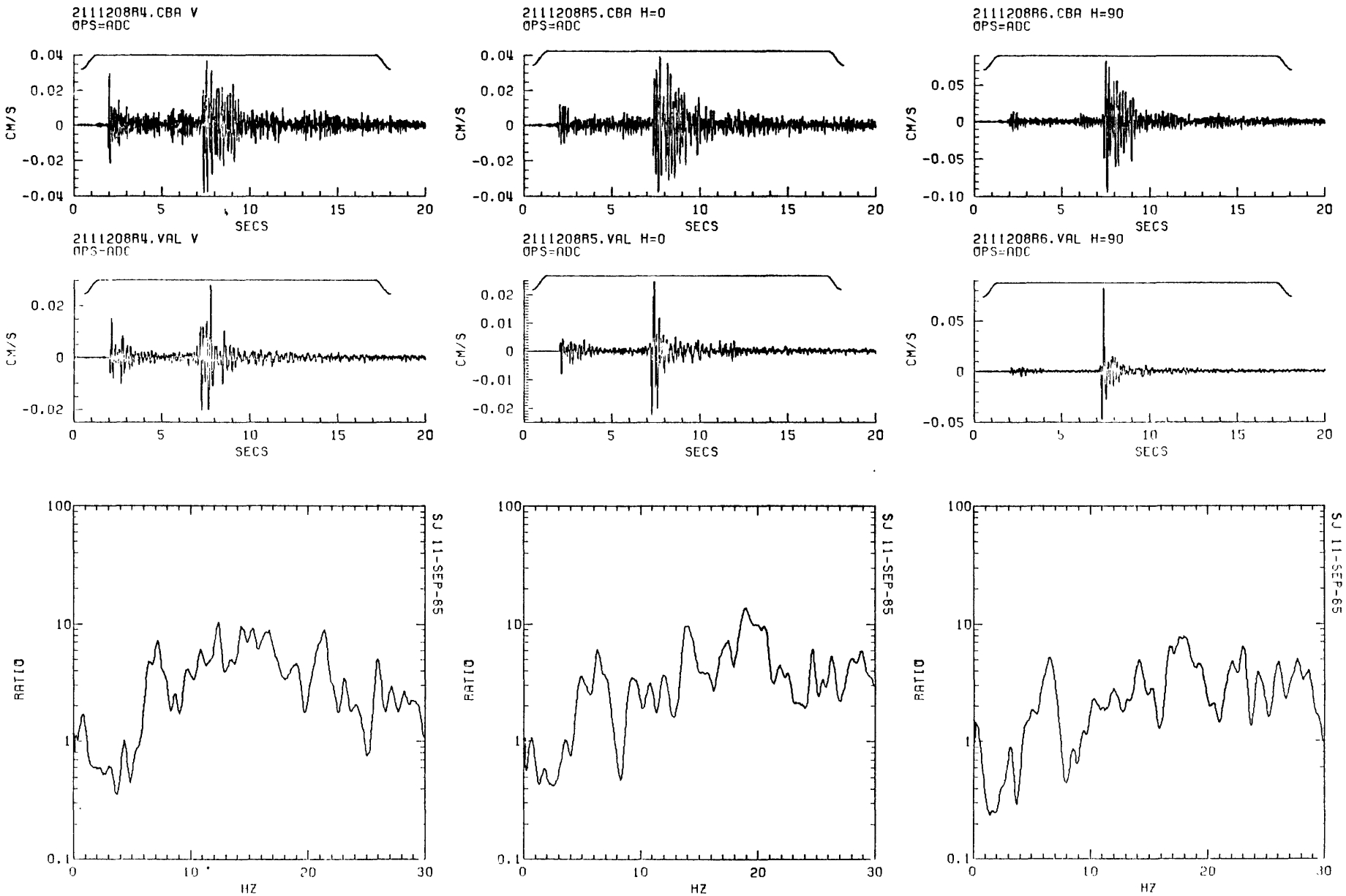

Figure A62. Scaled seismograms and spectral ratios of event on July 29, 1985 (Julian 211) at 12:08 for the vertical, horizontal (N-S and E-W) components, respectively, of stations CBA/VAL.

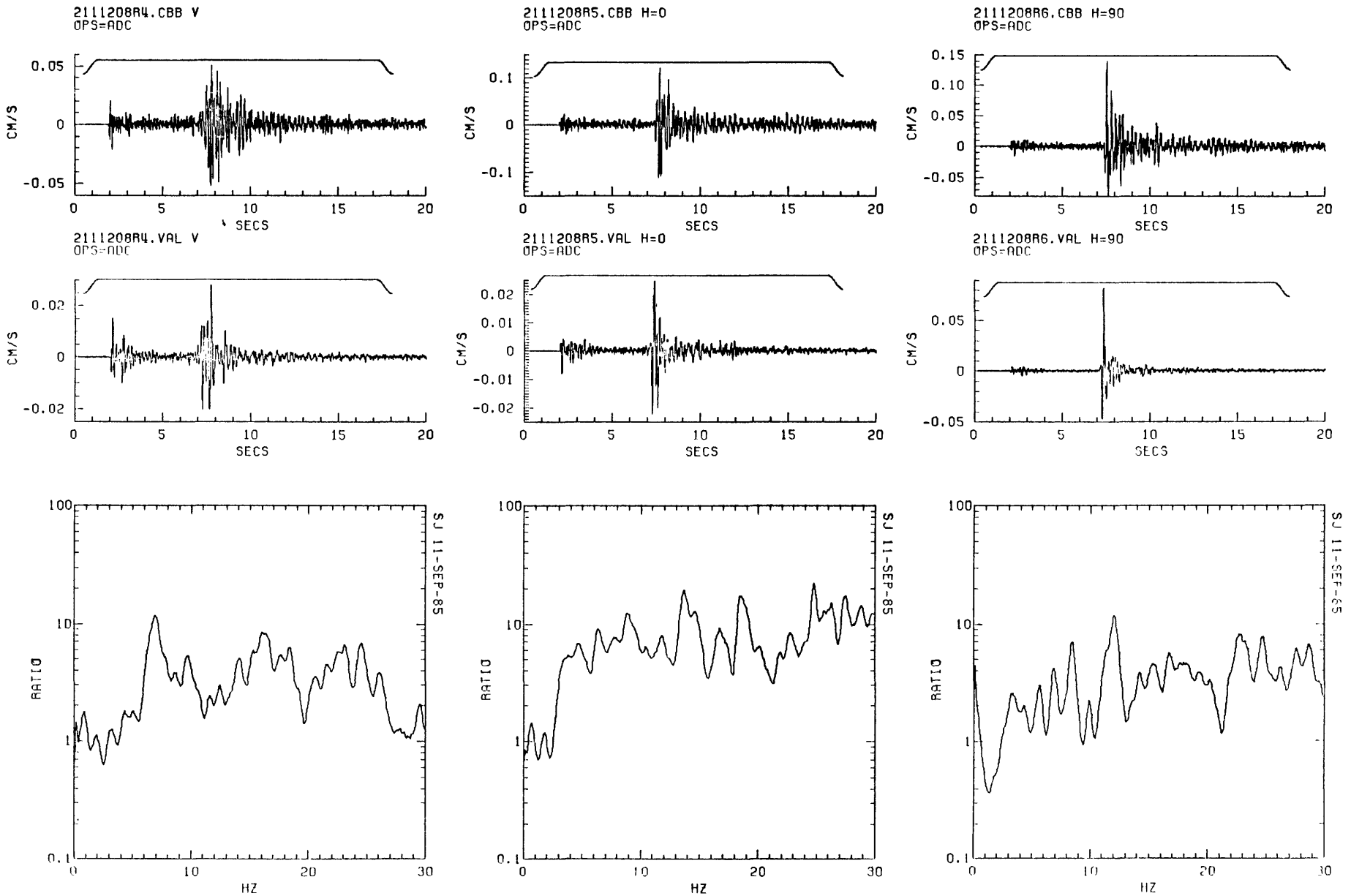

Figure A63. Scaled seismograms and spectral ratios of event on July 29, 1985 (Julian 211) at 12:08 for the vertical, horizontal (N-S and E-W) components, respectively, of stations CBB/VAL.

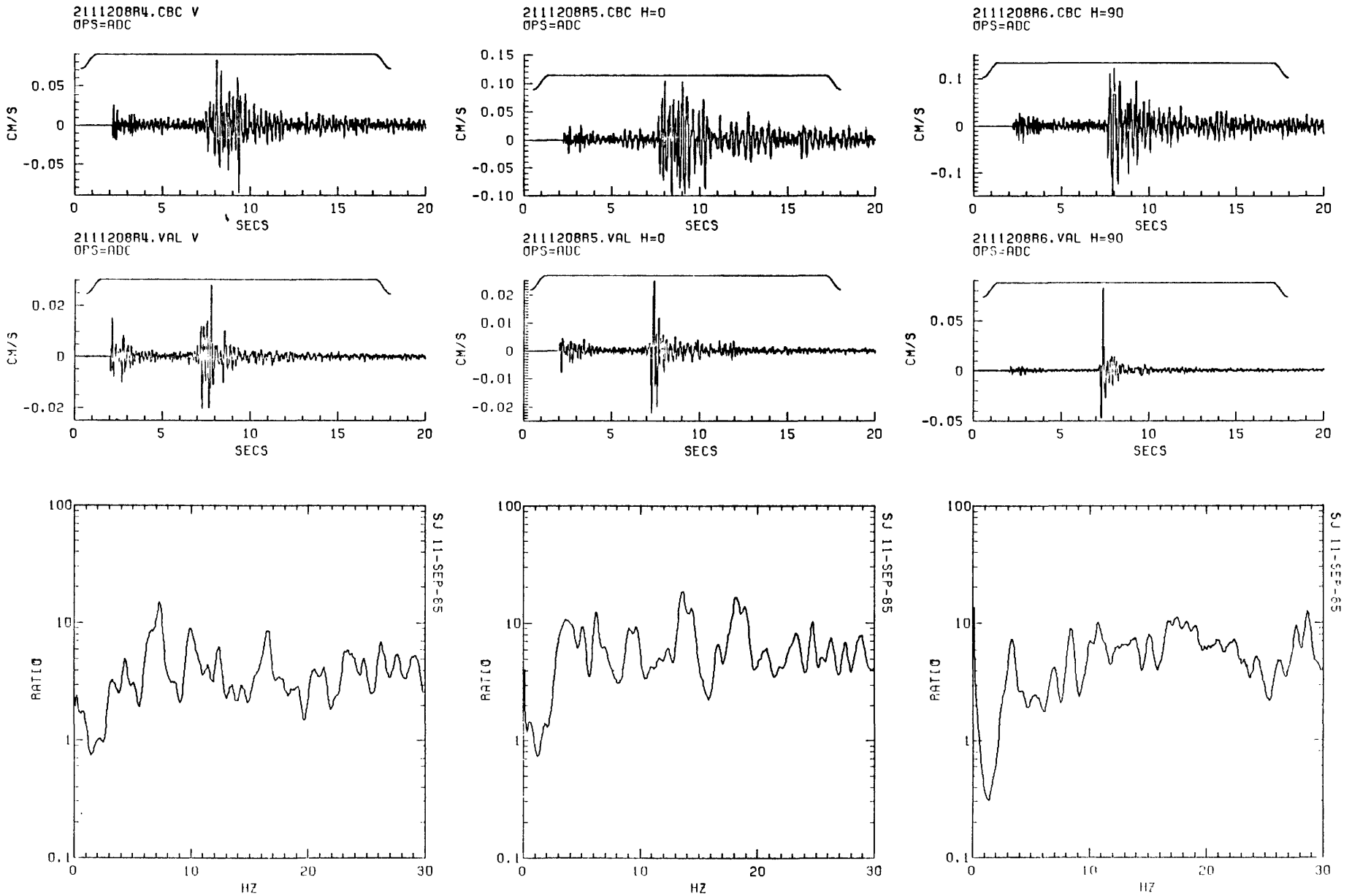

Figure A64. Scaled seismograms and spectral ratios of event on July 29, 1985 (Julian 211) at 12:08 for the vertical, horizontal (N-S and E-W) components, respectively, of stations CBC/VAL.

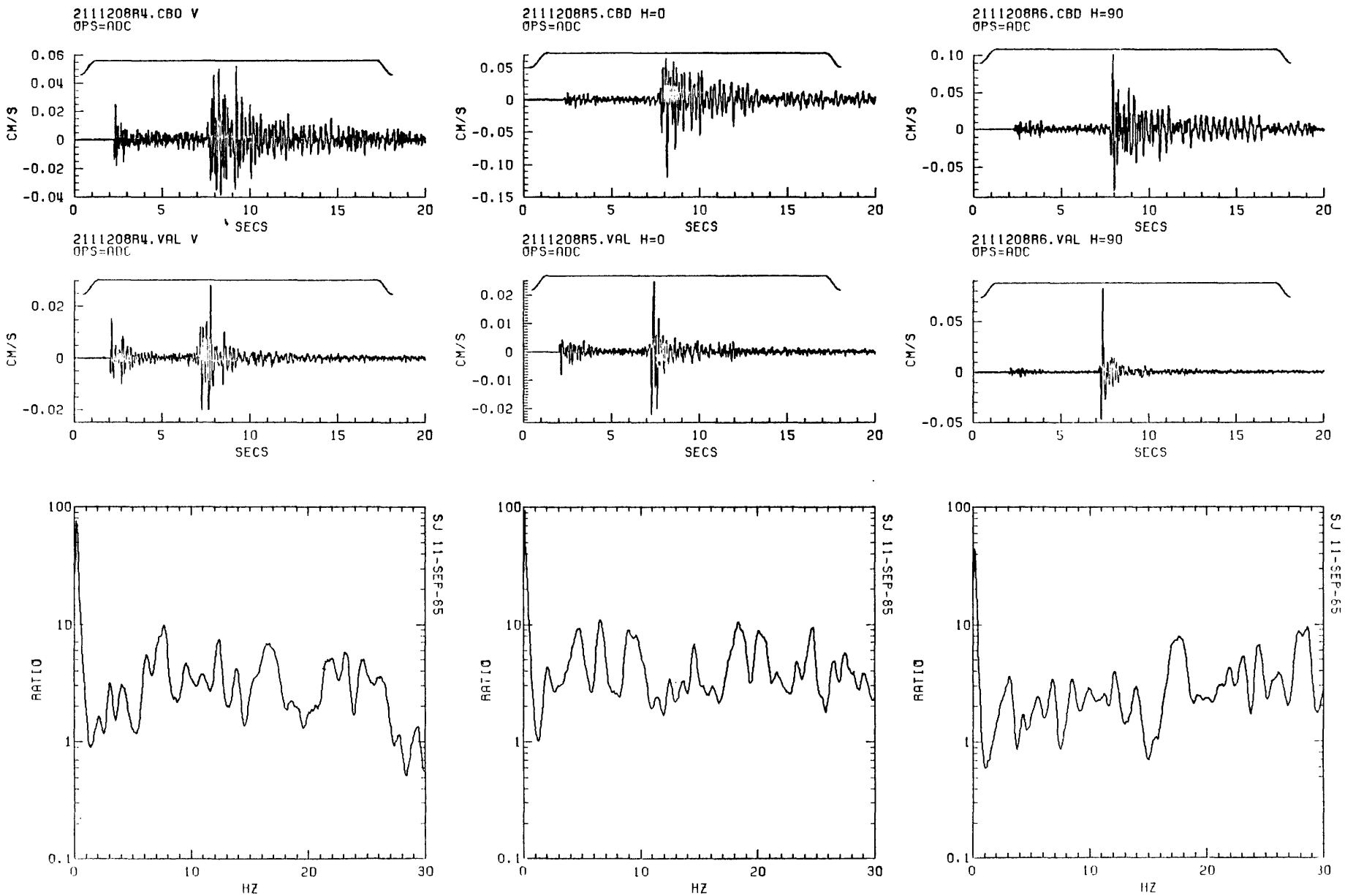

Figure A65. Scaled seismograms and spectral ratios of event on July 29, 1985 (Julian 211) at 12:08 for the vertical, horizontal (N-S and E-W) components, respectively, of stations CBD/VAL.

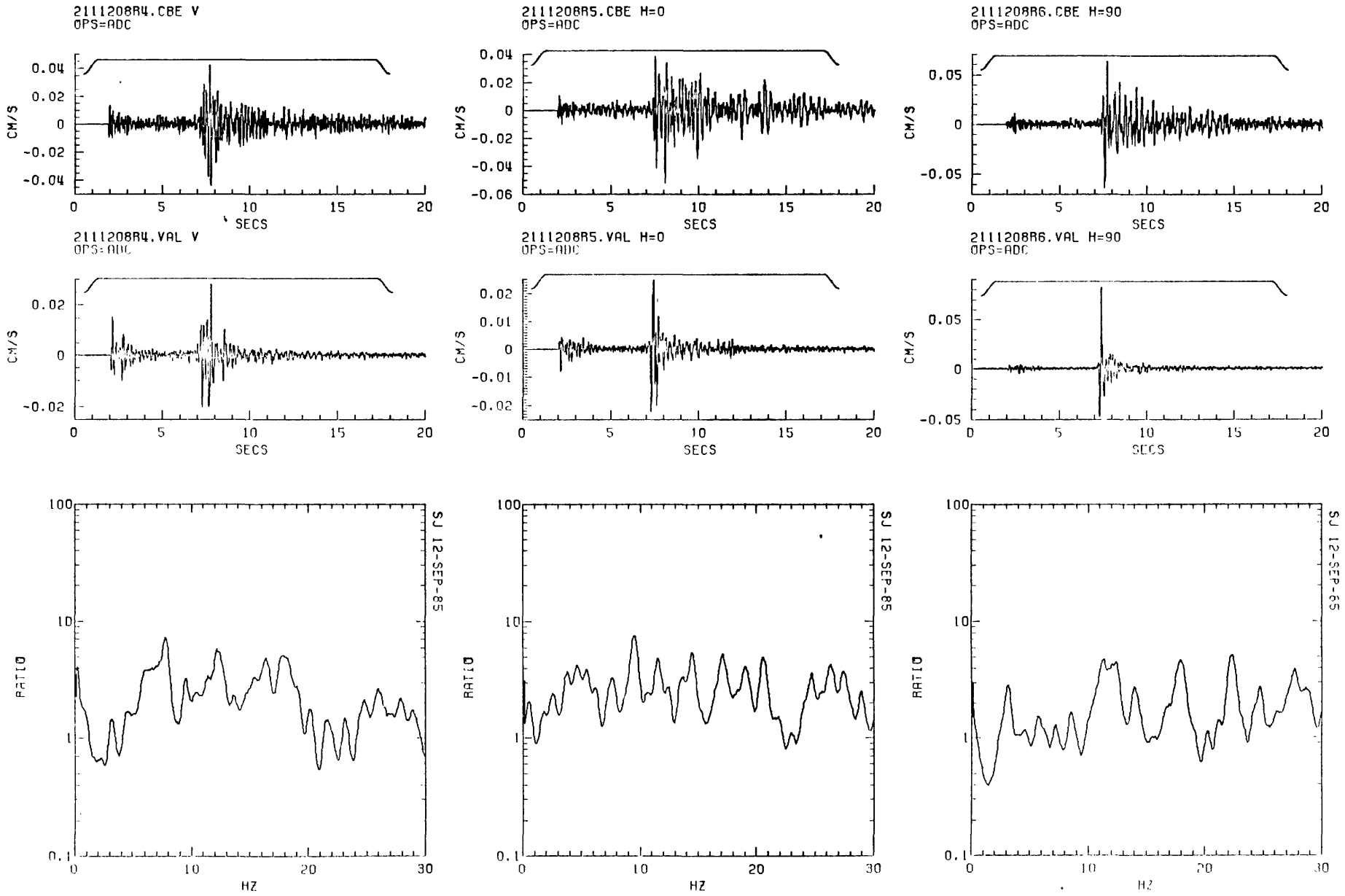

Figure A66. Scaled seismograms and spectral ratios of event on July 29, 1985 (Julian 211) at 12:08 for the vertical, horizontal (N-S and E-W) components, respectively, of stations CBE/VAL.

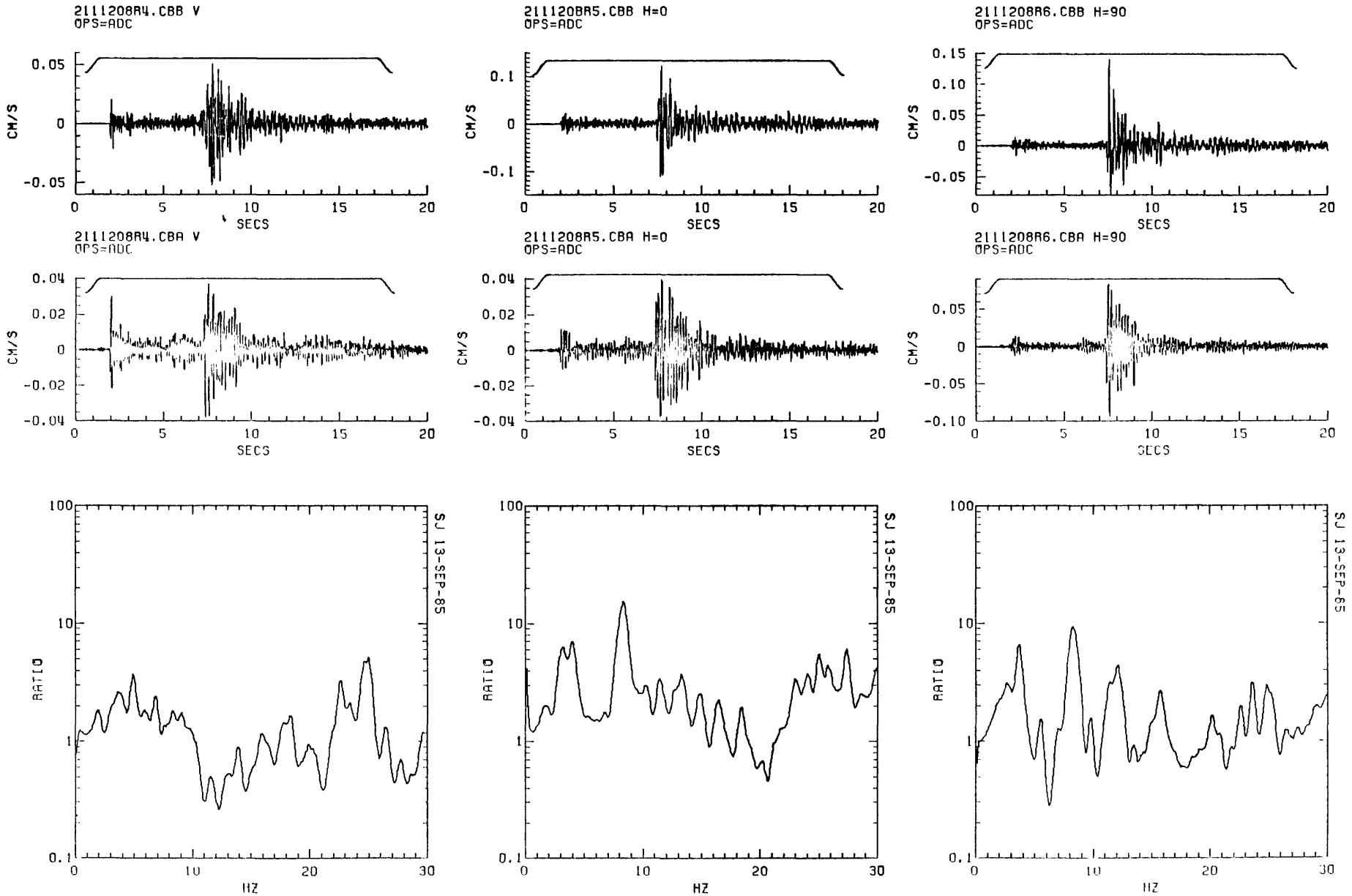

Figure A67. Scaled seismograms and spectral ratios of event on July 29, 1985 (Julian 211) at 12:08 for the vertical, horizontal (N-S and E-W) components, respectively, of stations CBB/CBA.

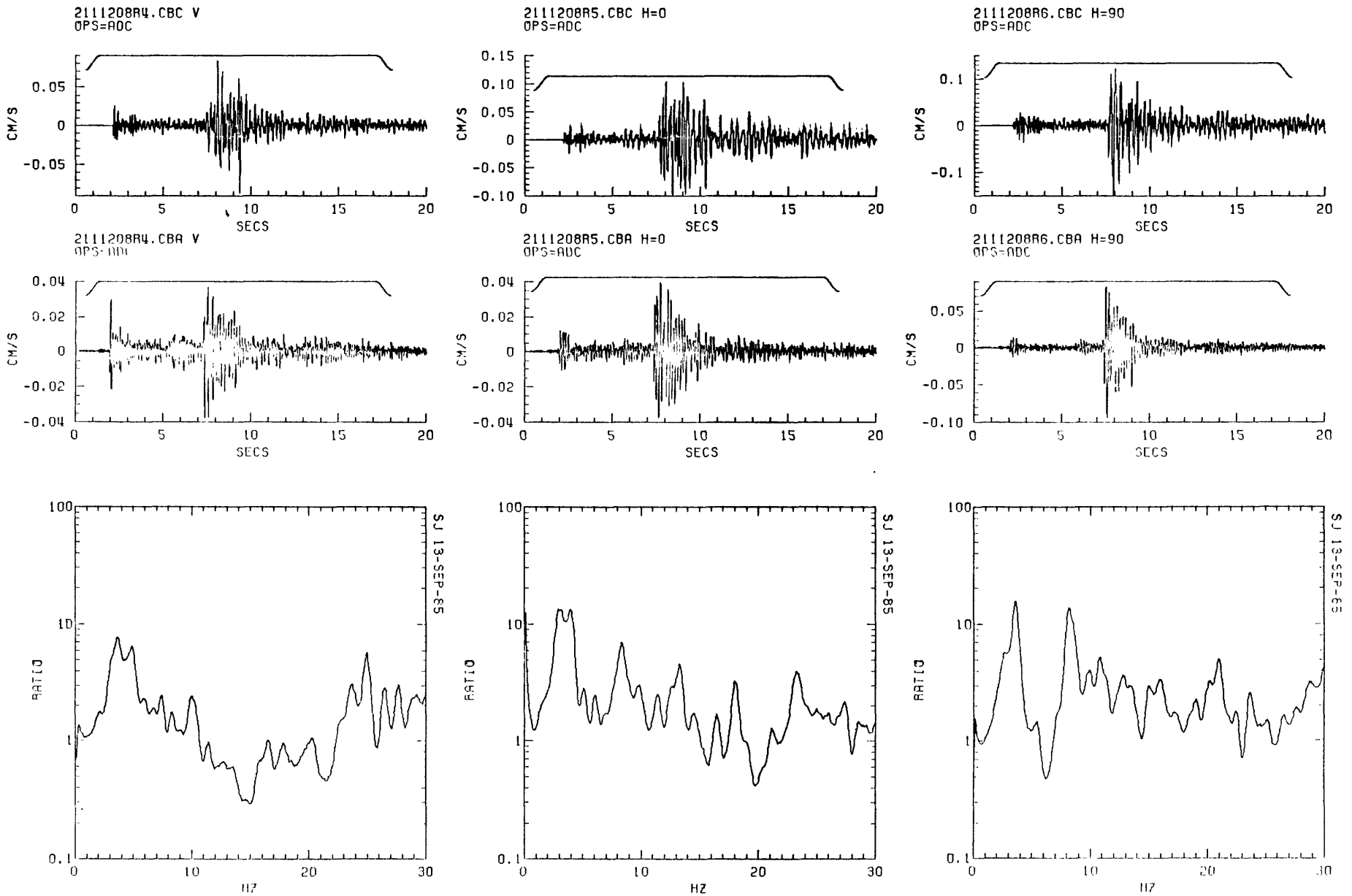

Figure A68. Scaled seismograms and spectral ratios of event on July 29, 1985 (Julian 211) at 12:08 for the vertical, horizontal (N-S and E-W) components, respectively, of stations CBC/CBA.

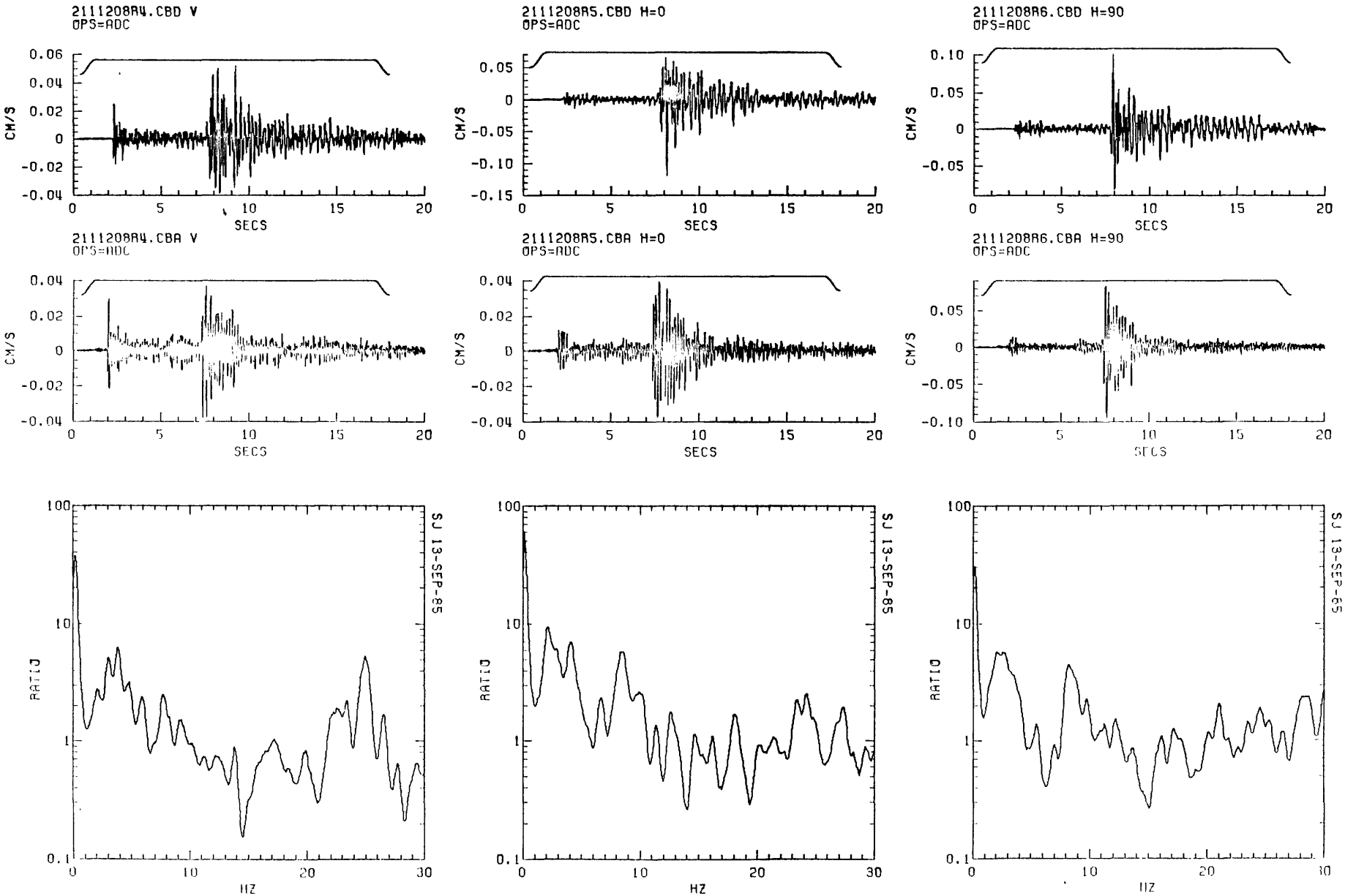

Figure A69. Scaled seismograms and spectral ratios of event on July 29, 1985 (Julian 211) at 12:08 for the vertical, horizontal (N-S and E-W) components, respectively, of stations CBD/CBA.

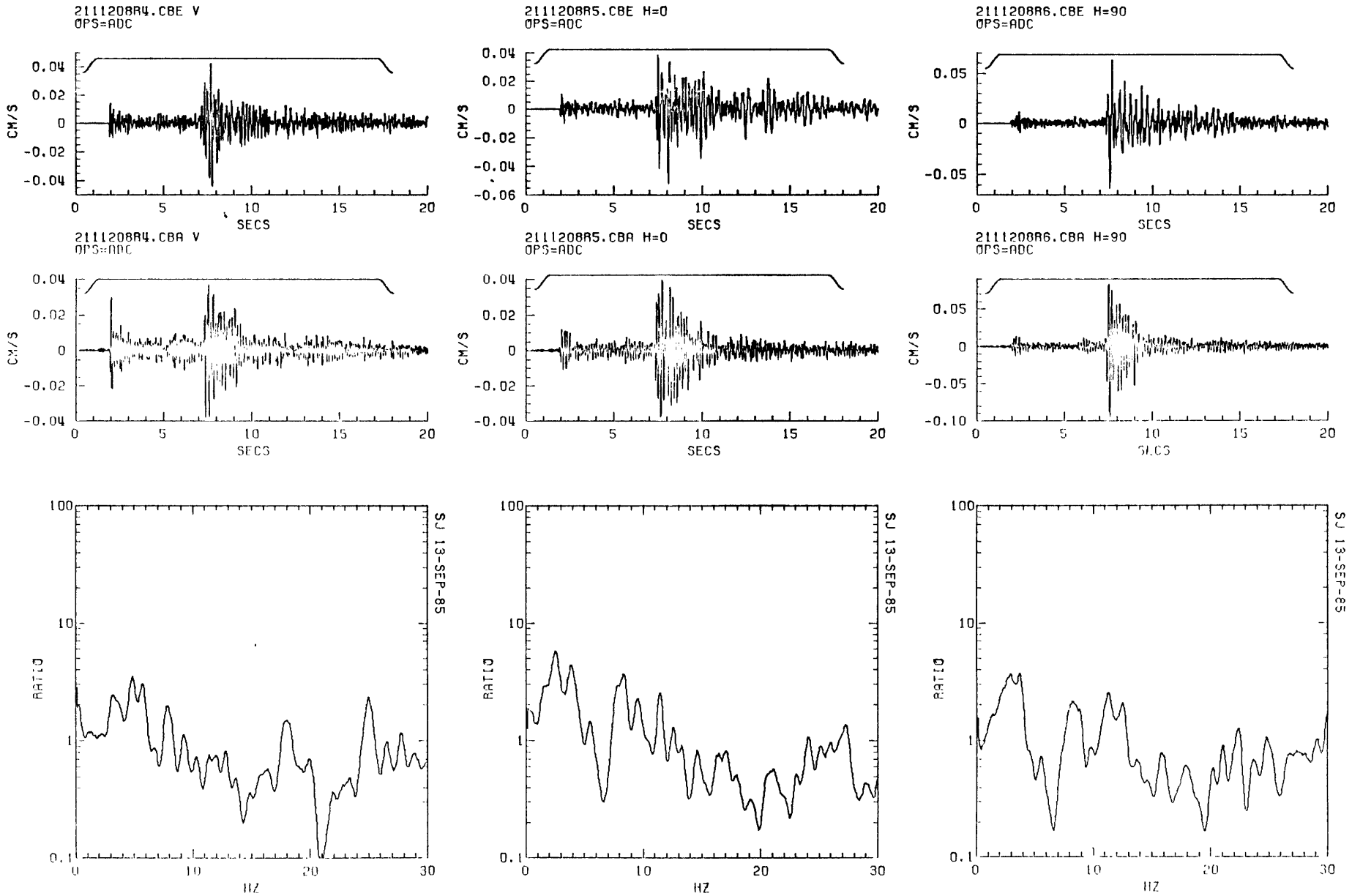

Figure A70. Scaled seismograms and spectral ratios of event on July 29, 1985 (Julian 211) at 12:08 for the vertical, horizontal (N-S and E-W) components, respectively, of stations CBE/CBA.

APPENDIX B
VIÑA EXPERIMENT
SEISMOGRAMS, FOURIER AMPLITUDE SPECTRA AND SPECTRAL RATIOS

The objective of this appendix is to provide the seismograms, Fourier amplitude spectras and spectral ratios related to the Viña experiments only. Selected plots of data processed by C. Mueller and J. Watson are presented herein.

The plots are organized as follows:

Event	Type of Plot	Figure(s)
2150204	Seismograms	B1-B3
	Fourier amplitude spectra	B4-B9
	Spectral ratios	B10-B14
2160657	Seismograms	B15-B17
2161006	Seismograms	B18-B20
2161857	Seismograms	B21-B23
	Fourier amplitude spectra	B24-B28
	Spectral ratio	B29-B32
2191002	Seismograms	B33-B35
	Fourier amplitude spectra	B36-B38
	Spectral ratio	B39-B40

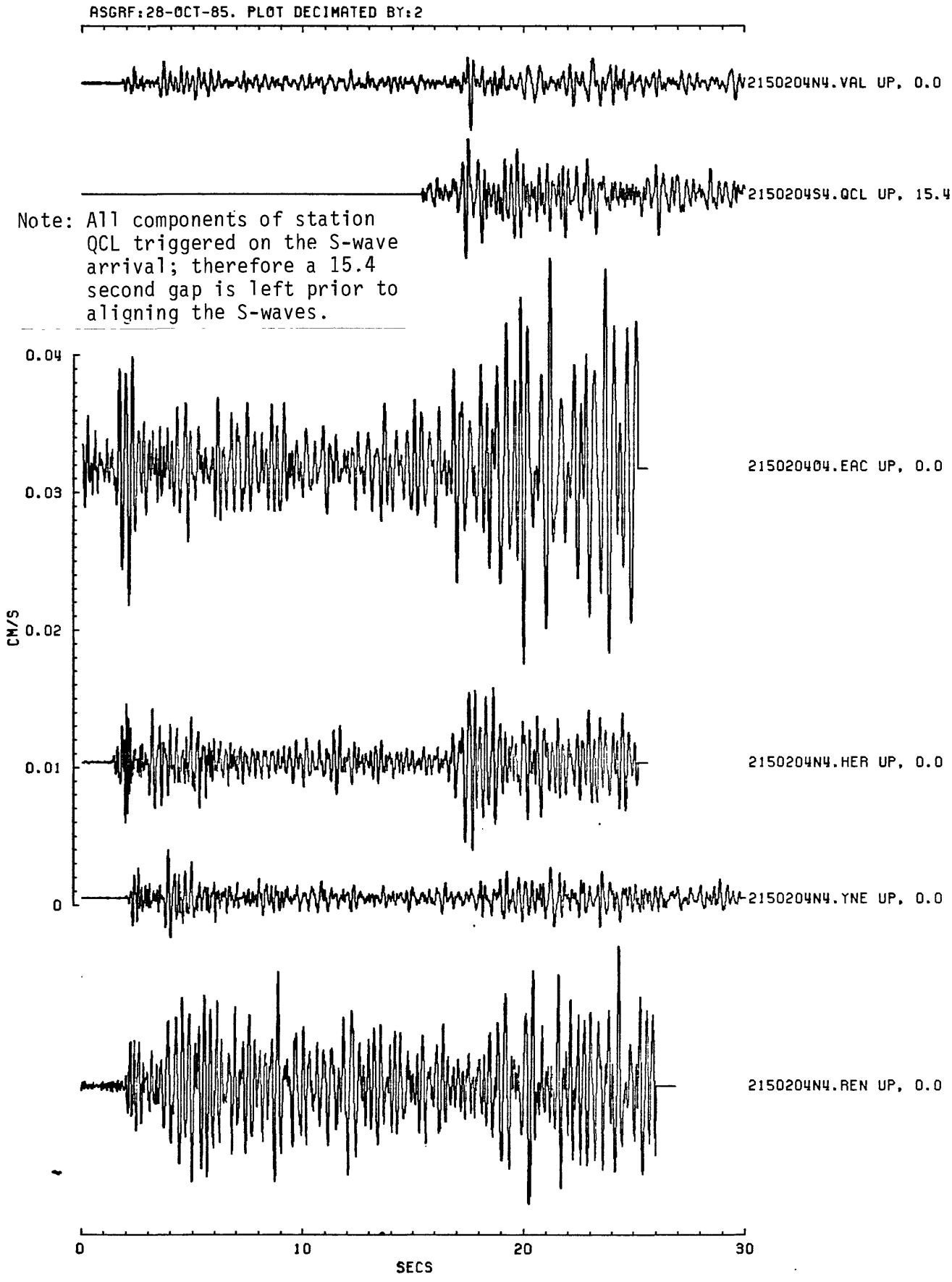

Figure B1. Scaled seismograms for event 2150204 (vertical components).

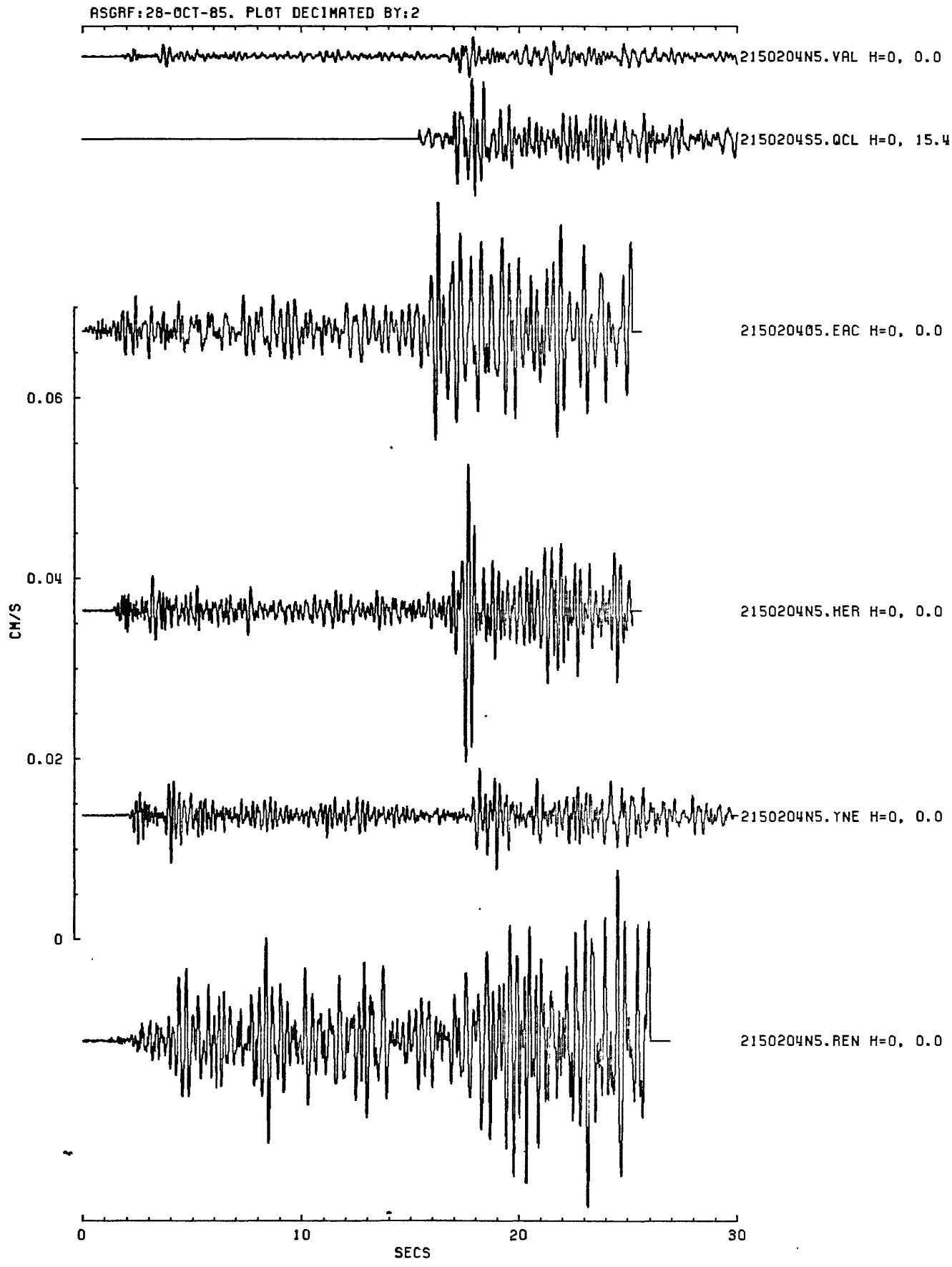

Figure B2. Scaled seismograms for event 2150204 (N-S components).

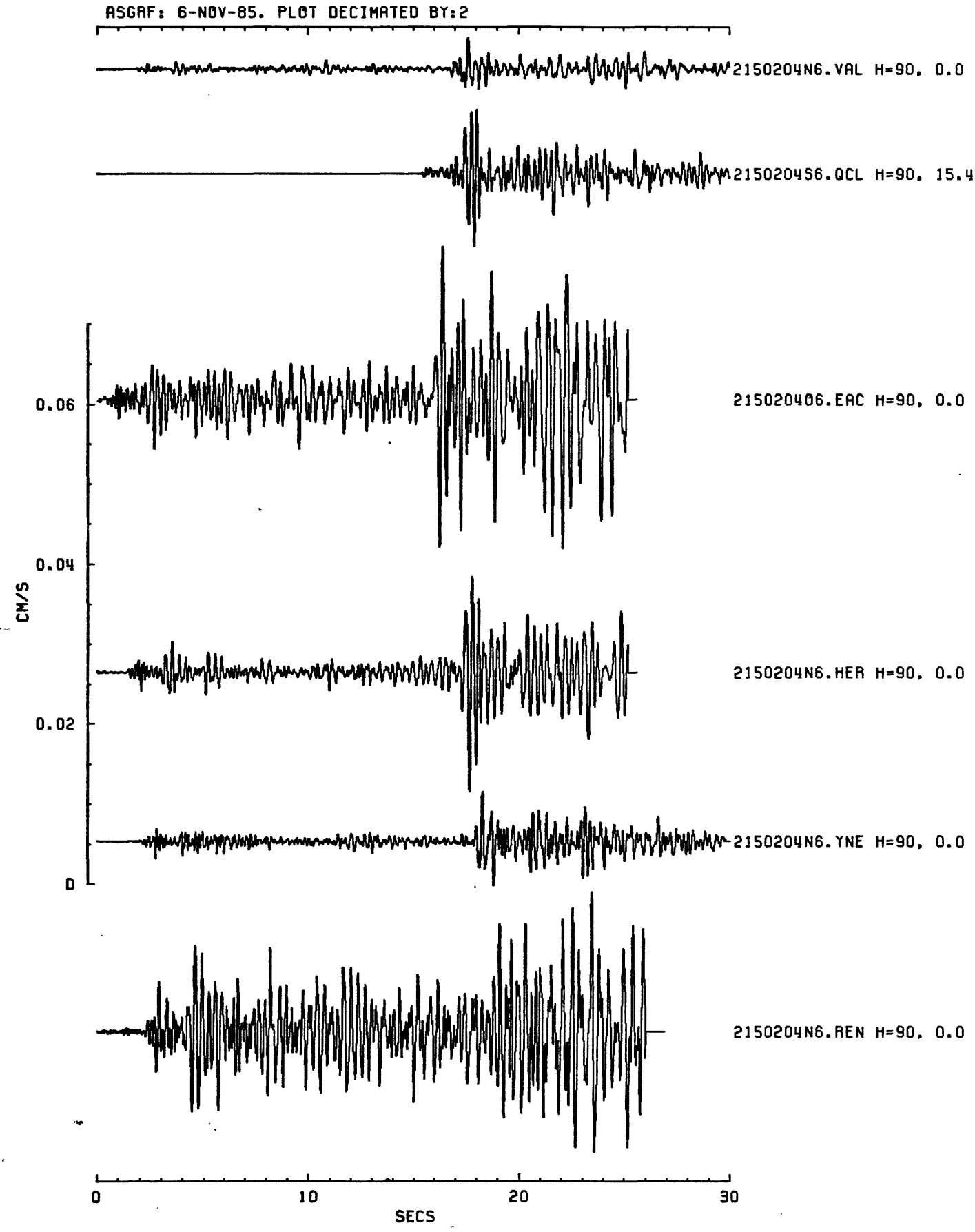

Figure B3. Scaled seismograms for event 2150204 (E-W components).

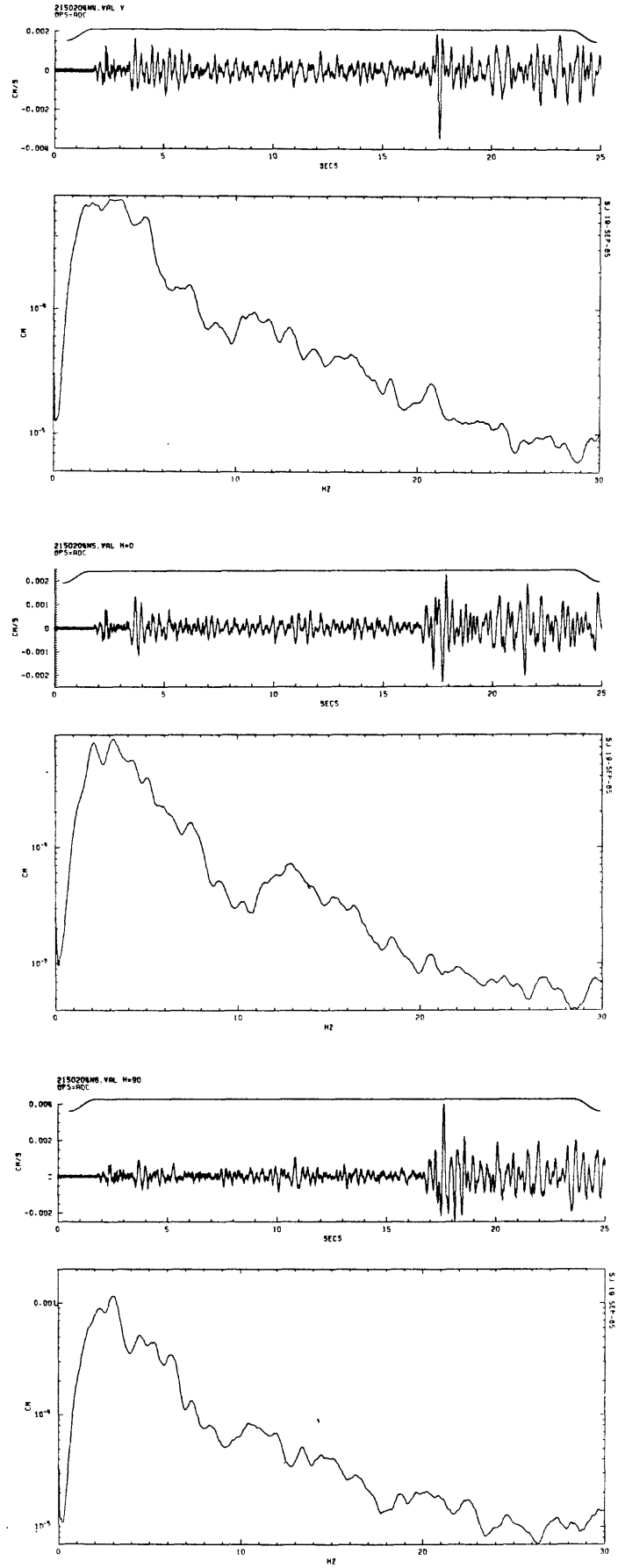

Figure B4. Time series and Fourier amplitude spectra of event on August 3, 1985 (Julian 215) at 02:04 for the vertical, horizontal (N-S and E-W) components, respectively, for station VAL.

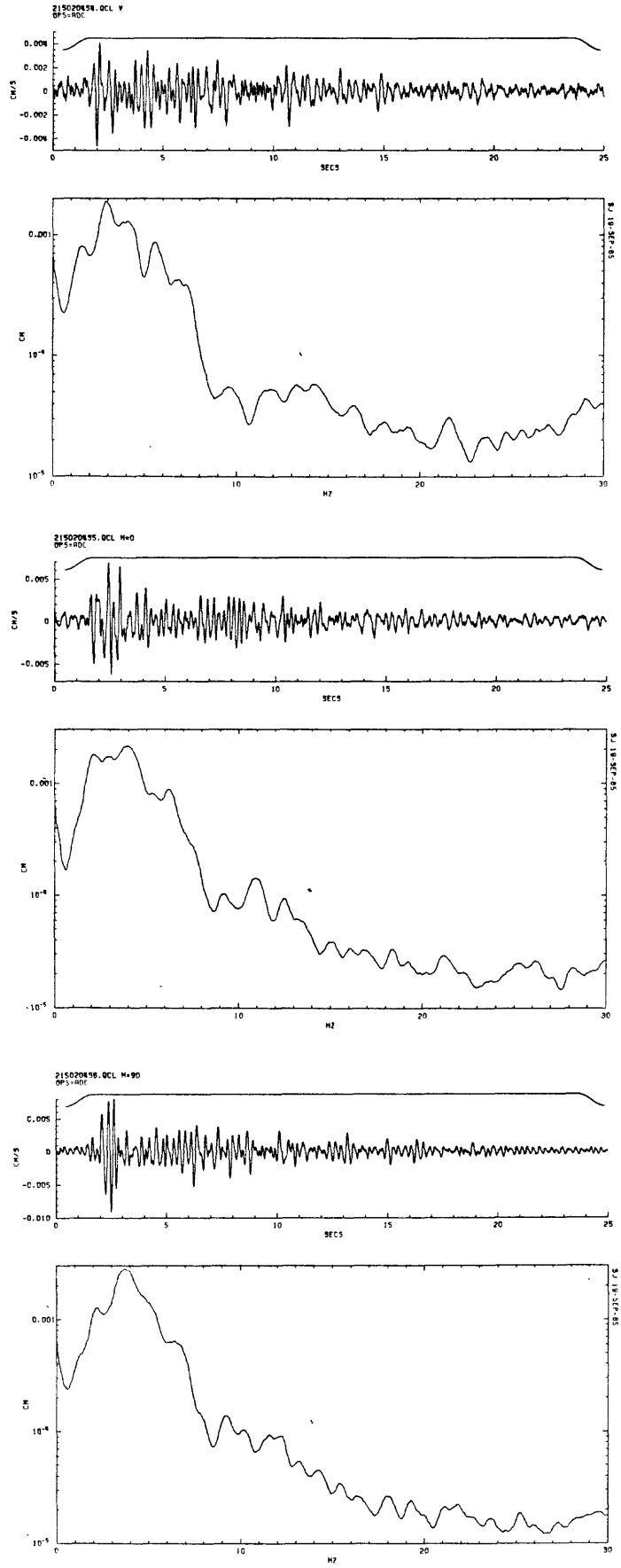

Figure B5. Time series and Fourier amplitude spectra of event on August 3, 1985 (Julian 215) at 02:04 for the vertical, horizontal (N-S and E-W) components, respectively, for station QCL.

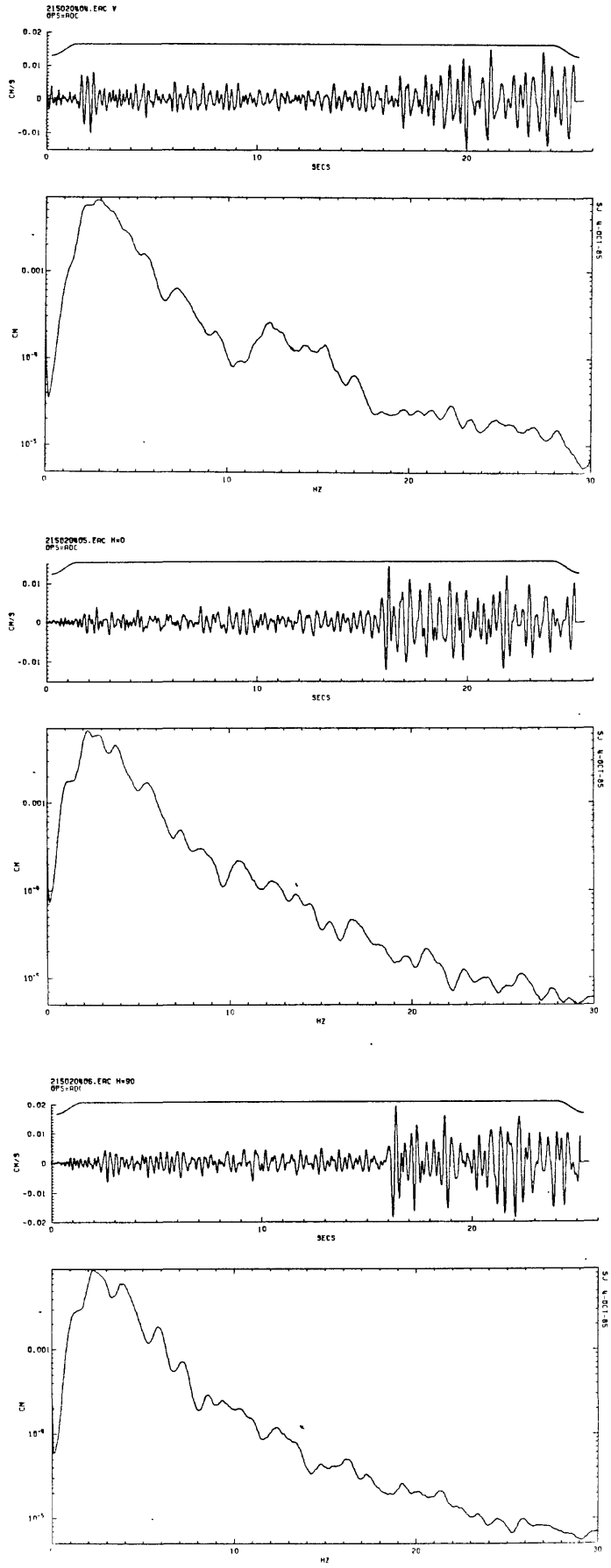

Figure B6. Time series and Fourier amplitude spectra of event on August 3, 1985 (Julian 215) at 02:04 for the vertical, horizontal (N-S and E-W) components, respectively, for station EAC.

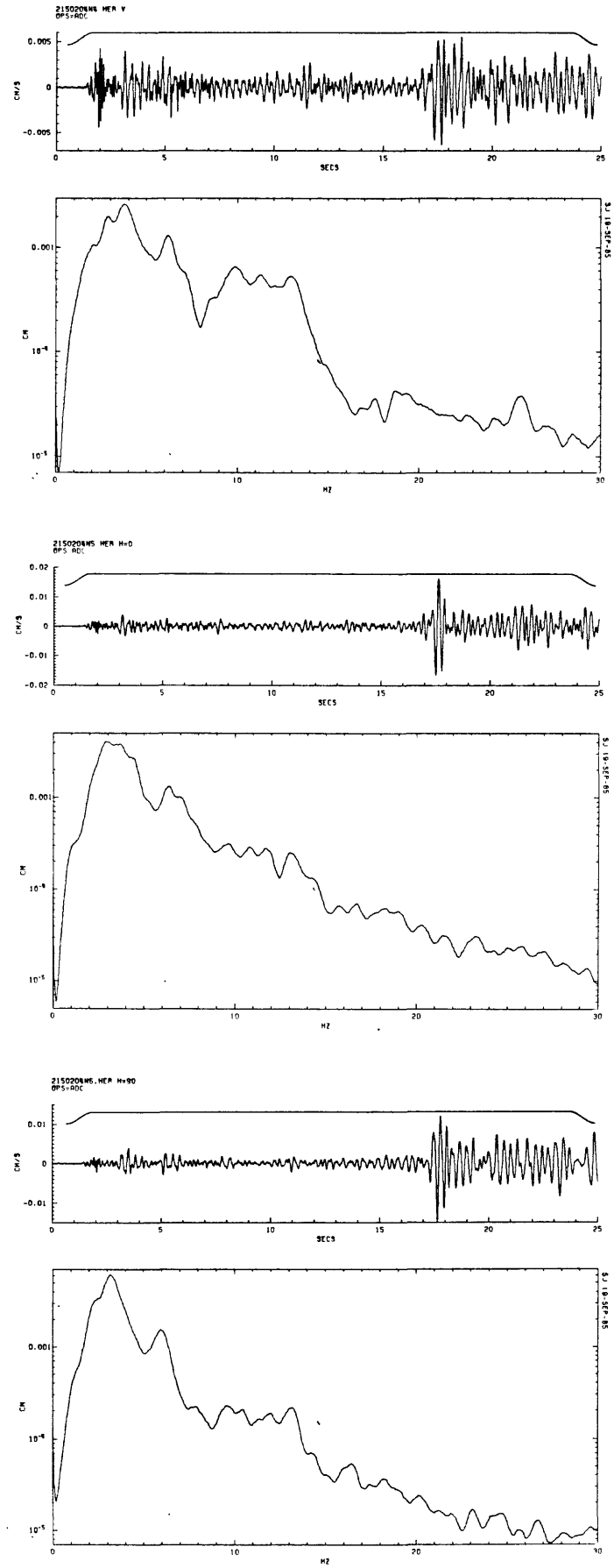

Figure B7. Time series and Fourier amplitude spectra of event on August 3, 1985 (Julian 215) at 02:04 for the vertical, horizontal (N-S and E-W) components, respectively, for station HER.

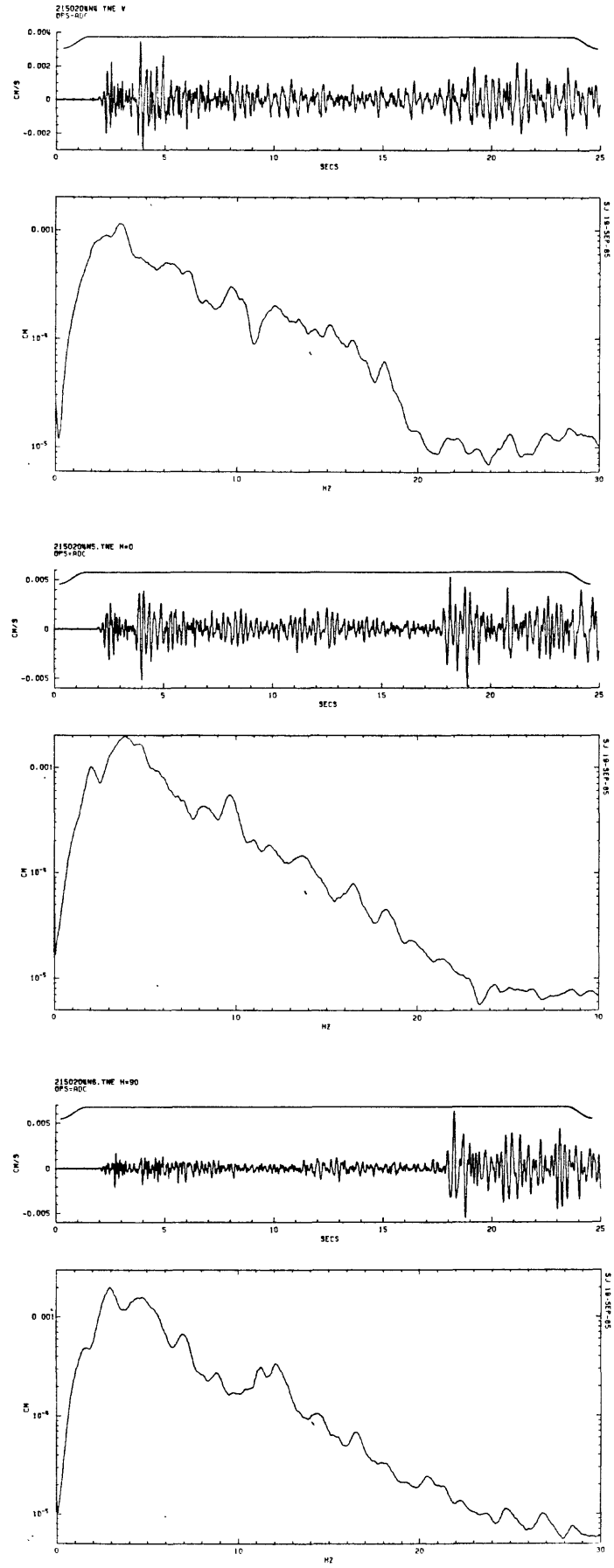

Figure B8. Time series and Fourier amplitude spectra of event on August 3, 1985 (Julian 215) at 02:04 for the vertical, horizontal (N-S and E-W) components, respectively, for station YNE.

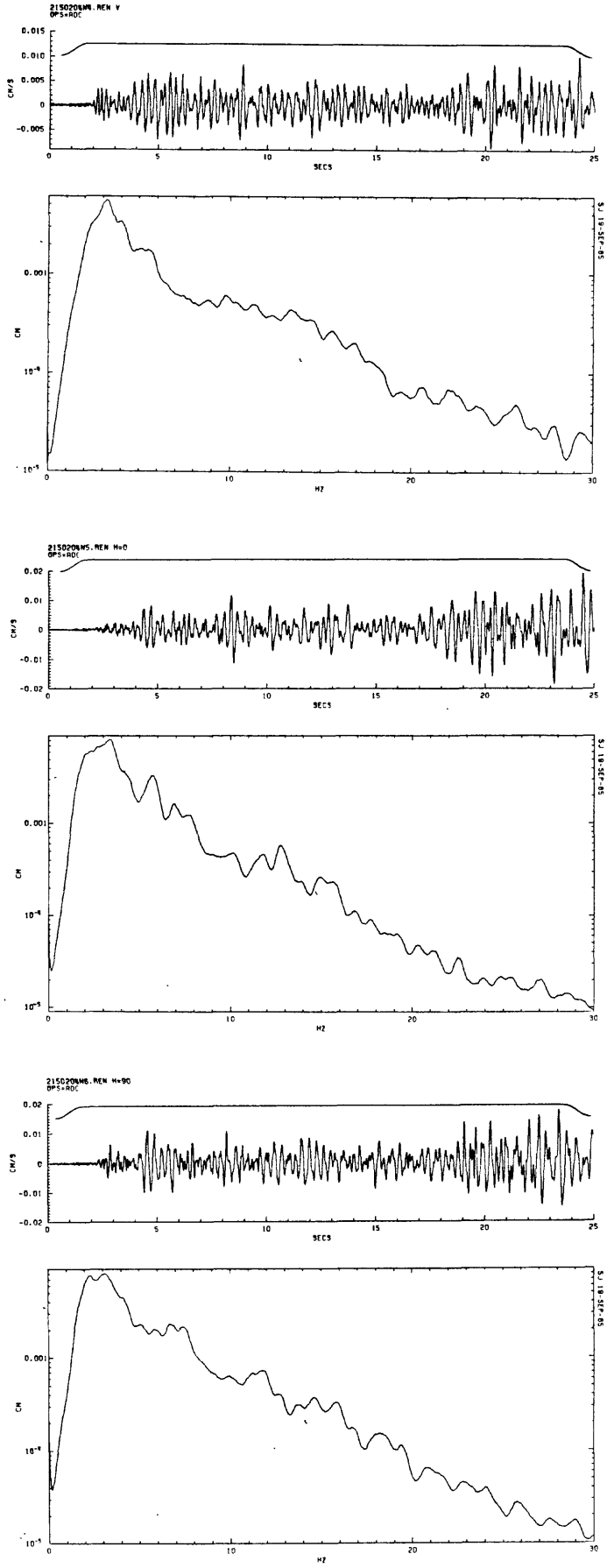

Figure B9. Time series and Fourier amplitude spectra of event on August 3, 1985 (Julian 215) at 02:04 for the vertical, horizontal (N-S and E-W) components, respectively, for station REN.

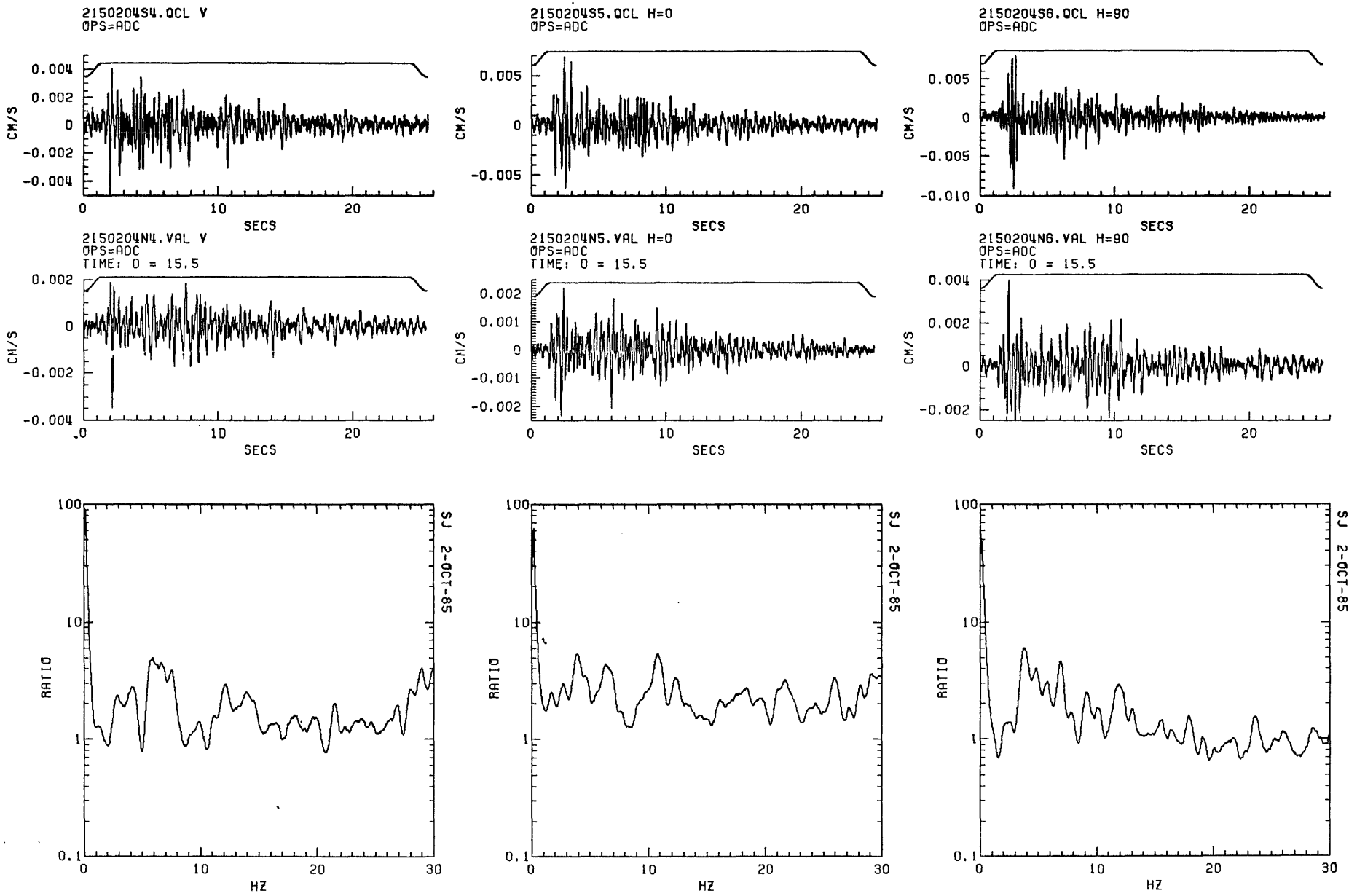

Figure B10. Scaled seismograms and spectral ratios of event on August 3, 1985 (Julian 215) at 02:04 for the vertical, horizontal (N-S and E-W) components, respectively, of stations QCL/VAL.

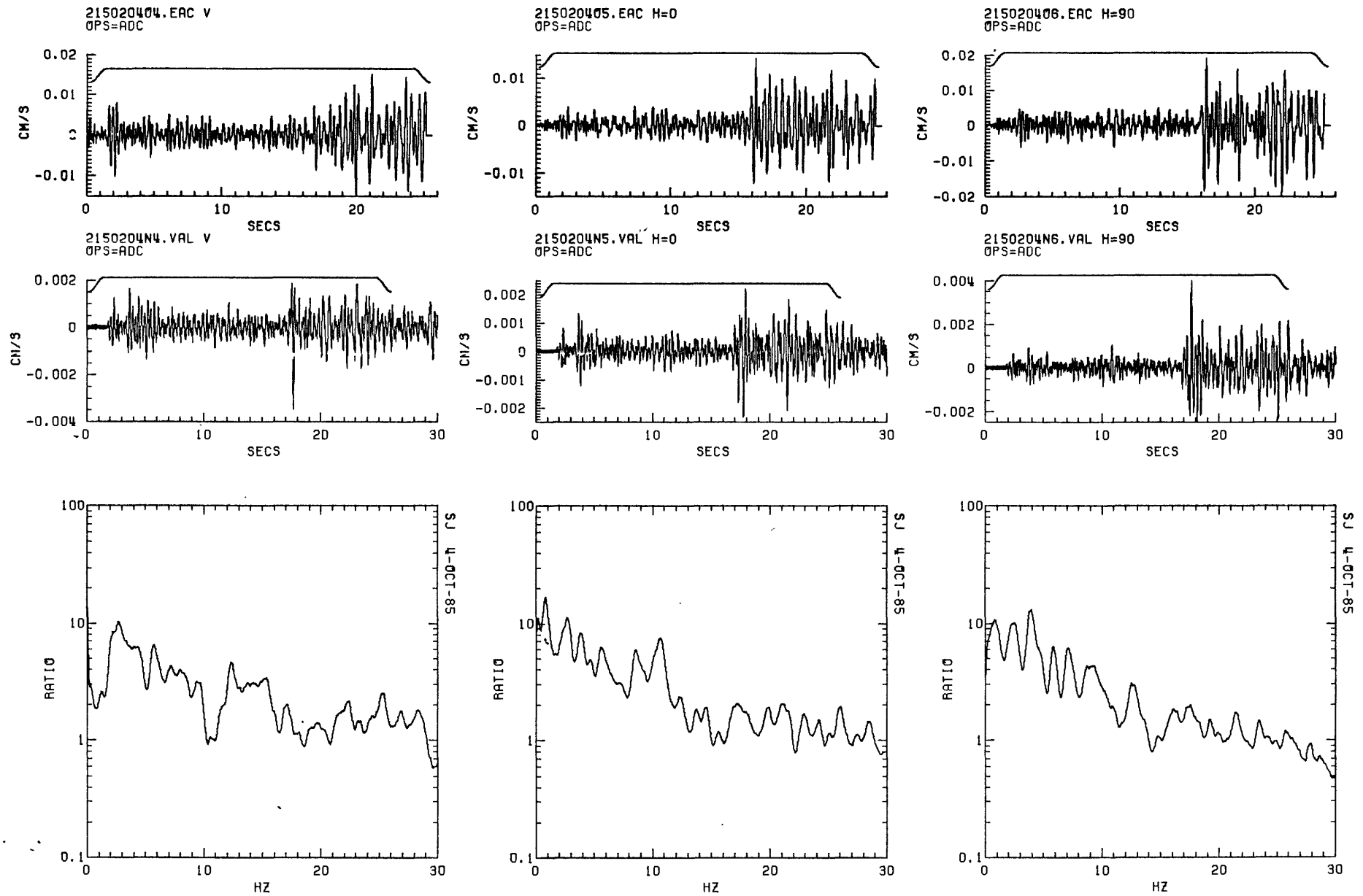

Figure B11. Scaled seismograms and spectral ratios of event on August 3, 1985 (Julian 215) at 02:04 for the vertical, horizontal (N-S and E-W) components, respectively, of stations EAC/VAL.

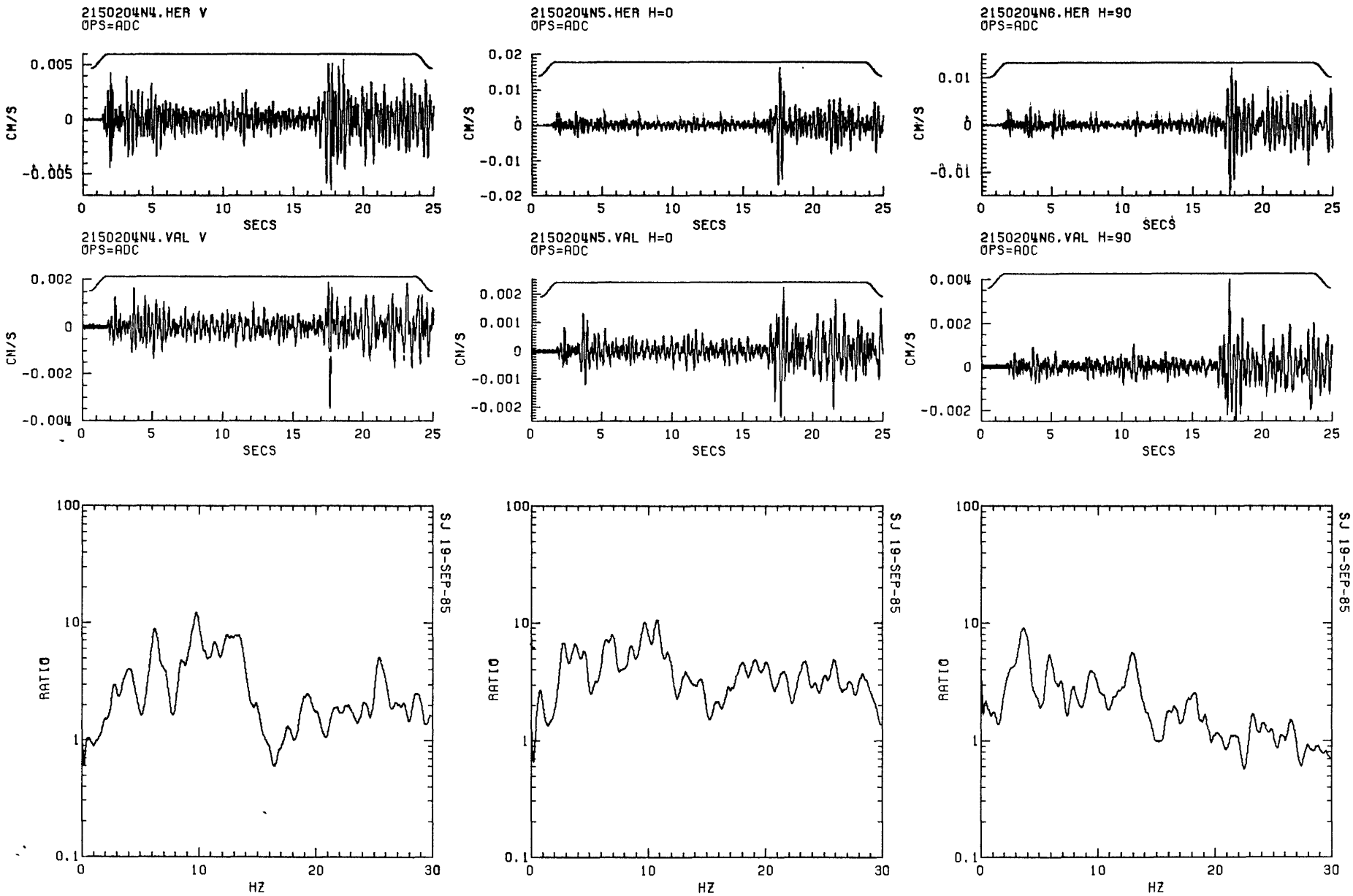

Figure B12. Scaled seismograms and spectral ratios of event on August 3, 1985 (Julian 215) at 02:04 for the vertical, horizontal (N-S and E-W) components, respectively, of stations HER/VAL.

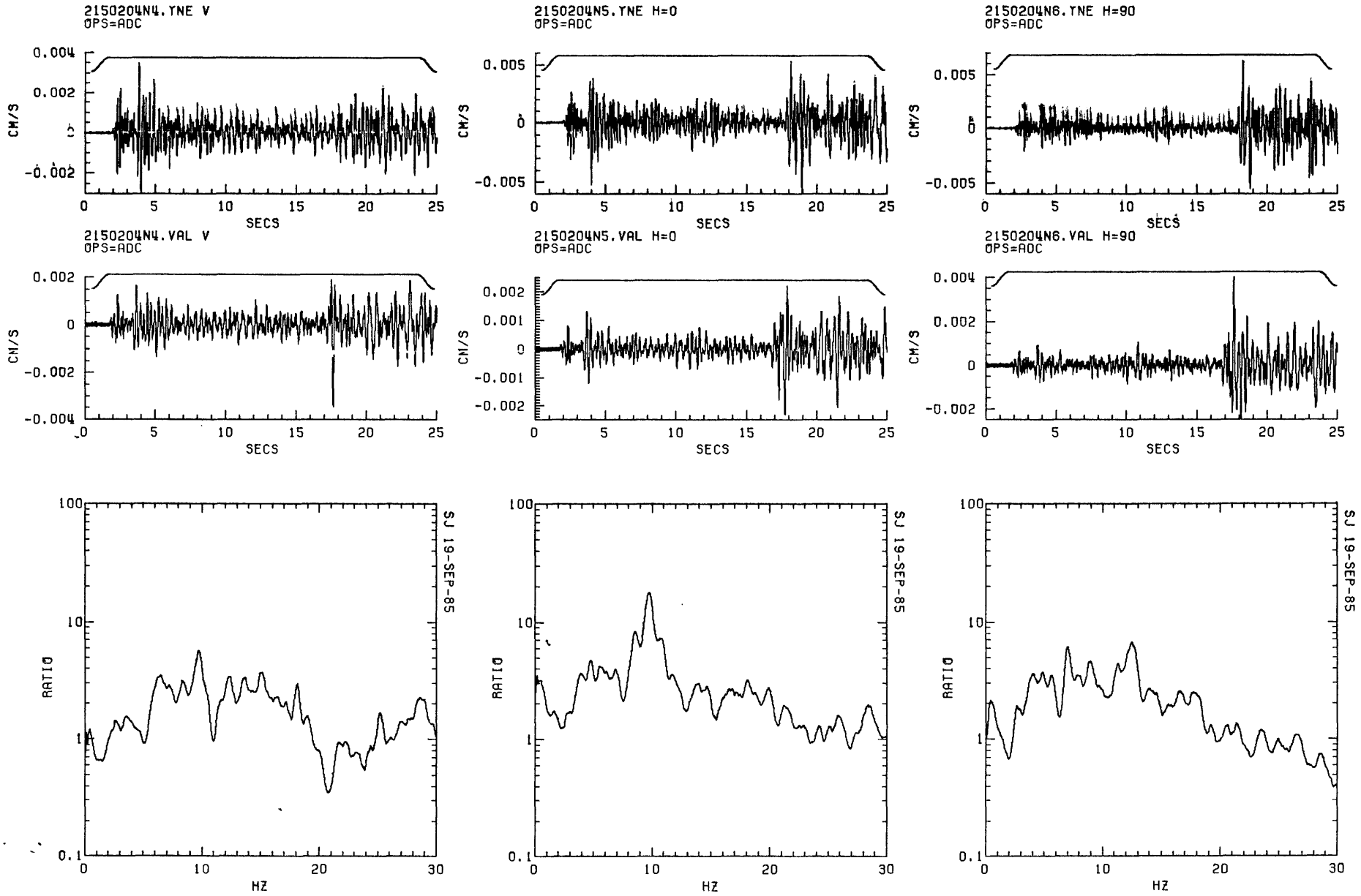

Figure B13. Scaled seismograms and spectral ratios of event on August 3, 1985 (Julian 215) at 02:04 for the vertical, horizontal (N-S and E-W) components, respectively, of stations YNE/VAL.

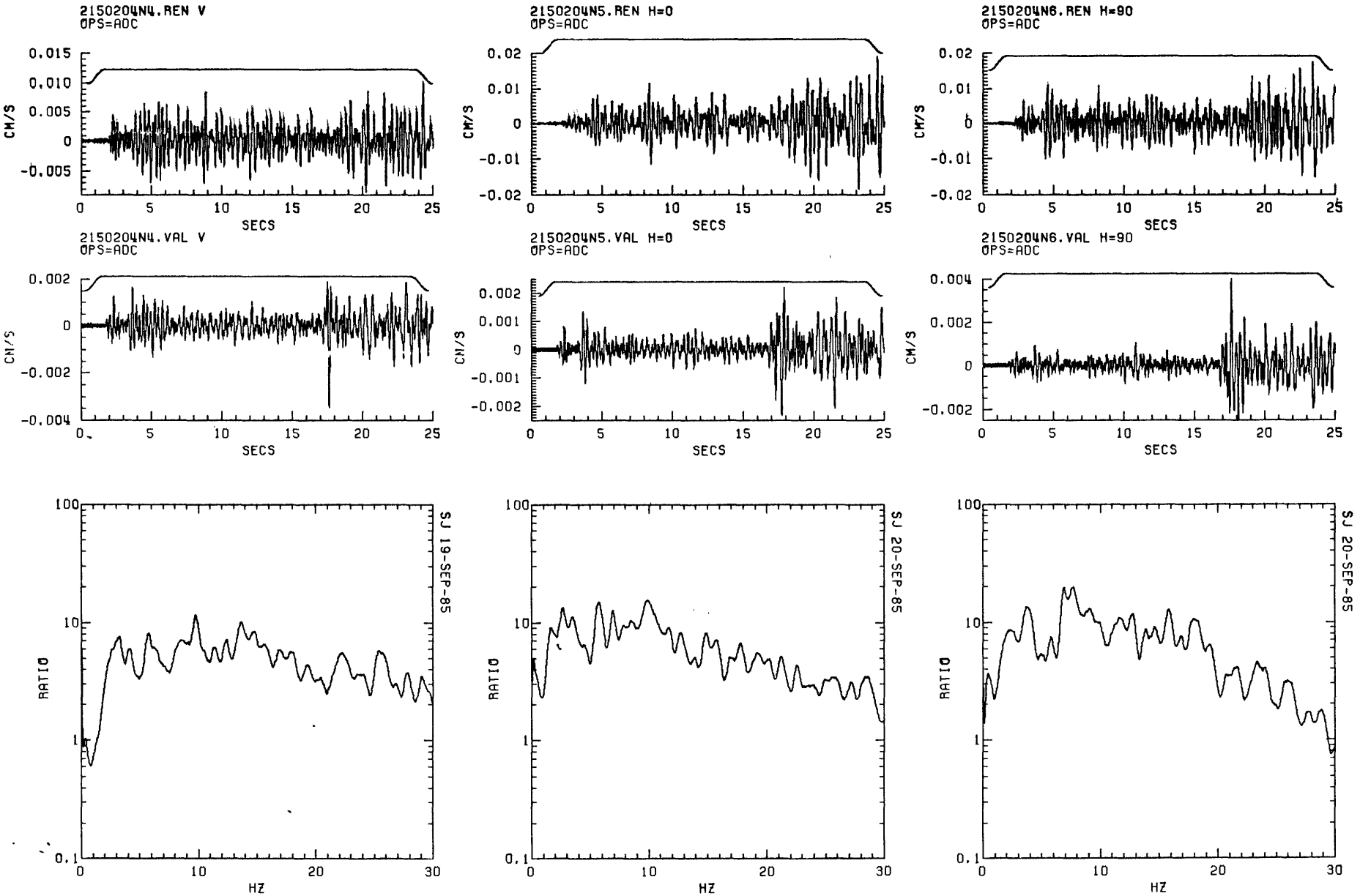

Figure B14. Scaled seismograms and spectral ratios of event on August 3, 1985 (Julian 215) at 02:04 for the vertical, horizontal (N-S and E-W) components, respectively, of stations REN/VAL.

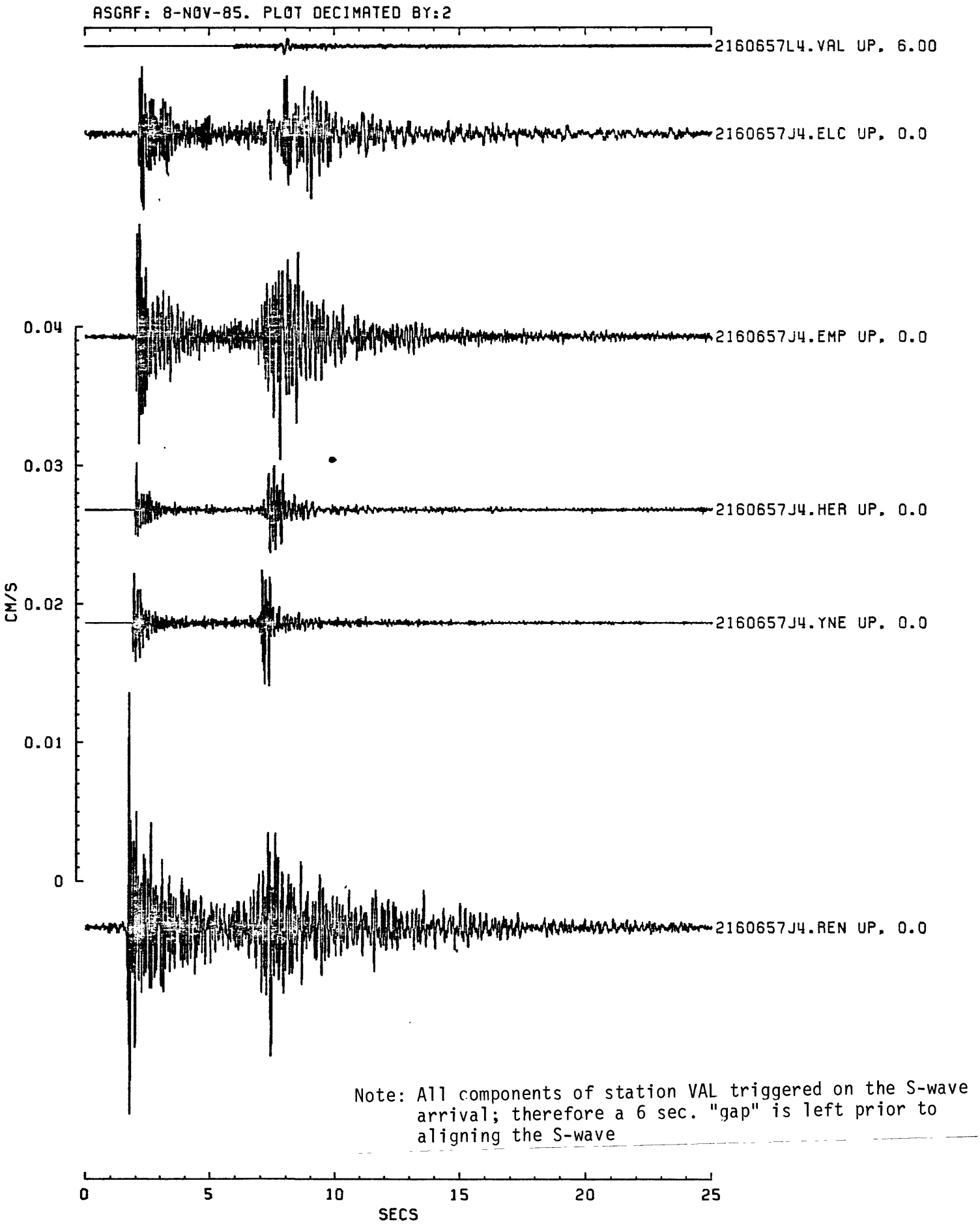

Figure B15. Scaled seismograms for event 2160657 (vertical components).

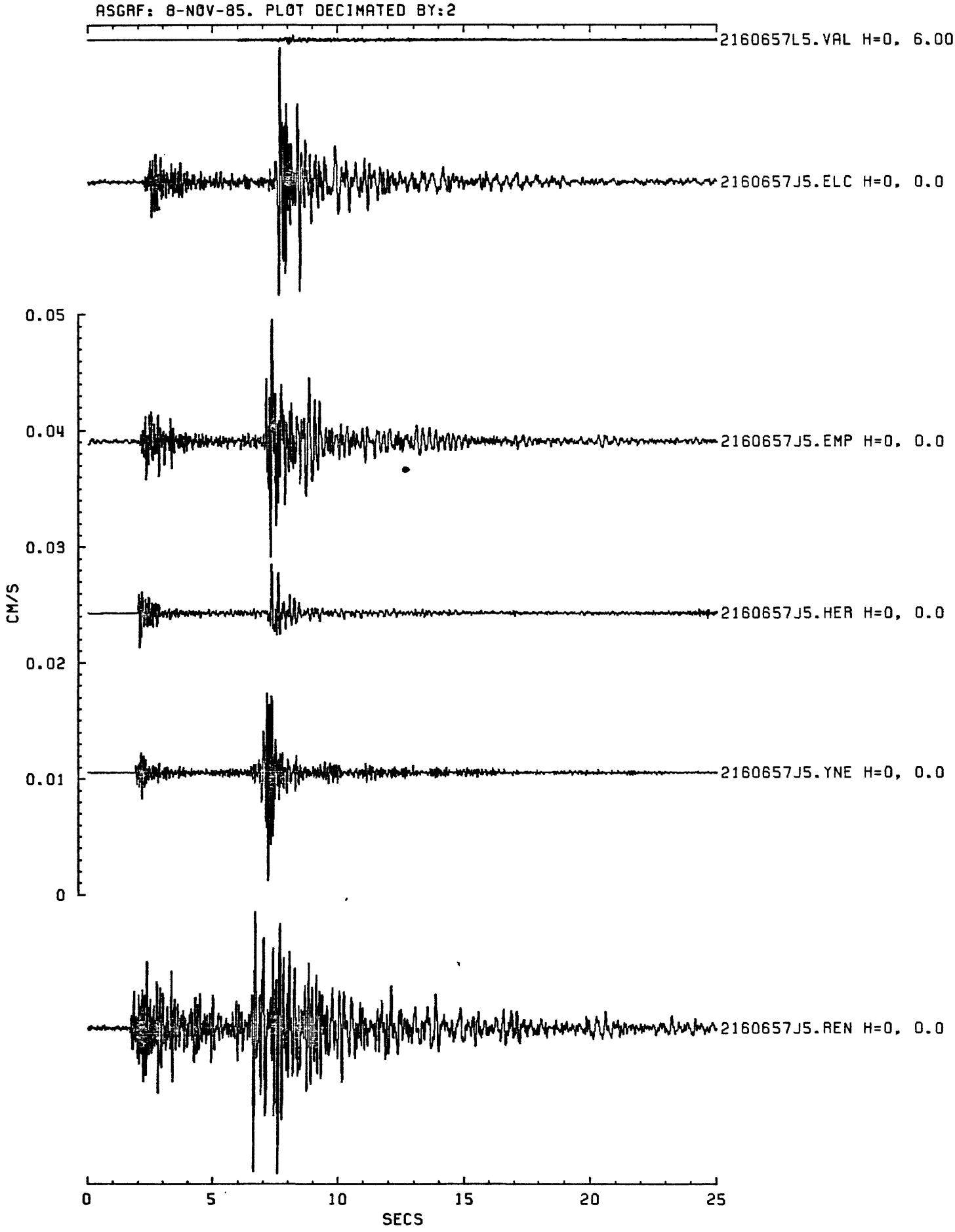

Figure B16. Scaled seismograms for event 2160657 (N-S components).

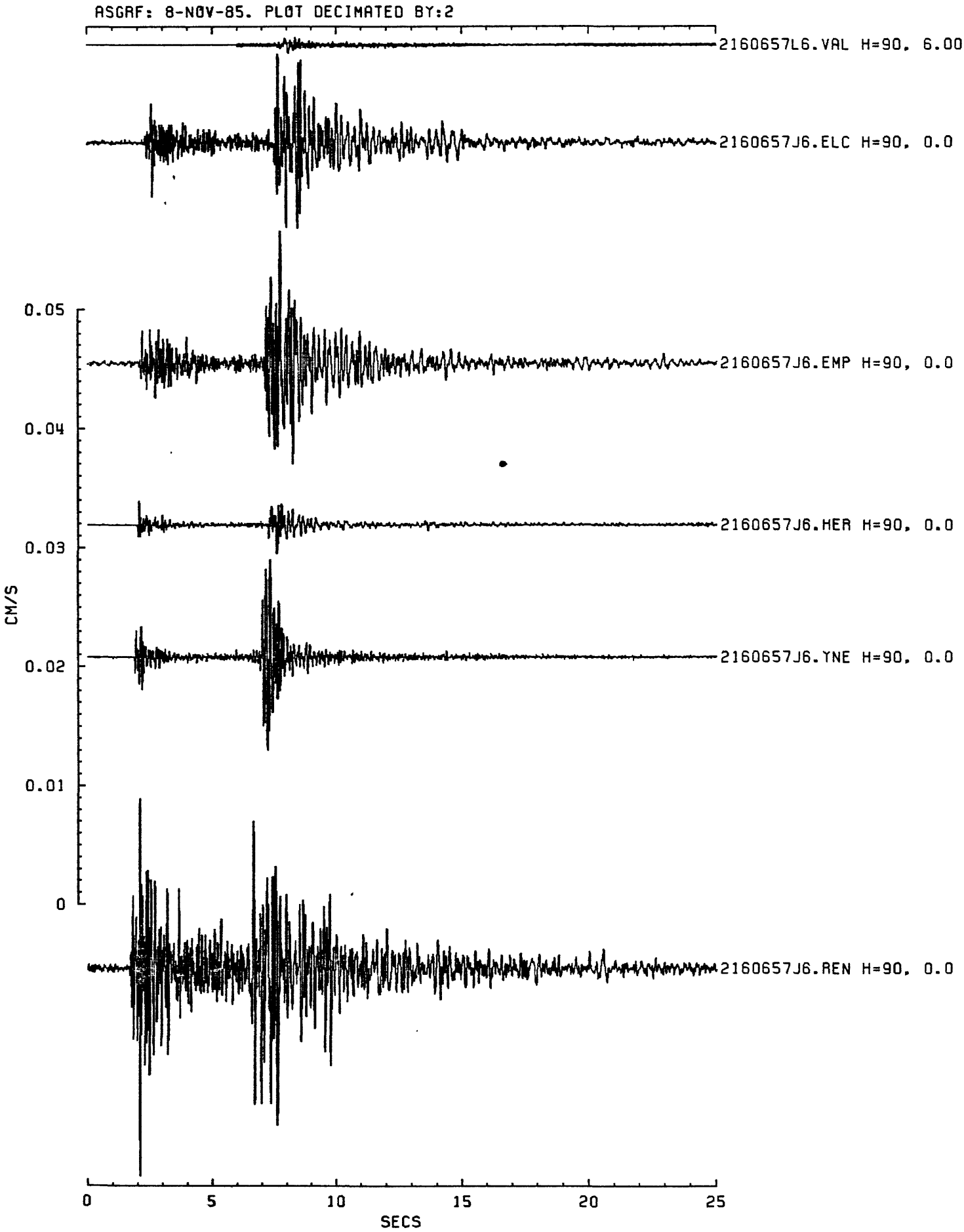

Figure B17. Scaled seismograms for event 2160657 (E-W components).

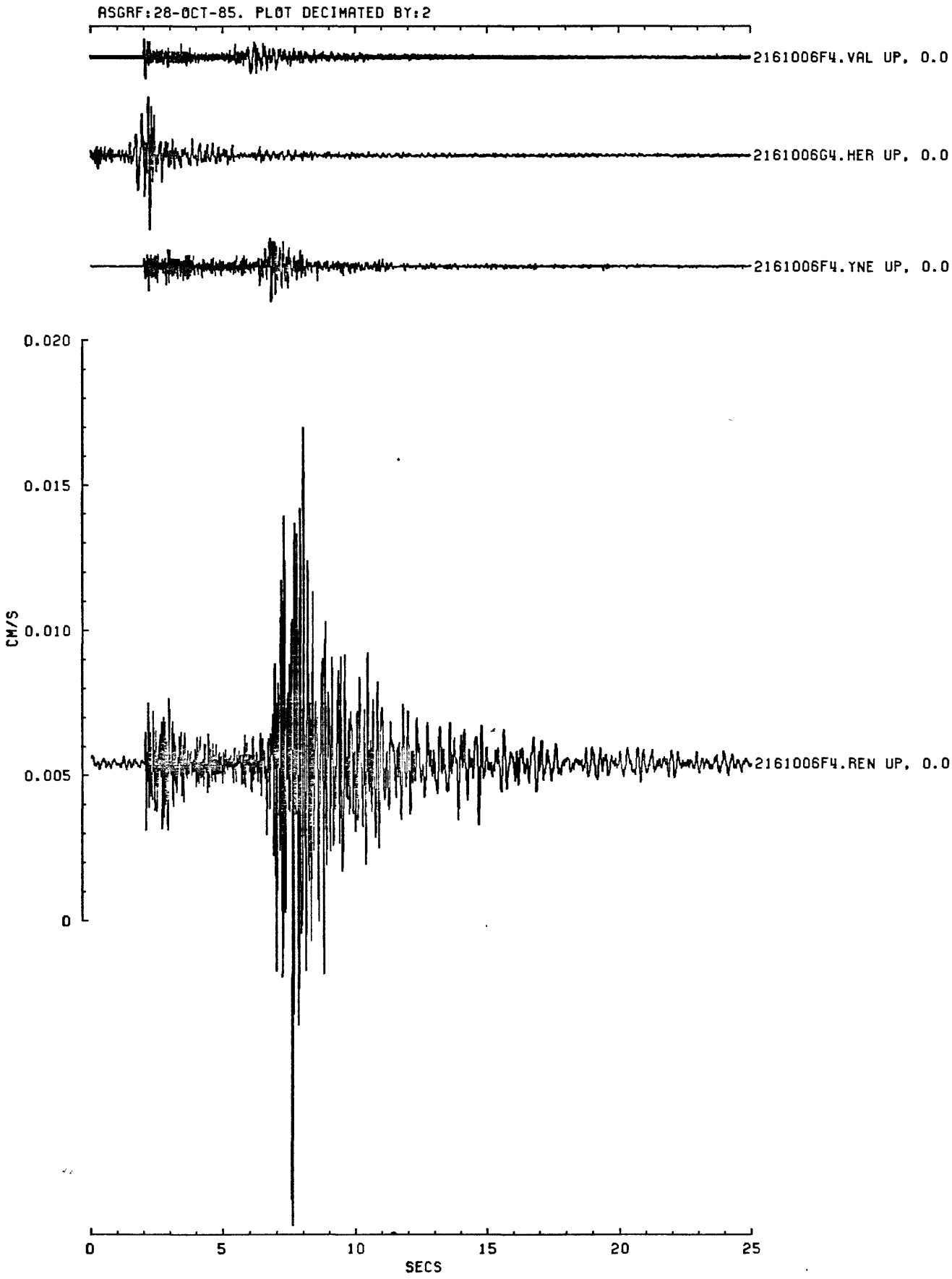

Figure B18. Scaled seismograms for event 2161006 (vertical components).

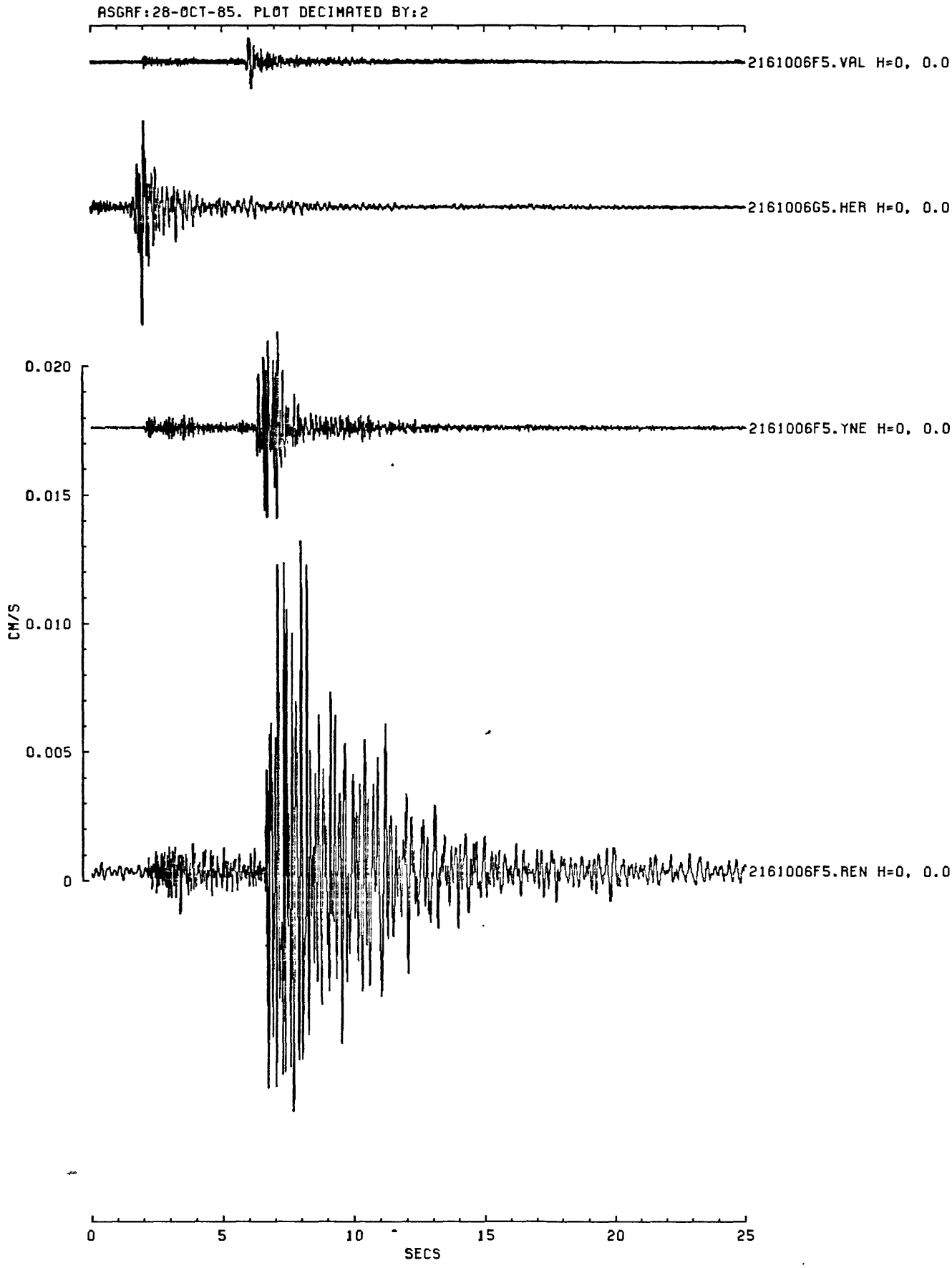

Figure B19. Scaled seismograms for event 2161006 (N-S components).

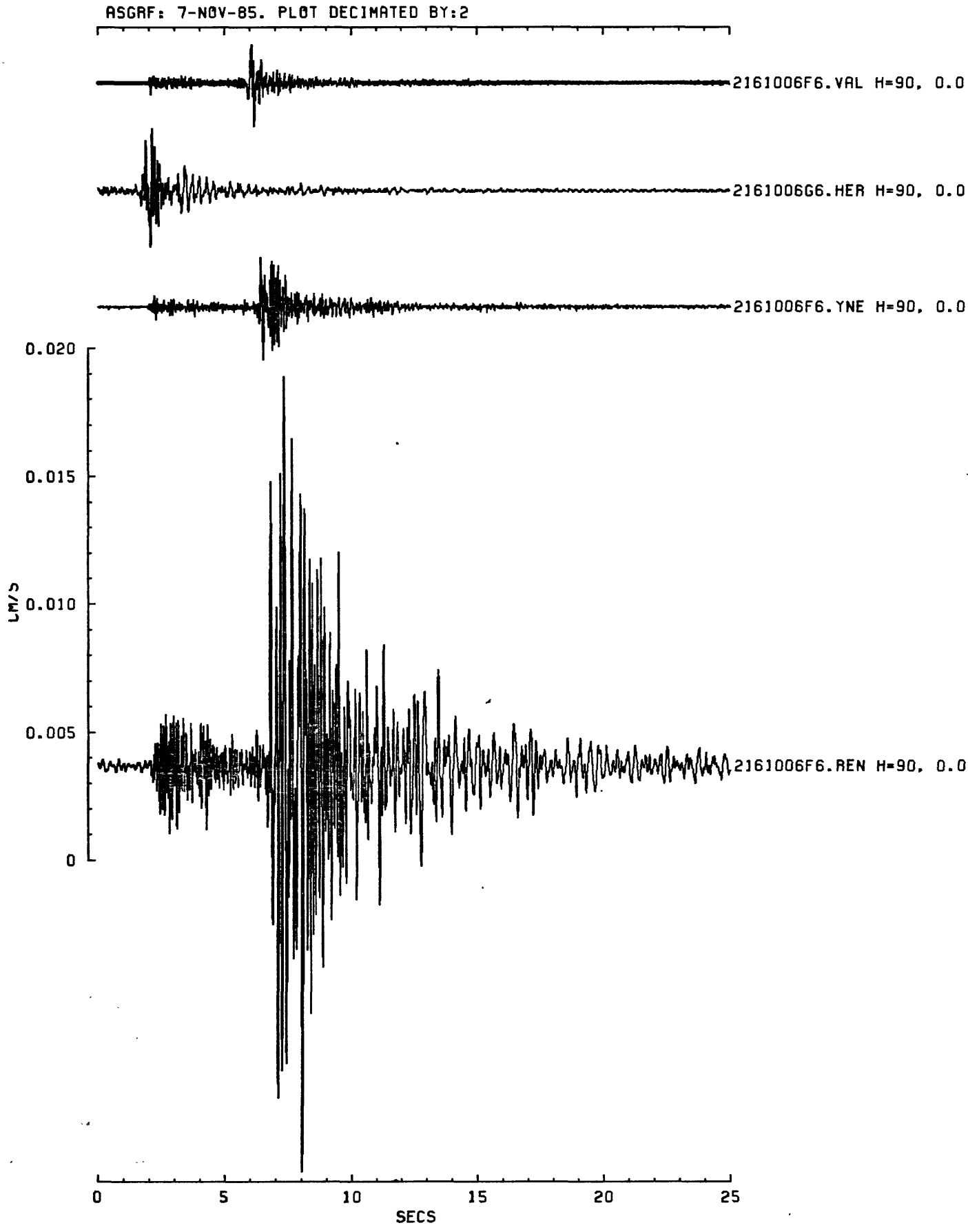

Figure B20. Scaled seismograms for event 2161006 (E-W components).

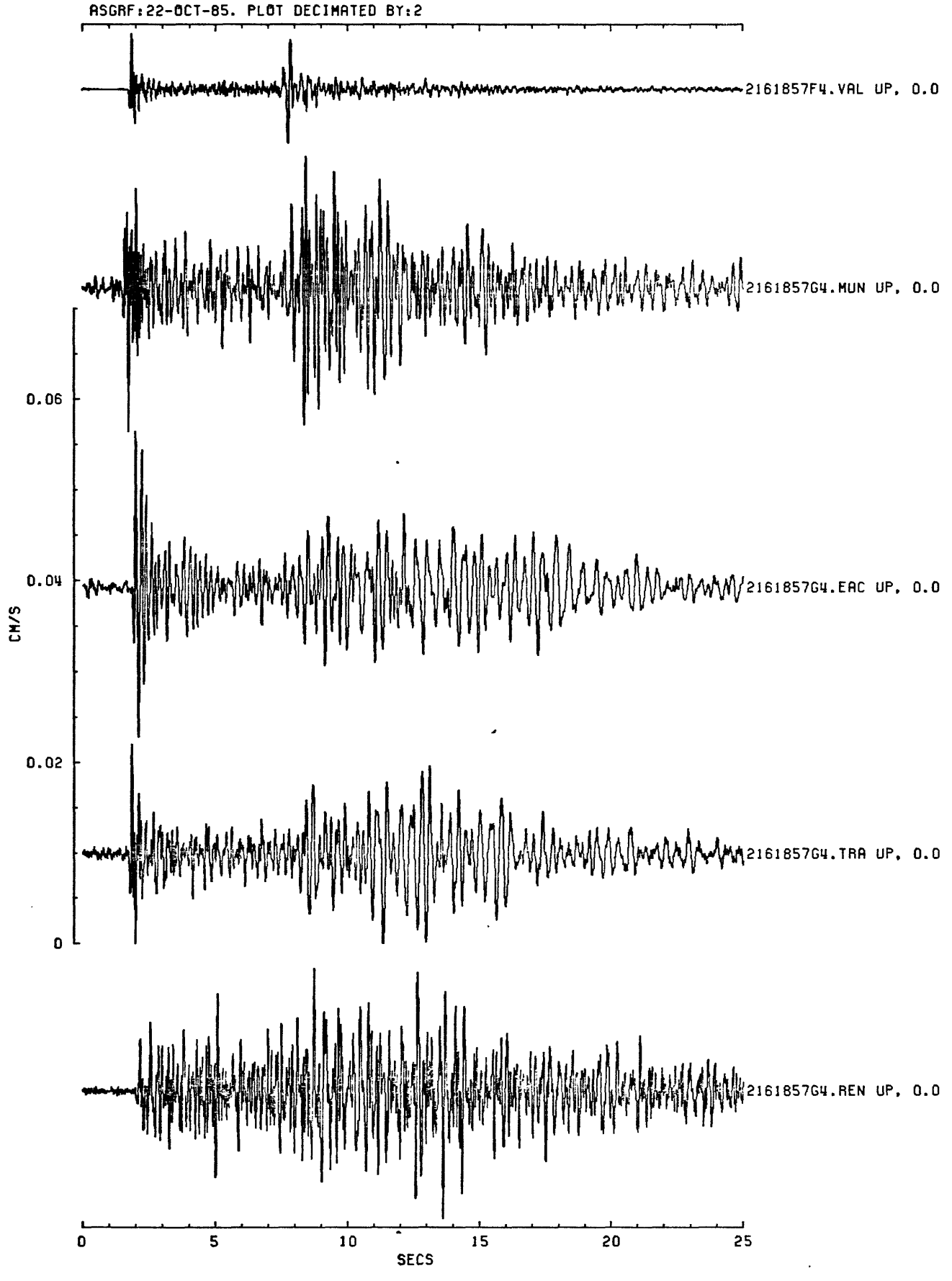

Figure B21. Scaled seismograms for event 2161857 (vertical components).

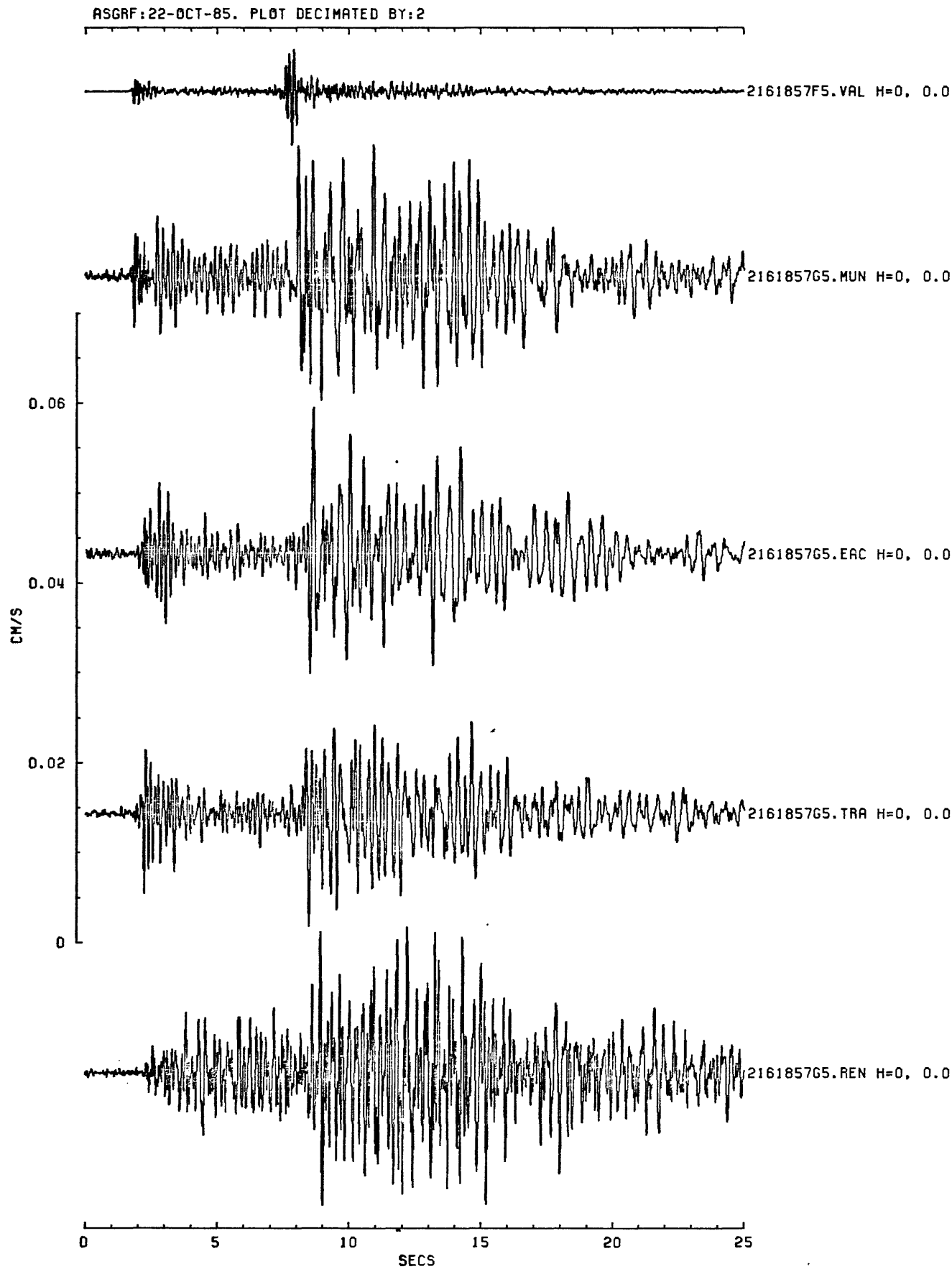

Figure B22. Scaled seismograms for event 2161857 (N-S components).

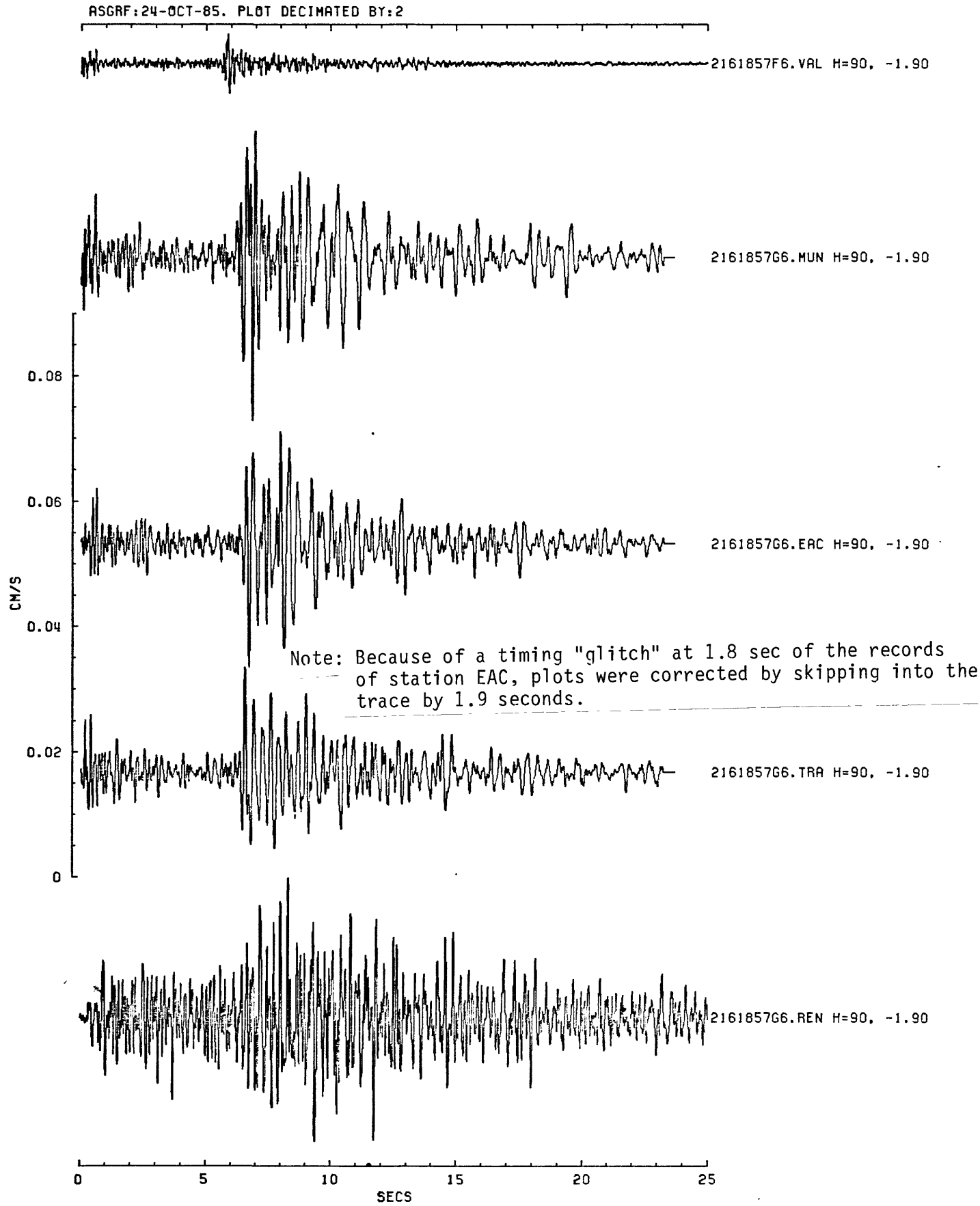

Figure B23. Scaled seismograms for event 2161857 (N-S components).

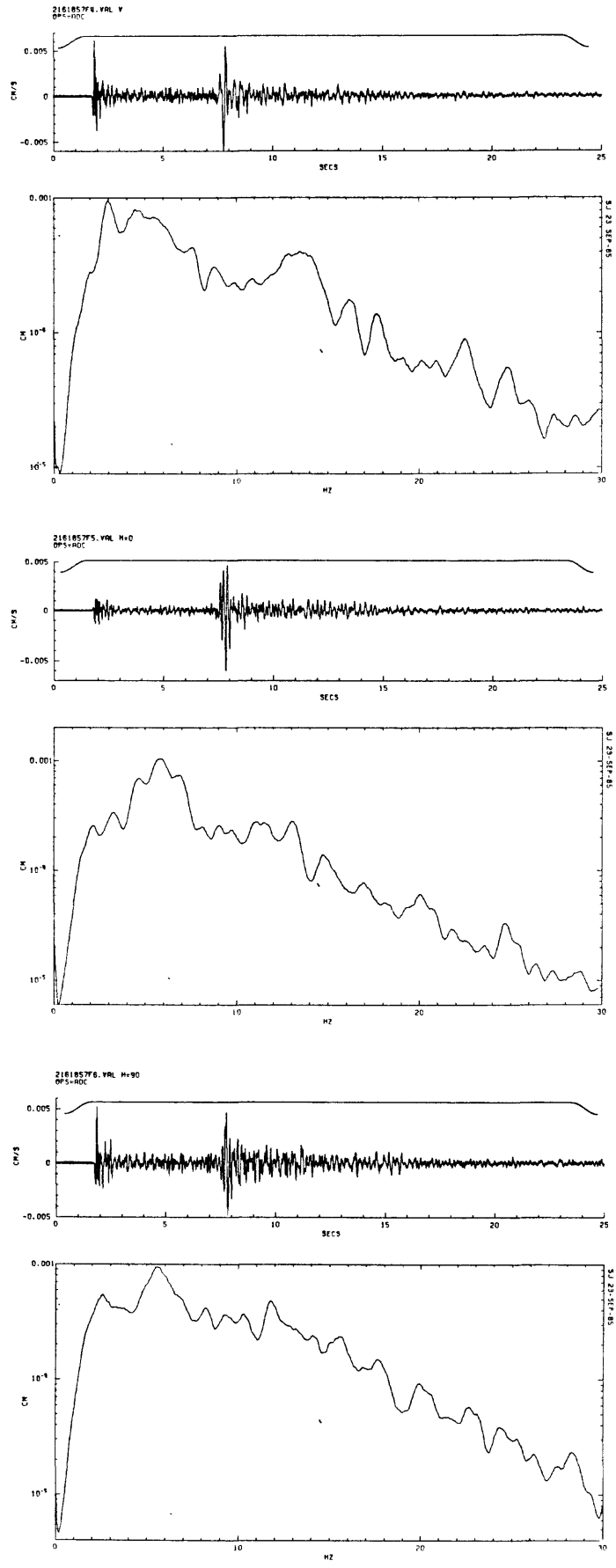

Figure B24. Time series and Fourier amplitude spectra of event on August 4, 1985 (Julian 216) at 18:57 for the vertical, horizontal (N-S and E-W) components, respectively, for station VAL.

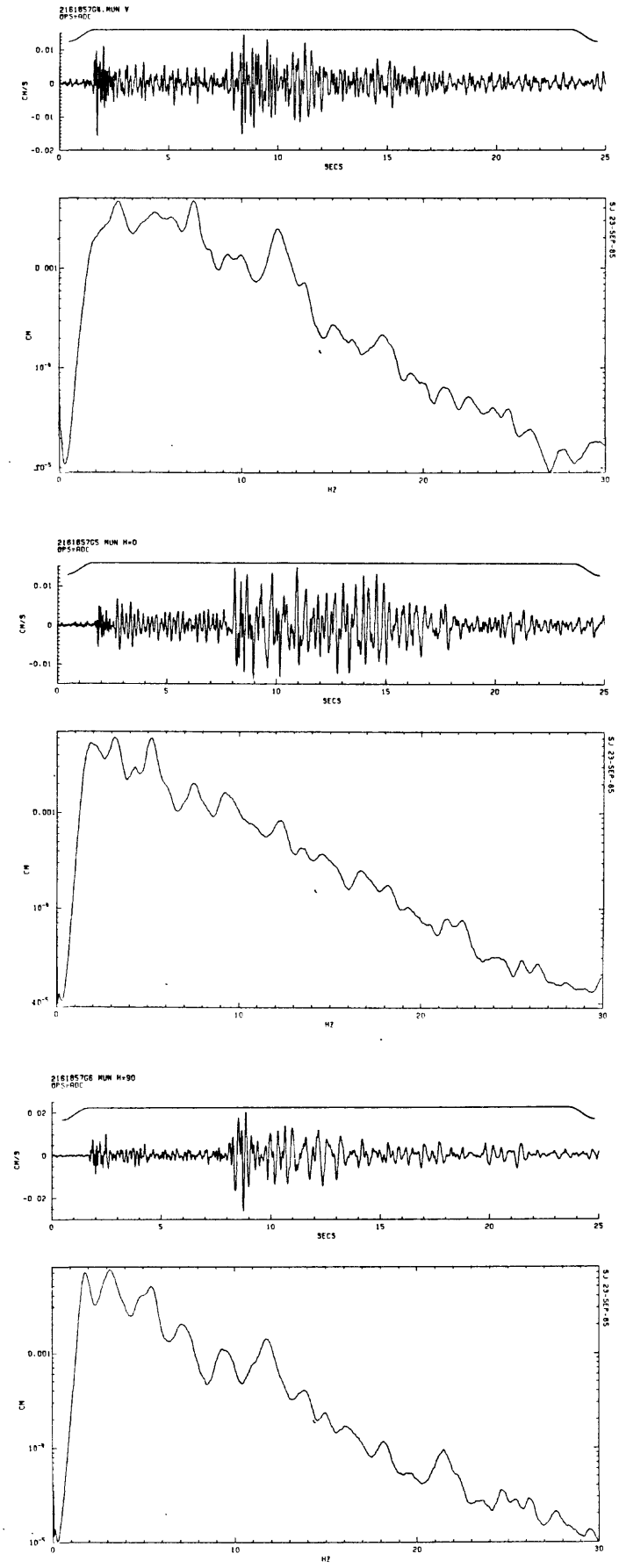

Figure B25. Time series and Fourier amplitude spectra of event on August 4, 1985 (Julian 216) at 18:57 for the vertical, horizontal (N-S and E-W) components, respectively, for station MUN.

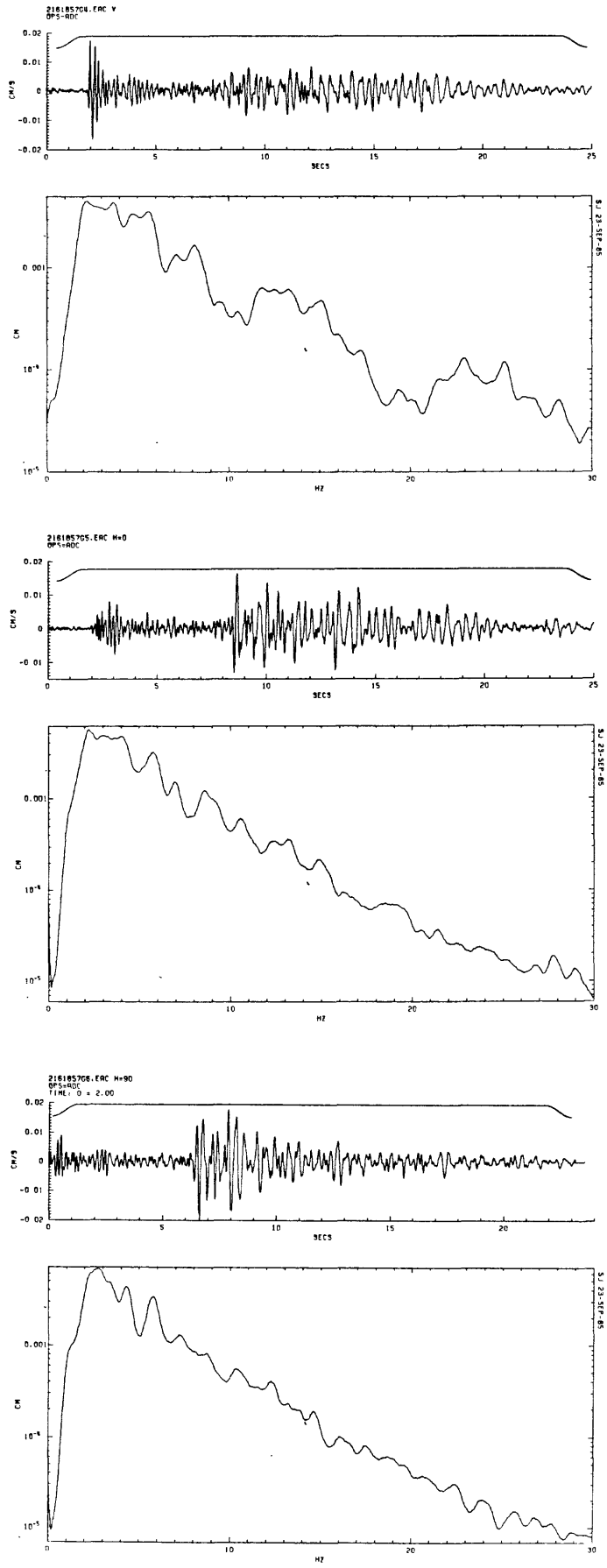

Figure B26. Time series and Fourier amplitude spectra of event on August 4, 1985 (Julian 216) at 18:57 for the vertical, horizontal (N-S and E-W) components, respectively, for station EAC.

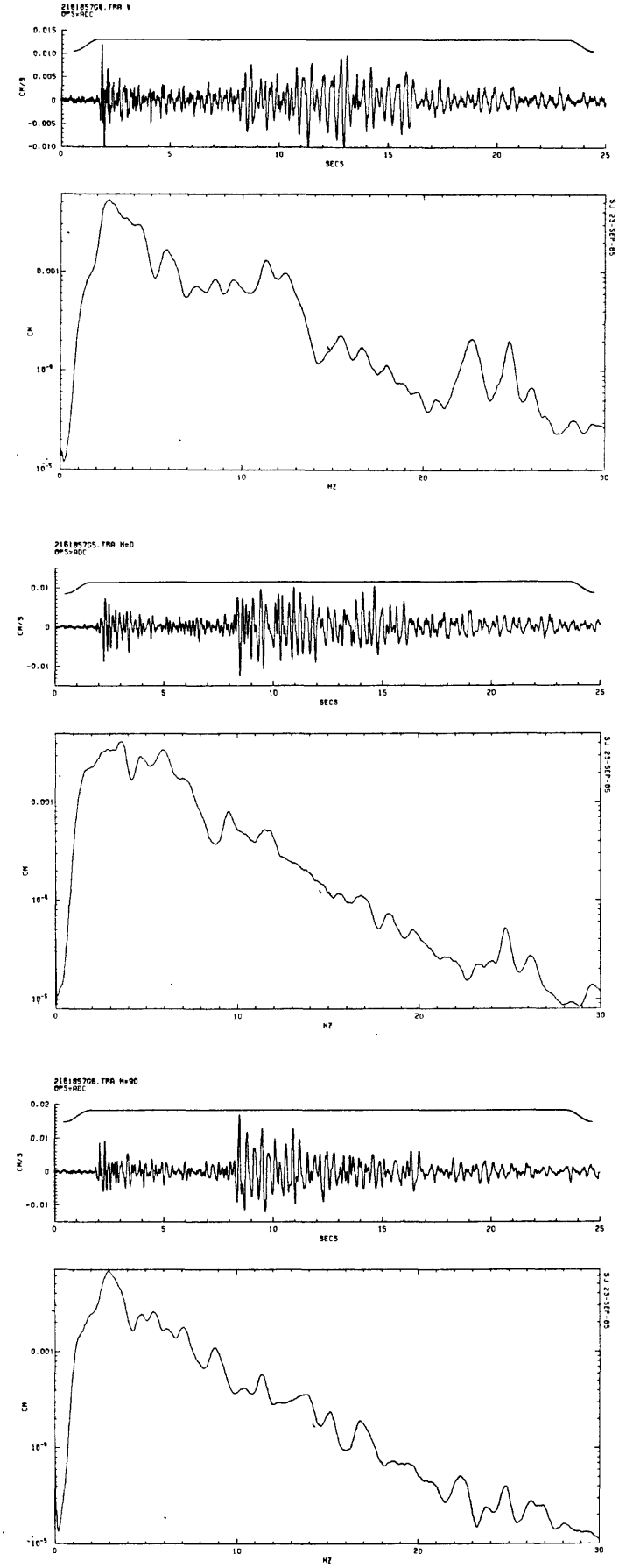

Figure B27. Time series and Fourier amplitude spectra of event on August 4, 1985 (Julian 216) at 18:57 for the vertical, horizontal (N-S and E-W) components, respectively, for station TRA.

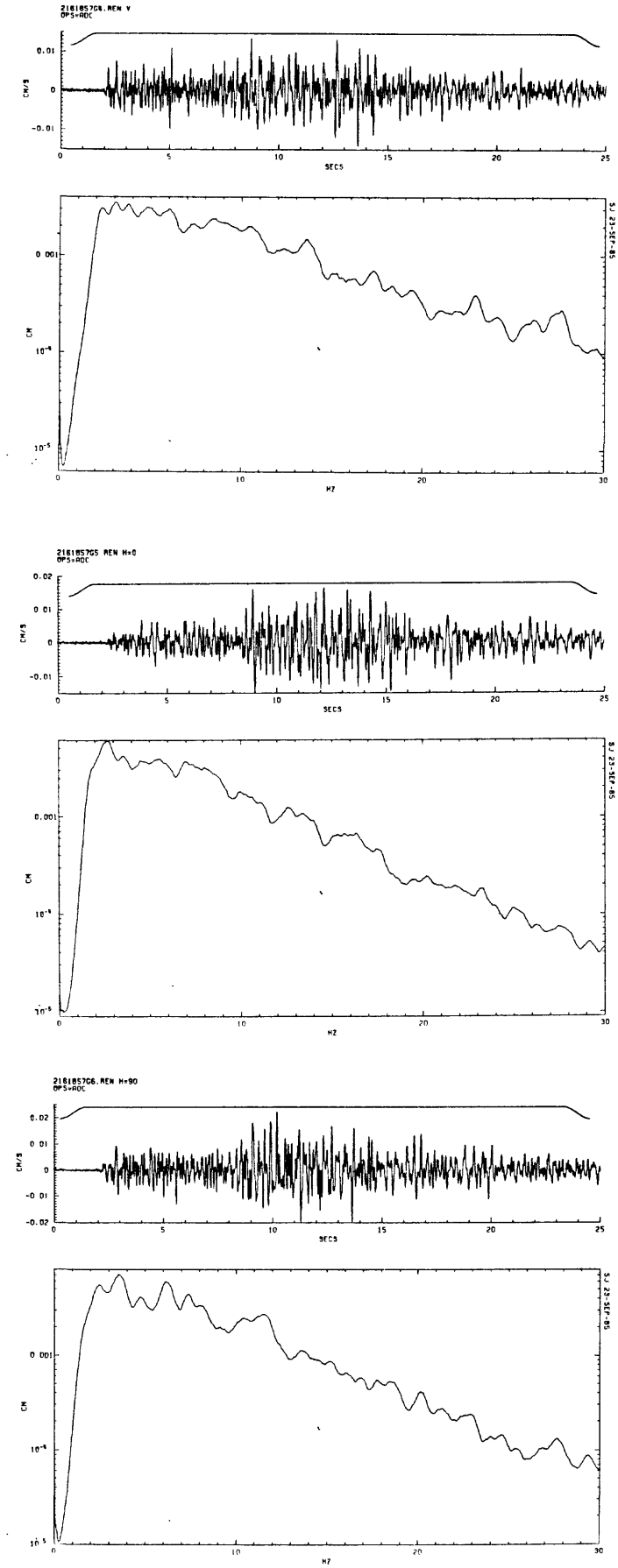

Figure B28. Time series and Fourier amplitude spectra of event on August 4, 1985 (Julian 216) at 18:57 for the vertical, horizontal (N-S and E-W) components, respectively, for station REN.

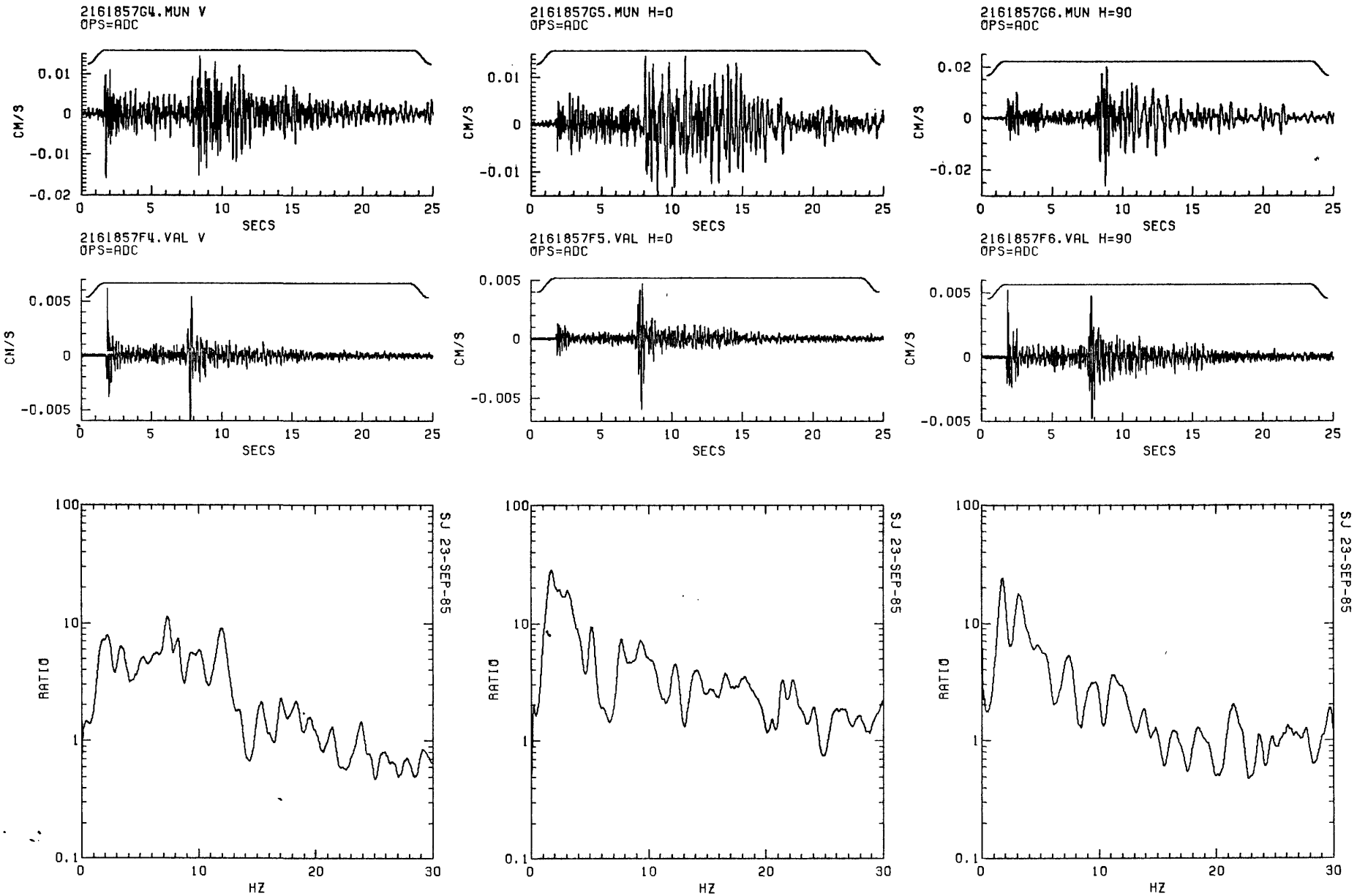

Figure B29. Scaled seismograms and spectral ratios of event on August 4, 1985 (Julian 216) at 18:57 for the vertical, horizontal (N-S and E-W) components, respectively, of stations MUN/VAL.

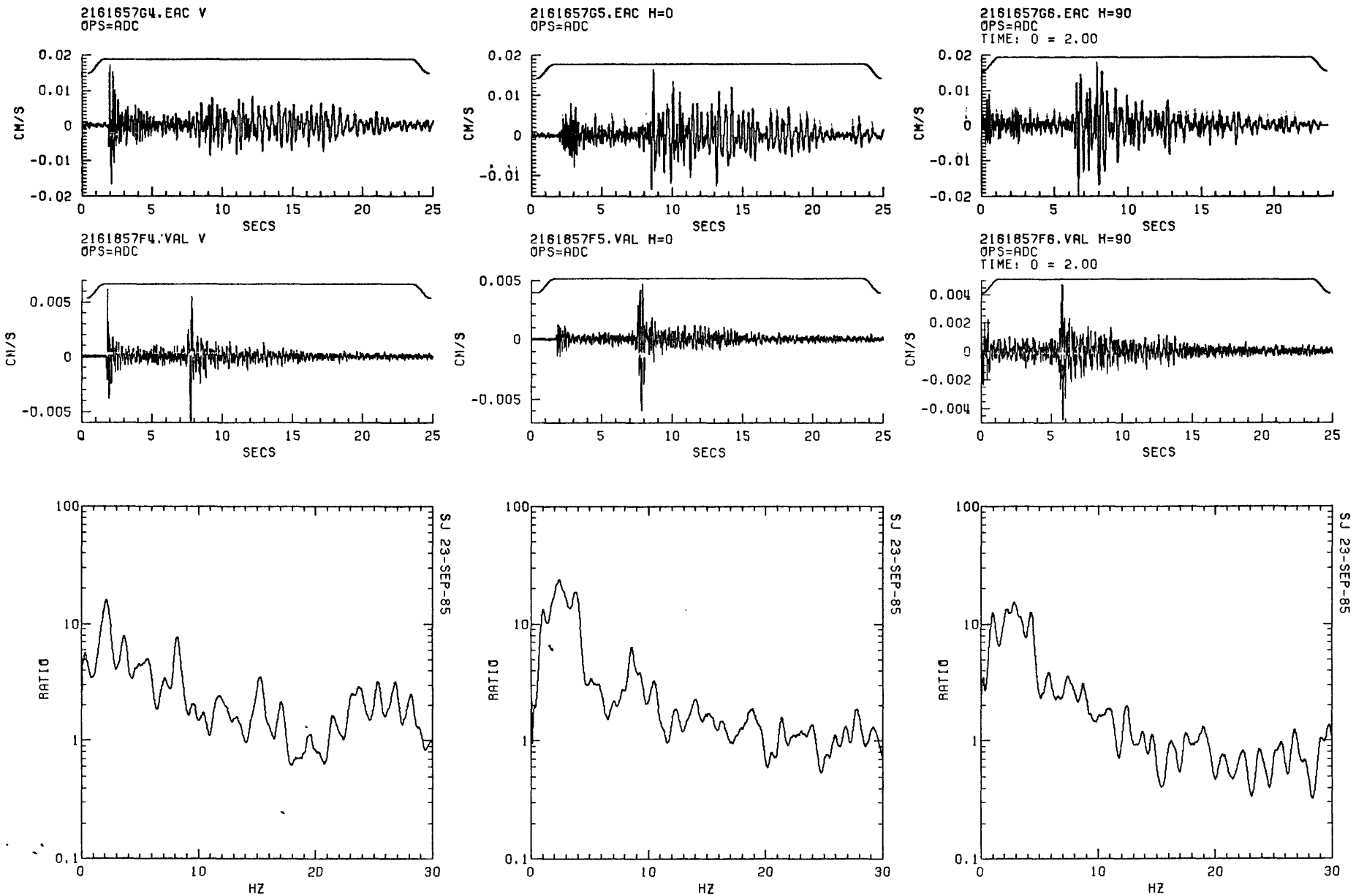

Figure B30. Scaled seismograms and spectral ratios of event on August 4, 1985 (Julian 216) at 18:57 for the vertical, horizontal (N-S and E-W) components, respectively, of stations EAC/VAL.

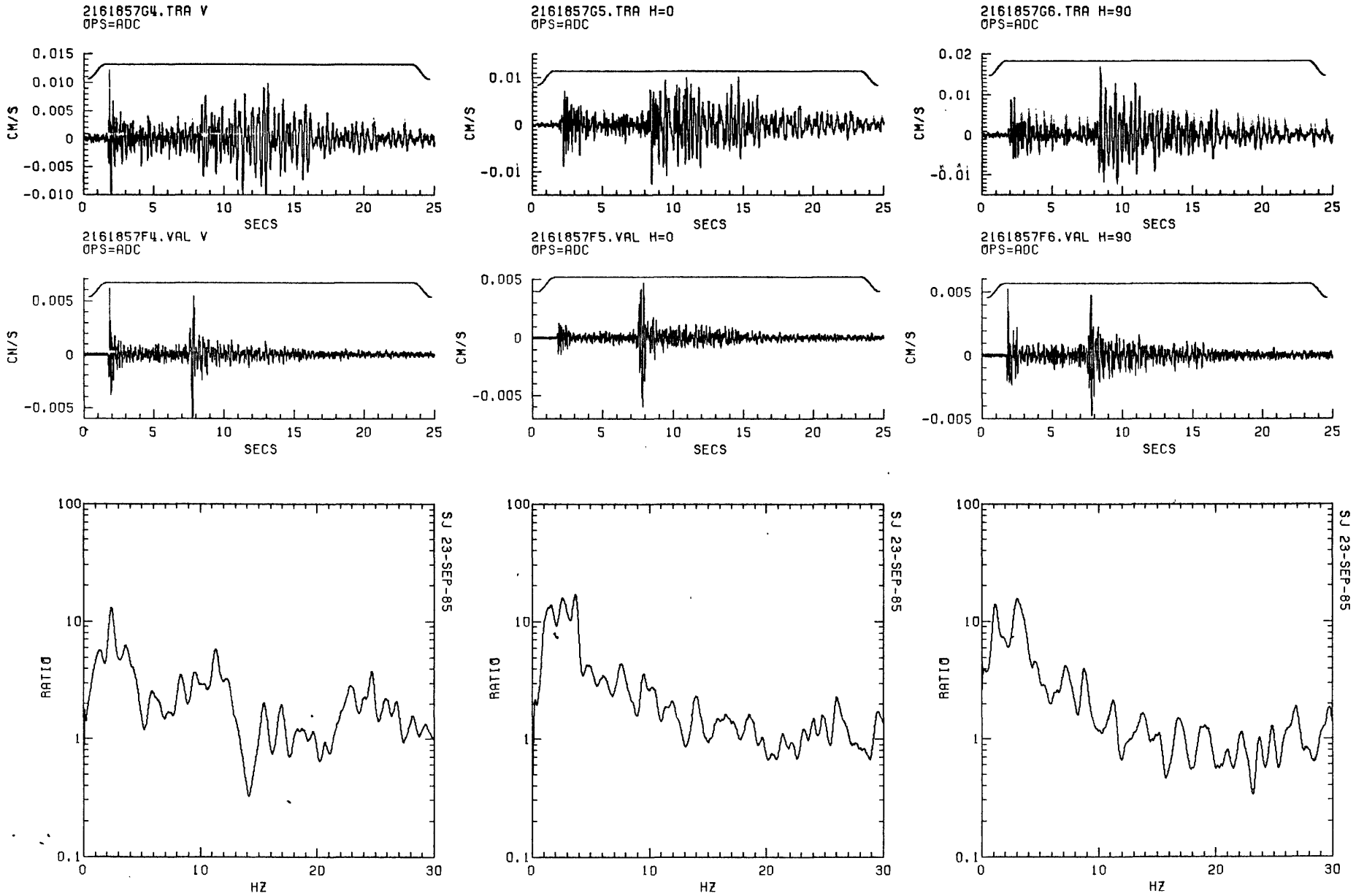

Figure B31. Scaled seismograms and spectral ratios of event on August 4, 1985 (Julian 216) at 18:57 for the vertical, horizontal (N-S and E-W) components, respectively, of stations TRA/VAL.

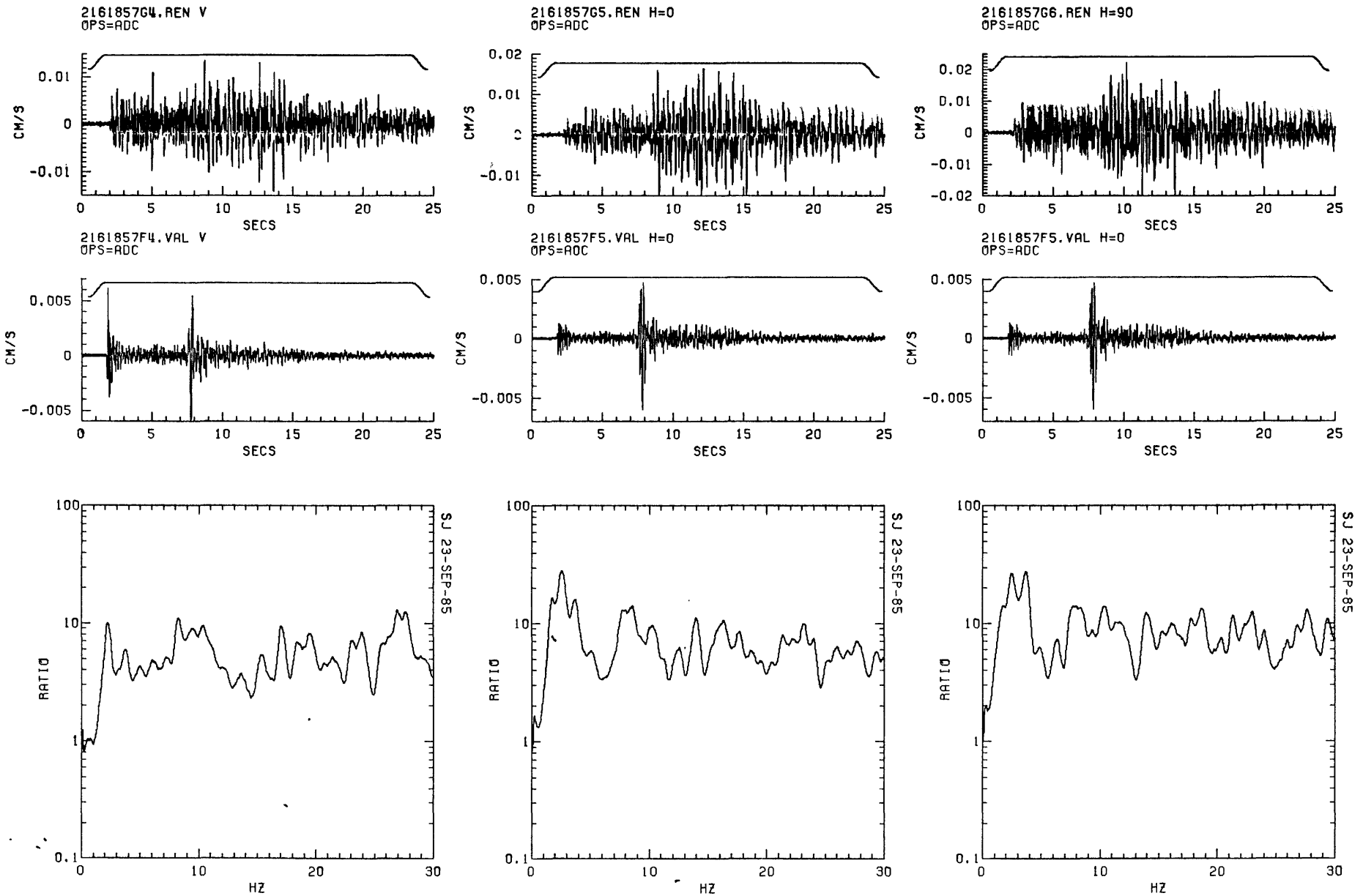

Figure B32. Scaled seismograms and spectral ratios of event on August 4, 1985 (Julian 216) at 18:57 for the vertical, horizontal (N-S and E-W) components, respectively, of stations REN/VAL.

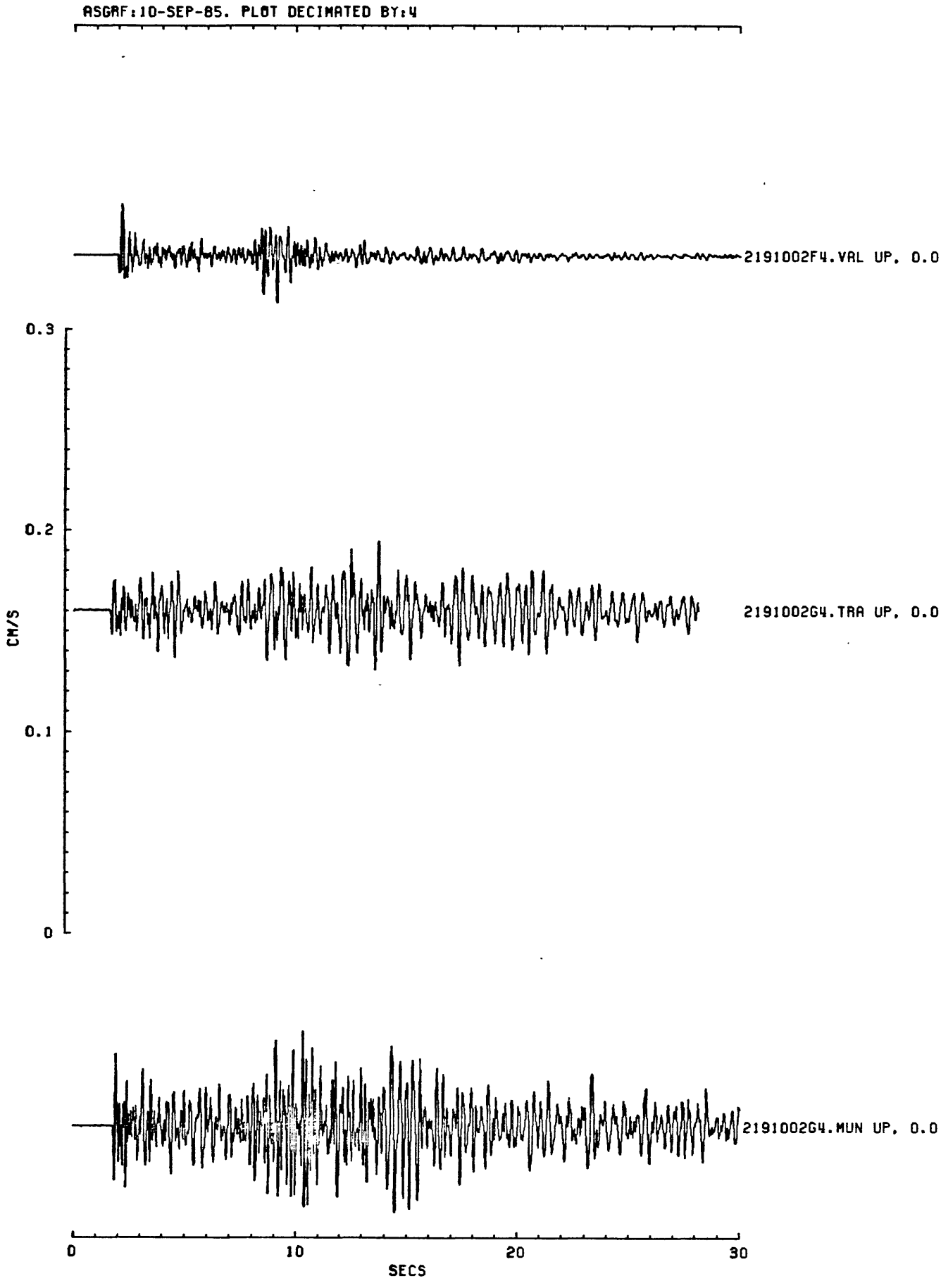

Figure B33. Scaled seismograms for event 2191002 (vertical components).

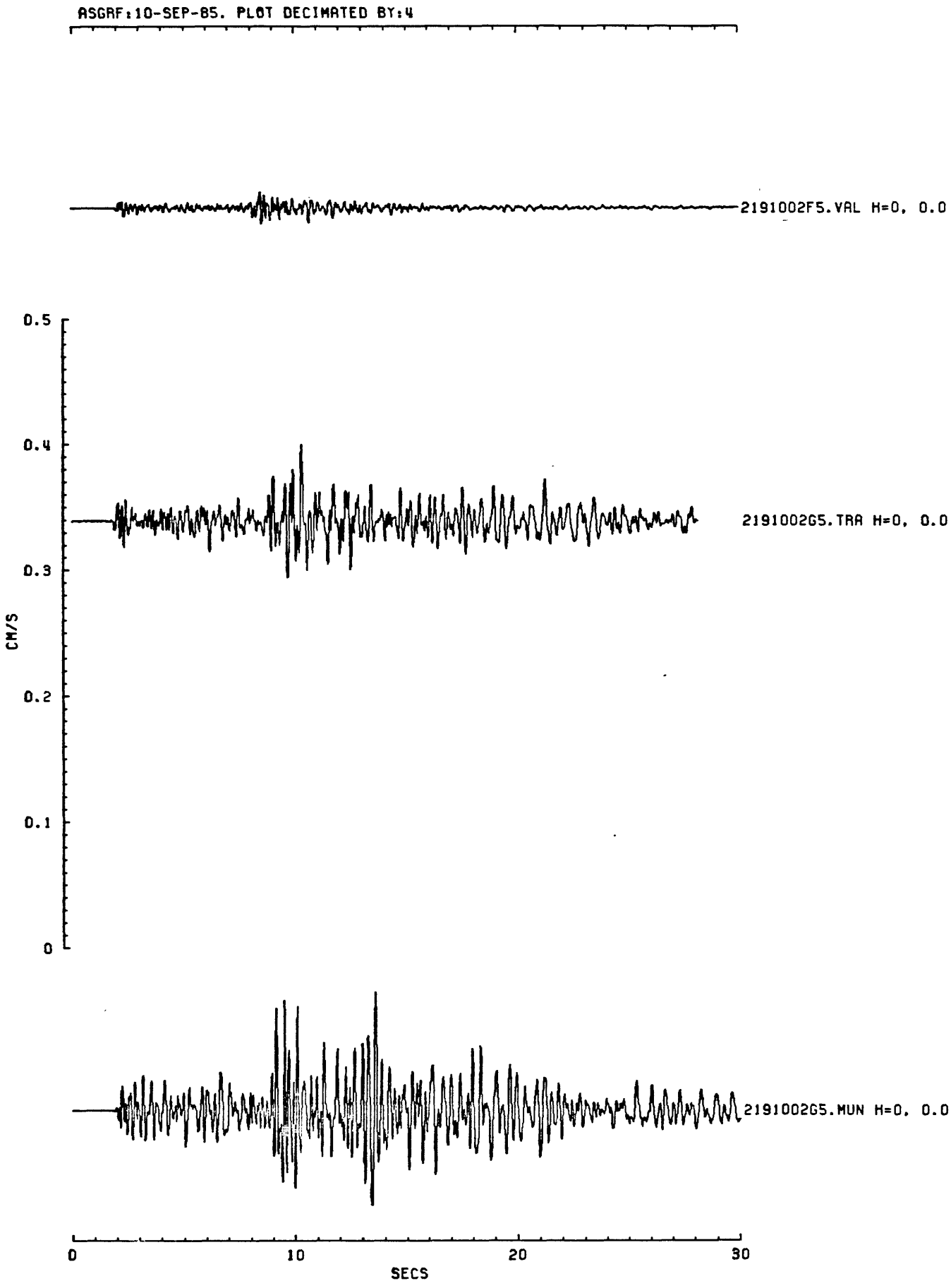

Figure B34. Scaled seismograms for event 2191002 (N-S components).

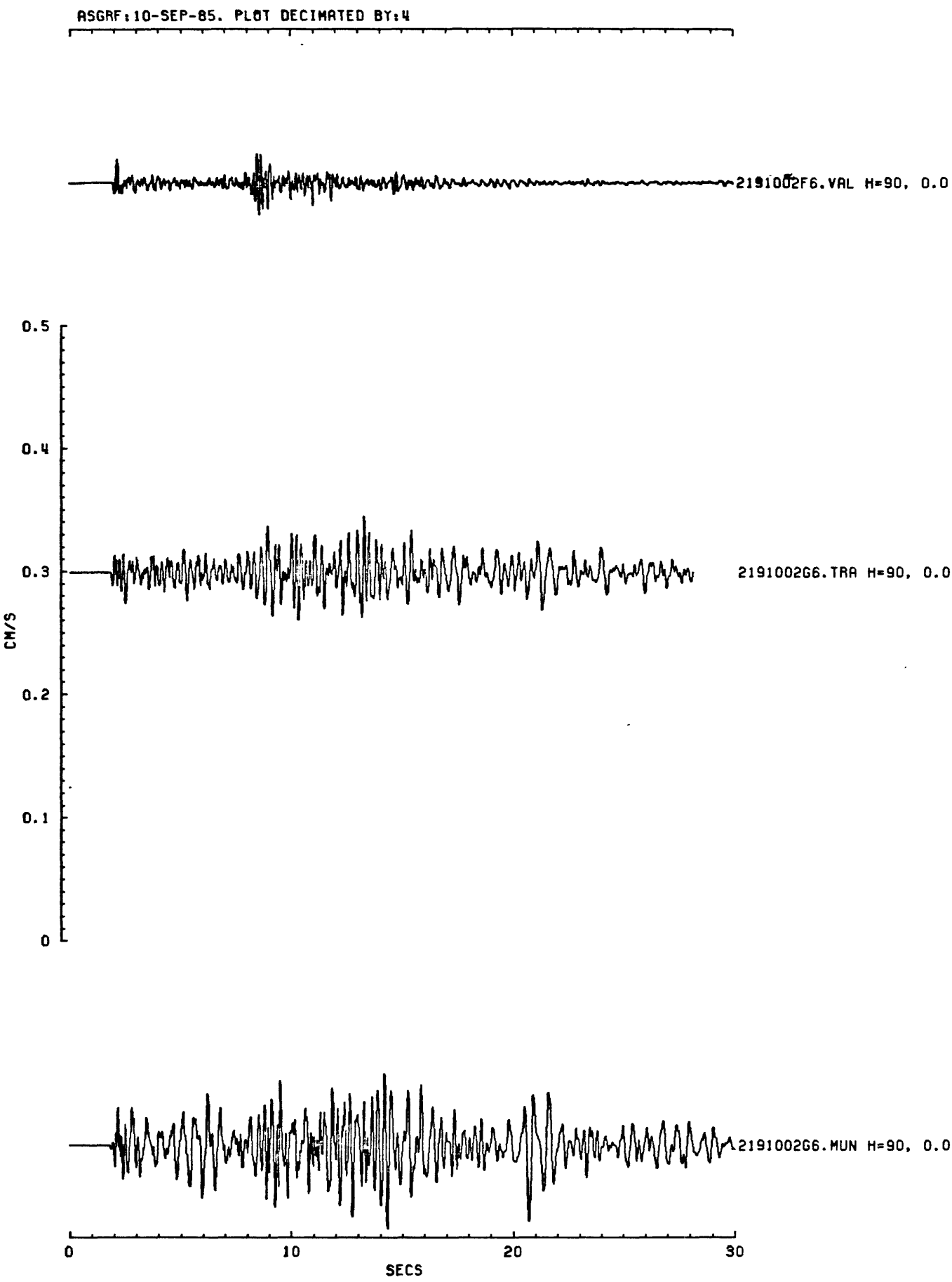

Figure B35. Scaled seismograms for event 2191002 (E-W components).

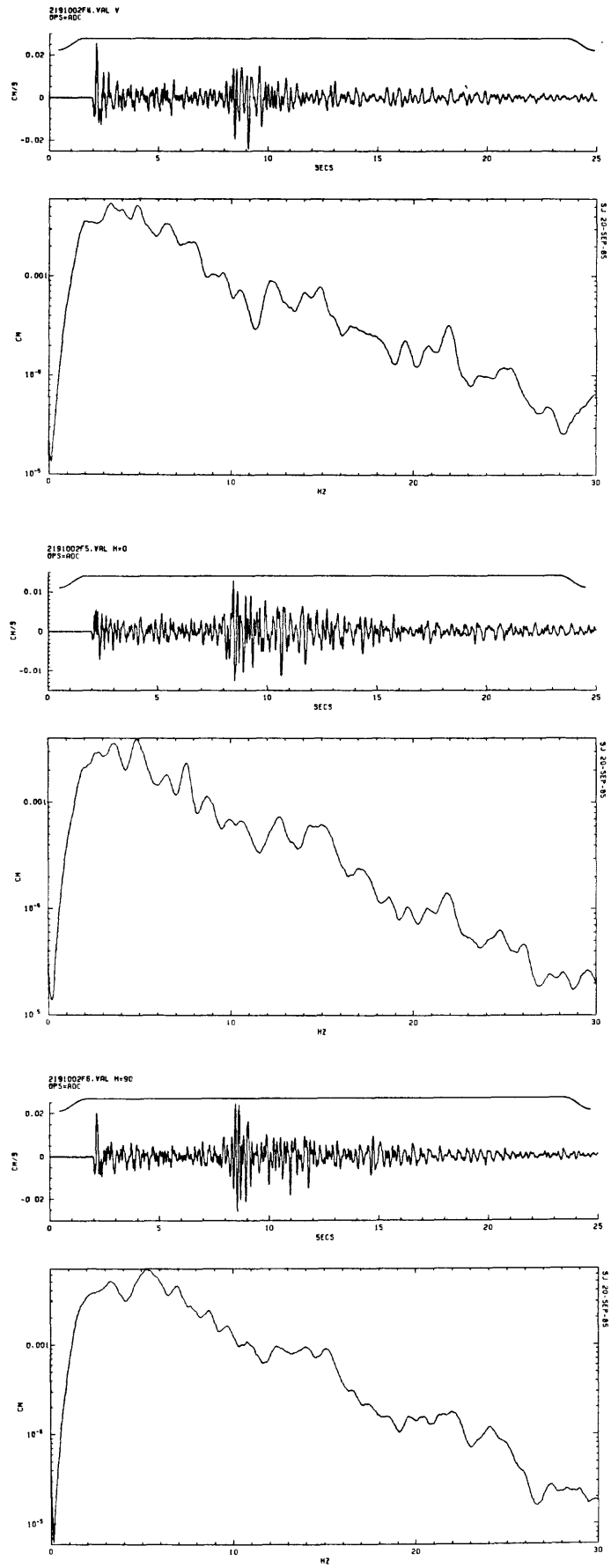

Figure B36. Time series and Fourier amplitude spectra of event on August 7, 1985 (Julian 219) at 10:02 for the vertical, horizontal (N-S and E-W) components, respectively, for station VAL.

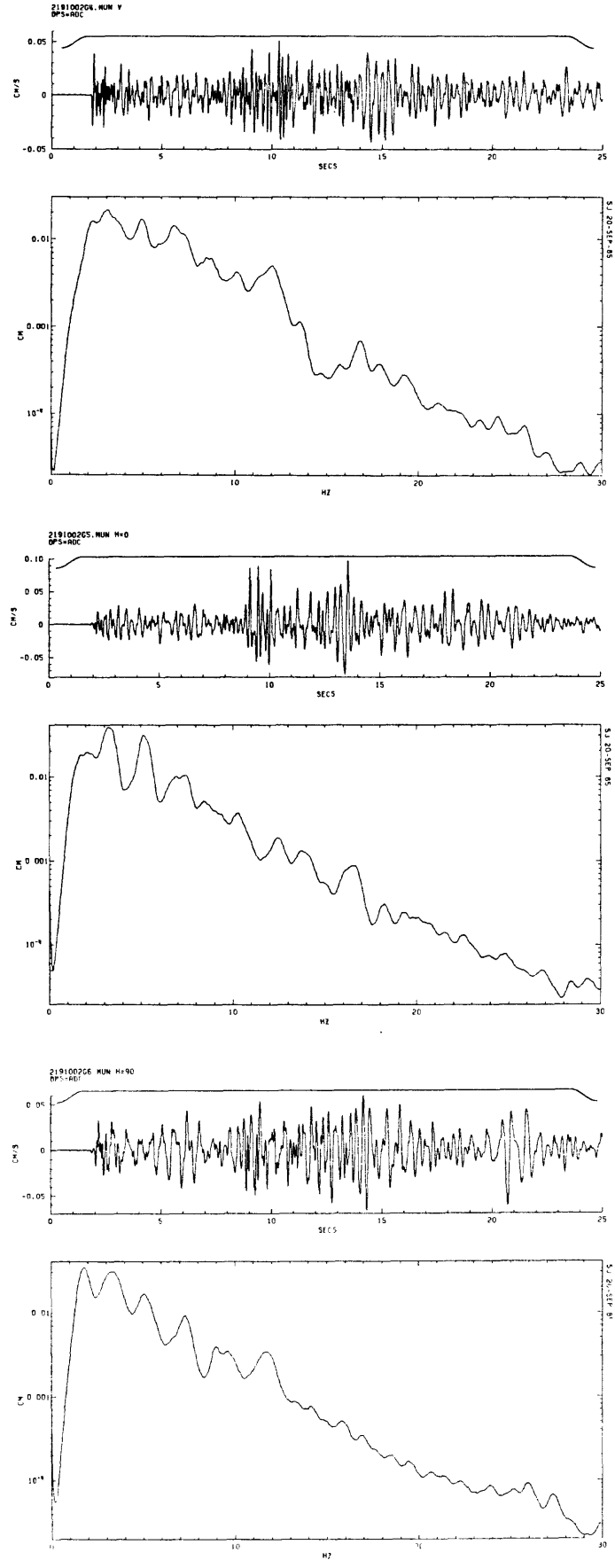

Figure B37. Time series and Fourier amplitude spectra of event on August 7, 1985 (Julian 219) at 10:02 for the vertical, horizontal (N-S and E-W) components, respectively, for station MUN.

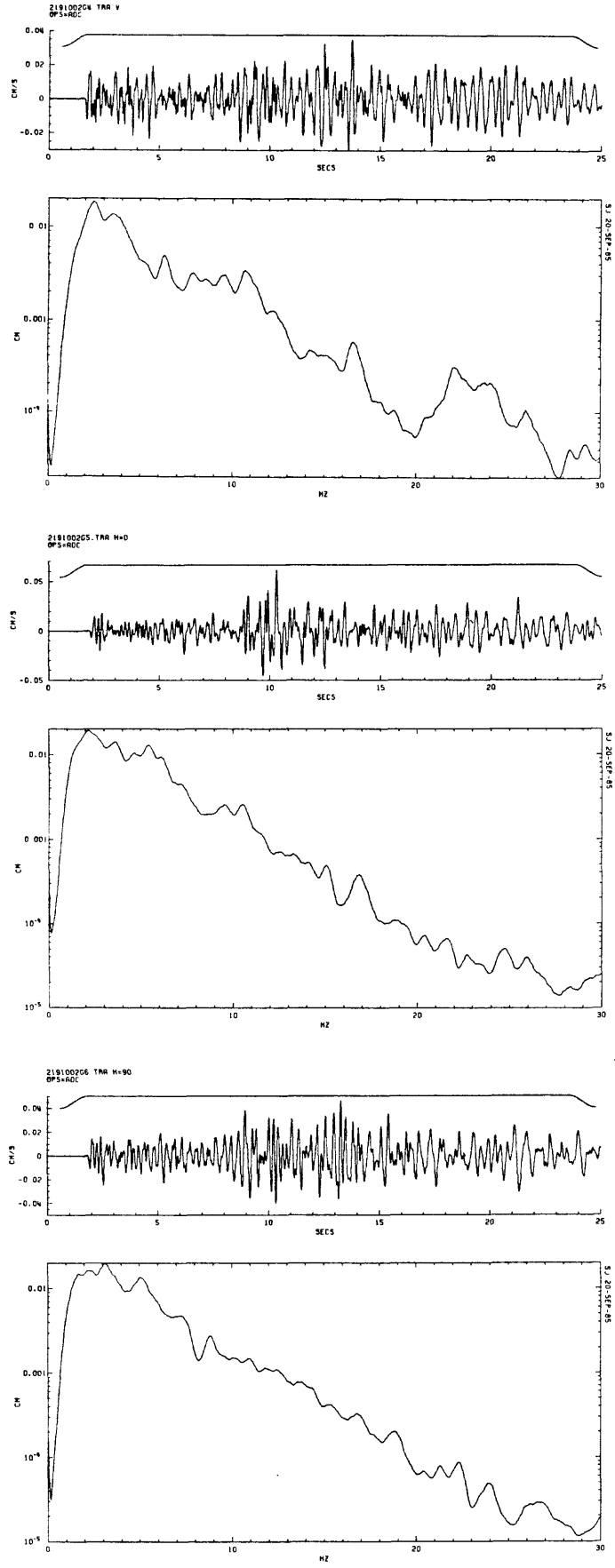

Figure B38. Time series and Fourier amplitude spectra of event on August 7, 1985 (Julian 219) at 10:02 for the vertical, horizontal (N-S and E-W) components, respectively, for station TRA.

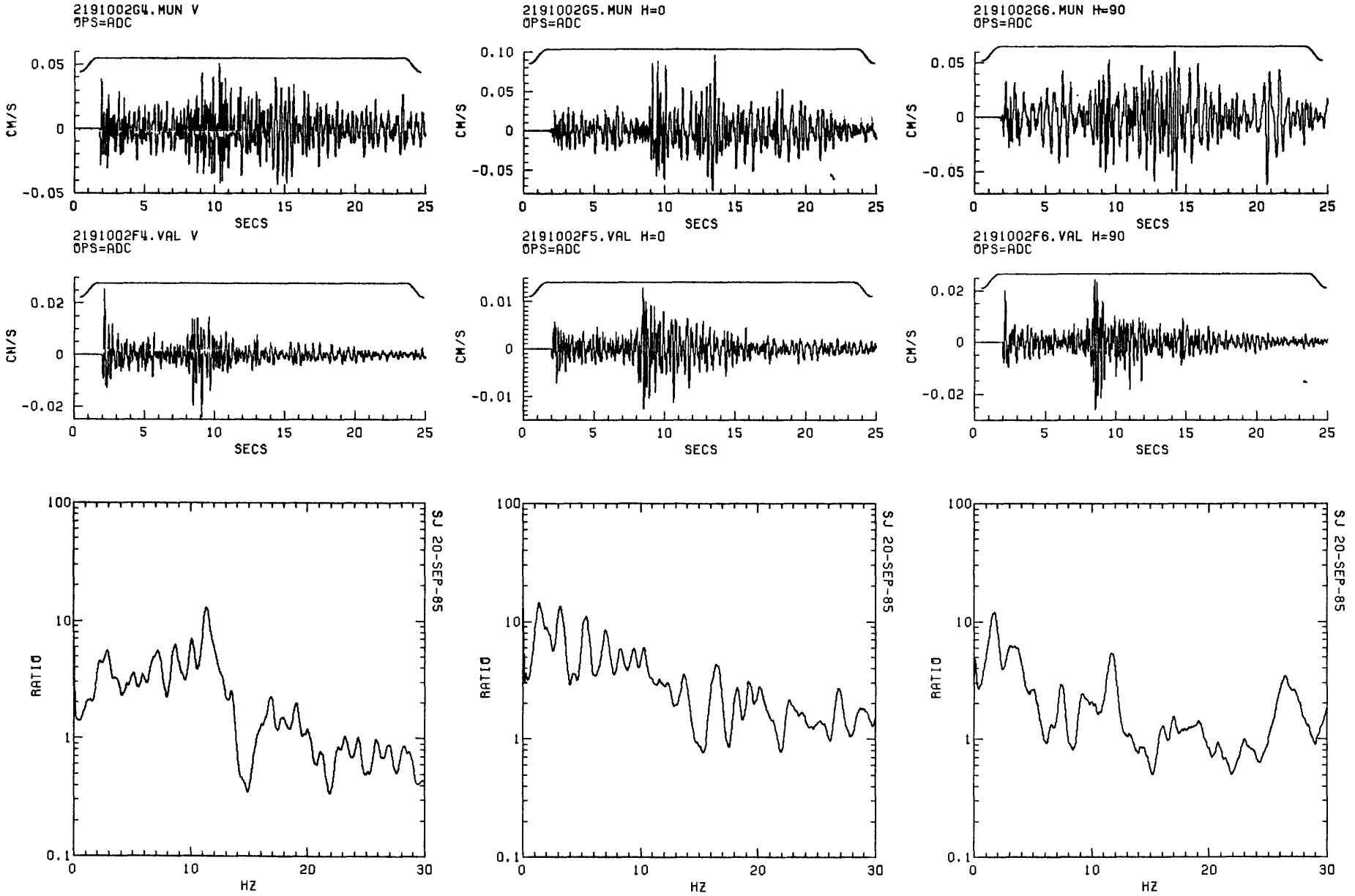

Figure R39. Scaled seismograms and spectral ratios of event on August 7, 1985 (Julian 219) at 10:02 for the vertical, horizontal (N-S and E-W) components, respectively, of stations MUN/VAL.

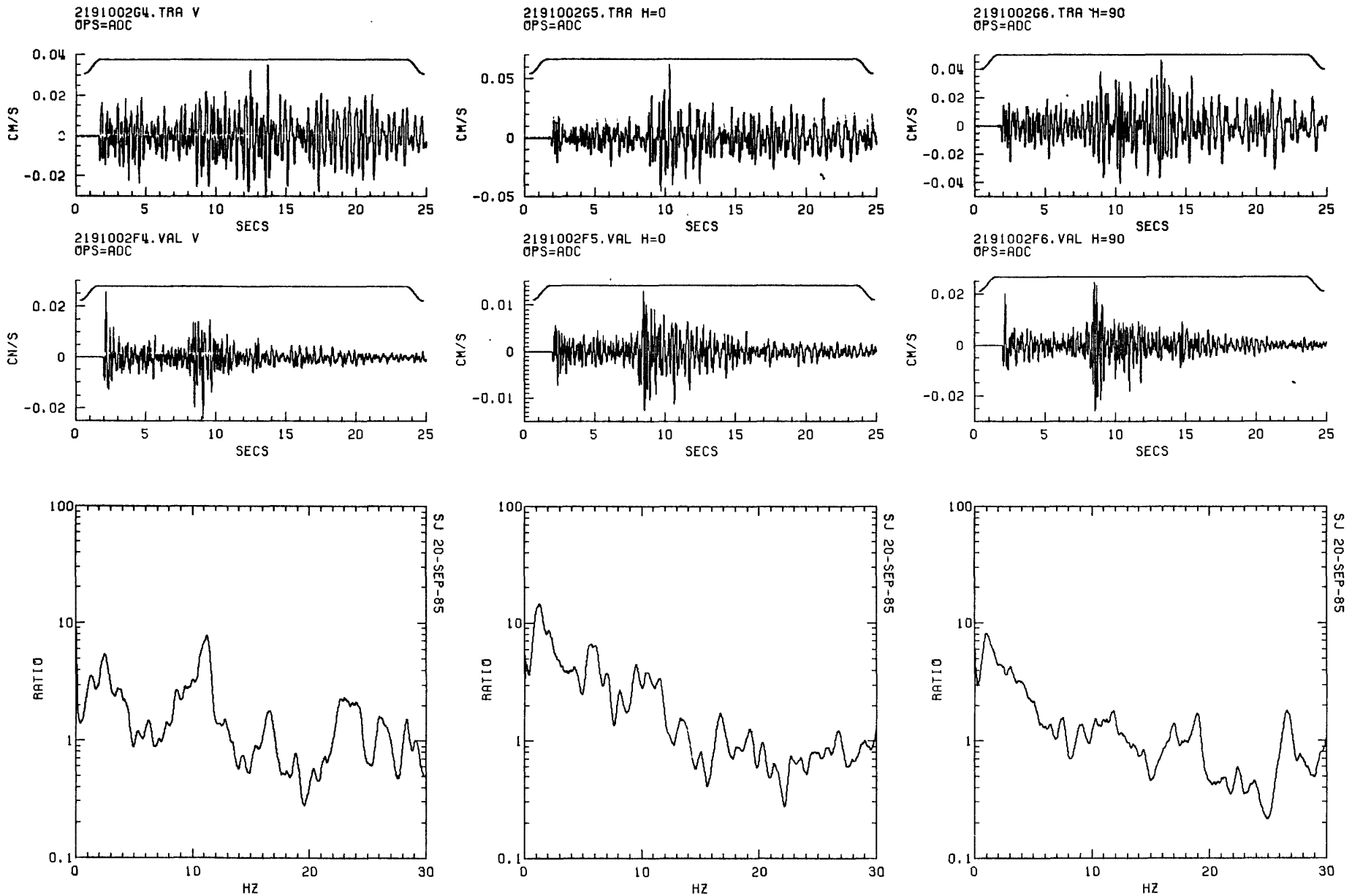

Figure B40. Scaled seismograms and spectral ratios of event on August 7, 1985 (Julian 219) at 10:02 for the vertical, horizontal (N-S and E-W) components, respectively, of stations TRA/VAL.